The Internal Properties of the Bioadhesive Bond

By Paul Marshall, B.Pharm. M.R. Pharm.S.

Thesis submitted to the University of Nottingham
for the degree of Doctor of Philosophy, May 2000

Abstract

The movement and concentration of water inside hydrophilic matrices and the bioadhesive bonds formed by them have been proposed as important factors in the bioadhesion of hydrophilic matrices (Smart *et al*, 1991, and Mortazavi and Smart, 1993). This thesis has developed a non-invasive magnetic resonance imaging (MRI) technique to spatially resolve the self-diffusion coefficient (SDC) and concentration profiles of water inside the bioadhesive bonds formed by dry and hydrated hydrophilic matrices. The bioadhesive interaction between mucin and adhesive may affect the network structure and diffusion retarding properties of either polymer. The mobility of solutes may be used as an indicator of such changes. This thesis has developed a fluorescence recovery after photobleaching (FRAP) technique to measure the mobility of fluorescently tagged dextrans in the mucin and adhesive polymer networks.

These methods were combined with basic studies of liquid uptake kinetics and bond strength through detachment force testing to study the bioadhesive bonds formed between alginate matrices and pig gastric mucus. These studies provided evidence to suggest that the bioadhesion of dry and hydrated alginate matrices involved several underlying mechanisms. In the case of bioadhesive bonds formed by dry alginate matrices, the SDC profiles indicated that the hydration of alginate and the formation of a viscous gel layer may cause the localised dehydration of mucus directly adjacent to the alginate matrix. Furthermore, the work of adhesion (W_a) of bioadhesive bonds formed between pig gastric mucus and dry alginate matrices suggested that polymer interpenetration and secondary chemical bonding might also be involved. In the case of bonds formed by hydrated alginate matrices, similar studies indicated that the bioadhesion of hydrated alginate matrices might involve polymer interpenetration and secondary chemical bonding as well as mucus dehydration, although the latter phenomenon appeared to be dependent on the molecular weight of alginate.

Acknowledgements

I would like to take this opportunity to express my sincere thanks to everybody that has helped and encouraged me throughout my PhD project.

I would especially like to thank Colin Melia for his support and friendship, in addition to providing an intuitively enlightened approach to academic research.

I would also like thank Peter Dettmar, Frank Hampson, Paul Dickson and all the people at Reckitt & Colman Products for all their support, help and advice over the years, as well as providing the financial incentive for this research project. My thanks also go out to everyone at Pronova Biopolymer, especially Edvar Onsoyen and Mike Dornish.

I am indebted to Angelien Snaar, Yao Ng and Richard Bowtell for all their hard work and patience in teaching me the principles of magnetic resonance imaging. Likewise, I am extremely grateful for the helpful advice and hard work that John Holden put into the development of fluorescence recovery after photobleaching.

I would like to thank Anne Price for her work in the liquid uptake studies as well as John Knight, Jeff Pearson and Adrian Allen for their work and advice in purifying pig gastric mucus. I would also like to thank Giles Saunders for the imaging of the alginate powders. I would also like to thank the teaching and research support staff of the School of Pharmacy, especially Christie, Barbara, Linda, Karen, Mick, Pravin, Steve, Lee and Dave, for all their hard work and help.

I would also like to thank the 'Lads', especially Col, Matt and Ian, but not forgetting Jack and Danny, for some memorable 'nights out on the tile'. I would also like to thank Clair, Helen and Linda for providing their own brand of feminine charm and insight. I would also like to thank Sandy, Sarah, Ying Hui and Arvind, for all their help.

I am very lucky to have been blessed with a supportive family that have given me their love and understanding during the years as well as encouraging me to complete and write-up this thesis. Subsequently, I would like to give my most heartfelt thanks to my parents, Barbara and Brian, my sister, Louise, and my wife, Joanna. In the same spirit, I would also like to express my sincere thanks to Joanna's parents, Maureen and Dudley, for their help and support (shame they couldn't teach her to cook!!).

To Mum,

This is for you!

Take care and don't worry…well not too much!

Ohe, iam satis est, ohe, libelle,
iam pervenimus usque ad umbilicos.
tu procedere adhuc et ire quaeris,
nec summa potes in schida teneri,
sic tamquam tibi res peracta non sit,
quae prima quoque pagina peracta est.
iam lector queriturque deficitque,
iam librarius hoc et ipse dicit
'Ohe, iam satis est, ohe, libelle.'

Marcus Valerius Martialis

Liber IV, Epigrammatum LXXXIX (Penguin Classics)

Contents

List of abbreviations and nomenclature

α	coefficient of Fickian (Case I) transport
A	ampere or alanine
Ala	alanine
ANOVA	analysis of variance
Arg	arginine
ASCII	American standard code for information interchange
Asp	aspartic acid
ATR-FTIR	attenuated total reflectance Fourier transform infra-red spectroscopy
a.u.	arbitrary units
AUC_F	area under fluorescence intensity profile
AUC_{FT}	area under force-time curve
β	coefficient of relaxational (Case II) transport
B_0	applied magnetic field strength
BP	British Pharmacopoeia
°C	degrees centigrade
CCKP-Z	cholecystokinin
CFM	continuous fluorescence microphotolysis
CFMM	continuous fluorescence multipoint microphotolysis
CLSM	confocal laser scanning microscope or confocal laser scanning microscopy
CMC	carboxymethylcellulose
Cp	centipoise
CPP	1,3-bis(ρ-carboxyphenoxypropane)
Cys	cysteine
δ	duration of magnetic gradient
Δ	time between the start of each magnetic gradient
D	aspartic acid
Da	Dalton
Dl	decilitre
DNA	deoxyribonucleic acid

DVLO	Derjaguin, Landau, Vervey and Overbeck colloid theory
E	glutamic acid
E_{app}	apparent Young's modulus
EDTA	ethylenediamine tetra-acetic acid
EPR	electron paramagnetic resonance
F	phenylalanine
F_x	frequencies – 'x' can be G, GG, GGG, GGM, MGM, MG/GM, MM or M.
F_0	fluorescence intensity immediately after photobleaching
F_∞	fluorescence intensity at very long times after photobleaching
F_{max}	maximum detachment force
FITC	fluorescein isothiocyanate
F_P	fluorescence intensity profile
FRAP	fluorescence recovery after photobleaching
FRAPP	fluorescence recovery after pattern photobleaching
FTIR	Fourier transform infra-red spectroscopy
Fuc	fucose
g	gramme or force of gravity or magnetic gradient amplitude
gH_20	gramme of water
G	guluronate or guluronic acid or glycine
G'	storage modulus
G"	loss modulus
Gal	galactose
GalNAc	N-acetylgalactosamine
GG	polyguluronate or polyguluronic acid blocks
GI	gastrointestinal
GlcNAc	N-acetylglucosamine
Glu	glutamic acid
Gly	glycine
H	histidine
HCl	hydrochloride

HPC	hydroxypropylcellulose
HPLC	high performance liquid chromatography
HPMC	hydroxypropylmethylcellulose
hr	hour
Hz	Hertz
I	isoleucine
k	kinetic constant
K	lysine
kDa	kiloDalton
keV	kiloelectron volt
kg	kilogram
L	leucine
LINESCAMP	line scanning microphotolysis
LVER	linear viscoelastic region
Lys	lysine
µg	microgram
µl	microlitre
µm	micrometre
m	diffusional exponent or metre
M	mannuronate or mannuronic acid or molar or methionine
MAP	mussel adhesive protein
M:G	ratio of mannuronate to guluronate
mJ	millijoule
mins	minutes
mg	milligram
ml	millilitre
mm	millimetre
mM	millimoles or millimolar
MM	polymannuronate or polymannuronic acid blocks
mol	moles
mPa	milliPascals
MRI	magnetic resonance imaging
ms	milliseconds

MUC	tandem repeat sequence
M_w	weight average
mW	milliwatts
MW	molecular weight
n	number of experiments
N	Newton or asparagine
NA	numerical aperture
NeuAc	N-acetyl neuramic acid or sialic acid
N_G	average G block length
$N_{G>1}$	average G block length, excluding single G blocks
N_M	average M block length
$N_{M>1}$	average M block length, excluding single M blocks
nm	nanometre
NMR	nuclear magnetic resonance
ns	nanosecond
NSAIDS	non-steroidal anti-inflammatory drugs
p	probability
P	proline
P_x	position of 'x' in the SDC profile; the subscript 'x' may be 'DF', 'zen' or 'nad' for diffusion front, zenith and nadir, respectively
Pa	Pascal
PAS	periodic acid-Schiff's base assay
PEG	polyethylene glycol
PEhd	high density polyethylene
PHEMA	polyhydroxyethylmethacrylic acid
PMA	polymethacrylic acid
Pro	proline
PSA	poly(sebacic anhydride)
PTFE	polytetrafluoroethylene
PVA	polyvinyl alcohol
PVC	poly(vinyl chloride)
PVP	polyvinylpyrolidone

Q	glutamine
R	arginine
r^2	correlation coefficient
RF	radiofrequency
R_P	fluorescence recovery profile
rpm	revolutions per minute
R_T	rate of transport
S	serine
S_0	ground energy state of an electron pair
S_1	first higher energy state of an electron pair
SA	N-acetyl neuramic acid or sialic acid or sebacic acid
SCAMP	scanning microphotolysis
SD	standard deviation
SDC	self-diffusion coefficient
SDC_x	SDC of 'x' in the SDC profile; the subscript 'x' may be 'DF', 'zen' or 'nad' for diffusion front, zenith and nadir, respectively
SDS-PAGE	sodium dodecylsulphate polyacrylamide gel electrophoresis
secs	seconds
SEM	scanning electron microscope or scanning electron microscopy
Ser	serine
SGF	simulated gastric fluid
SIF	simulated intestinal fluid
τ_D	characteristic diffusion time
τ	characteristic recovery time
t	time
T	tesla or threonine
T_1	spin-lattice relaxation
T_2	spin-spin relaxation
T_a	actual time between fluorescence recovery images
T_{bl}	photobleaching time

T_i	desired time between fluorescence recovery images
tan δ	G''/G'
TE	echo time
TFA	2,2,2-trifluoroacetamide
Thr	threonine
TIR-FRAP	total internal reflectance fluorescence recovery after photobleaching
TR	repetition time
V	valine
W_a	work of adhesion
w/v	weight by volume
w/w	weight by weight
Y	tyrosine

Chapter 1

Introduction

1.1. Sodium alginates

1.1.1. Source and chemical composition of alginates

Alginates are anionic polysaccharide polymers found in the intercellular matrix of brown seaweed (Phaecophyacae), forming up to 40% of the dry weight of seaweed and providing strength and flexibility (Smidsrod and Draget, 1996). The chemical composition of alginate is dependent on several factors, including the species of Phaecophyceae, age, part of the plant, season and environmental conditions (table 1.1). For example, *Laminaria hyperborea*, which grows in the rough seas off the coast of Norway, needs to be structurally resilient and subsequently contains a high level of guluronic acid. In comparison, *Macrocystis pyrifera* grows in the calm waters off the west coast of USA and has a high mannuronic acid content. Alginates may be produced by several microbial species such as *Azotobacter vinelandii* (Gacesa, 1988) and *Pseudomonas aeruginosa* (Linker and Jones, 1964 and 1966).

Table 1.1 Composition of some seaweed (data taken from Clare, 1993).

Source	Composition parameters					Alginate content (% dry weight)
	F_G	F_M	F_{GG}	F_{MM}	$F_{GM,MG}$	
Laminaria digitata	0.41	0.59	0.25	0.43	0.16	18-26
Laminaria hyperborea (leaf)	0.55	0.45	0.38	0.28	0.17	25-38
Laminaria hyperborea (stipes)	0.68	0.32	0.56	0.20	0.12	
Laminaria hyperborea (outer cortex)	0.75	0.25	0.66	0.16	0.09	
Lessonia nigrescens	0.33	0.62	0.19	0.43	0.19	28-71
Ecklonia maxima	0.45	0.55	0.22	0.32	0.32	30-40
Macrocystis pyrifera	0.39	0.61	0.16	0.38	0.23	20-31
Durvillea antarctica	0.29	0.71	0.15	0.57	0.14	-
Ascophyllum nodosum	0.10	0.90	0.04	0.84	0.06	
Ascophyllum nodosum	0.36	0.64	0.16	0.44	0.20	19-30

1.1.2. Extraction and manufacture of alginates

The first chemical extraction of alginate was patented by Stanford in 1881 and has since been improved, for example by Green in 1936 and Le Gloahec in 1938. The current extraction and purification process is outlined in figure 1.1.

1.1.3. Chemical structure of alginates

Alginates are linear binary copolymers of β-D-mannuronic (M) and α-L-guluronic acids (G) (figures 1.2a and 1.2b), which are linked by either α1-4- or β1-4-glycosidic bonds (figures 1.2c, 1.2d and 1.2e) (Grasdalen *et al*, 1977). Polymannuronate and polyguluronate blocks adopt extended ribbon and buckled ribbon conformations, respectively (figures 1.2c and 1.2d) (Gascesa, 1988).

In early work, Haug *et al*, 1965 and 1966, showed that alginates were composed of three main fractions: polyguluronate blocks (GG), polymannuronate blocks (MM) and heteropolymeric guluronate-mannuronate (MG or GM) blocks. Further work using specific degrading enzymes and nuclear magnetic spectroscopy revealed that sequences of MMG and GGM were also present in the heteropolymeric sequences. Mathematical analysis of this data showed that the monomer sequence could be described by a second order Markov model (Smidsrod and Draget, 1996). ^{1}H-NMR and ^{13}C-NMR are used to determine the two monad frequencies (F_M and F_G), the four nearest neighbouring diad frequencies (F_{GG}, F_{MM}, F_{MG} and F_{GM}) and the eight nearest triad frequencies (Smidsrod and Draget, 1996).

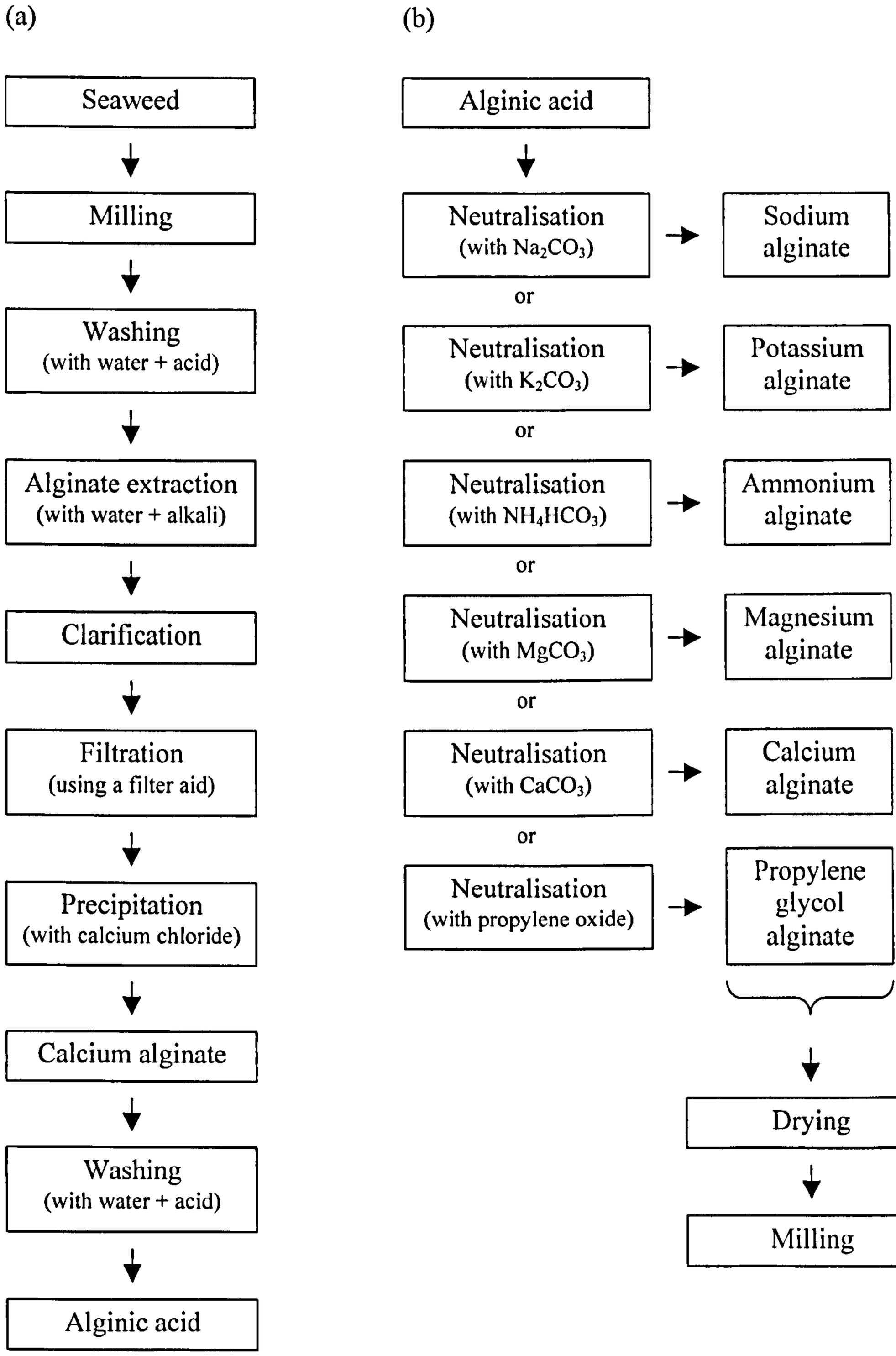

Figure 1.1 The process used by Pronova Biopolymer for (a) the production of alginic acid and (b) the manufacture of alginate salts.

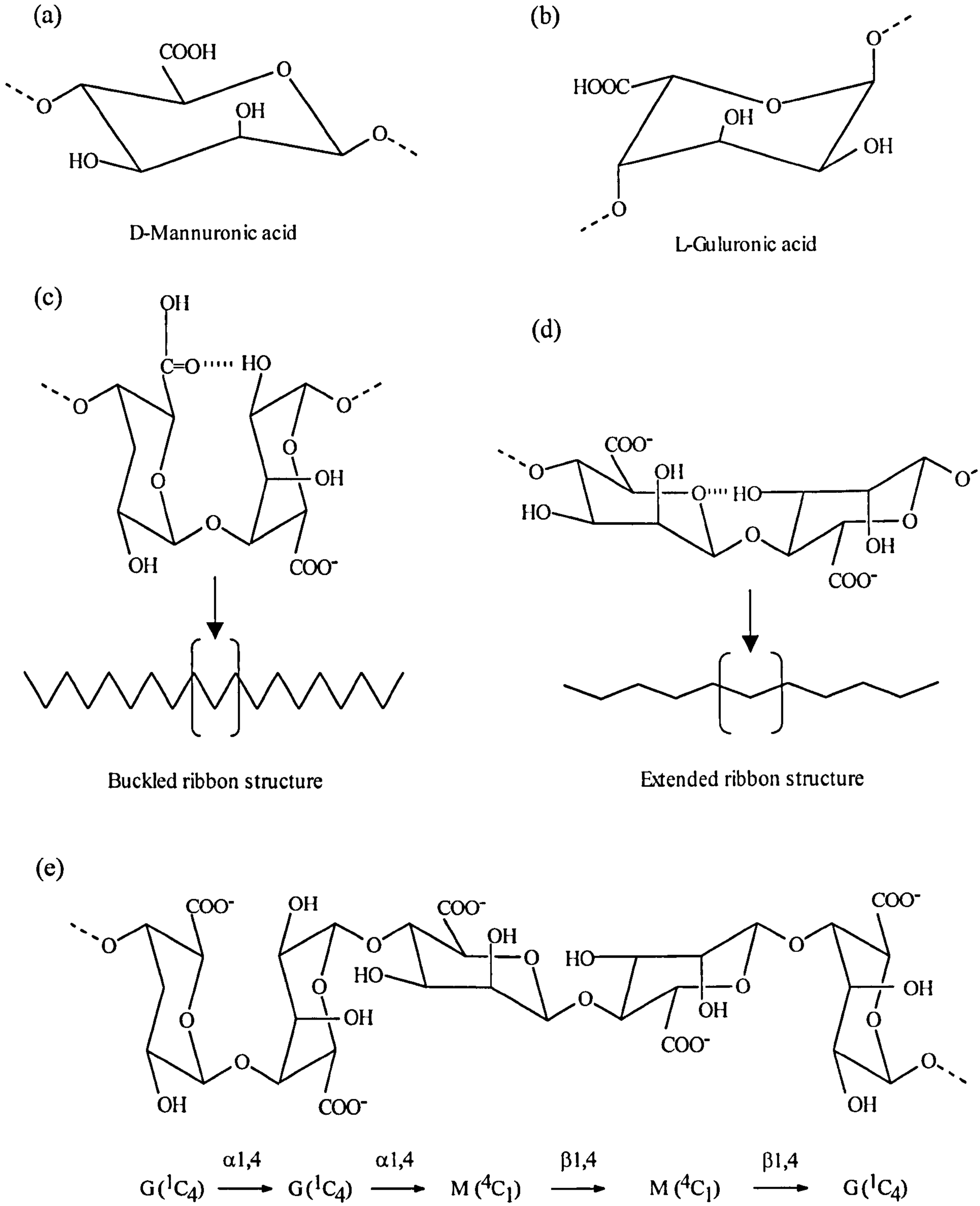

Figure 1.2 Structural components of alginate

(a) Mannuronic acid monomer (b) guluronic acid monomer (c) polyguluronate conformation (d) polymannuronate conformation (e) heterogeneous block conformation.

These frequencies can then be used to calculate the average block lengths, including single monomer blocks

$$\overline{N_G} = \frac{F_G}{F_{MG}} \tag{1.1}$$

$$\overline{N_M} = \frac{F_M}{F_{MG}} \tag{1.2}$$

or excluding single monomer blocks.

$$\overline{\overline{N_{G>1}}} = \frac{(F_G - F_{MGM})}{F_{GGM}} \tag{1.3}$$

$$\overline{\overline{N_{M>1}}} = \frac{(F_M - F_{GMG})}{F_{MMG}} \tag{1.4}$$

where $\bar{N}_x$ is the average block length, including single blocks, $\bar{N}_{x>1}$ is the average block length, excluding single blocks. The subscript 'x' may represent either G for guluronate blocks or M for mannuronate blocks.

The average lengths and frequencies of the blocks give some indication of the structure of alginate.

1.1.4. Functional properties of alginates

The composition and sequence of the monomers may influence some of the properties of alginate. Other factors such as molecular weight and polydispersity may also influence alginate properties. For example, low molecular weight polymers, containing short guluronate block fragments, tend not to participate in gel formation. Subsequently, the resulting gel strength is lower than predicted from the G content of the alginate (Smidsrod and Draget, 1996).

1.1.4.1. Gel forming properties of alginate

The addition of polyvalent cations to sodium alginate causes the Na^+ ions in the alginate to be displaced in favour of the cations, resulting in the formation of an alginate gel. Polyguluronate blocks bind cations more greatly and more strongly than either heteropolymeric or polymannuronate blocks, which have similar cation binding affinities (Smidsrod, 1974).

The selective binding of some polyvalent cations and the structural conformation of polyguluronate implies that alginate chelates cations in a highly specific auto-co-operative reaction. For example, a single Ca^{2+} ion may co-ordinate with the oxygen molecules in the hydrophilic cavity between two neighbouring guluronic acid residues (figure 1.3a) (Clare, 1993). The chelated Ca^{2+} ion is then able to co-ordinate with a second di-guluronate block from a neighbouring alginate chain. The Ca^{2+} ion effectively acts as a cross-linker between two alginate chains. The molecular size of the hydrophilic cavity influences the binding affinity of cations, such that $Ba^{2+} > Sr^{2+} > Ca^{2+} >> Mg^{2+}$ (Smidsrod, 1974). The structural conformation of a calcium alginate gel has been considered analogous to an egg-box, with Ca^{2+} ions as the eggs and polyguluronate as the packaging (figure 1.3b) (Grant *et al*, 1973).

As Ca^{2+} ions are added to a solution of sodium alginate, the alginate chains start to align and viscosity increases. As more Ca^{2+} is added, the solution becomes thixotropic and then finally gel-like. The influence of Ca^{2+} ion concentration on gel rheology is shown in figure 1.4a (Clare, 1993). The strength of the calcium alginate gel is influenced by the length of the polyguluronate blocks and is proportional to the square of alginate concentration (Smidsrod and Grasdalen, 1984). Alginates rich in guluronate tend to produce strong and brittle gels. The high degree of cross-linking produces a polymer structure that is relatively rigid and inflexible. In comparison, alginates rich in mannuronate tend to produce weak and elastic gels since the low degree of cross-linking produces a flexible polymer structure (Mitchell and Blanshard, 1976, and Smidsrod and Draget, 1996). Molecular size and binding affinity of polyvalent cations also influence gel strength, such that $Ba^{2+} > Sr^{2+} > Ca^{2+} >> Mg^{2+}$ (Smidsrod, 1974).

(a)

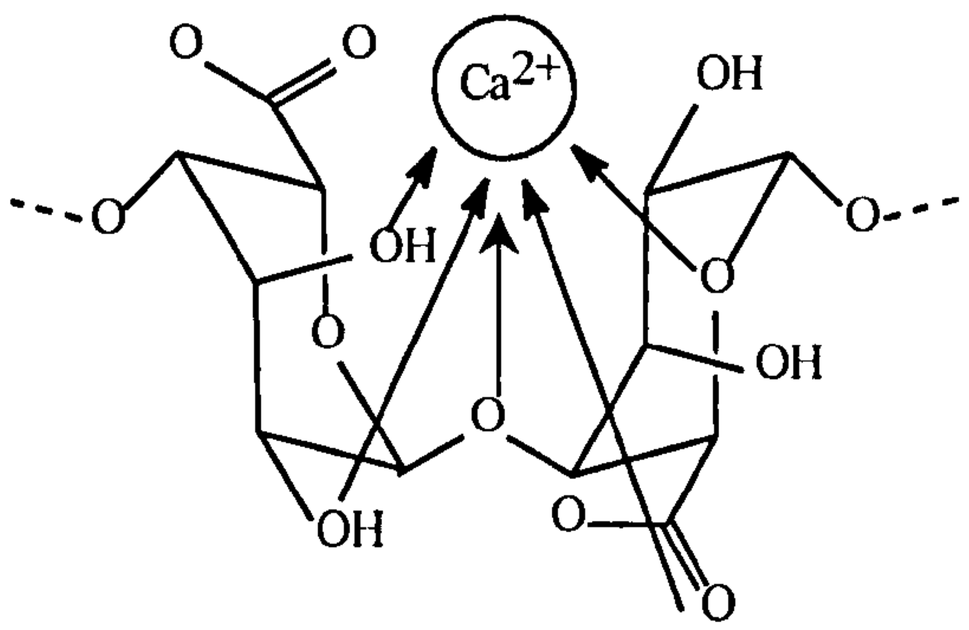

(b)

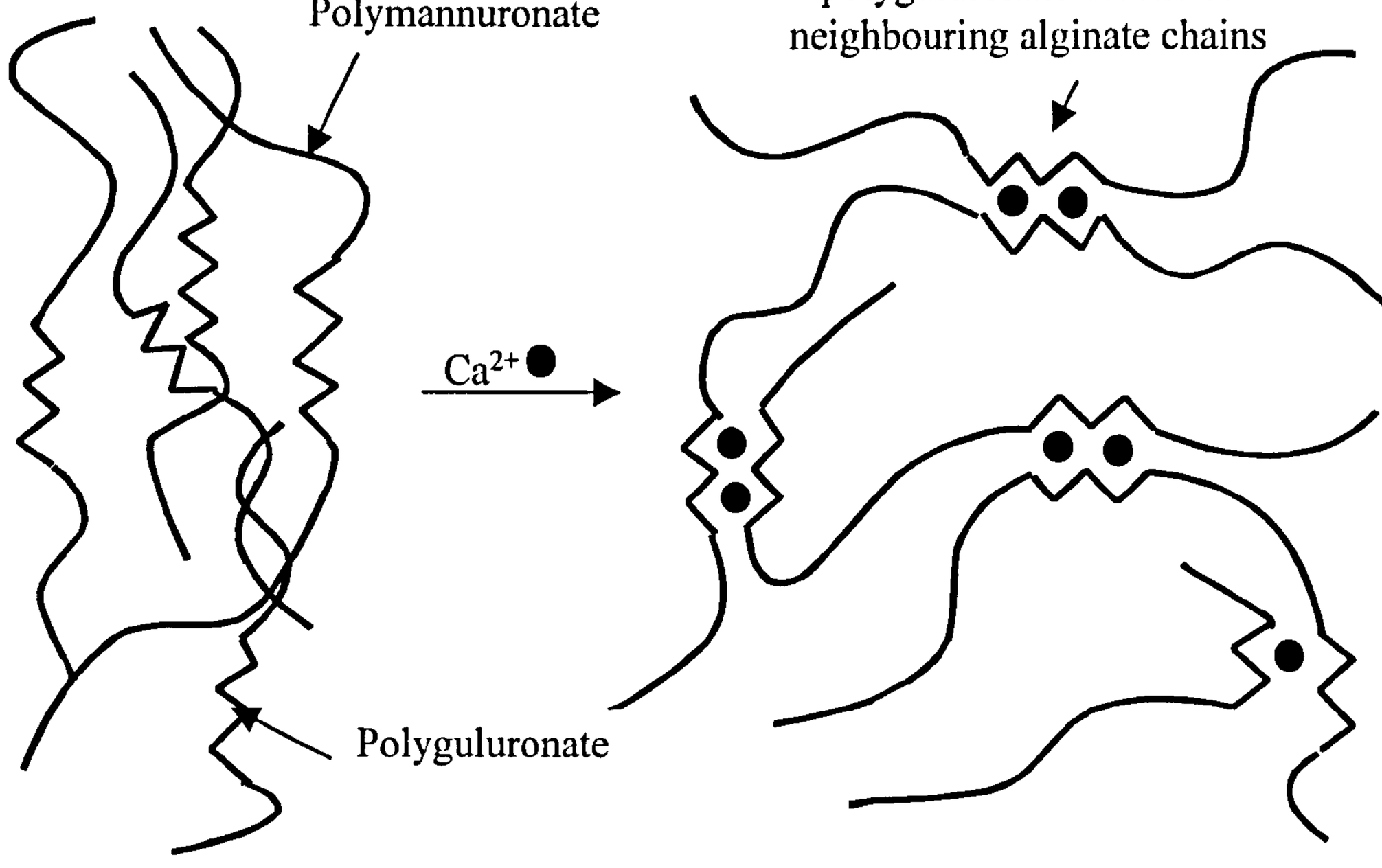

Figure 1.3 (a) The binding sites of calcium in the hydrophilic cavity between two guluronate monomers and (b) the 'egg-box' model of alginate gel.

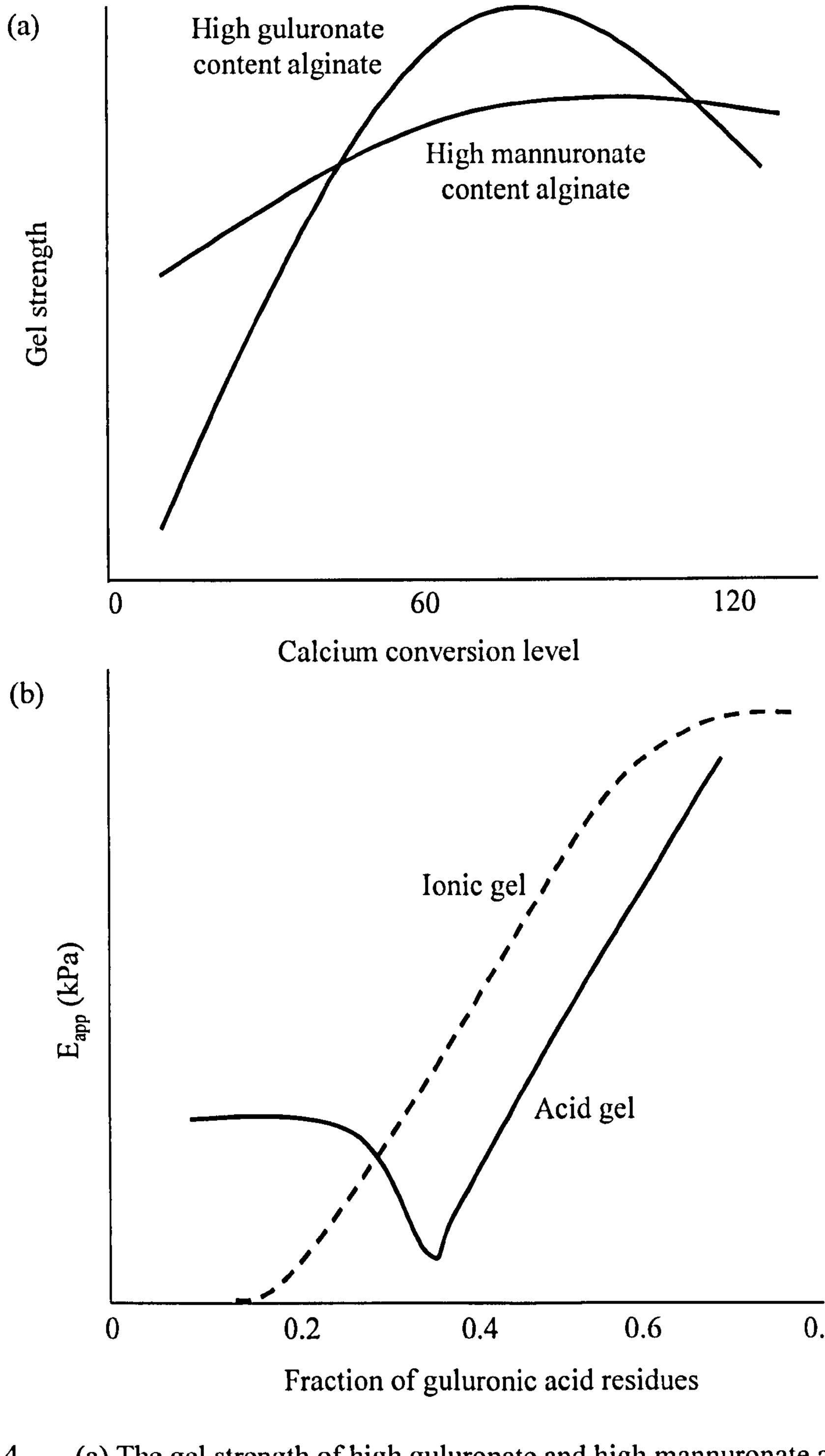

Figure 1.4 (a) The gel strength of high guluronate and high mannuronate alginates at different calcium conversion levels, which is the ratio of Ca^{2+} ions to sodium alginate monomers (Clare, 1993). (b) The apparent Youngs modulus (E_{app}) of alginic acid gels and ionic alginate gels as a function of the guluronic acid content (Draget *et al*, 1994).

1.1.4.2. Formation and properties of heterogeneous and homogeneous gels

The solubility of a calcium salt determines the amount of Ca^{2+} ions available to react with the alginate and thus can influence the physical nature of an alginate gel. Calcium salts are either totally water-soluble (e.g. calcium chloride), sparingly water-soluble (e.g. calcium sulphate dihydrate) or insoluble at neutral pH but fully soluble in acid conditions (e.g. anhydrous dicalcium phosphate).

In the case of highly soluble salts, such as calcium chloride, Ca^{2+} ions are readily available to react with sodium alginate, resulting in instant gel formation and the formation of an inwardly moving gelling zone. This type of gel formation is described as 'diffusion or dialysis setting'. Gels formed in this way are characteristically strong but heterogeneous (Smidsrod and Draget, 1996, and Gorden *et al*, 1991). In the case of poorly soluble salts such as dicalcium phosphate anhydrous, a small amount of Ca^{2+} ions is available to react with the sodium alginate. Consequently, the calcium salt may be mixed with a sodium alginate solution to produce a non-gelling homogenous suspension. The alginate gel forms when the solution is exposed to a trigger, such as a change in temperature, excess water or acid, which causes the calcium salt to dissolve. This type of gel formation is described as 'internally setting' and produces typically homogeneous gels (Gorden *et al*, 1991, and Smidsrod, and Draget, 1996).

1.1.4.3. The effect of low molecular weight G block polysaccharide on gel properties

Draget *et al*, 1998a and 1998b, showed that the addition of low molecular weight polyguluronate fragments or polygalacturonate fragments from pectin can modulate the formation and rheology of an alginate gel, thus influencing its viscosity, stability and elasticity. At concentrations of Ca^{2+} less than 20 mM, the alginate gel strength is inversely proportional to the concentration of low molecular weight G block fragments. This may be due to the polyguluronate fragments being able to bind calcium ions without actually contributing to the gel network. At Ca^{2+} concentrations greater than 20 mM, the alginate gel strength becomes proportional to the concentration of the G block fragments. Draget *et al* suggested that the G block fragments may be acting as cross-linkers between neighbouring alginate chains (Draget *et al*, 1998). This may have

important implications for the polymer structure of alginate gels, suggesting that the 'egg-box' model is over simplistic view of the gel structure.

1.1.4.4. Formation and properties of acid alginate gels

Alginates are also able to form stable soft acid gels because polymannuronate and polyguluronate blocks are able to form cross-links between like blocks in neighbouring alginate chains, which are stabilised by intermolecular hydrogen bonding. This occurs when the carboxyl groups of sodium alginate are protonated and uncharged, i.e. pH < pK_a values of both mannuronic acid (pK_a=3.38) and guluronic acid (pK_a=3.65) and (figure 1.4b) (Draget *et al*, 1994). Heteropolymeric blocks may interfere with this cross-linking, except in alginates where strictly alternating MG/GM blocks can act as repeating sequences, capable of forming intermolecular cross-links (Draget *et al*, 1994 and 1996). Factors that influence the properties of an ionic gel, such as alginate concentration and molecular weight, may also influence the properties of an acid gel. An exception is that the polymannuronate blocks may form stable intermolecular cross-links at pH values below the pK_a, but not in the presence of divalent ions.

1.1.4.5. Factors influencing the properties of sodium alginate solutions

Several factors influence the solubility of alginates, for example molecular weight, and polydispersity. The thermodynamic equilibrium of free counter-ion mixing also influences both the dissolution rate and solubility of alginate. This suggests that alginate solubility decreases with the binding of polyvalent ions (e.g. Ca^{2+}) or with increasing salt concentration, which reduces the entropy of counter-ion mixing with water. At pH values below the pK_a, intermolecular interactions of homopolymeric and heteropolymeric blocks also reduce alginate solubility, such that MG-blocks>MM-blocks>GG-blocks (Smidsrod and Draget, 1996).

Physical variables such as temperature, alginate molecular weight, concentration, pH and ionic strength also influence solution rheology. Molecular weight influences solution viscosity, with high molecular weight alginates producing highly viscous solutions at low concentrations. The stiffness of the alginate polymer chains can also influence solution viscosity, such that MG<MM<GG with respect to chain stiffness and

solution viscosity. This is because rotation about the diaxial glycosidic linkages in polyguluronate blocks is sterically hindered (Pronova).

Temperature and alginate concentration also influences solution viscosity. As a general rule, increasing the temperature of a 1% w/v sodium alginate solution by 1°C decreases the solution viscosity by 2.5% due to the increased thermal motion of the alginate chains (Pronova). If alginate concentration increases, the number of intermolecular entanglements may increase, resulting in an increase in solution viscosity. At low concentrations (<1% w/v), alginate solutions are almost Newtonian but at higher concentrations(>2% w/v), they become psuedoplastic (Clare, 1993).

Varying the pH of an alginate solution between 5 and 11 does not greatly influence solution viscosity. The vast majority of ionisable groups on the alginate chains remain ionised, resulting in the alginate attaining a net negative charge that stabilises the viscosity of the solution. At pH values less than 5, the carboxyl groups start to become protonated, resulting in an increase in viscosity and the eventual formation of an acid gel (Clare, 1993). The levels of residual calcium in commercial alginates can vary between trace amounts and 50%. This may obviously influence the rheology of an alginate solution, although this is dependent on pH. For example, calcium levels greater than 1% w/v can produce solutions of high viscosity with shear-thinning properties at pH≈5, whereas equivalent solutions are attained with calcium levels less than 0.5% w/v at pH<4 (Clare, 1993).

The density and number of charged groups also influence solution viscosity since the repulsion of like charges extends the chain length and increases the intrinsic viscosity. If monovalent salts are added, the counter-ions may neutralise charged groups on the alginate, reducing charge repulsion, chain extension and, ultimately, intrinsic viscosity (Smidsrod and Draget, 1996, and Kelco). The relation between viscosity and ionic-strength is dependent on the alginate, the degree of polymerisation, concentration and type of salt (Kelco).

1.1.5. Pharmaceutical applications of alginates

The unique physicochemical properties of alginate ensure its use in a wide range of industries, for example food, medical, manufacturing and pharmaceutical industries. This section will only describe the pharmaceutical and medical applications of alginate (table 1.2). Other industrial applications are listed in the promotional literature of both Pronova and Kelco companies (Pronova and Kelco).

Table 1.2 Pharmaceutical and medical applications of alginate salts

Application	Property	Examples
Tablets	1. Disintegrates tablet by polymer swelling. 2. Promotes drug dissolution.	
Sustained release tablets	1. Calcium alginate and acid-gel network retards matrix hydration and drug release.	
Raft-forming antacids	1. A floating calcium alginate and acid gel raft acts as a physical barrier preventing reflux acid damage to the oesophagus.	Gaviscon Algicon Gastrocote Topal
Wound management	1. Increases wound temperature and granulation. 2. Highly adsorbent and promotes haemostatis.	Kaltostat, Tegagen, etc
Dental impression powders	1. Internally set calcium alginate gels take accurate dental impressions.	

1.2. Gastrointestinal mucus

Gastrointestinal mucus is a high molecular weight glycoprotein, which is secreted by goblet cells in the gastrointestinal epithelium to form a continuous adherent semi-solid gel layer covering the gastrointestinal mucosa. The mucus layer provides a protective diffusion barrier to lumen contents, which may include acid, alkali, proteases, toxins

and macromolecules. It is also able to bind bacteria, viruses, parasites and heavy metals. Mucus may also retard the diffusion of nutrients, ions and more importantly, from a pharmaceutical viewpoint, drugs. Other functional properties of mucus include lubricating epithelial surfaces and interacting with the immune system (Forstner and Forstner, 1994). Gastrointestinal mucus exists in three main physical phases: presecreted mucus stored in Goblet cells; a layer of mucus gel firmly adhered to the epithelial surface; a mobile, mostly soluble mucus mixed with lumen contents (Allen *et al*, 1993).

1.2.1. Composition of mucus

Native mucus usually contains approximately 1% of salts and other dialysable components, 0.5-1% of proteins, 0.5-1% of a carbohydrate-rich glycoprotein and approximately 95% water. The remainder consists of non-dialysable components such as nucleic acids and lipids (Harding, 1989, Allen, 1981, and Carlstedt *et al*, 1985). The glycoprotein fraction is recognised as the component responsible for the viscoelastic properties and viscous nature of mucus (Bell *et al*, 1984 and 1985, Sellars *et al*, 1988). Nucleic acids and proteins, such as secretory IgA, lyzozyme and lactoferrin (Clamp and Creeth, 1984), are present in the mucus as a result of cell breakdown and passive transduction through the cell membrane, respectively. Various lipids such as cholesterol, free fatty acids, glycolipids and phospholipids are also present and may be covalently bound to the mucin molecules (Hutton, 1991).

1.2.2. Primary structure of mucus glycoprotein

Mucus glycoproteins may be membrane-bound (e.g. MUC1) or secreted (e.g. MUC2). Membrane-bound mucins form part of the cell-surface glycocalyx, which protects the mucosa from pathogens and may also prevent cell adhesion, although over-expression may result in the dissemination of malignant tumour cells and the blockage of certain membrane receptors (Gum, 1995). In comparison, secretory mucins are found in the lumen and have a considerably different structure to membrane-bound mucins.

The mucin molecule contains a protein core (apomucin), which is composed of repeating amino acid sequences (tandem repeats), and the structure of which depends on

the type of mucin. The tandem repeat forms the molecular signature of the mucin molecule (Forstner and Forstner, 1994), for example MUC1 to MUC7 (table 1.3). In all cases, repeat sequences start with a unique non-repetitive N-terminus and finish with a unique C-terminus amino acid sequences.

Table 1.3 The sequence of the tandem repeat peptides encoded by mucin genes MUC1-MUC7

Mucin type	Peptide sequence of tandem repeat	Tissue with high-level of expression
MUC1	PDTRPAPGSTAPPAHGVTSA[a] GSTAPPAHGVTSAPDTRPAP[b]	Breast, pancreas
MUC2	PTTTPITTTTTVTPTPTPTGTQT[a b]	Colon, small intestine, gall bladder[a]
MUC3	HSTPSFTSSITTTETTS[a b]	Colon, small intestine, gall bladder[a]
MUC4	TSSASTGHATPLPVTD[a b]	Tracheobronchial [a]
MUC5	TTSTTSAP[a b]	Tracheobronchial, stomach[a]
MUC6	SPFSSTGPMTATSFQTTTTTPTPSHPQTT LPTHVPPFSTSLVTPSTGTVITPTHAQM ATSASIHSTPTGTIPPPTTLKATGSTHTA PPMTPTTSGYSQAHSSTSTAAKTSTSLH SHTSSTHHPEVTPTSTTTITPNPTSTGTS TPVAHTTSATSSRLPTPFTTHSPPTGS[a]	Stomach, gall bladder[a]
MUC7	TTAAPPTPSATTPAPPSSSAPG[a]	Salivary glands[a]
MUC8	-	Respiratory tract[c]

[a] (Gum, 1995)

[b] (Forstner and Forstner, 1994)

[c] (Harding *et al*, 1999)

1.2.2.1. Protein backbone of mucus glycoprotein

The large central protein core (apomucin) contains a large number of serine, threonine and proline residues (table 1.4). These amino acid residues can form O-glycosidic linkages with carbohydrate moieties and these moieties protect the protein backbone from proteolysis (Allen and Pearson, 1993, and Forstner and Forstner, 1994). The cysteine rich amino acid sequences that flank either side of the apoprotein are non-glycosylated and may form intermolecular disulphide linkages between other mucin monomers. However, these 'naked' non-glycosylated regions are protease sensitive. Recombinant gene work on the MUC2 mucin monomer, found in the colonic and small intestinal mucus (Gum, 1995), has shown that there is a non-glycosylated cysteine-rich region in the middle of the glycosylated protein core, separating two tandem repeat units (Forstner and Forstner, 1994). This suggests that MUC2 mucin is capable of forming branched polymers as well as the usual linear polymers.

Table 1.4 Amino acid composition of pig gastrointestinal mucus glycoproteins (Allen, 1981)

Amino acid composition	**Source**		
(mol/100 mol protein)	**Gastric**	**Small intestinal**	**Colonic**
Thr	18.1	26.5	24.1
Ser	15.8	10.4	12.2
Pro	15.3	15.4	14.8
Glu	7.7	4.2	5.3
Asp	4.8	4.6	4.8
Ala	4.7	3.8	5.2
Gly	5.8	5.6	5.5
Arg	3.2	2.2	3.5
Lys	3.9	2.2	2.6
Cys	3.1	4.3	-

1.2.2.2. Oligosaccharide side chains of mucus glycoprotein

The length of the oligosaccharide chain depends on the type of mucin. For example, colonic mucins can have up to 12 sugars per chain (Forstner and Forstner, 1994), gastric mucins up to 19 sugars per chain and small intestinal mucins up to 5 sugars per chain (table 1.5).

The oligosaccharide chain can be divided into three regions. The first is composed of an N-acetylgalactosamine residue that forms an alkali labile O-glycosidic linkage with either serine or threonine in the protein backbone. The oligosaccharide chain then extends by alternating β-linked galactose and N-acetylglucosamine residues. The oligosaccharide chain branches mainly through β(1-3) or β(1-6) linkages between N-acetylglucosamine and galactose (figures 1.5a-d) (Forstner and Forstner, 1994). The peripheral region of the chain consists of fucose, sialic acid, N-acetylgalactosamine, galactose or N-acetylglucosamine (figures 1.5a-d). It is frequently branched and may also express blood group antigens (Allen and Pearson, 1993) (figures 1.5e and 1.5f).

Sulphate residues in the ester linkages between N-acetylglucosamine, galactose and sialic acid residues convey an overriding negative charge to the oligosaccharide chains. The negative charges repel each other, causing the chain to expand and have a large hydrodynamic volume. In addition to O-linked oligosaccharides, some mucin monomers have alkali-stable N-linked oligosaccharides, accounting for the frequently reported presence of mannose in mucus. These types of oligosaccharides are found at the amino acid end sequence and are believed to play a part in mucin polymerisation (Forstner and Forstner, 1994, and Allen and Pearson, 1993).

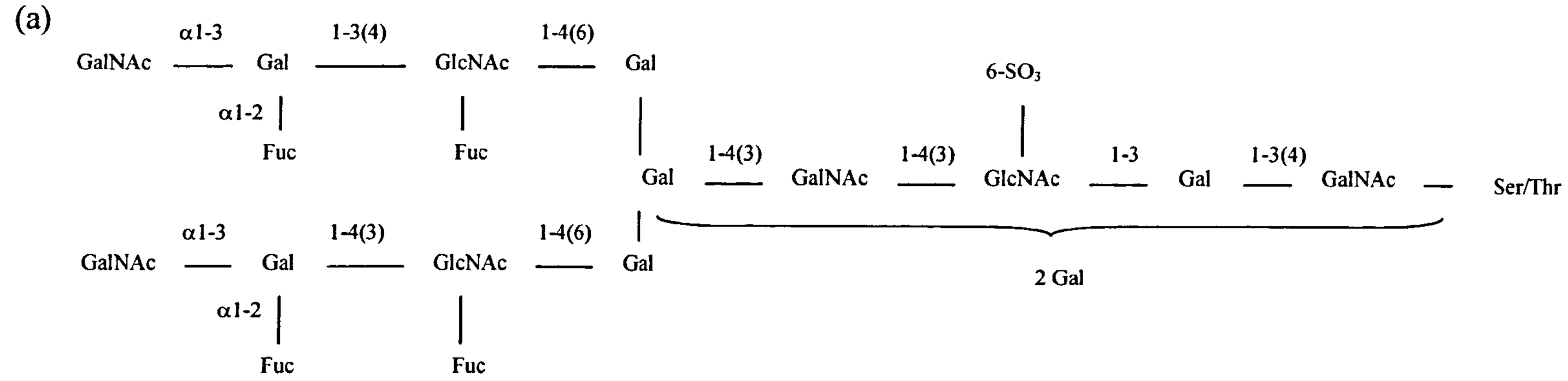

Figure 1.5 Amino acid structure of some carbohydrate side chains of gastrointestinal mucus glycoproteins

(a) Pig gastric mucus (A secretor) (b) human colonic mucus (c) sheep/cow submaxillary mucus (d) pig submaxillary mucus (e) human non-secretor and (f) human H(O) secretor blood group antigen (Allen, 1981). Abbreviations: Gal - galactose; GlcNAc - N-acetylglucosamine; GalNAc – N-acetylgalactosamine; Fuc – fucose; SA – sialic acid

Table 1.5 Composition of pig gastrointestinal mucus glycoproteins (figure 1.6) (Allen *et al*, 1984).

Constituents	**Percentage dry weight composition**		
	Gastric	**Small intestine**	**Colonic**
Carbohydrate	82.9	77.5	83.4
Ester sulphate	3.2	2.8	3.4
Protein	13.3	19.6	13.7
	Molar ratio		
N-acetylgalactosamine	1.0	1.0	1.0
N-acetylglucosamine	2.8	0.6	2.9
Galactose	2.9	0.7	2.5
Fucose	1.9	0.3	1.5
Sialic acid	0.2	0.5	0.2

1.2.2.3. The link protein

Previous studies combining thiol reduction and proteolysis with SDS-PAGE have shown the existence of a small molecular weight link protein, which was thought to cross-link four glycoprotein sub-units to form a mucin polymer. However, recent recombinant gene work has shown that this so-called 'link' protein is actually a constituent of the C-terminus of the apomucin backbone (Forstner and Forstner, 1994, and Bansil *et al*, 1995). The link protein had been produced as a result of a specific step in the purification process, which resulted in bonds between aspartate and proline residues being cleaved and followed by thiol reduction (Forstner and Forstner, 1994).

1.2.3. Secondary glycoprotein structure

The monomer structure of mucus glycoproteins generally consists of a central heavily glycosylated protein backbone, which is flanked on either side by non-glycosylated protein regions and has a molecular weight of approximately $2\text{-}3\text{x}10^6$ Da. Early electron microscopy and proteolysis work showed that the heavily glycosylated protein regions have protease sensitive globular regions at regular periodic intervals along the protein

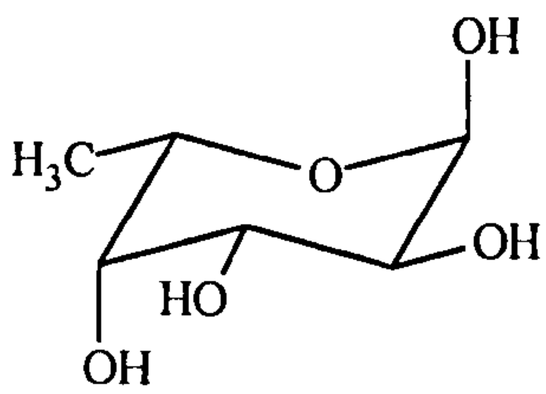

L-fucose (Fuc)

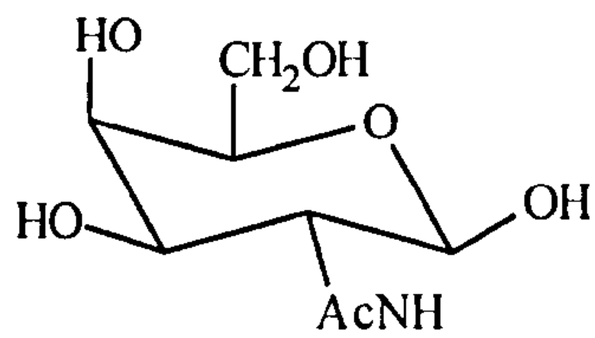

N-acetylgalactosamine (GalNAc)

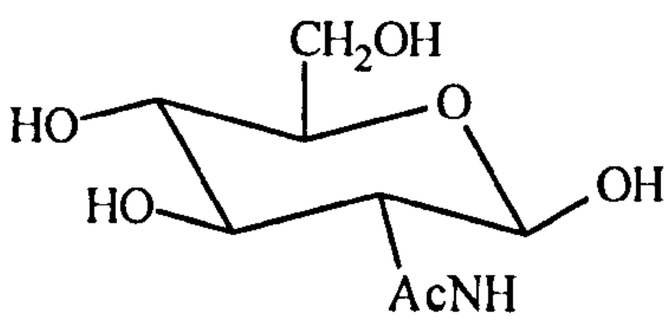

N-acetylglucosamine (GlcNAc)

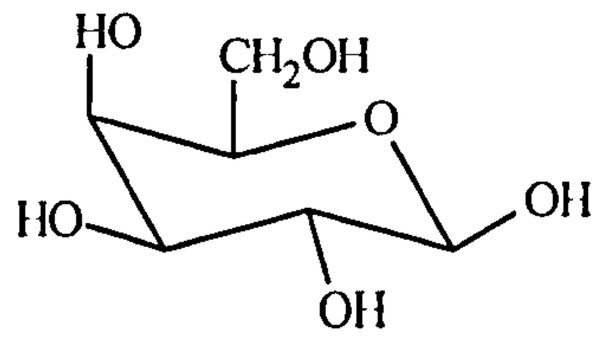

Galactose (Gal)

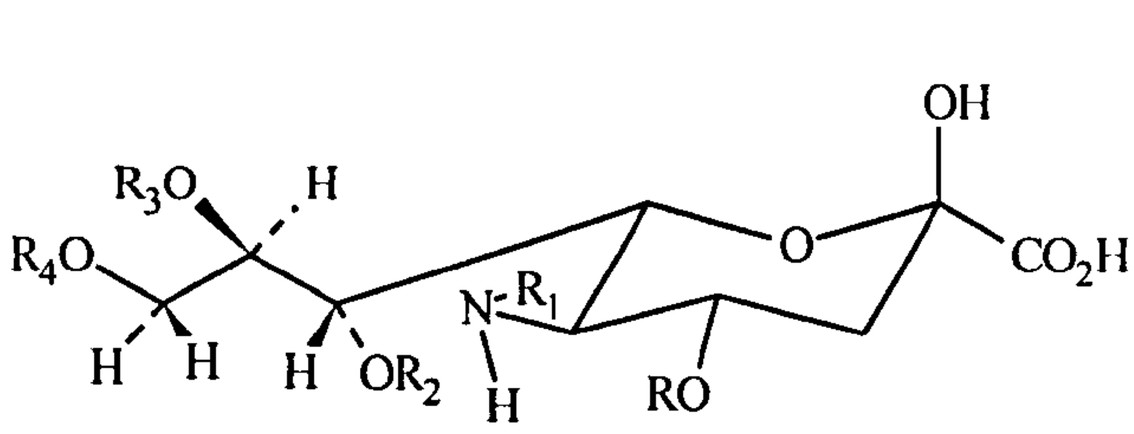

N-acetylneuramic acid (NeuAc)

Figure 1.6 The chemical structures of monosaccharides found in the carbohydrate side chains of mucus glycoprotein (Harding, 1989).

core, allowing the mucin monomer to flex and bend (figure 1.7a) (Harding, 1989). The non-glycosylated end regions of the protein core have a more folded conformation and are rich in cysteine residues that can form intra- and intermolecular disulphide bonds. Protease digestion of the mucin monomer produces the glycosylated 'bottle-brush' regions (sub-units) of approximately 3-7x10^5 Da (Allen and Pearson, 1993, and Harding, 1989) (figure 1.7a).

1.2.4. Tertiary glycoprotein structure

Several models have been proposed to describe the polymeric structure of mucus. Early work indicated that four 3-7x10^5 Da mucin sub-units may be linked by a small molecular weight 'link protein' to form a 'windmill' model of 2-3x10^6 Da (figure 1.8) (Allen, 1981 and 1983). In contrast, recent work has shown that 3-7x10^5 Da mucin sub-units form 2-3x10^6 Da monomer units. These monomer units are then linked by intermolecular disulphide bonds to form linear polymeric structures of up to 4.4x10^7 Da (figure 1.7b) (Allen and Pearson, 1993, Forstner and Forstner, 1994, Carlsedt *et al*, 1985, and Harding, 1989). The molecular weight of mucin is characteristically polydisperse, which may result from the different types of mucin sub-units as well as different degradative processes with different levels of enzymatic activity (Allen and Pearson, 1993). There has been substantial confusion over the structure of mucin, resulting from taking inadequate precautions against protease degradation during mucus purification. This caused the mucin to be proteolytically degraded into monomers and 'bottle-brush' sub-units (Allen and Pearson, 1993).

In solution, the mucin molecule is enormously expanded and becomes a semi-flexible or kinked linear coil that occupies a large roughly spherical hydrated domain (Forstner and Forstner, 1994, and Harding, 1989). Studies measuring the dynamic solution viscosities of proteolytically digested and thiol reduced mucins have elucidated possible intermolecular interactions between the glycosylated regions of the mucin sub-units (Sellars *et al*, 1988, and Bell *et al*, 1984). The proposed model describes the intermolecular interdigitation of the carbohydrate side-chains to form relatively stable and long-lived interactions (figure 1.9). This implies that the mechanical strength of the gel network is dependent on the number of these interactions and the size of the mucin polymer. At low mucin concentrations (<20 mg ml^{-1}), the polymer expands to occupy

(a)

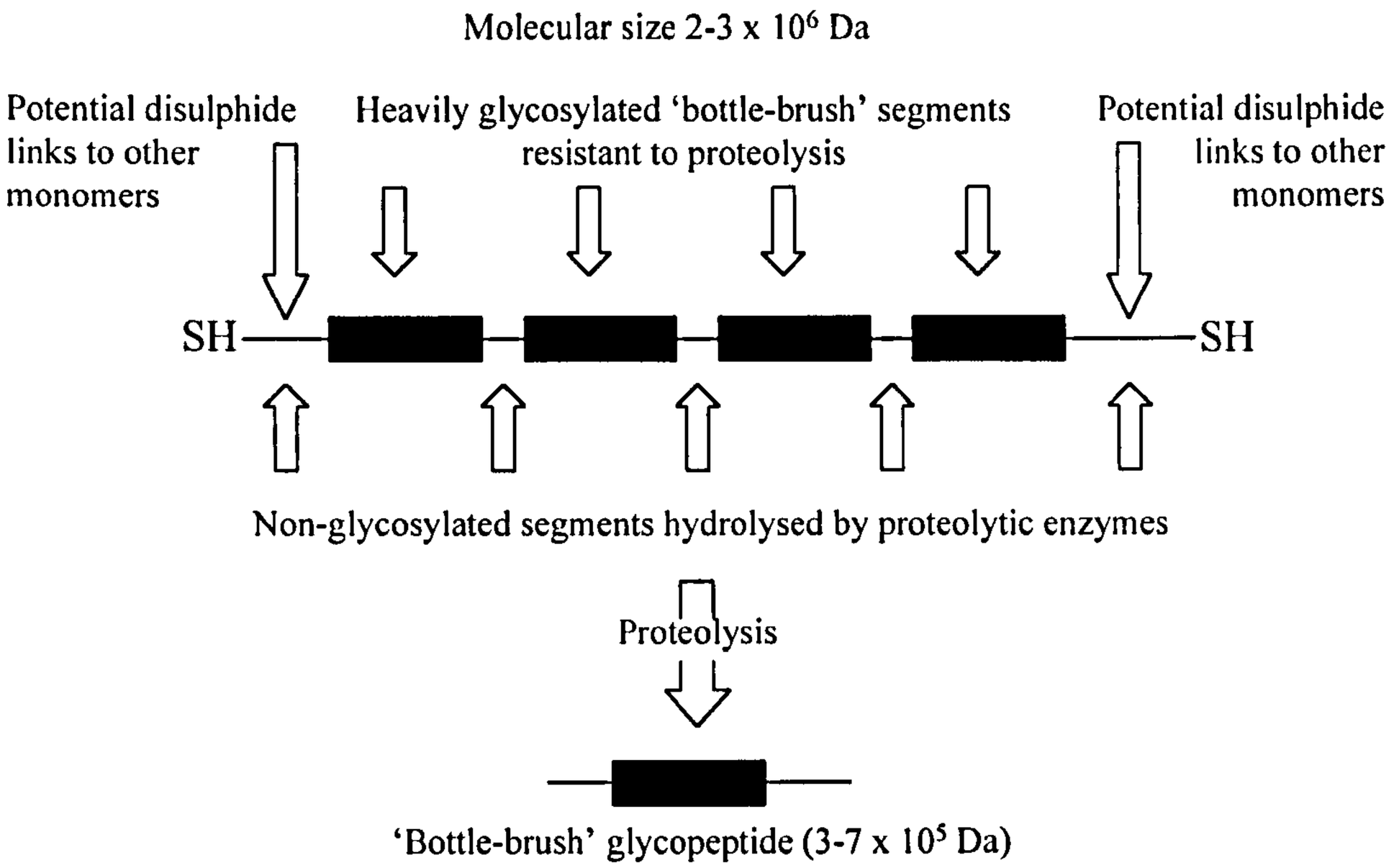

(b)

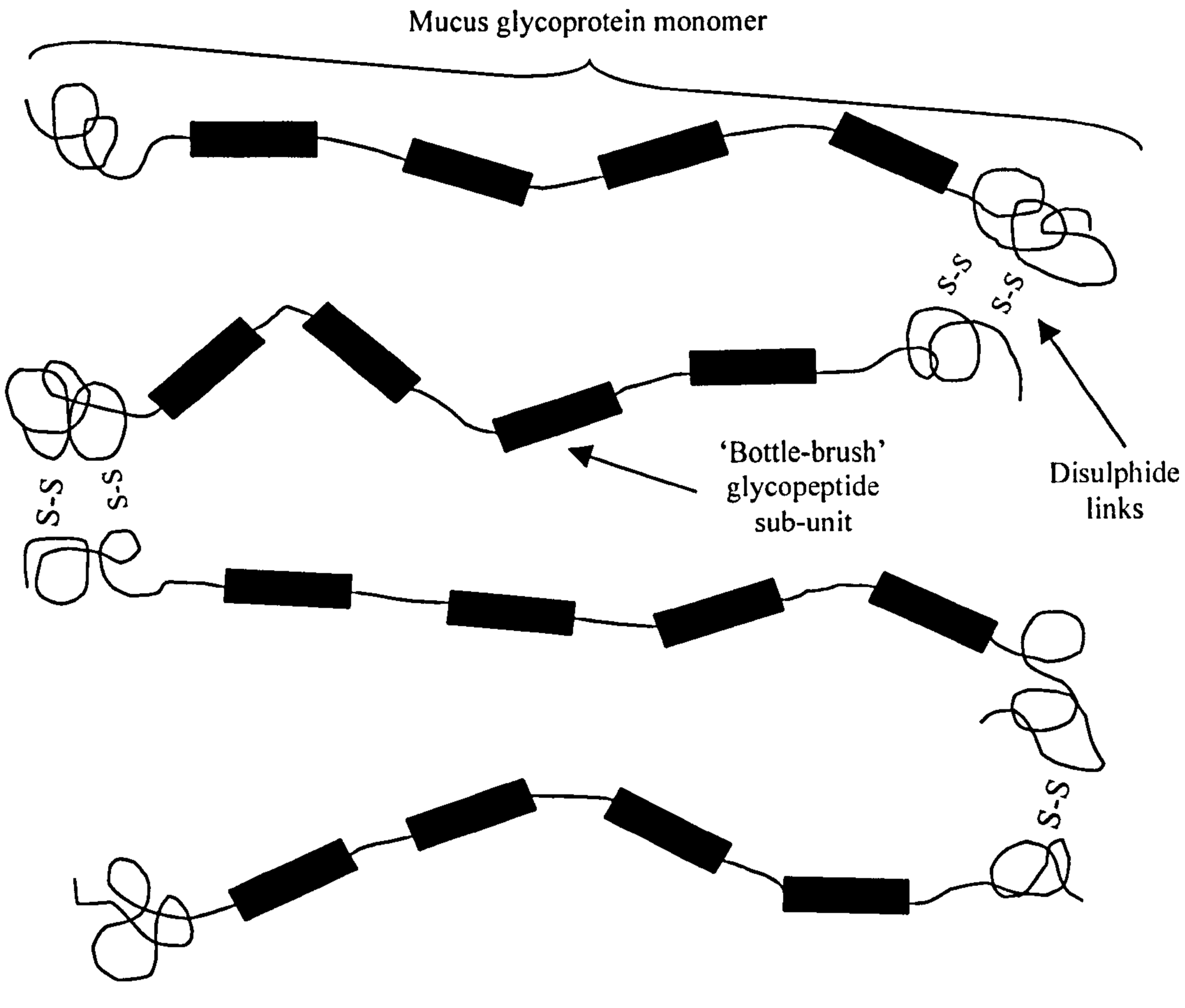

Figure 1.7 (a) The monomer and 'bottle-brush' sub-unit structure of mucin and (b) the linear mucin polymer.

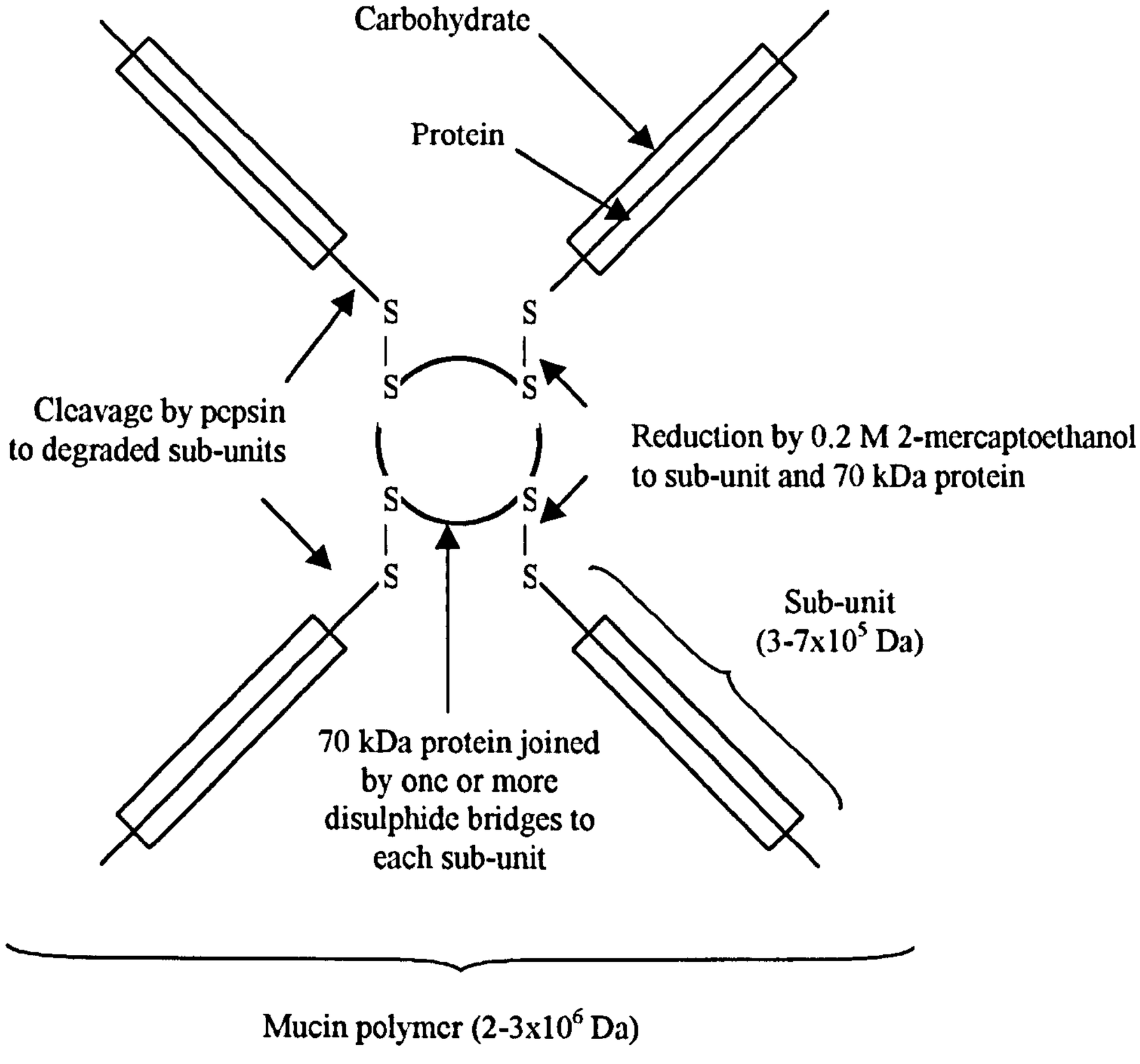

Figure 1.8 The branched 'windmill' model of mucin, proposed by Allen and co-workers (Harding, 1989).

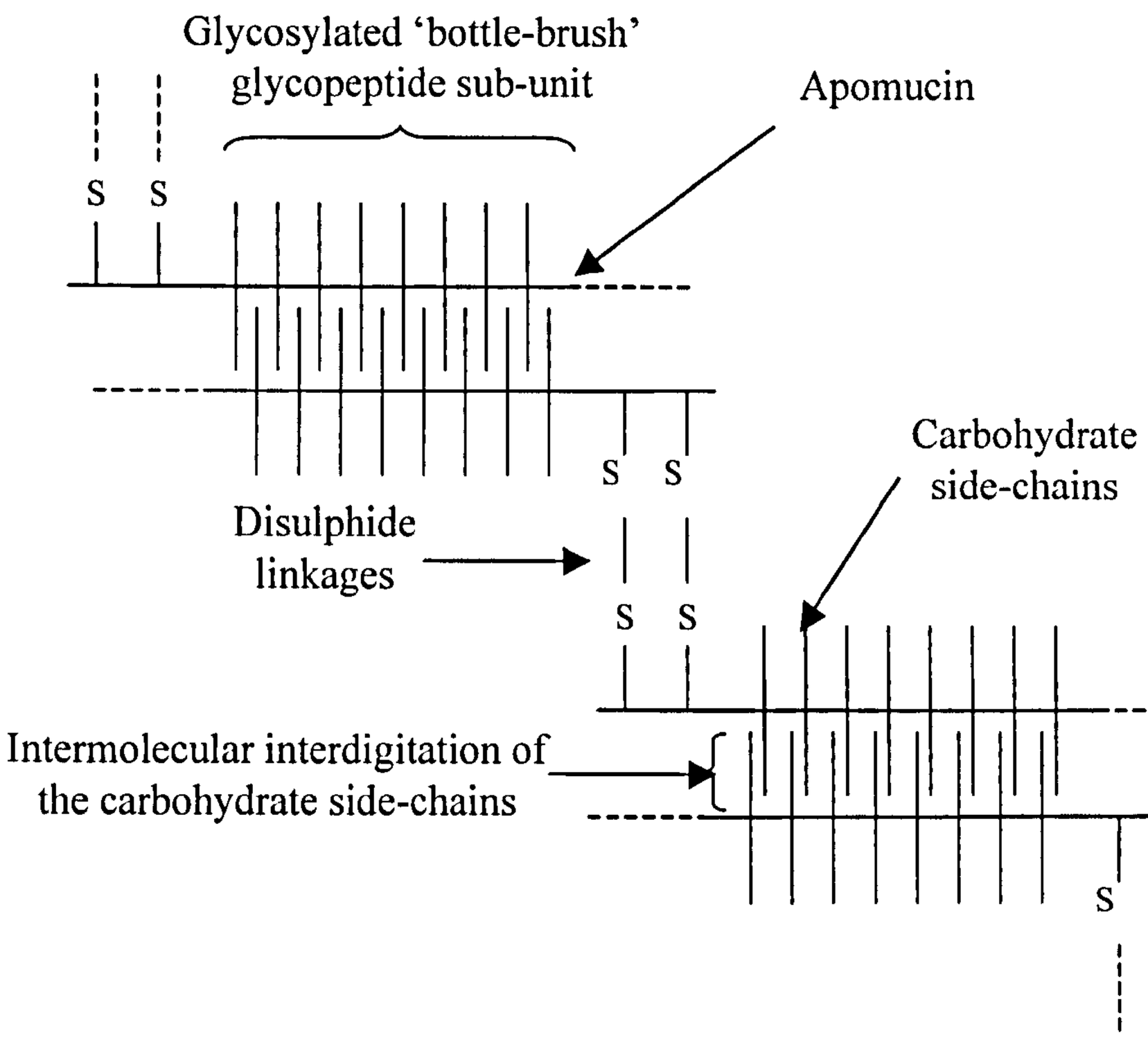

Figure 1.9 Schematic diagram showing the interpenetration of carbohydrate side chains of the glycosylated region of mucin.

The mucus glycoproteins form a cross-linked gel structure as a result of the intermolecular interactions and entanglements of the carbohydrate side-chains of heavily glycosylated 'bottle-brush' glycopeptide sub-units.

the whole solution volume. As mucin concentration increases, mucin polymers begin to interact, resulting in a sharp increase in solution viscosity. In the case of pig gastric mucus, this point occurs at about 20 mg ml^{-1} mucin. Further increases in mucin concentration results in a stronger, thicker and more stable gel due to increased number of interactions (Hutton, 1991). The gel forming ability of mucus glycoproteins appears to mainly depend on two structural features, the structure of the mucin polymer and the non-covalent intermolecular interactions between glycosylated regions (Sellars *et al*, 1988, and Hutton, 1991).

1.2.5. Presecreted, adherent and soluble mucus secretions

1.2.5.1. Presecreted mucus

In presecreted mucus, the negatively charged mucin is charge-shielded by cations, resulting in a collapsed and highly condensed polymeric structure (Forstner and Forstner, 1994). Electron probe analyses have shown a high calcium content in the intra-cellular mucus granules. Also, the *in vitro* volume of mucus is reduced by divalent cations (Allen, 1989). As soon as the mucin molecule is secreted from the goblet cell, the cationic charge shielding is lost, resulting in the mucin hydrating and rapidly swelling to form gel-like mucus (Forstner and Forstner, 1994). Mucus may then exist either as a thin layer of stable water insoluble gel, which is firmly adhered to the epithelium or as a viscous soluble mucus solution that mixes with lumen contents.

1.2.5.2. Adherent mucus

Adherent mucus forms a translucent gel layer that covers the epithelial surfaces of the stomach, intestines and colon of the gastrointestinal tract. Some sections, such as the oesophagus, do not have many goblet cells and have very little mucus, if any, covering the epithelium (Allen and Pearson, 1993). The thickness of the mucus gel layer has been shown to vary along the length of the gastrointestinal tract and may be influenced by the type of animal species and feeding (table 1.6). Mucus thickness may also be influenced by certain disease states, such as Crohn's disease, and by some chemical substances, such as prostaglandins and sodium salicylate (Kerss *et al*, 1982, and Sandzen *et al*, 1988).

Table 1.6 The thickness of gastrointestinal mucus in different species.

Species	**Location of mucus**	**Fasted**	**Mean thickness (± SD) (μm)**	**Range of thickness (μm)**
Rat[a]	Stomach	Yes	73 ±5	5-550
Rat[a]	Stomach	No	48 ±5	-
Rat[b]	Duodenum	-	80	-
Rat[c]	Stomach	Yes	145 ±22	-
Frog[d]	Stomach	Yes	55 ±5	5-550
Frog[d]	Stomach	No	95 ±8	-
Frog[e]	Stomach	Yes	75 ±5	5-550
Mouse[b]	Colon	-	180	-
Human[f]	Stomach	-	192 ±7	5-550

[a] Male Wistar rats (Kerss *et al*, 1982)

[b] (Winne *et al*, 1990)

[c] Male Sprague-Dawley rats (Sandzen *et al*, 1988)

[d] *Rana pipiens* (Kerss *et al*, 1982)

[e] *Rana temporaria* (Kerss *et al*, 1982)

[f] Abnormal tissue (Kerss *et al*, 1982)

1.2.5.3. Purified adherent mucus

Native mucus from the stomach, duodenum, small intestine and colon has a viscoelastic shear-thinning rheology as well as being able to flow and anneal, if mechanically damaged (Sellars *et al*, 1988 and 1991, Bell *et al*, 1984 and 1985, and Allan and Pearson, 1993). Bell *et al*, 1984, and Sellars *et al*, 1988, developed methods to remove the lipid, protein and nucleic acid impurities from native gastric, duodenal and colonic adherent mucus gels and leave a purified mucin fraction. Purified mucins are able to form gels at *in vivo* concentrations of 46-50 mg ml^{-1} (gastric), 35-40 mg ml^{-1} (duodenal) and 19-22 mg ml^{-1} (colonic), which have the same rheology as their respective native mucus gels. However, there are some subtle differences between purified mucin gels

and native adherent mucus, the main one being the resistance of native mucus to solubilisation.

1.2.5.4. Properties of adherent mucus gel

The physical properties of mucus can be described by the storage modulus (G'), the loss modulus (G") and the tan δ value, which is G"/G' (Madsen *et al*, 1996). Elastic gel-like structures tend to have tan δ<1, whereas viscous liquids tend to have tan δ>1. Native and purified gastric, intestinal and colonic mucus gels usually have tan δ values between 0.13 and 0.2, which indicates a gel-like structure. However, at low shear frequencies, the storage modulus suggests that mucus gels behave like a viscous liquid rather than an elastic gel and this property may allow the mucus to flow and anneal.

The mucin polymer remains intact and stable in a range of hostile conditions. Native and purified gastric and duodenal mucus gels are not disrupted by exposure to pH 1 to pH 8, hypertonic salt solutions (2.0M NaCl) or bile salts. Even concentrations of ethanol up to 60% do not affect the mechanical properties of the gel. Native and purified colonic mucus gels are also resistant to hostile conditions such as pH 1, exposure to bile salts and 6M guanidium chloride (Bell *et al*, 1985 and Sellers, *et al*, 1991).

Small intestinal mucus gels behave very differently from other gastrointestinal mucus gels. Native small intestinal mucus is present in copious amounts and is very easily removed from the mucosa to give an opaque and heterogeneous sample, which is heavily contaminated with mucosal cells (Sellars *et al*, 1991). It is also noticeably weaker and of a poorer quality than other gastrointestinal mucus gels. Exposure to pH 1, bile salts and 6M guanidium chloride causes the collapse of the mucin gel structure. However, removal of protein and lipid impurities increases the quality and strength of an *in vivo* equivalent purified mucin gel (28-33 mg ml^{-1}). The purified intestinal mucin gel is not disrupted by exposure to pH 1, bile salts and 6M guanidium chloride, but becomes so if the protein impurities are returned to the mucin gel (Sellars *et al*, 1991).

Certain rigorous treatments can affect the structural integrity of mucus gels. The commonly used practice of freezing fresh mucus samples until required may actually

affect the quality and strength of mucus. However, the mechanical properties of the mucus gel return to normal after two hours (Bell *et al*, 1984). The treatment of mucus with agents that disrupt disulphide linkages or proteases that digest the non-glycosylated protein regions results in the solubilisation of mucus and an irreversible loss of mechanical structures (tan δ>2) (Sellars *et al*, 1988).

1.2.5.5. Soluble mucus

Soluble mucus can be defined as being freely soluble in the lumen or not being physically adhered to the mucosal surface (Allen and Carroll, 1985). Soluble mucus mixes with other gastrointestinal secretions as well as with ingested liquid and solid material. The composition of soluble mucus is the same as adherent mucus except that the concentration and molecular weight of mucin are significantly lower. Soluble non-degraded polymeric mucin can be directly secreted into the lumen as a result of physiological or pharmacological stimulation. Endogenous substances such as secretin, 5-hydroxytryptamine, vasoactive intestinal peptide, prostaglandins, CCKP-Z, gastrin and histamine may induce secretion of soluble mucus. Intermittent exposure to mucosal irritants such as ethanol and NSAID's can also stimulate soluble mucus production although continued exposure can result in the inhibition of all mucus output (Allen and Carroll, 1985). The increased production of soluble mucus does not necessarily result in an increased production of adherent mucus, although this occurs for carbachol and prostaglandins (Allen and Carroll, 1985).

1.2.6. Permeability of the adherent mucus layer

The adherent mucus gel layer may act as a diffusional barrier, protecting gastrointestinal mucosa from damage by irritant substances. From a pharmaceutical viewpoint, this mucus gel layer may also retard the diffusion of drugs across the mucosal barrier (Kearney and Marriott, 1987, Bhat *et al*, 1995, and Larhed *et al*, 1997).

The structure and composition of mucus gels suggest that the mucin gel network immobilises water molecules to form the equivalent of an unstirred water layer, which retards diffusion. Several studies measuring the diffusion of solutes and ions in mucus

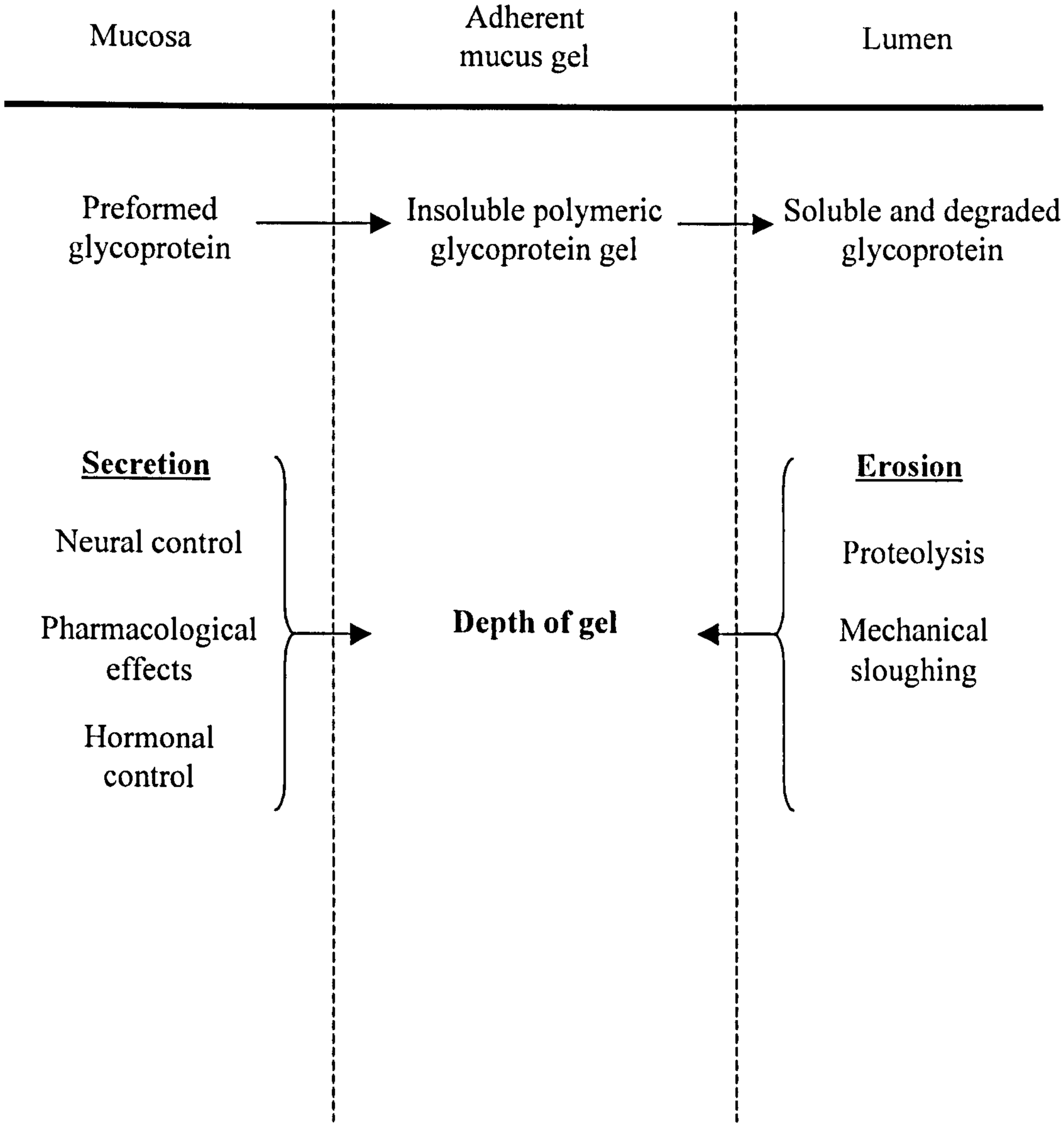

Figure 1.10 Schematic diagram of the dynamic processes controlling the thickness of gastrointestinal mucus.

and unstirred water layers have concluded that a simple unstirred water layer model cannot solely account for the slowing-down of diffusion (Desai *et al*, 1991, Winne and Verheyen, 1990, Smith *et al*, 1986, Smithson *et al*, 1981 and Williams and Turnberg, 1980). Some studies have suggested other mechanisms, such as an ionic exclusion effect (Lee and Nicholls, 1987, Desai *et al*, 1991).

The permeability of mucus to low molecular weight solutes is dependent on the molecular size of the diffusing species (up to a molecular weight of 14400 Da) (Desai and Vagdama, 1991, and Allen and Pearson, 1993). Mucus is not permeable to large molecular weight proteins such as myoglobin (17000 Da) and lumenal pepsins (35000 Da) (Hutton, 1991), suggesting that the mucin network structure has some sort of molecular permeability threshold. This functional property of mucus restricts the proteolytic degradation by pepsins to the lumenal surface. However, pepsin is able to surface digest a 70-80μm thick layer of mucus in just 20 min (Kerss *et al*, 1982) although a continuous secretion of mucus maintains the patency of the mucus layer. Figure 1.10 illustrates the dynamic processes involved in the maintenance of the thickness and patency of the adherent mucus gel layer.

In the case of the gastric and duodenal mucus layers, the mucus may also be degraded by hydrochloric acid, which can easily permeate the entire thickness of a mucus layer. The active secretion of bicarbonate by gastric mucosa neutralises the lumenal influx of hydrogen ions. This results in the formation of a pH gradient across the mucus layer, from pH 7 on the mucosal side to pH 2 on the lumenal side (Allen, 1989, Allen and Pearson, 1993, Allen *et al*, 1993, and Livingston *et al*, 1995). Mucus is also able to inherently buffer hydrogen ions in conditions above pH 2, (Turner *et al*, 1985).

1.3. Bioadhesion and drug delivery

The gastrointestinal tract, particularly the oral route, represents the most convenient and preferred site for systemic delivery of drugs. Oral controlled release dosage forms allow the sustained maintenance of effective systemic concentrations of drugs, resulting in the reduction of dosage frequency and drug-induced side-effects. In the current climate of polypharmacy, the use of controlled drug delivery devices can dramatically simplify a complicated disease management regimen and improve patient compliance.

To date, a wide range of drug delivery technologies have been developed to achieve sustained release of drug from an oral dosage form. Examples include osmotic pump devices and hydrophilic matrices. The rate of drug absorption and the transit of a dosage form along the gastrointestinal tract can vary (Helliwell, 1993). This may alter the performance and effectiveness of a controlled drug delivery device, particularly if the drug exhibits pH-dependent solubility or is only absorbed in a specific region of the gastrointestinal tract.

Drug delivery devices that adhere to the gastrointestinal mucosa may be able to slow or otherwise control the transit time of a dosage form, perhaps maintaining its position in areas of the gastrointestinal tract where drug absorption is favourable (Veillard, 1990). Furthermore, an adhered dosage form has the potential to improve drug absorption across the mucosa by maintaining a constant drug concentration gradient at the site of absorption (Lehr, 1996). Other applications of bioadhesive dosage forms include the inhibition of proteolytic enzymes, increasing the epithelial permeability, the provision of localised drug therapy, the targeting of specific diseased tissues and receptor mediated endo- and transcytosis (Lehr, 1996 and 1998).

1.3.1. Bioadhesion

Bioadhesion has been defined as the state in which two materials, at least one of which is a biological substrate, are held together for extended periods of time by interfacial forces (Longer and Robinson, 1986). Bioadhesion may be classified with respect to the physicochemical nature of both the adhesive and substrate (Park and Park, 1990, and Helliwell, 1993). Type I bioadhesion refers to the adhesion between two biological substrates without the involvement of artificial materials. Examples include cell fusion and cell aggregation. Type II bioadhesion is the adhesion of biological substrates to artificial material. Examples include cell adhesion to culture dishes. Type III bioadhesion is the adhesion of an artificial material to a biological substrate. Examples include adhesion of polymers to skin or soft tissue. The hydration state of the adhesive polymer may affect the process of adhesion and subsequently bioadhesion may also be further classified as either 'wet' or 'dry' (Lehr *et al,* 1992a).

In pharmaceutical science, bioadhesion implies the adhesion of a drug dosage form to a specific biological location. If the biological substrate is mucus, the adhesive process may be referred to as mucoadhesion (Park, 1989, Helliwell, 1993, and Ahuja, 1997).

1.3.2. Chemical and physical interactions involved in bioadhesion

It has been postulated that bioadhesion may involve the formation of primary or secondary chemical bonds as well as macromolecular mechanical interactions.

1.3.2.1. Mechanical interactions

The rheological nature of an adhesive polymer is an important factor that determines its ability to form mechanical interactions. A mechanical interaction may occur if the adhesive can flow into but not back out of macroscopic crevices in a biological substrate (Peppas and Buri, 1985, and Mikos and Peppas, 1990b). A likewise opposite situation may occur if a biological substrate is able to flow into crevices in a dosage form. An example of a biological substrate exhibiting this property is mucus. A purely mechanical interaction would not involve the formation of chemical bonds between the two substrates (Longer and Robinson, 1986) but would be affected by the surface roughness of the substrates. For example, it has been reported that smooth surfaces, that is those with an aspect ratio of less than 1:20, do not mechanically interact (Peppas and Buri, 1985b).

1.3.2.2. Primary chemical bonding

Primary chemical bonds are formed if the functional groups of the biological substrate and the bioadhesive polymer covalently bond to produce a permanent high strength bond. In certain situations such as hard tissue adhesion in dentistry and orthopaedics, a primary bond is essential. In the case of bioadhesive dosage forms, which do not need to be permanently adhered to the soft tissue, a semi-permanent bond lasting a few minutes to several hours is often only required (Longer and Robinson, 1987, Peppas and Buri, 1985, and Mikos and Peppas, 1990).

1.3.2.3. Secondary forces

Secondary forces of attraction occurring in bioadhesion include electrostatic, van der Waals, hydrogen and hydrophobic bonds. Sialic acid and sulphate residues in mucus may confer a net negative charge, which may attract and form electrostatic bonds with oppositely charged adhesives. Mucus and many bioadhesive polymers have a high population of chemical residues, which are capable of hydrogen bonding, for example -OH and –COOH (Peppas and Buri, 1985). Hydrogen bonding may occur when the hydrogen atom of a polarised covalent donor molecule is attracted to an electronegative atom in an acceptor molecule. Apolar regions in both the mucus and polymer may also associate to form hydrophobic bonds

Molecules that have either temporary or permanent dipoles can interact via van der Waals forces, which may be classified as London dispersion, Keesom or Debye forces. London dispersion forces result from the natural oscillations of the electron cloud inducing synchronous oscillations in neighbouring electron clouds and forming temporary dipoles (Morra and Cassinelli, 1997). Polar Keesom forces result from the orientation of permanent dipoles whereas Debye forces occur when a permanent dipole induces a dipole in another molecule (Longer and Robinson, 1986). Polar Keesom and induced Debye forces tend to be relatively stronger than London dispersion forces (Longer and Robinson, 1986, and Peppas and Buri, 1985).

1.4. The theories of bioadhesion

Bioadhesion may be conveniently divided into three main stages. The initial stage involves the formation of an intimate contact between the adhesive polymer and the biological substrate. In the second stage, the adhesive and substrate form a semi-permanent bond. The final stage involves the maintenance of the adhesive bond. The last two decades of research into bioadhesion have produced several theories to explain various aspects of the bioadhesive process.

1.4.1. The wetting theory

Bioadhesion can be analysed in terms of the interfacial tension and surface energy of both the adhesive and the biological substrate. The wetting of the biological substrate and adhesive is crucial in the formation of an intimate contact. However, this theory does not account for phenomena such as capillary suction, which may occur in porous dry adhesives.

The relationship between contact angle and surface tension of a liquid droplet on a solid surface is described by the Young equation (Duchene and Ponchel, 1992 and Larsson, 1980).

$$\gamma_{SV} = \gamma_{SL} + \gamma_{LV} \cos\theta \tag{1.5}$$

γ_{SL} is the solid-liquid surface tension, γ_{SV} is the solid-vapour surface tension, γ_{LV} is the liquid-vapour surface tension and θ is the liquid contact angle.

The liquid contact angle is an indicator of the wetting ability of the liquid, that is, the ability of the liquid to spread across a solid surface. If a liquid does not spread on a solid surface, it will have a large contact angle. In contrast, a freely spreading liquid has a contact angle of zero.

Interfacial tensions between liquid and solid can be used to describe the thermodynamic work of adhesion and is given by the Dupre equation (Duchene and Ponchel, 1992, and Peppas and Buri, 1985).

$$W_{TA} = \gamma_{LV} + \gamma_{SV} - \gamma_{SL} \tag{1.6}$$

W_{TA} is the thermodynamic work of adhesion

However, W_{TA} is difficult to determine using the Dupre equation because some of the interfacial tensions are difficult to measure. Since both γ_{LV} and θ can be easily and directly measured, the Young and Dupre equations may be combined to give equation 1.7.

$$W_{TA} = \gamma_{LV}(1+\cos\theta) \qquad (1.7)$$

W_{TA} is usually much smaller than the work of adhesion determined from detachment force studies and consequently it suggests that other factors other than interfacial phenomena are involved in bioadhesion (Duchene and Ponchel, 1992).

1.4.1.1. Thermodynamic models of interfacial interaction

The thermodynamic description of bioadhesion uses the Young equation as a starting point. To date, three approaches have been developed to describe bioadhesion in terms of thermodynamic equilibria and interactions. These are the Neumann approach, the polar-dispersion approach and the Lewis acid-Lewis base approach.

1.4.1.2. The Neumann approach

The Neumann approach considers the interfacial tensions described by the Young equation as functions of the component surface tensions. The model assumes that negative interfacial tensions are impossible and that interfacial and surface free energies cannot be divided into components that describe intermolecular forces. The model is experimentally simple since it uses a single contact angle to characterise the interfacial interactions of a solid surface (Morra and Cassinelli, 1997). A version of the Neumann approach has been used by Li *et al*, 1998, to evaluate a bioadhesive buccal patch for peptide drug delivery.

1.4.1.3. The polar-dispersion approach

The polar-dispersion approach considers surface tensions to have polar and disperse components, which correspond to Keesom forces and London dispersion forces, respectively. This model assumes that like forces will interact with each other. The captive bubble technique (Andrade *et al*, 1979) measures the contact angles of air and octane bubbles in order to determine both polar and disperse components of surface tensions. The advantage of this technique is that equilibrium contact angles are measured in a constant environment (Lehr *et al*, 1992a).

The relevant surface tensions can be rewritten, using a geometric mean equation, to account for both disperse and polar components (equation 1.8).

$$\gamma = \gamma^{P} + \gamma^{D} - 2\left\{\left(\gamma_1^{D}\gamma_2^{D}\right)^{1/2} + \left(\gamma_1^{P}\gamma_2^{P}\right)^{1/2}\right. \tag{1.8}$$

The geometric mean model is relatively simple and may be inappropriate for some complex systems involving organic liquids, polymers and water. However, Shojaei and Li, 1997, showed that the bioadhesive potential of acrylic acid and polyethylene glycol monomethylether monomethacrylate copolymers predicted using this model were in good agreement with experimentally determined values.

The harmonic mean model is an alternative to the geometric mean model (Sahlin and Peppas, 1997). Esposito *et al*, 1994, used the harmonic mean model to relate the surface thermodynamics of a range of polymers, including polyacrylic acid and sodium alginate, to their bioadhesive bond strength.

Models of bioadhesion derived from the captive bubble technique assume that both surfaces are regular, and as a result, ignore the possibility that the polymers may interpenetrate. This approach also assumes that the polar component is symmetrical and interacts through forces arising from permanent dipoles, which contradicts current opinion regarding the nature of intermolecular interactions. It is thought that the contribution of the permanent dipole to intermolecular interactions may be negligible (Morra and Cassinelli, 1997).

Lehr and co-workers have extensively used the polar-dispersion approach. For example, Lehr *et al*, 1992a, investigated the bioadhesiveness of polycarbophil and pig intestinal mucosa in physiological fluids. Bodde *et al*, 1990, have also used the polar-dispersion approach to assess the bioadhesiveness of a series of acrylic acid copolymers with respect to buccal peptide drug delivery.

1.4.1.4. The Lewis acid-Lewis base approach

Dividing surface energies into disperse and polar components may be an inadequate approach to modelling some practical situations. A more rigorous alternative has been proposed, which analyses surface free energies in terms of electron donation and acceptance, i.e. Lewis acid-base interactions. Interfacial interactions are dominated by the ability of compounds to act as either electron donators or electron acceptors (Rillosi and Buckton, 1995a and 1995b and Buckton and Cappucinello, 1998). The surfaces of a two-phase system may be completely characterised by three surface tension parameters, γ^-,γ^+ and γ^{LW}, representing electron donation, electron acceptance and apolar (Lifshitz van der Waals) parameters, respectively (Rillosi and Buckton, 1995a and 1995b and Buckton and Cappucinello, 1998). However, the experimental determination of interfacial interactions according to the Lewis acid-Lewis base approach requires the measurement of contact angles of at least three liquids of known parameters.

1.4.1.5. Spreading coefficients

The main disadvantage of analysing bioadhesion thermodynamically is that contact angle models only describe two-phase systems. The bioadhesive bond usually forms in the presence of a third phase, that is, a physiological fluid. In 1993, Lehr *et al* adapted the three-phase surface thermodynamic analysis developed by Kaeble and Moacanin and applied it to the mucus-polymer-liquid system of a bioadhesive bond. The interfacial interactions of all three phases are described by equations 1.9 to 1.11.

$$S_B = \gamma_{ML} - \gamma_{BM} - \gamma_{BL} \tag{1.9}$$

$$S_M = \gamma_{BL} - \gamma_{BM} - \gamma_{ML} \tag{1.10}$$

$$S_L = \gamma_{BM} - \gamma_{BL} - \gamma_{ML} \tag{1.11}$$

S_B is the adhesive spreading coefficient, S_M is the mucus spreading coefficient, S_L is the liquid spreading coefficient, γ_{ML} is the mucus-liquid surface tension, γ_{BM} is the adhesive-mucus surface tension and γ_{BL} is the adhesive-liquid surface tension.

The liquid spreading coefficient is directly related to the Griffith surface energy of fracture by equation 1.12

$$\gamma_G = -\frac{S_L}{2} \tag{1.12}$$

γ_G is the Griffith surface energy of fracture.

According to equations 1.9 to 1.11, bioadhesion may only occur when S_L is negative, S_B or S_M are positive and γ_G is positive. Since the surface properties of both mucus and physiological liquids remain relatively constant, equations 1.9 to 1.11 can be rewritten using the geometric mean equation to give a single combined spreading coefficient given by equation 1.13 (Lehr *et al*, 1993 and Shojaei and Li, 1997).

$$S_C = (\gamma_G)^{1/2}\left(\frac{S_B}{2}\right)^{1/2} \qquad (1.13)$$

S_C is the combined spreading coefficient.

1.4.2. The electronic theory

The electronic theory is based on the DVLO theory of colloid flocculation (Larsson, 1980). Initially, negatively charged mucus may adsorb counter-ions to form an electrical double layer. An adhesive of like charge may experience weak attractive forces at distances greater than 10 μm, but these are easily sheared. As the adhesive and mucus surfaces move closer together (2-10 μm), a strong repulsion is experienced, due the presence of an energy barrier. If this energy barrier is overcome, the mucus and adhesive experience a strong attractive force, which results in the formation of a semi-permanent bond. In the situation where the mucus and adhesive surfaces are oppositely charged, the electrostatic forces will be attractive, although there may be some repulsive van der Waals forces (Larsson, 1980). Some cases of bioadhesion may involve a salt bridging effect between mucus and adhesive (Park and Robinson, 1985, and He *et al*, 1998). Several studies have successfully explained the adhesive behaviour of microparticles in terms of electrostatic repulsion and attraction (Teng and Ho, 1987, Durrer *et al*, 1994a and 1994b, and Tur and Ch'ng, 1998).

1.4.3. The adsorption theory

The bioadhesive process can be described in terms of the thermodynamic adsorption of an adhesive polymer to a mucosal surface (equation 1.14) (Duchene and Ponchel, 1992).

$$\Delta G_{AD} = \Delta H_{AD} - T\Delta S_{AD} \qquad (1.14)$$

ΔH_{AD} is the enthalpy change on adsorption, ΔS_{AD} is the entropy change on adsorption, ΔG_{AD} is the free energy of adsorption and T is temperature.

The adhesive is adsorbed onto the mucosal surface as a result of an exothermic process involving secondary forces such as van der Waals forces and hydrogen bonding (Peppas and Buri, 1985). The adsorption theory tends to be an underlying mechanism in other bioadhesion theories.

1.4.4. The fracture theory

The strength of the bioadhesive bond can be related to the strain required to separate the adhered polymer from mucus. The fracture strength of bioadhesion is described by equation 1.15 (Peppas and Buri, 1985, Ahuja *et al*, 1997, and Jabbari and Peppas, 1994). The underlying assumption of this model is that the fracture occurs at the adhesive-mucus interface. However, several studies have shown that the fracture may occur near the mucus-adhesive interface (Peppas and Buri, 1985).

$$\sigma = \left(\frac{E\varepsilon}{l}\right)^{1/2} \qquad (1.15)$$

σ is the fracture strength, E is the Young's modulus, ε is the fracture energy (the sum of reversible and irreversible work of adhesion) and l is the critical crack length.

The fracture energy is composed of the reversible work of adhesion and the irreversible work of adhesion. However, if both surfaces are thermodynamically similar and the rate

of detachment is very slow, the work required for adhesive failure can be considered as reversible (Ponchel *et al*, 1987, and Duchene and Ponchel, 1992).

In this case, equation 1.15 can be rewritten as equation 1.16 (Ponchel *et al*, 1987)

$$\sigma = \left(\frac{EW_R}{l} \right)^{1/2} \tag{1.16}$$

W_R is the reversible work of adhesion.

The removal of an adhesive polymer from a mucosal surface can be characterised by a force-distance profile. Ponchel *et al*, 1987, mathematically analysed various parts of the profile in order to determine the characteristic parameters of equations 1.15 and 1.16, which describe the underlying mechanisms of bioadhesion.

The fracture strength of a bioadhesive bond may also be related to the thermodynamic surface equilibria of both mucus and adhesive by equation 1.17 (Peppas and Buri, 1985).

$$\sigma = \left[\left(\frac{E\varepsilon}{A} \right) \left(1 + \frac{\gamma_T - \gamma_B - \gamma_{BT}}{2\gamma_B} \right) \right]^{1/2} \tag{1.17}$$

γ_T is the tissue surface tension, γ_B is the bioadhesive surface tension, γ_{BT} is the tissue-bioadhesive interfacial surface tension and A is the characteristic length of the area where adhesion occurs.

1.4.5. The diffusion-interpenetration theory

If the adhesive polymer is able to form an intimate contact with mucus, polymer concentration gradients are established, which may drive a mutual interdiffusion and entanglement of mucin and adhesive chains. Secondary forces of attraction, such as van der Waals, hydrogen bonding and ionic bonding, may then form between the mucin and adhesive. The underlying assumption of this theory is that either one or both polymers

are freely mobile. In the case of highly cross-linked polymers, where chain diffusion is restricted and interpenetration is unlikely to occur, smaller polymer chains or chain ends may be able to diffuse and interpenetrate (Peppas and Buri, 1985).

The interpenetration depth and extent of polymer entanglement directly influences the strength of adhesion (Jabbari and Peppas, 1994). In turn, the mobility and flexibility of the 'penetrating' polymer chains as well as the rigidity and mesh size of the 'receiving' polymer structure will influence both the rate and depth of interpenetration. Polymer hydration also plays a key role in this mechanism since hydrated adhesive chains are more mobile and more able to form secondary forces of attraction than dry adhesives. The critical depth of polymer interpenetration required for effective bioadhesion is not known. For compatible polymers it may be in the order of microns (~ 0.2-0.5 μm), whereas for poorly compatible polymers, it may be in the order of nanometers (~ 1-100 nm) (Sahlin and Peppas, 1996). Polymer diffusion rates in mucus are typically in the order of 10^{-10} to 10^{-16} cm^2 sec^{-1} (Peppas and Buri, 1985, and Mikos and Peppas, 1990b). The relation between polymer diffusion and polymer interpenetration depth may be described by equation 1.18 (Peppas and Buri, 1985)

$$P = (D_b t)^{1/2} \tag{1.18}$$

P is the interpenetration depth, D_b is the polymer diffusion coefficient and t is time.

This theory suggests that successful bioadhesives will be similar to mucus, that is, they will be hydrophilic and contain a high proportion of ionic and polar groups, for example -OH, -COOH, $-NH_2$, $-SO_2H$ (Peppas and Buri, 1985, and Leung and Robinson, 1990).

In 1993, Jabbari *et al* used attenuated total reflectance infrared spectroscopy (ATR-FTIR) to show that polymer swelling and chain interpenetration positively influenced the bioadhesion of polyacrylic acid films when adhered to Sigma bovine submaxillary mucus. Rheological studies (e.g. Mortazavi and Smart, 1994b) have indirectly shown that polymer chain entanglement between adhesive and mucus may increase bioadhesion. Furthermore, Sahlin and Peppas have shown that the incorporation of polyethylene glycol (PEG) in polyacrylic acid hydrogel matrices improves the self-adhesion of matrices. Near-field FTIR have shown that the PEG molecules diffuse

across the hydrogel-hydrogel interface and enhance the strength of the bond (Sahlin and Peppas, 1997). In contrast, Lehr *et al* in 1990, did not find any evidence that polymer interpenetration was involved in the bioadhesion of polycarbophil-coated microspheres to fresh rat intestinal mucus.

1.4.5.1. Scaling concepts and diffusion models

Scaling or proportionality concepts analyse the dependence of a set of parameters on a nominated quantity without particular concern for obtaining numerical coefficients. Examples of this include describing the relationship between polymer network structure and diffusion in a polymer network in terms of scaling concepts (Mikos and Peppas, 1990b). The mucus network may be characterised in terms of an average mesh size, which describes the effective space available for diffusion and defines 'spheres of influence' in which a polymer chain does not interact with other chains. Consequently, bioadhesion may be described in terms of scaling concepts of diffusion and polymer relaxation.

Mikos and Peppas, 1990, have shown how scaling concepts can help determine the mechanism of polymer interdiffusion across the mucus-polymer interface. Rouse diffusion may occur if the degree of polymerisation is less than the entanglement limit, permitting the polymer chain to move in three dimensions. As a result, the polymer mix behaves like a viscous liquid with the polymer self-diffusion coefficient being inversely scaled to the molecular weight of the chain. (Jabbari and Peppas, 1994, and Sahlin and Peppas, 1996). If molecular weight of the polymer is less than a critical molecular weight and is greater than the entanglement limit, polymer diffusion may occur by reptation with the polymer self-diffusion coefficient being inversely scaled to $[\text{molecular weight}]^{1/2}$. However, if polymer molecular weight is greater than a critical value, the diffusion coefficient becomes independent of molecular weight.

Peppas and co-workers have published several comprehensive reviews both on polymer interpenetration and scaling concept analysis. For example, Sahlin and Peppas, 1996, Peppas, 1998, Mikos and Peppas, 1990, Peppas and Buri, 1985, and Jabbari and Peppas, 1994.

1.4.6. The dehydration theory

The rheology of mucus may allow it to flow into macroscopic and microscopic crevices in the adhesive in order to form an intimate contact with the adhesive. In hydrophilic polymers, a stiff gel layer forms as the adhesive starts to hydrate, which may have a high cohesive strength resulting from entanglement of the adhesive polymer chains. The hydration of the adhesive polymer may also dehydrate the adjacent mucus layer, forming a stiff and highly cohesive mucus gel layer. This results in the 'setting' of a stiff, cohesive interfacial region that has components of both macro- and microscopic mechanical bonds. In contrast, over-hydrated adhesives may form a slippery gelatinous mucilage, which can be easily sheared, resulting in poor bioadhesive bond strengths (Smart *et al*, 1984).

The ability of a hydrating adhesive to dehydrate mucus was first shown by Smart *et al* in 1984, who reported that dry polymer films became adhesive as a result of extracting hydration water from the mucus. In 1993, Mortazavi and Smart studied how matrices and gels of Carbopol 934P influenced the dehydration of mucus and related these observations to their bioadhesive bond strength. The study found that dry matrices and concentrated gels began to dehydrate the mucus after just 1 minute and that both the cohesiveness and adhesiveness of mucus gels increased as the water content decreased (Mortazavi and Smart, 1993). In a study investigating the influence of hydration on bioadhesion, Woolfson *et al*, 1992, discovered that a dry sodium CMC or sodium carbopol polymer films produced stronger bioadhesive interactions compared to hydrated polymer films. A likewise trend was observed in hyaluronic acid benzyl ester films by Sanzgiri *et al*, 1994. Using a different approach, Robert *et al*, 1988, reported that an adhesive polymer adhered better to a mucin-free epithelium than to a mucus covered epithelium due to incomplete hydration of the adhesive.

1.5. Factors important to bioadhesion

1.5.1. Polymer-related factors

1.5.1.1. Molecular weight

Early work showed that bioadhesion was proportional to molecular weight up to 100,000 Da but was independent at higher molecular weights (Peppas and Buri, 1985). However, other studies have showed this relationship to be polymer specific, related to the size, configuration and structure of the adhesive as well the critical macromolecular chain length required for interpenetration and entanglement. For example, sodium CMC polymer films exhibit maximum bioadhesive bond strengths at molecular weights greater than 78,600 Da (Smart *et al*, 1984). In comparison, polyacrylic acid compacts reach their maximum bioadhesive potential at 750,000 Da, but become less bioadhesive at higher molecular weights (Mortazavi and Smart, 1994b, and Tobyn *et al*, 1996b).

1.5.1.2. Concentration of bioadhesive polymer

Numerous studies have shown that increasing the concentration of adhesive increases the bioadhesive bond strength of a dosage form, with dosage forms containing 100% polymer exhibiting maximum bioadhesive potential (Jimenez-Castellanos *et al*, 1993, Leung and Robinson, 1990, and Hassan and Gallo, 1990). However, adhesive polymers may interact with other adhesive polymers rather than with mucin at high concentrations of adhesive, reducing the bioadhesive potential of the dosage form (Ahuja *et al*, 1997 and Peppas and Buri, 1985).

1.5.1.3. Cross-linking of polymer chains

Cross-linking of a polymer effectively reduces the length and mobility of the polymer chains and decreases the ability of these chains to interpenetrate and entangle the mucus network. However, it is thought that bioadhesion may still occur in highly cross-linked adhesives if smaller branch chains are able to effectively diffuse into the mucin polymer network (Peppas and Buri, 1985). The influence of cross-linking and chain flexibility is seen in the bioadhesion of polyacrylic acids and acrylamide co-polymers to rabbit

gastric mucosa, in which the bioadhesion of the co-polymer increased as the degree of cross-linking decreased and chain flexibility increased (Park and Robinson, 1985 and 1987).

1.5.1.4. Density of adhesion sites

The number, density and type of chemical groups on an adhesive can dramatically influence bioadhesion. It has been shown that polymers containing ionisable hydrophilic groups, such as -COOH, -OH, $-SO_4H$ and $-NH_2$, tend to be more bioadhesive than polymers containing other chemical groups, although the adhesive must posses a minimum of these chemical groups in order to be bioadhesive (Park and Robinson, 1987). Above this threshold quantity, the bioadhesive bond strength tends to be proportional to the number and density of the groups (Park and Robinson, 1984 and 1985, and Smart *et al*, 1984).

The type of adhesive group also appears to influence bioadhesion. For example, polymers with -COOH groups may be more bioadhesive than neutral polymers or sulphonated polymers (Park and Robinson, 1984, Leung and Robinson, 1990, and Gupta *et al*, 1990). The bioadhesive potential of an adhesive may be reduced if the conformational structure of the polymer shields the adhesion sites. Subsequently, simple linear polymers such as polyethylene glycol tend to be more adhesive than highly conformational polymers on a molecular weight basis (Ahuja *et al*, 1997, Peppas and Buri, 1985, and Park and Robinson, 1985).

1.5.1.5. Polymer swelling

The swelling of an adhesive polymer may influence bioadhesion in several ways. For example, the swelling of an adhesive may disrupt inter-polymer bonds, which may expose adhesive chemical groups and allow the polymer to interact with mucin. Further hydration and swelling of the adhesive may reduce the cohesion of the polymer gel, forming a slippery mucilage that is easily sheared (Smart *et al*, 1984).

The ability of the adhesive to swell may be influenced by several factors, including the density of cross-linking and the ionic strength of the hydration medium. For example,

the addition of sodium chloride to polyacrylic acid-mucin mixes decreases the gel strength (G' modulus) of the mix. It is thought that increasing the ionic strength may charge shield both mucin and adhesive, resulting in a less expanded network and fewer interactions (Mortazavi and Smart, 1994b). In contrast, the bioadhesion of polyacrylic acids have been shown to increase in calcium concentrations greater than 20%. It is thought that the calcium ions form salt bridges between the adhesive chains, resulting in an expanded polymer network (Leung and Robinson, 1990).

1.5.2. Physiological factors

1.5.2.1. Type of mucus

Native gastrointestinal mucus is a unique material, but is not easy to manipulate experimentally, since it can be both adhesive and slippery. Subsequently, most adhesive tests tend to pre-treat or purify mucus before use. However, the pre-treatment or purification processes may actually destroy the unique functional properties of mucus, especially those that confer its adhesive potential. Freeze-dried purified mucins are also available commercially, for example Sigma Type I (bovine submaxiallary mucin), Sigma type II (pig gastric mucin) and Sigma type III (partially purified pig gastric mucin) mucins (Sigma, Poole, UK).

Several studies have investigated how the origin, composition, treatment and structure of mucus influences bioadhesion (Rossi *et al*, 1995, Kocervar-Nared *et al*, 1997, and Madsen *et al*, 1996). Both Kocervar-Nared *et al*, 1997, and Madsen *et al*, 1996, have shown that the rheological properties of reconstituted freeze-dried gastric mucins were completely dissimilar to native gastric mucus. Rossi *et al*, 1995, used dynamic oscillatory rheology to demonstrate that commercially available freeze-dried mucins contained salts that decreased the bioadhesive potential of polyacrylic acids.

Bioadhesion may also be influenced by the composition of native mucus. For example, increasing the concentration of dry solids in mucus increases the bioadhesive potential of polyacrylic acids (Tobyn *et al*, 1995, Mortazavi and Smart, 1993). The bioadhesive properties of an adhesive may be influenced by its location in the GI tract. For example,

carbopol matrices adhere more strongly to the fundus of the stomach than to the cardiac region (Tobyn *et al*, 1995).

The continual sloughing off of the native mucus gel layer may limit the bioadhesive potential of a polymer. Lehr *et al*, 1991, determined that rat intestinal mucus had a turnover time of between 47 mins and 270 mins. An additional implication is that the sloughed off, solubilised mucus sits in the lumen and may interact with the adhesive in the same way as adherent mucus gel.

1.5.2.2. Pathological mucus

The functional properties of a bioadhesive dosage form must be able to withstand changes in the structure and properties of mucus that occur in pathological disease states such as cystic fibrosis, gastroduodenal ulcers, Crohn's disease and inflammatory bowel syndrome (Marriot and Gregory, 1990).

In general, pathological disease states result in either hyposecretion or hypersecretion of mucus, as well as changes in mucin structure. Hyposecretion of mucus is generally linked with ulcerative conditions, although some patients with Crohn's disease may produce mucus normally. Also, patients with ulcerative colitis tend not to produce any mucus in their colon due to a complete absence of goblet cells (Marriott and Gregory, 1990). Mucins in patients with gastric ulcers tend to be more acidic and degraded than normal mucins (Allen, 1981), whereas patients with adenocarcinoma produce mucins containing more sialic acid and antigenic material.

Cystic fibrosis sufferers tend to hypersecrete thick mucus containing a large amount of sulphated glycoproteins that blocks intestinal, pancreatic and bronchial mucosal glands. In inflammatory diseases, DNA and albumin may leach into the gastrointestinal tract, resulting in an increase in the viscosity of mucus (Marriott and Gregory, 1990).

1.5.3. Other factors

1.5.3.1. Bathing fluid

The pH of the bathing fluid may influence bioadhesion by affecting the ionisation states of both adhesive and mucus. For example, polyacrylic acid is an anionic polymer and is bioadhesive when unionised. When pH is greater than its pK_a of 4.75, bioadhesion dramatically decreases as a result of the polymer becoming increasingly more ionised (Park and Robinson, 1985). At pH greater than 6, polyacrylic acids swell considerably due to electrostatic repulsion, dramatically reducing the density of carboxyl groups and its bioadhesive potential (Park and Robinson, 1987). However, this increases the mobility and entanglement of polyacrylic acid chains, accounting for the increase in storage moduli of polymer-mucus mixes with increasing pH (Hassan and Gallo, 1990).

1.5.3.2. State of hydration

Several contradictory studies have investigated the influence of prehydration time on the bioadhesiveness of hydrophilic matrices. For example, Ponchel *et al*, 1987, determined that matrices of polyacrylic acid hydrated for 10 mins exhibited maximum bioadhesive potential. In contrast, Tobyn *et al*, 1995, showed that dry polyacrylic acid matrices produced the strongest bioadhesive bonds.

1.5.3.3. Polymer contact force

Solid bioadhesive dosage forms may require the application of an initial contact force to aid the formation of a bioadhesive bond. Several studies (e.g. Park and Robinson, 1985, Tobyn *et al*, 1995 and Lejoyeux *et al*, 1989a and 1989b) have shown that increasing the initial contact force increases the bioadhesive bond strength due to improved wetting, improved swelling and increased polymer interdiffusion. The influence of contact force is important in situations where dosage forms are applied to mucosal surfaces by patients, for example buccal drug delivery dosage forms.

1.5.3.4. Initial contact time

Several studies have shown that bioadhesion increases the longer an adhesive remains in contact with the mucus (Smart *et al*, 1984, Leung and Robinson, 1990, Sanzgiri *et al*, 1994, Tobyn *et al*, 1995). The influence of contact time is also important in situations where the dosage form is applied to the mucosal surface by the patient.

1.5.3.5. Removal rate

The rate at which an adhesive is removed from mucus may influence the observed bioadhesion. Increasing the removal rate often increases the observed bioadhesive strength of the polymer (Tobyn *et al*, 1995, and Smart, 1991). This is because the bioadhesive bond is viscoelastic in nature. Rapid removal rates do not allow the polymer and mucin chains to deform and flow, resulting in a stronger and more brittle tensile fracture (Smart, 1991).

1.5.3.6. Duration of bioadhesion

The majority of bioadhesive studies have concentrated on investigating the strength of bioadhesive bonds, rather than the duration of bioadhesion. In 1994, Mortazavi and Smart measured how long different adhesives remained adhered to mucosal tissue when placed under a constant tensile stress (Mortazavi and Smart, 1994a). It was shown that the strongest adhesives did not necessarily produce the most durable bonds, but rather the moderately adhesive HPMC formed the most durable bioadhesive bonds. The duration of a bioadhesive bond seems to be influenced by the rate of polymer swelling, polymer network cohesion and the stresses placed on the bond. This suggested that an adhesive which swells rapidly to form a long lasting cohesive rigid gel is more likely to produce a more stable and durable bioadhesive joint than other types of polymer (Mortazavi and Smart, 1994a).

1.5.3.7. Formulation factors

The type of dosage form may significantly influence the bioadhesive potential of a polymer. In polymer films, bioadhesive bond strength is improved if the film thickness

is increased but is decreased if a plasticiser is added (Woolfson *et al*, 1992, 1995a and 1995b). The plasticiser reduces the mechanical strength of the polymer film and increases the flexibility of the film, changing the mechanism of detachment from a brittle tensile fracture to a viscoelastic peel-type mechanism. Peeling mechanisms tend to produce lower fracture strengths than tensile mechanisms (Jacques and Buri, 1992). The size of the dosage form may also influence the bioadhesive potential of a formulation. In general, larger dosage forms tend to be more bioadhesive than smaller dosage forms, since a larger area of adhesive polymer interacts with the mucus (Sam *et al*, 1992, Mikos and Peppas, 1990a, and Durrer *et al*, 1994a and 1994b). The porosity of a tablet dosage form seems not to influence the bioadhesive properties of the polymer (Lejoyeux *et al*, 1989a and 1989b, and Duchene and Ponchel, 1992).

1.6. Bioadhesive polymers

Adhesives may be classified according to their chemical nature or their principal mechanism of adhesion. Adhesives used in drug delivery devices should be non-toxic, non-irritant, adhere quickly, easily formulated, stable and inexpensive (Ahuja *et al*, 1997).

1.6.1. Anionic polymers

Anionic polymers such as polyacrylics and polysaccharides are regarded as good adhesives since they fulfil most of the requirements necessary for bioadhesion. An example of a 'good' anionic adhesive is the polyacrylic family, which are synthetic, high molecular weight, cross-linked branched and linear polymers of acrylic acid (Tobyn, 1994). The polymers are flexible and can easily diffuse into the mucus network. They also possess a large number of carboxyl groups, which may hydrogen bond with mucus (Tobyn *et al*, 1992). Polyacrylics also have a large capacity to take up water and the surface of the hydrated polymer thermodynamically favours adhesion to mucus (Tobyn, 1994). In contrast, the salts of polyacrylic acids tend not to be adhesive (Park and Robinson, 1985).

Another example of a 'good' anionic adhesive is sodium CMC, which is a water-soluble polymer, possessing a large number of carboxyl groups. Sodium CMC is used in several

adhesive pharmaceutical preparations, for example, skin adhesive in some ostomy products. Xanthan gum is another example of a high molecular weight heteropolysaccharide, containing carboxyl, hydroxyl and ester groups, that is used as a controlled release and bioadhesive agent. HPMC also makes Suscard Buccal tablets weakly bioadhesive in addition to its principal role as a controlled release agent (Smart, 1993).

1.6.2. Cationic polymers

Cationic polymers are not commonly used in pharmaceutical devices since they tend to be poorly adhesive and may be toxic. An exception to this is chitosan, which is non-toxic, biocompatible and biodegradable (He *et al*, 1998). Chitosan is a linear, flexible polymer, which is able to diffuse into the mucus network, allowing its large number of hydroxyl and amine groups to hydrogen bond with mucus. At pH values below its pK_a, chitosan carries a positive charge that may electrostatically interact with negative charges in mucus. It also seems able to open up cellular tight junctions, which may aid the absorption of drugs, in particular, peptide drugs.

1.6.3. Neutral polymers

Neutral polymers such as polyvinylpyrrolidine are typically 'poor' adhesives (Smart *et al*, 1984) and tend to rank below their ionic counterparts (Park and Robinson, 1984).

1.6.4. Bioadhesive polymers with specific adhesive receptors

Polymers that might bind to specific receptors on cell surfaces could dramatically improve and alter the entire concept of bioadhesive drug delivery (Helliwell, 1993). The process of specific, receptor mediated polymer adhesion has been demonstrated *in vitro* by investigators such as Lehr *et al*, 1992b, and Naisebett and Woodley, 1994. However, in a study of the adhesion of tomato lectins to isolated pig enterocytes and human Caco-2 cells, Lehr *et al*, 1992b, reported that specific cell mediated adhesion may be inhibited by the mucus layer. Therefore, pharmaceutical applications of specific adhesives will require such polymers to rapidly diffuse through the mucus layer in order to bind with

cell receptors and, once there, resist removal forces such as mucus turnover and peristalsis.

1.6.4.1. Lectins

Lectins are naturally occurring plant glycoproteins that have an unique ability of being able to recognise and bind to exposed carbohydrate residues on glycoproteins, such as those on intestinal epithelial cells (Naisebett and Woodley, 1994). They are able to resist lumenal digestion and do not affect cell integrity upon binding (Helliwell, 1990). However, most lectins are considered to be reasonably toxic, for example the kidney bean lectin.

1.6.4.2. Proteins

The blue mussel (*Mytilus edulis*) uses adhesive proteins to adhere to underwater surfaces, such as ship hulls or coastal rocks where they experience terrific shear forces. A mussel adhesive protein (MAP) has been isolated and purified by Schnurrer and Lehr in 1996, who then demonstrated that MAP coated slides performed equally well as polycarbophil coated slides when adhering to freshly slaughtered pig duodenum mucosa. These strong adhesive properties were attributed to carbachoyl residues, positively charged lysine residues and a high content of hydroxylated amino acids in the mussel adhesive protein. Pathogenic bacteria such as *Pseudomonas aeruginosa* and *Escherichia coli* may also have adhesive proteins and pili to help the bacteria adhere to the cell membrane (Hugo and Russell, 1987).

1.6.5. Rank orders of bioadhesion

Whilst scientists may refer to 'good' and 'poor' adhesives in a particular context, the abstract ranking of an adhesive proves difficult since the type of test and the experimental conditions can affect the observed bioadhesion. This must be borne in mind when comparing results from different bioadhesive studies, especially those that have attempted to rank the adhesiveness of different polymers (for example, Park and Robinson, 1984, Smart *et al*, 1984, and Robert *et al*, 1988).

1.6.6. Pharmaceutical applications

The use of adhesive polymers in surgery and dentistry is commonplace, for example, cyanoacrylates in orthopaedic surgery. In contrast, relatively few bioadhesive drug delivery devices are commercially available, although the use of bioadhesive polymers in drug delivery devices has been extensively researched. The products that have been designed as bioadhesive dosage forms and that are commercially available are listed in table 1.7.

Table 1.7 Pharmaceutical products that are intended for bioadhesion

Polymers	Bioadhesive Product
Alginate (calcium and sodium salts)	Algosteril, Comfeel SeaSorb, Kaltogel, Kaltostat, Sorbsan and Tegagan
Carbomer 940P	Viscotears and GelTears
Carbomer 934P and polycarbophil	Replens
Hydroxyethylcellulose	Minims and Artificial Tears
Hypromellose	Isopto Alkaline, Isopto Plain and Moisture-eyes
Hypromellose and dextran '70'	Tears Naturale
Karaya gum powder	Salts and Hollister stoma products
Modified carboxymethylcellulose	Intrasite gel
Modified HPMC	Suscard
Polyvinylalcohol	Liquifilm Tears and Sno Tears
Polyvinylalcohol and macrogol '8000	Hypotears
Sodium carboxymethylcellulose	Rhinacort, Nystan pessaries, Luborant, Glandasone, Comfeel and Comfeel Plus
Sodium carboxymethylcellulose, gelatin and pectin	Orahesive, Orabase, Adcortyl in Orabase, Granuflex, DuoDERM and Stomahesive
Xanthan gum	Buccastem

1.7. Methods used to study bioadhesion

A wide range of methods has been used to study bioadhesion and may be broadly classified as either *in vitro* or *in vivo* tests. *In vitro* tests may be further classified by the parameter studied, for example, adhesive strength, number of adhered particles and duration of adhesion (Park and Park, 1990).

1.7.1. In vitro tests

1.7.1.1. Detachment force testing

This type of test is widely used to study bioadhesion and measures the force or work required to break a bioadhesive bond. The test involves applying a contact force for a period of time to aid formation of a bioadhesive bond and then removing the adhesive from the mucosal surface at a controlled rate until it is completely detached. This type of test can determine several parameters that may be used to describe the properties of the bioadhesive bond (Ponchel *et al*, 1987). The most commonly determined parameters are the work of adhesion (W_a) and the maximum detachment force (F_{max}).

There are several mechanisms by which an adhesive polymer may be removed from the mucosal surface; these are tensile, shear or peel forces (Jacques and Buri, 1992). In the case of tensile and shear tests, the stress is uniformly distributed over the adhesive bond. This type of mechanism is usually predominant when both adhesive and mucosal surface are relatively inflexible, with the only flexible part of the system being the adhesive interface (Sahlin and Peppas, 1996). This results in a high breaking strength, which may be attributed to either adhesive or cohesive failure.

If one of the substrates is flexible, the applied stress becomes limited to a fine line along the adhesive interface and the flexible substrate is 'peeled' off the other substrate. The failure of the joint predominantly occurs at the adhesive interface, resulting in the observed breaking strength being lower than either tensile or shear fractures (Jacques and Buri, 1992). The flexibility and thickness of both adhesive and mucosal substrate may significantly influence the observed bioadhesive strength of an adhesive polymer. Therefore, studies comparing adhesive polymers should take appropriate measures to

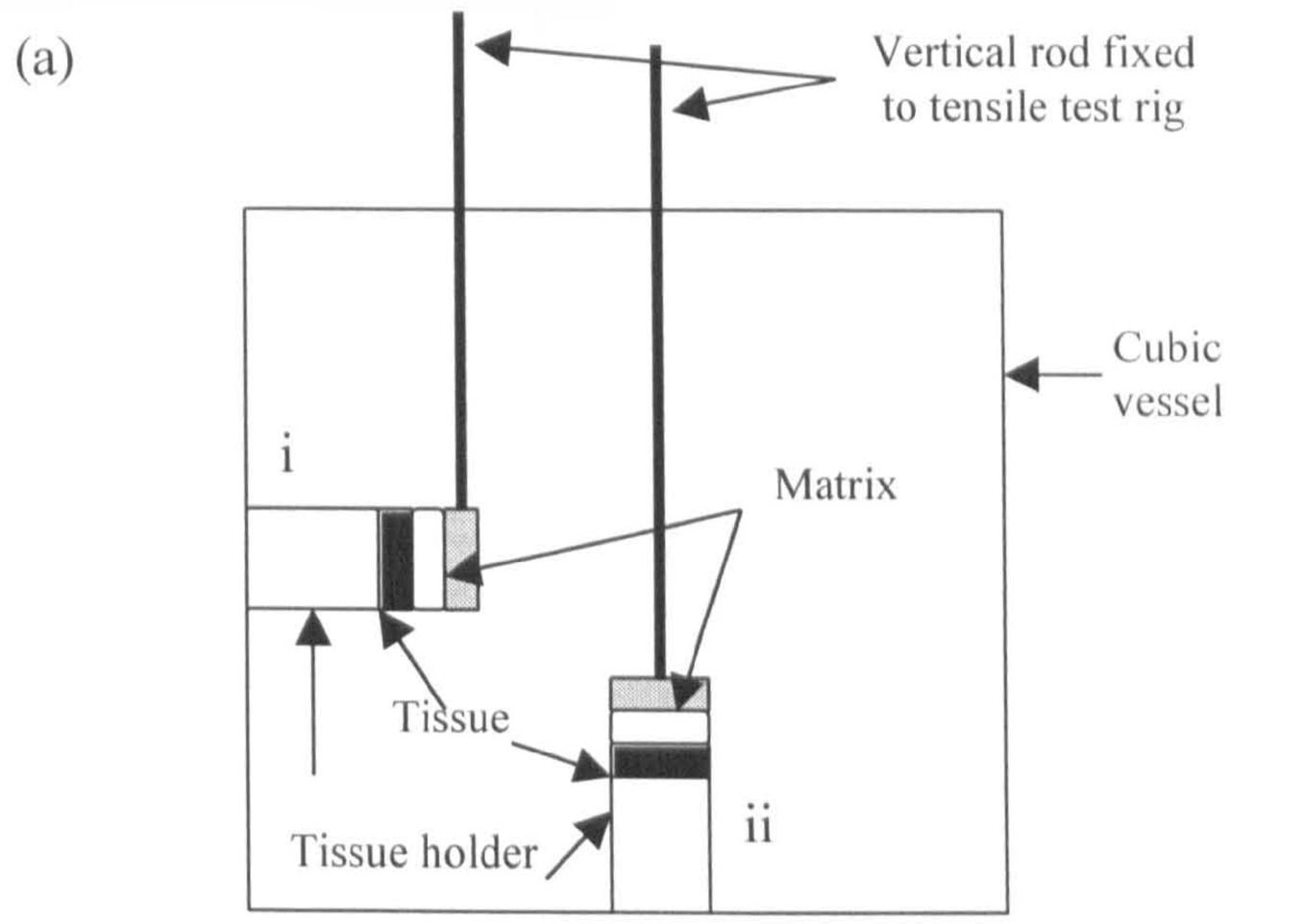

Figure 1.11 (a) An example of a sample cell geometry to determine the (i) shear and (ii) tensile forces of detachment (Jimenez-Castellanos *et al*, 1993). (b) The sample cell geometry used in the Wilhelmy plate method (Smart *et al*, 1984).

(a)

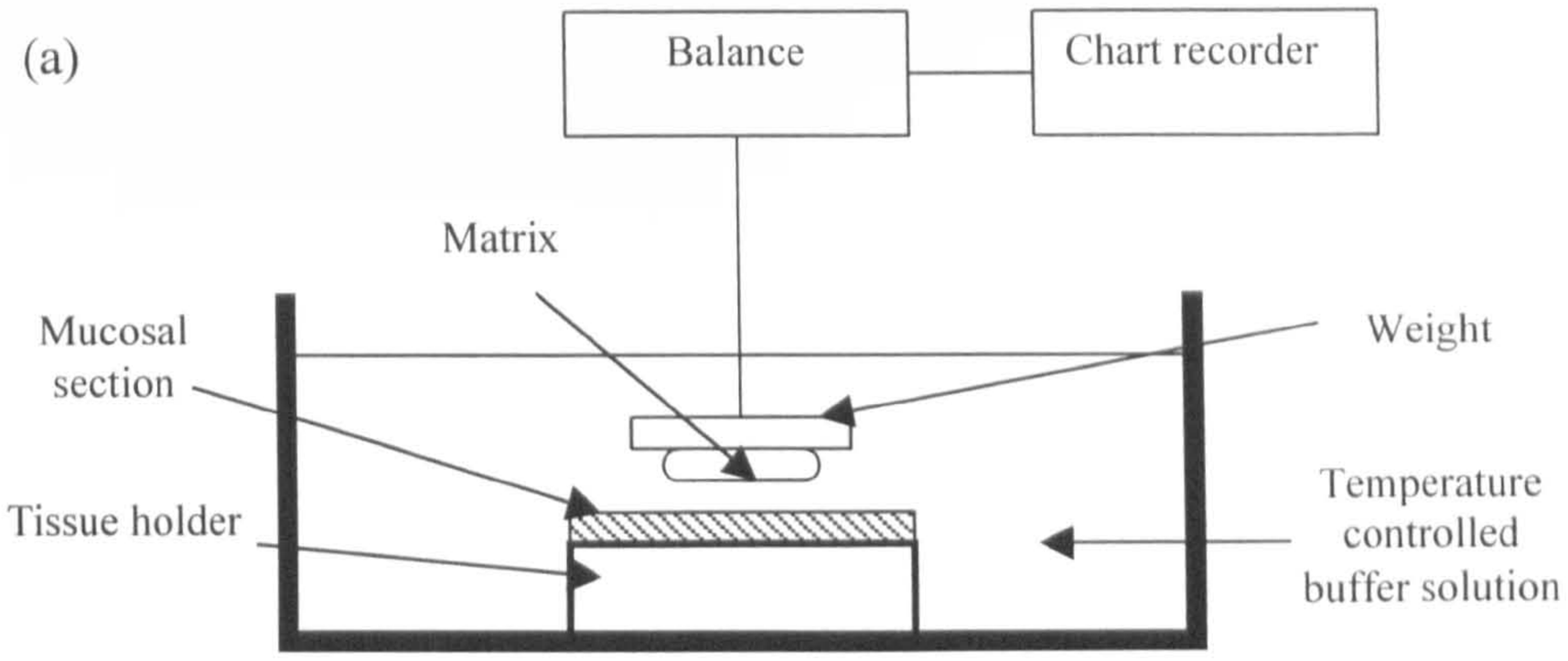

(b)

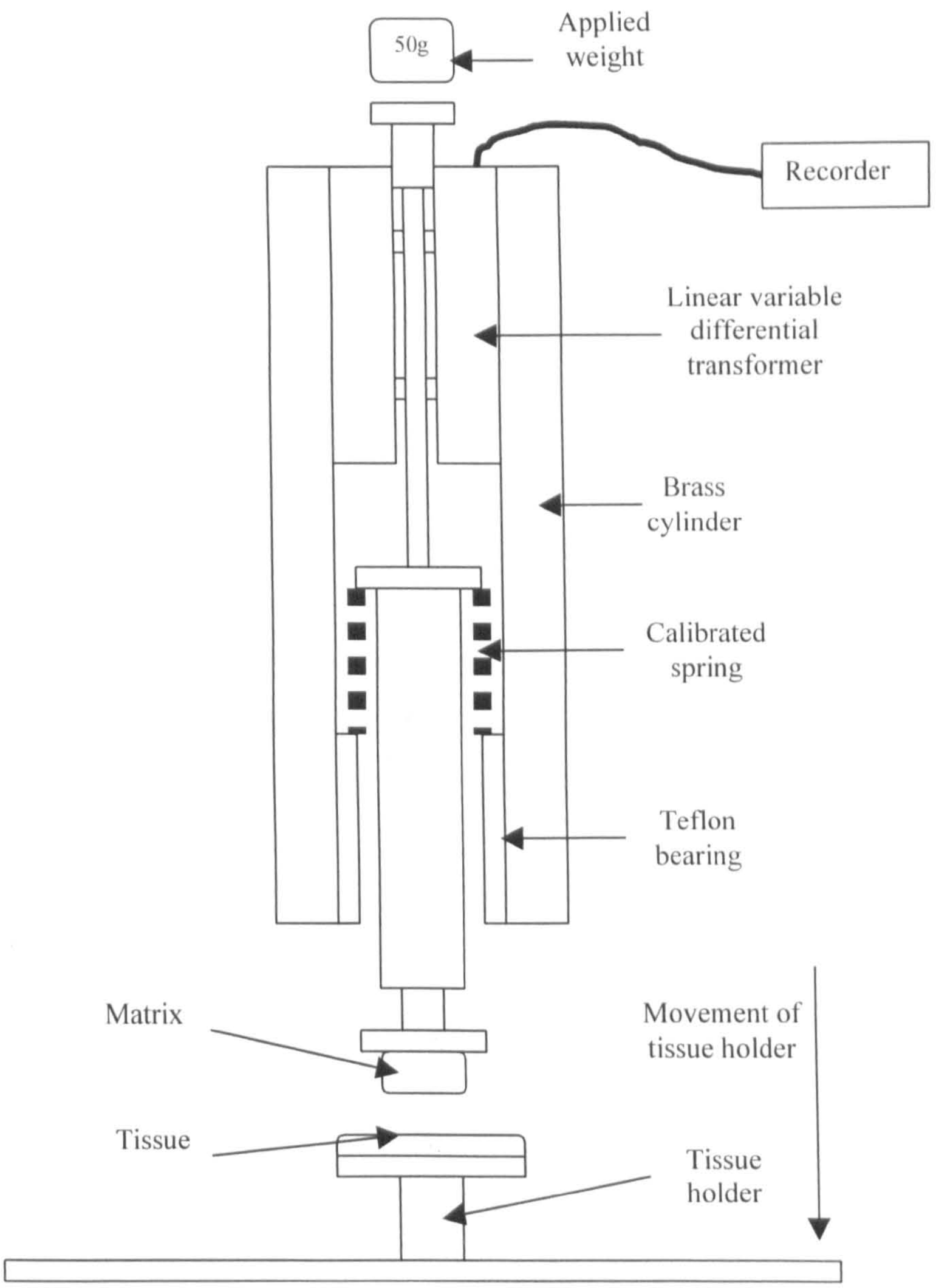

Figure 1.12 (a) An example of a sample cell geometry using a modified top pan balance as a tensile test rig (Smart, 1991). (b) A sample cell geometry of a tensile test rig using a linear variable differential transformer to measure the bioadhesive bond strength (Woolfson *et al*, 1992).

control the thickness of the substrates, particularly the mucosal tissue. This may be achieved by using the same mucosal section to test different adhesive polymers.

These types of tests are commonly undertaken on tensile testing rigs. Tensile testers usually determine either the tensile or peel strength of a bioadhesive bond. It is also possible to use tensile tests to apply shear forces to a bioadhesive bond by rearranging the sample cell geometry (figure 1.11a) (Jimenez-Castellanos *et al*, 1993, and Mortazavi and Smart, 1995). The Wilhelmy plate technique can be used to apply a shear force to a polymer film (figure 1.11b) (Sam *et al*, 1992, Smart *et al*, 1984 and Smart *et al*, 1991).

Several studies have used custom-built tensile test testers: modified tensiometers (Park and Robinson, 1985 and 1987, Robert *et al*, 1988, Leung and Robinson, 1990, Schnurrer and Lehr, 1996, and Sanzgiri *et al*, 1994); modified top pan balances (figure 1.12a) (Smart, 1991, and Mortazavi and Smart, 1993); linear variable differential transformers (figure 1.12b) (Woolfson *et al*, 1992, 1995a and 1995b). Other studies have used commercially available machines such as Instron tensile tester (Ponchel *et al*, 1987, Lejoyeux *et al*, 1989a and 1989b, and Anlar *et al*, 1994), texture analyser (Tobyn *et al*, 1995, 1996a and 1996b, and Jones *et al*, 1997), DuNoy tensiometer (Robert *et al*, 1988) and Lloyd tensile tester (Blanco-Fuente *et al*, 1996). The highly sensitive microbalance on the Cahn DCA contact angle analyser has been used to measure the bioadhesiveness of small area samples such as microspheres (Chickering *et al*, 1995a and 1995b).

Detachment force tests are quick, inexpensive and easy to perform, allowing a rapid throughput of samples. However, the observed bioadhesive indicators may be extremely sensitive to experimental conditions and parameters, such as contact time, contact pressure, probe withdrawal speed and hydration time (Helliwell, 1993).

1.7.1.2. Surface tension and wetting

The surface thermodynamics of mucosal tissue and adhesive may considerably influence the formation of a bioadhesive bond. Several methods can determine contact angles, surface tensions and spreading coefficients of the tissue and the polymer. These

include the pendant drop method, the sessile bubble method, the rotating bubble method, the Wilhelmy plate method and the captive bubble method.

In 1989, Mikos and Peppas used the pendent drop method to study how electrolyte, pH and concentration of mucin influences the surface tension of mucin solutions and bioadhesion. Lehr *et al*, 1993, also used this method to measure surface spreading coefficients of a bioadhesive bond and to develop the combined spreading coefficient model to describe bioadhesion. As described in section 1.4.1.3, the captive bubble technique can determine the disperse and polar components of the adhesive and mucosal surface tensions (Lehr *et al*, 1990 and 1992a). This method has been used to assess the surface polarity and wetting characteristics of a range of acrylic acid and butyl acetate copolymers influence bioadhesion (Bodde *et al*, 1990).

1.7.1.3. Rheological testing

The rheological properties of an adhesive-mucus dispersion may provide valuable information on the possible mechanisms of bioadhesion. The rheology of a dispersion may be described in terms of the elastic gel (G') and viscous liquid (G") components. If mucus and adhesive polymer chains interact, the polymer network may become more cross-linked and gel-like, resulting in an increase in G' and a decrease G". The difference between the G' of an adhesive-mucus dispersion and the sum of G' of individual substrates may be indicative of the extent of chain interaction.

Kerr *et al*, 1990, used dynamic oscillatory rheology and electron spin resonance to study how molecular weight influenced the bioadhesive interaction between carbopol and purified pig gastric mucus. Mortazavi *et al*, 1992, showed that Carbopol 934P and purified pig gastric mucus exhibited a high degree of rheological synergism, which was markedly affected below pH 4.5 and above pH 8, but was unaffected by temperatures up to 45°C. Madsen *et al*, 1998a and 1998b, tested different adhesive polymers to show that macromolecules possessing numerous hydrogen bond forming groups and an open expanded network produce a pronounced rheological synergism. Rheological testing has also provided invaluable information on the structure of mucus, purified mucus and commercially available freeze-dried mucins. Both Madsen *et al*, 1996, and Kocevar-

Nared *et al*, 1997, determined that rheology of commercial mucins showed little similarity to native or purified mucus.

In 1990, Hassan and Gallo developed a simple viscosity method, which used a Brookfield viscometer to quantify and measure the interactions between mucus and adhesive. In comparison to rheological testing, this technique is quicker, more simple and cheaper. It is also able to test a wide range of adhesive polymers in a wide range of conditions.

1.7.1.4. The falling film method

This technique was initially developed by Teng and Ho in 1987. It consists of an inclined supporting platform, a perfusion system and an effluent collector. The mucosal tissue, which is attached to the supporting platform, is perfused firstly with an adhesive suspension then secondly with physiological fluid. The amount of adhesive adhering to the mucosal surface is related to the bioadhesive potential of the dosage form. This technique is particularly useful to study the bioadhesion of particulate formulations. Perfusion rate, inclination angle of the platform and length of tissue are factors that may influence the observed bioadhesion. Ranga Rao *et al*, 1989, and Gaserod *et al*, 1998, have used versions of this technique to study the adhesion of microparticles to the gastrointestinal mucosal surface.

1.7.1.5. Flow channel method

Mikos and Peppas, 1990a, developed the sealed flow channel method to study the bioadhesion of single microspheres. This method involves carefully placing a single microsphere on the mucosal tissue and dislodging the microsphere by passing humid air through the sealed channel. The movement and detachment of the particle is recorded on video tape.

1.7.1.6. Colloidal gold staining

Colloidal gold particles adsorb to mucin molecules to form red coloured mucin-gold conjugates. Adhesives that interact with the stabilised conjugates are stained red.

Absorbance spectroscopy may be used to quantify the intensity of staining, which is related to the bioadhesive potential of the polymer (Park, 1989). In 1998, Tur and Ch'ng used colloidal gold staining, amongst other techniques, to study the interactions of 0.3% cross-linked polyacrylic and polymethacrylic acids with Sigma bovine submaxillary mucin.

1.7.1.7. Fluorescent probe method

In 1984, Park and Robinson labelled the lipid bilayer of cultured human conjunctival epithelial cells with a fluorescent probe to study how bioadhesion was affected by the electrostatic charge and backbone structure of a polymer. The technique relates the bioadhesive potential of a polymer to both fluorescence and viscosity of the lipid bilayer.

1.7.1.8. Attenuated total internal reflectance-Fourier transform infra-red spectroscopy

Attenuated total internal reflectance-Fourier transform infra-red spectroscopy (ATR-FTIR) has been used to study the interdiffusion of polymers at the adhesive-mucus interface. In a key paper, Jabbari *et al*, 1993, used ATR-FTIR to provide evidence that polyacrylic acid polymers diffuse into the mucus network during bioadhesion. ATR-FTIR has also been used to determine the diffusion of water through a hydrating polymer film (Degim *et al*, 1998) and to measure the number of latex microparticles adsorbing to rat small intestine (Durrer *et al*, 1994a and 1994b).

1.7.1.9. Hydration and swelling studies

A number of studies (e.g. Park and Robinson, 1985 and 1987, and Leung and Robinson, 1990) have related polymer swelling to bioadhesive potential. The interaction and entanglement of both adhesive and mucus is thought to increase as the adhesive polymer network expands. However, the continued expansion of the adhesive network may produce a poorly cohesive slippery mucilage, which can be easily sheared (Smart *et al*, 1984, and Mortazavi and Smart, 1994a and 1994b). The importance of hydration and swelling in bioadhesion has been highlighted by Smart *et al*, in 1991, and then by

Mortazavi and Smart, in 1993, who indicated that some polymers may be adhesive as a result of their ability to dehydrate mucus.

1.7.1.10. Other in vitro techniques

Several other methods have been used to indirectly and directly study bioadhesion. A novel shear stress test uses the 'dunking' action of a disintegration test apparatus to measure microsphere adhesion to an agar plate (Nakamura *et al*, 1996). Analytical ultra-centrifugation, static light scattering and turbidimetry have been used to investigate how chitosan interacts with pig gastric glycoprotein (Fiebrig *et al*, 1994 and 1995). In a further study, Fiebig *et al*, 1997, used electron microscopy and colloidal gold labelling of the chitosan to show that chitosan concentrates in the centre of a chitosan-mucin aggregate. HPLC has also been used to measure the amount of tomato lectin-latex conjugates adsorbing to pig gastric mucin (Irache *et al*, 1994).

1.7.2. In vivo methods

The four main techniques used to study the *in vivo* effects of bioadhesive dosage form are gamma scintigraphy, perfused intestinal loops, gastrointestinal transit studies and pharmacokinetic studies (Helliwell, 1993). The first three techniques may be used to monitor the bioadhesive performance of a dosage form in the gastrointestinal tract. The last technique is the 'litmus test' of the controlled release properties of a bioadhesive dosage form and provides evidence for the clinical performance of a drug delivery device.

1.7.2.1. Gamma scintigraphy

In gamma scintigraphy, the bioadhesive dosage form is labelled with a radionuclide such as ^{99m}Te or ^{125}I. Once an animal or human volunteer swallows the radiolabelled dosage form, a gamma camera is used to image the transit of the dosage form through the gastrointestinal tract. This technique is non-invasive and relatively safe but is limited by high purchase and high running costs of the instrument. In an analogous technique, the gastrointestinal journey of a dosage form, loaded with radio-opaque

material such as ^{137}Ba, has been imaged using X-ray radiography (Chickering *et al*, 1997).

1.7.2.2. The perfused loop

The perfused intestinal loop method involves isolating and maintaining a viable section of intestine, which is then used to study the bioadhesion of a dosage form (Helliwell, 1993). The advantages of this method are that nerve connections and blood vessels to the isolated section remain intact and as a result mucus biosynthesis and secretion still occur. Furthermore, it is relatively inexpensive and the animal may be used as its own control. However, disadvantages include complicated and lengthy surgery, high risk of intestinal infection, the possibility of abnormal mucus secretion and possible effects of intestinal starvation.

1.7.2.3. Transit studies

Transit studies administer radiolabelled dosage forms to animal subjects, which are then sacrificed at set time-points, dissected and the radioactivity in individual tissue segments determined by scintillation. This technique may provide accurate information on the site of adhesion and is substantially cheaper than gamma scintigraphy, although animal wastage can be high. The targeted oral drug delivery of tomato lectins (Naisebett and Woodley, 1994 and 1995) and the gastrointestinal transit time of Carbopol 934P coated ^{99m}Te labelled ion resin particles (Smart and Kellaway, 1989) were investigated using this type of method.

1.7.2.4. Pharmacokinetic studies

In pharmacokinetic studies, a drug delivery device containing an active drug is given to an animal or human volunteer and the *in vivo* concentration of drug is measured. The rate at which drug appears in the physiological fluid is an indicator of the controlled drug delivery properties of the dosage form, which may be related to the bioadhesiveness of the dosage form but may be related to other phenomena. This method is expensive and requires complex analysis to measure drug concentrations in body fluids, but has been successfully used to study buccal drug delivery using

bioadhesive dosage forms (Bouckaert *et al*, 1993, Luessen *et al*, 1996, and Mumtaz *et al*, 1995, Illan *et al*, 1996).

1.8 Aims and objectives of the project

1.8.1. Development of methods to study the bioadhesion of sodium alginate matrices

The movement of water and the pattern of hydration inside a bioadhesive bond are factors thought to be important in the bioadhesion of hydrophilic matrices. A method to spatially resolve the diffusion and concentration of water inside a bioadhesive bond has yet to be developed. Therefore, the first aim of this project was to develop such a method using MRI to measure the concentration and SDC of water inside bioadhesive bonds formed by dry and hydrated alginate matrices.

The hydration state of a polymer can influence the tortuosity of the polymer network. This can be inferred and monitored from measuring the mobility of solutes in the polymer network. Therefore, a second aim of this project was to develop a FRAP method to measure the transport rates of FITC-dextrans inside bioadhesive bonds formed by dry and hydrated alginate matrices.

The discussion in this chapter indicated that various experimental factors and conditions may influence the observed bioadhesive bond strength of a polymer. Therefore, a third aim of this project was to investigate the influence of such factors on the observed bioadhesive bond strength of alginate matrices determined using a detachment force test.

1.8.2. The influence of some physicochemical factors on the bioadhesion of sodium alginate

The discussion in this chapter also indicated that the bioadhesion of a polymer may be influenced by some physicochemical factors. Therefore, a forth aim of this project was to use the methods developed above to study how molecular weight, M:G ratio and particle size influence the bioadhesion of dry and prehydrated alginate matrices. Liquid

uptake studies were also used to determine the influence of these factors on the hydration properties of alginate matrices.

Chapter 2

Characterisation of pig gastric mucus and sodium alginate

2.1. Introduction

The discussion in chapter 1 indicated that some physicochemical properties of the adhesive and mucus may influence bioadhesion and the properties of the bioadhesive bond. Therefore, the aim of this chapter was to characterise the properties of sodium alginate and pig gastric mucus.

2.2. Characterisation of sodium alginate

2.2.1. Physicochemical properties of sodium alginates

The aim of this section was to characterise the physicochemical properties of the sodium alginates used in the project.

Pronova Biopolymer (Drammen, Norway) provided data on the physicochemical properties and chemical composition of the sodium alginates. These are summarised in tables 2.1 and 2.2.

Table 2.1 Physicochemical properties of sodium alginates (data provided by Pronova Biopolymer)

Property	**Sodium alginate**				**Units**	**Test**
	LFR5/60	**SF120**	**SF/LF**	**LF120**		
Source	*Laminaria hyperborea*	*Laminaria hyperborea*	*Laminaria hyperborea*	*Lessonia nigrescens*	-	-
Viscosity	6.5	110	390	121	mPa	1% solution
Intrinsic viscosity	-	9.1	12.5	9.91	dl/g	-
Gel strength	-	71	-	27	g H_2O	FIRA
pH	6.8	7.2	6.1	7.3	-	1% solution
Ash content	-	-	0.02	-	%	Dry material content
Ca^{2+} content	-	0.02	-	0.19	%	-
Na^{+} content	-	9.23	-	9.63	%	-
Weight average	35,000	220,000	-	240,000	Da	-
Weight average	-	225,000	315,000	245,000	Da	Intrinsic viscosity
Poly-dispersity	-	2.5	-	2.7	-	-

Table 2.2 Block composition of sodium alginates (data provided by Pronova Biopolymer)

Polymeric blocks	**Sodium alginate**			
	LFR5/60	**SF120**	**SF/LF**	**LF120**
F_G	0.73	0.694	0.63	0.444
F_M	0.27	0.306	0.37	0.556
F_{GG}	0.61	0.552	0.58	0.258
F_{MM}	0.15	0.164	0.32	0.37
$F_{GM,MG}$	0.12	0.141	0.05	0.196
F_{GGG}	0.58	0.511	0.55	0.215
F_{GGM}	0.028	0.041	0.03	0.043
F_{MGM}	0.09	0.101	0.02	0.143
Average block length	(calculated using equations 1.1 to 1.4)			
N_G	6.1	4.9	12.6	2.3
$\bar{N}_M$	2.3	2.2	7.4	2.8
$\bar{N}_{G>1}$	22.9	14.5	20.3	7.0
$\bar{N}_{M>1}$	-	-	-	-

F is the frequency of polymeric blocks in the alginate determined by NMR spectroscopy, for example, F_{GG} is the frequency of GG blocks in the alginate.

Tables 2.1 and 2.2 show that LFR5/60, SF120 and SF/LF alginates have different molecular weights and viscosities but approximately the same guluronate content. The $\bar{N}_{G>1}$ value of SF120 is considerably lower than the $\bar{N}_{G>1}$ value of either LFR5/60 or SF/LF. The guluronate content of LF120 is lower than the other alginates, but its molecular weight and viscosity are approximately the same as SF120. The alginates used in this project were taken from single batches and are typical examples of commercially available sodium alginates.

For the purpose of this project, LFR5/60, SF120 and SF/LF were considered as high G alginates and LF120 as a low G alginate. LFR5/60, SF120 and SF/LF were used to investigate the influence of molecular weight on bioadhesion and LF120 and SF120 were used to study the influence of the M:G ratio on bioadhesion.

2.2.1.1. Method to determine the water content of sodium alginate

The BP 'Loss on Drying' method was used to determine the water content of sodium alginate. 0.1000g of sodium alginate was dried to a constant weight in an oven at 100°C to 105°C. The loss of mass was attributed to the evaporation of water from the alginate. Alginates kept at a constant 4°C in sealed containers were used as reference alginates to monitor the amount of water absorbed by the alginates during experimental manipulation.

Pronova Biopolymer provided data for the reference alginates and Reckitt & Colman Products (Hull, UK) provided data for the individual particle size fractions.

2.2.1.2. Results

Table 2.3 Water content of sodium alginates (data provided by Pronova Biopolymer and Reckitt & Colman Products)

Alginate		N	Water content (% w/w)
LFR5/60	Reference	-	13.5
	90-125 μm	2	13.4
SF120	Reference	-	9.0
	63-90 μm	2	10.0
	90-125 μm	2	10.5
SF/LF	Reference	-	13.2
	90-125 μm	2	13.6
LF120	Reference	-	9.4
	63-90 μm	2	8.9
	90-125 μm	2	9.7
	128-180 μm	2	9.1

The water content of experimentally used alginates and the respective reference alginate samples did not seem be different. SF120 and LF120 alginates contained ≈10% w/w water. LFR5/60 and SF/LF alginates contained ≈13% w/w water.

2.2.2. Particle size distribution of sodium alginates

Particle size is known to influence the hydration kinetics and gel forming properties of hydrophilic matrices (Alderman, 1984), which may subsequently influence the bioadhesive properties of alginate matrices. Therefore, the aim of this section was to characterise the particle size distributions of alginates.

2.2.2.1. Method

50.0 g of sodium alginate was shaken for 10 min in a nest of sieves (500 μm, 355 μm, 250 μm, 180 μm, 125 μm, 90 μm and 63 μm) and the cumulative percentage undersize distribution was determined.

2.2.2.2. Results

Table 2.4 Particle size distribution of sodium alginates determined by sieve analysis

Particle size (μm)	Cumulative percentage undersize			
	LFR5/60	**SF120**	**SF/LF**	**LF120**
500	-	-	99.82	-
355	99.97	99.95	99.81	99.90
250	99.78	99.88	97.73	99.69
180	89.63	99.80	60.34	99.45
125	64.92	99.09	26.53	57.68
90	42.99	42.37	7.15	42.72
63	26.54	1.75	1.38	22.33
0	0.00	0.00	0.00	0.00

The results in table 2.4 reveal that particle size distributions of the alginates were different, with the range of particle sizes being approximately ranked: SF/LF > LFR5/60 > LF120 > SF120. The different particle size ranges of the alginate may influence the properties of the matrices and their bioadhesive potential. Therefore, the 90-125 μm particle size fraction was used in future experiments studying the influence of molecular

weight and M:G ratio on bioadhesion. This fraction was chosen because each alginate could yield enough powder for matrix manufacture. The 63-90 μm, 90-125 μm and 125-180 μm particle size fractions of LF120 were used in future studies investigating the influence of particle size on bioadhesion.

2.2.3. Morphology of the sodium alginates

The shape of alginate particles may also influence the properties of the matrix, for example by affecting the porosity of a matrix, which may in turn influence the bioadhesive properties of the alginate matrices. Therefore, the aim of this section was to image and characterise the morphology of alginate particles by optical microscopy.

2.2.3.1 Method

Approximately 100 mg of sodium alginate was evenly dispersed on a microscope slide and transmission light micrographs were acquired using an inverted Nikon Optiphot microscope fitted with a x10 (NA 0.25) Nikon objective.

2.2.3.2. Results

Figures 2.1a, 2.1b and 2.1d-f show that LFR5/60, SF120 and LF120 particles used in this project were spheroidal and granular. In contrast, SF/LF particles were fibrous and may be up to 450 μm long (figure 2.1c). The micrographs of LF120 show that the 63-90μm, 90-125μm and the 125-180μm particles also contained a number of fines (figures 2.1d to 2.1f), but the origin and chemical composition of these fines could not be determined from the micrographs. The fines may be fragments that have been chipped off larger alginate particles during sieving or may be residues of the manufacturing process. The number of fines in the fractions seemed to increase as particle size increased.

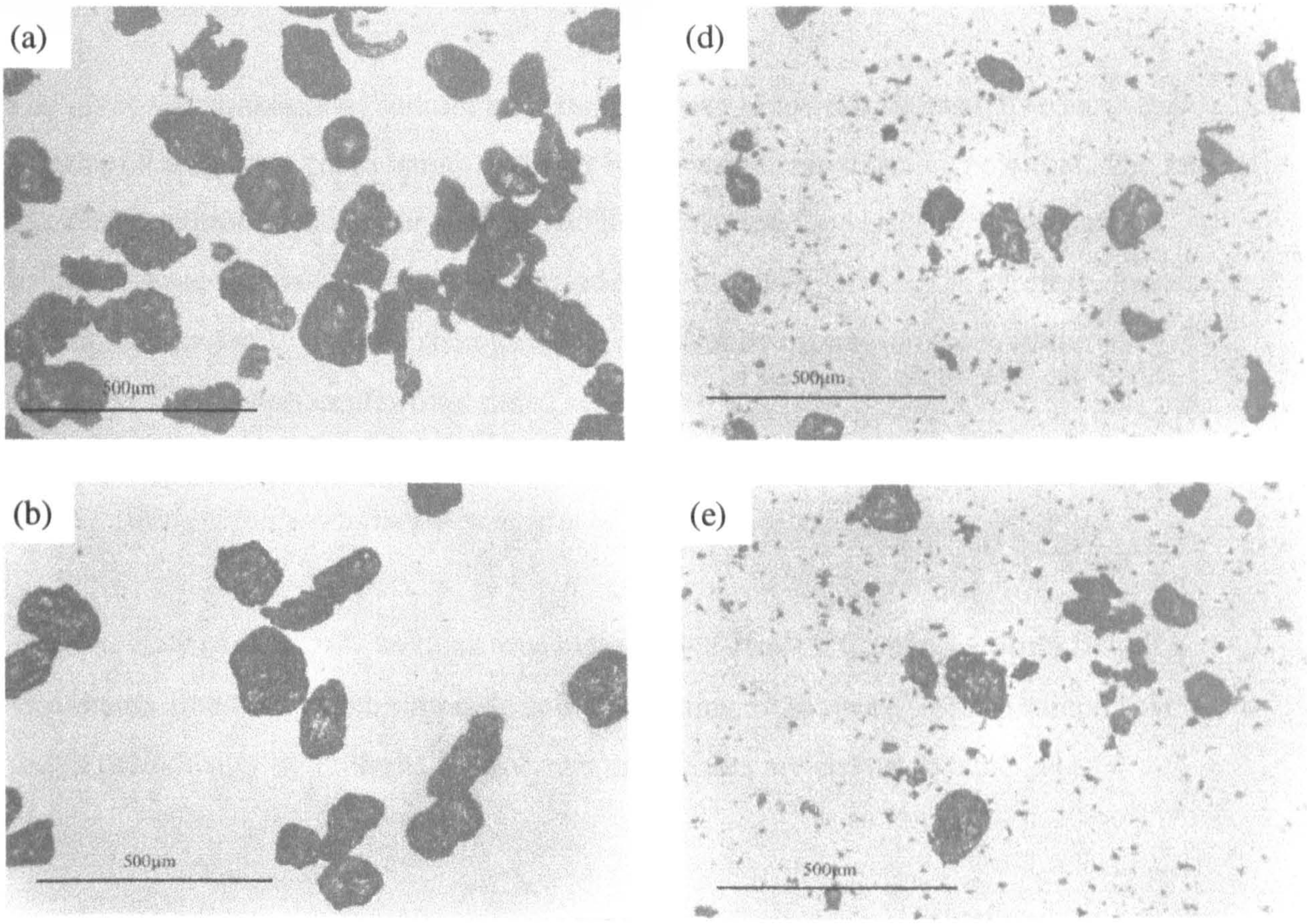

Figure 2.1 Optical micrographs of sodium alginates

(a) LFR5/60 (90-125 µm), (b) SF120 (90-125 µm), (c) SF/LF (90-125 µm), (d) LF120 (63-90 µm), (e) LF120 (90-125 µm) and (f) LF120 (125-180 µm).

2.2.4. Storage and stability of sodium alginate

The glycosidic linkages of sodium alginate are prone to hydrolysis, which reduces the length of the alginate chain length and may influence the bioadhesive potential. The rate of alginate degradation may be determined by measuring the viscosity of alginate solutions since viscosity is related to chain length in linear polymers. Therefore, the aim of this section was to monitor the rate of degradation by measuring the solution viscosity of alginate samples over time.

2.2.4.1. Method to determine the viscosity of alginate solutions

The viscosity of a 1% w/v solution was measured at 20±0.5°C, using a Brookfield RV viscometer fitted with an appropriate spindle rotating at 20 rpm. Alginate samples were tested periodically by Pronova Biopolymer and results are shown in table 2.4.

2.2.4.2. Results

Table 2.4 Solution viscosity of sodium alginates (data provided by Pronova Biopolymer)

Alginate		1% w/v solution viscosity (cp)			
		0 month	17 months	18 months	34 months
LFR5/60	Reference	6.5	-	6.5	4.3
	90-125 µm	-	-	-	4.1
SF120	Reference	110	-	105	95
	Bulk[a]	-	-	94	-
	63-90 µm	-	-	89	84
	90-125 µm	-	-	98	94
SF/LF	Reference	390	410	406	-
	90-125 µm	-	-	-	-
LF120	Reference	121	106	-	107
	Bulk[a]	-	90	-	-
	63-90 µm	-	-	-	108
	90-125 µm	-	-	-	92
	125-180 µm	-	-	-	92

[a] Bulk alginates have not been separated into particle size fractions.

Table 2.4 shows that the solution viscosity of reference alginates and alginate samples decreased over a period of 34 months. The viscosities of the reference alginates decreased by ≈10% of their original value over the time period and differed from the alginate samples by no more than 10%.

2.2.5. Determination of a suitable matrix manufacturing compression pressure

The aim of this section was to obtain compression-hardness profiles of SF120 and LF120, which would be used to chose a suitable compression force to manufacture alginate matrices for future studies.

2.2.5.1. Method

10 mm diameter circular flat face sodium alginate matrices were manufactured from 90-125μm particles of SF120 and LF120 on a Manesty F3 tablet press fitted with tablet compression monitor model TCM1 (Copley Instruments Ltd, Nottingham). The matrices were compressed using different upper punch compression pressures. The diametrical crushing strengths of five matrices at each compression pressure were determined using a CT-40 hardness tester (CT-40 Engineering Systems, Nottingham) to obtain a compression/hardness profile.

2.2.5.2. Results

Figure 2.2 shows the compression-hardness profiles of SF120 and LF120. The linear sections of the profiles were between 243-721 mPa for SF120 and 351-1190 mPa for LF120. The linearity of the relationship indicates that matrix crushing strength is directly proportional to the log of compression pressure. Matrices could not be manufactured at pressures greater than 721 mPa for SF120 and 1190 mPa for LF120 without damaging the compression tooling. Therefore, a compression pressure of 400-410 mPa was used to manufacture sodium alginate matrices for future studies. This value is the approximate median compression pressure for both linear sections.

2.2.6. Surface characterisation of sodium alginate matrices

The surface characteristics of alginate matrices may affect how alginate forms an intimate contact with mucus and may subsequently affect the mechanisms of bioadhesion as well as the properties of the bioadhesive bond. Therefore, the aim of this section was to image and characterise the surfaces of both dry and hydrated alginate matrices using scanning electron microscopy (SEM).

2.2.6.1. Principles of scanning electron microscopy

SEM uses a focused stream of electrons to image the surface of the sample. The stream of electrons is generated by an electron gun and accelerated towards an anode by using a differential potential of 1-50 keV. The stream is focused to a 5-50 nm spot using three

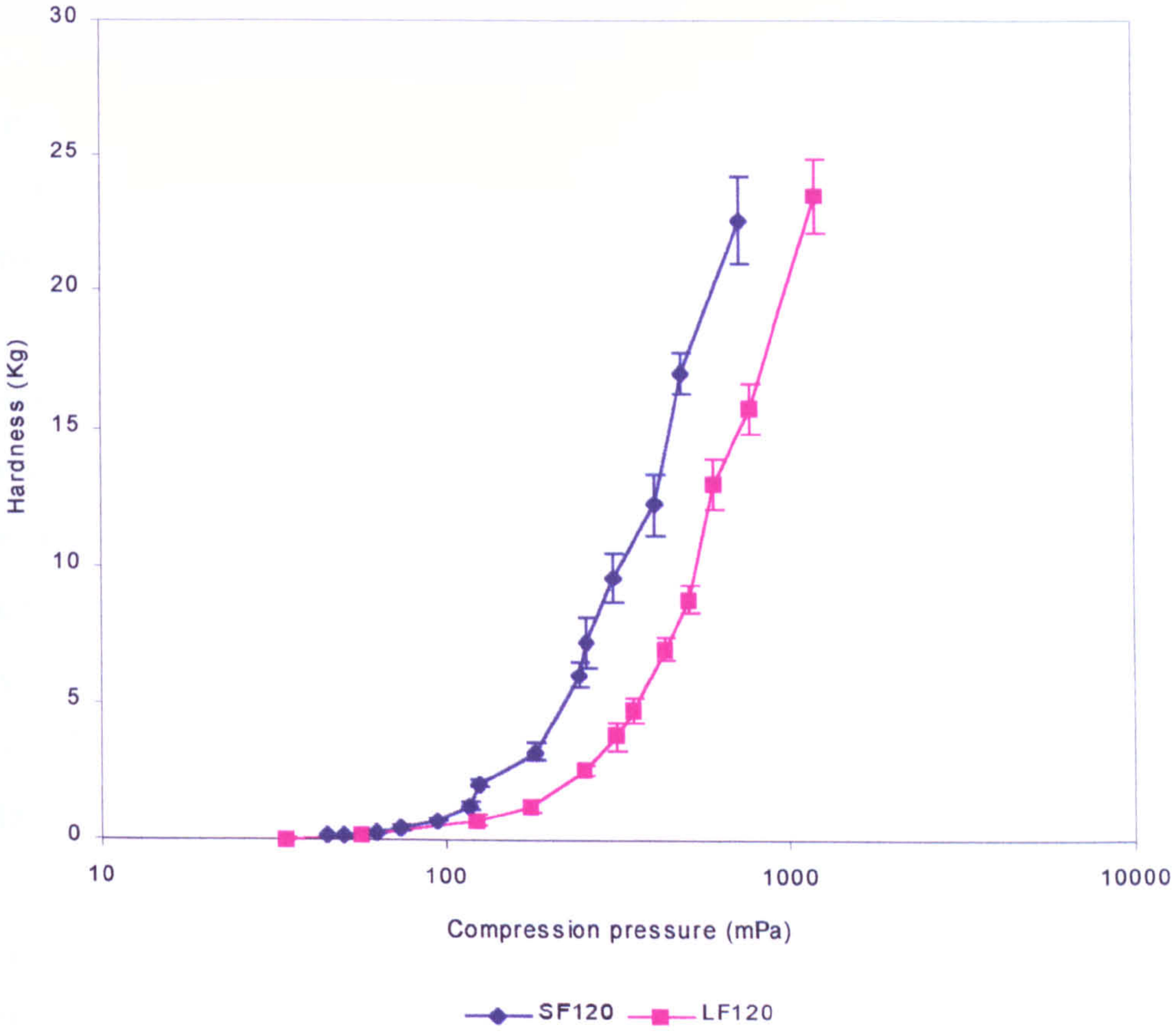

Figure 2.2 Compression pressure-hardness profile of sodium alginate matrices.

The compression-hardness profile of 10 mm diameter circular, flat face matrices manufactured from 90-125 μm particles of SF120 and LF120 (mean, n=5, ± 1 SD).

sets of negatively charged electron lenses and raster scanned across the specimen. This causes electrons to be generated from the sample, which are then collected by a positively charged electron detector, producing an image of the sample surface. Since the stream of electrons do not travel far in air, the entire imaging process has to be performed under vacuum.

Hydrated samples can be imaged using cryo-SEM, which uses the same principles as conventional SEM. The technique rapidly freezes the sample to -180°C and then slowly heats it to approximately -80°C under vacuum, which sublimes and removes any surface water. Although, ice formation is inevitable in thick specimens, the rapid freezing process has the advantages that dynamic processes are immobilised and ice crystal growth is minimised, preventing damage to fine structures in the sample (Sargent, 1988).

2.2.6.2. Method to characterise surfaces of dry matrices using scanning electron microscopy

10 mm diameter, circular flat face sodium alginate matrices were manufactured using a standard compression force of 400-410 mPa. The lower surface of a matrix was attached to a sample stub using carbon paste and then coated with gold in a stream of argon for 4-6 mins, using a Balzer SCD030 sputter coater, to prevent surface charging. Matrices were imaged using a Phillips 505 SEM at an applied accelerated voltage of 25.0 keV and a spot size of 20 nm.

2.2.6.3. Results

Figures 2.3a to 2.3f show micrographs (78x magnification) of the dry surface of sodium alginate matrices. Figures 2.4a to 2.4f show the same samples at a higher magnification (312x magnification). The matrices illustrated in the figures are typical examples of matrices used in this project.

The surfaces of LFR5/60 and SF120 matrices (figures 2.3a and 2.3b) appeared to be similar and reflected the shape of the particles. SF120 matrices appeared to be more

porous than LFR5/60. The surfaces of SF/LF matrices (figure 2.3c) reflected the fibrous nature of the alginate particles. The surfaces of LF120 matrices (figures 2.3d to 2.3f) are similar to those of LFR5/60 and SF120, except that the matrices seem to contain a number of fines. The proportion of fines appeared to increase as particle size increased. Also, LF120 matrices manufactured from 90-125 μm particles appeared to be more porous than matrices manufactured from either 63-90 μm or 125-180 μm particles and LFR5/60 and SF120 matrices.

Increasing the magnification provides more detail on the structures observed in figures 2.3a to 2.3f. The surfaces of LFR5/60 and SF120 (figures 2.4a and 2.4b) seem to have large inter-particulate pores. In comparison, SF/LF matrices (figure 2.4c) tend to have smaller intra- and inter-particulate crevices. Figures 2.4d to 2.4f show that the fines are closely associated with particles of LF120. The origin of these fines has been discussed previously in section 2.2.3.2 and it is unlikely that are formed during matrix manufacture. The higher magnification shows that LF120 matrices manufactured from 90-125 μm particles have larger inter-particulate pores than those manufactured from either 63-90 μm or 125-180 μm particles.

2.2.6.4. Method to characterise surfaces of hydrated matrices using cryogenic scanning electron microscopy

The viscous alginate gel layers of hydrated matrices were characterised according to the method of Hodson *et al*, 1994. The lower punch surface of a 10 mm diameter, circular flat face sodium alginate matrix, manufactured by compression at 400-410 mPa, was attached to a sample stub, using carbon paste, and hydrated in physiological saline at 37±1°C for 10 mins. Excess saline was removed without disturbing the gel layer, and the matrices rapidly cooled in nitrogen slush at -180°C. Frozen samples were transferred, under vacuum to prevent frost formation, to the cryo-preparation chamber (-180°C) (Hexland CT 1000A) and freeze fractured using a cold knife. Etching of the surface (-90°C) to remove any unbound surface water was carried out on the electrically heated main stage of a Phillips 505 SEM. The samples were then coated in the cryo-preparation chamber with gold in a stream of argon for 4-6 mins. Maintaining the

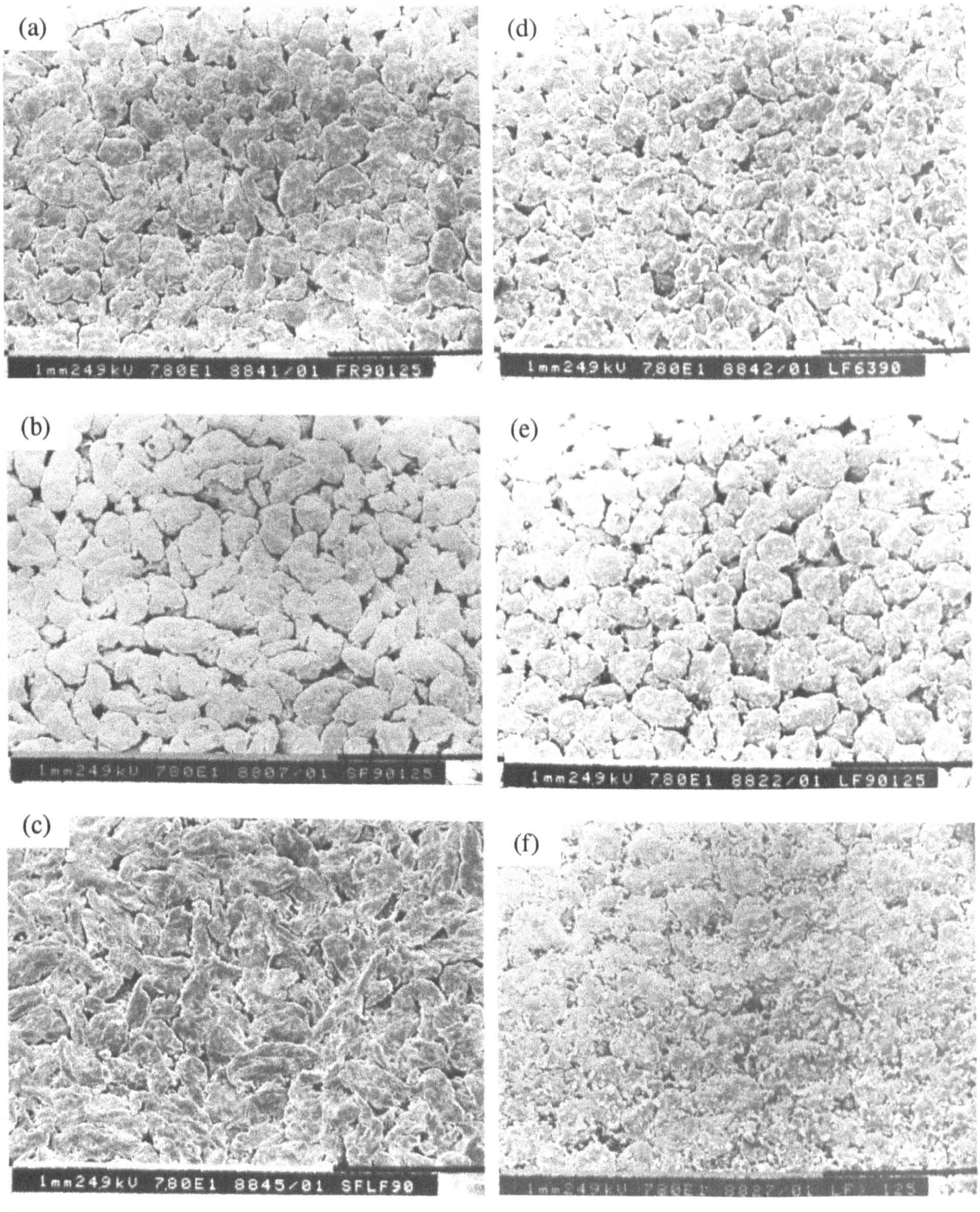

Figure 2.3 Scanning electron micrographs (78.0x magnification) of the upper surfaces of dry alginate matrices

(a) LFR5/60 (90-125 µm), (b) SF120 (90-125 µm), (c) SF/LF (90-125 µm), (d) LF120 (63-90 µm), (e) LF120 (90-125 µm) and (f) LF120 (125-180 µm).

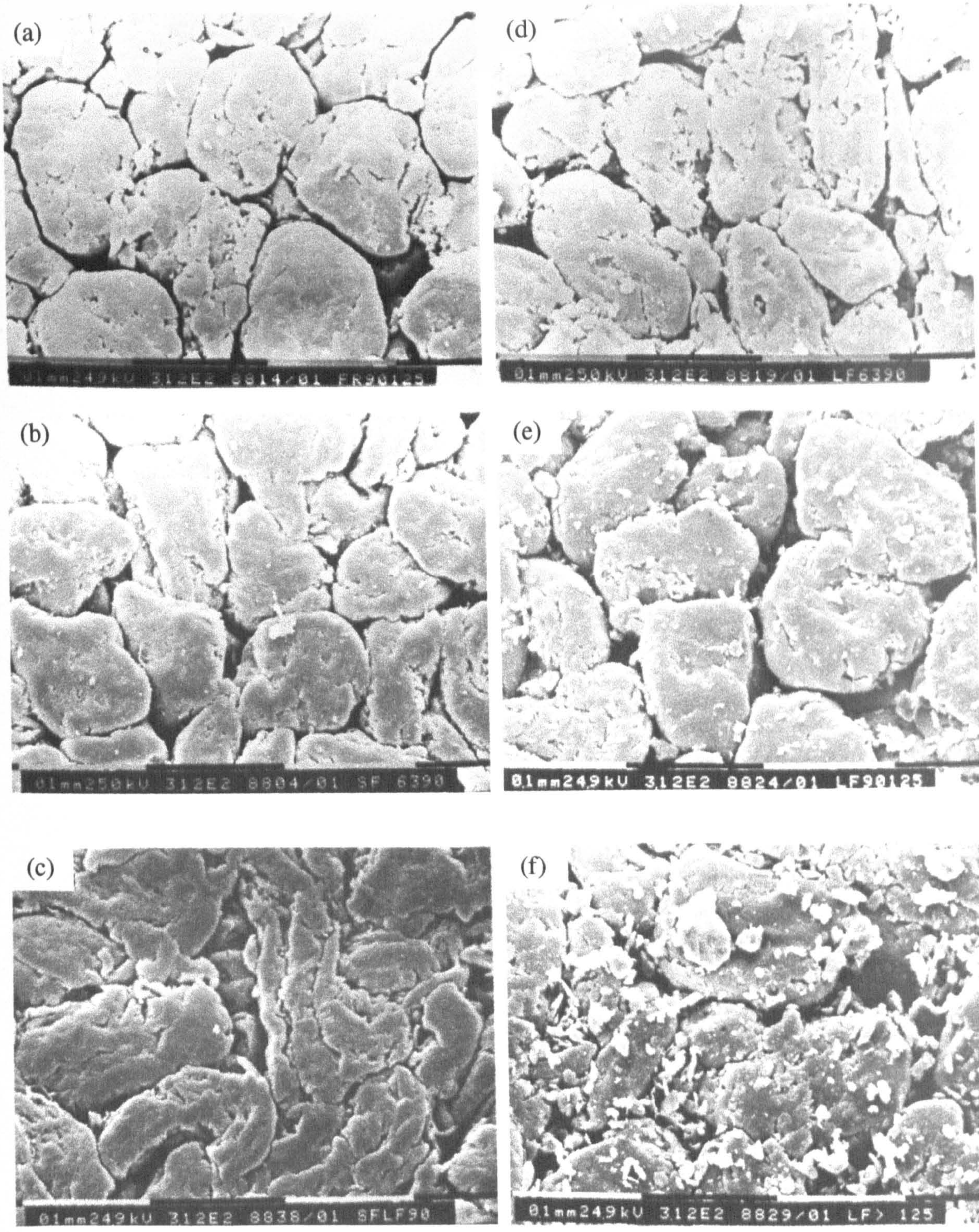

Figure 2.4 Scanning electron micrographs (312x magnification) of upper surfaces of dry alginate matrices

(a) LFR5/60 (90-125 μm), (b) SF120 (90-125 μm), (c) SF/LF (90-125 μm), (d) LF120 (63-90 μm), (e) LF120 (90-125 μm) and (f) LF120 (125-180 μm).

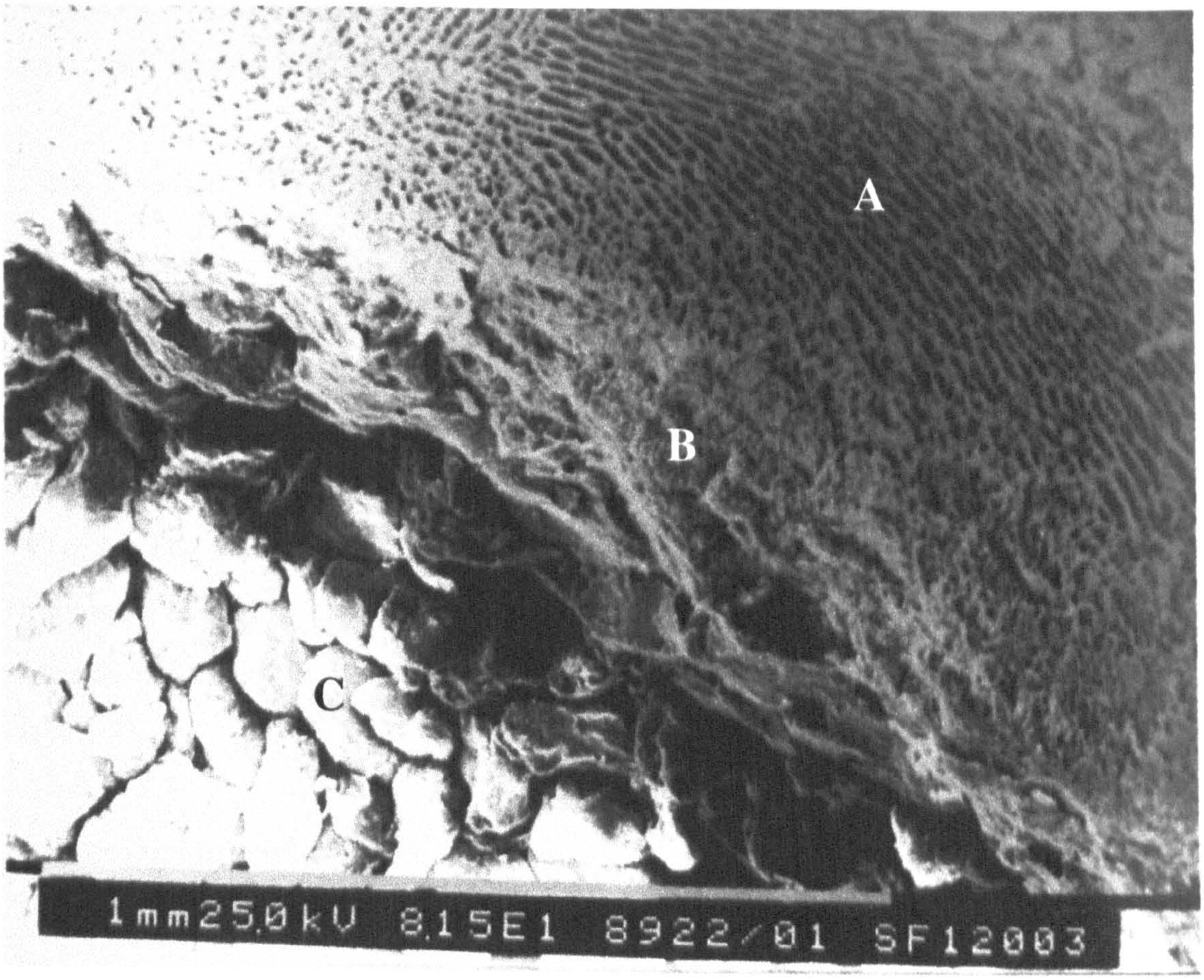

Figure 2.5 A scanning electron micrograph of a typical viscous alginate gel layer.

A 220,000 Da sodium alginate matrix prehydrated in physiological saline at 37±1°C for 10 mins, frozen in nitrogen slush and freeze fractured using a cold knife: A – extensively hydrated outer viscous gel layer; B – poorly hydrated inner gel layer; C – dry matrix core.

samples at -180°C, images were obtained using an applied accelerated voltage of 25.0 keV and a spot size of 20 nm.

2.2.6.5. Results

The micrographs of prehydrated matrices did not reveal any significant differences in the viscous gel layers formed by different alginates. Figure 2.5 shows a hydrated outer gel layer and an inner dry core of a SF120 matrix. This is a typical example of an alginate viscous gel layer that has been hydrated in physiological saline at 37±1°C for 10 mins. The micrographs show that there is extensive ice crystal formation in the outer regions of the gel layer, which indicates a high level of hydration. Unfortunately, the growth of ice crystals may have also destroyed the finer structures in the viscous gel layer.

Adjacent to this highly hydrated gel layer, is a less extensive, poorly hydrated inner gel layer, which is adjacent to the dry matrix core. The structure of the viscous alginate gel layer agrees with previous work carried out by Hodson *et al*, 1995, who imaged the structure of alginate matrices that had been hydrated in simulated intestinal fluid.

2.2.7. Discussion

2.2.7.1. Properties of alginate molecules

The sodium alginates used in this project had different M:G ratios, molecular weights and solution viscosities. Molecular weight and solution viscosity of the alginates can be ranked: LFR5/60 << SF120 ≈ LF120 < SF/LF (table 2.1). The ranking of molecular weight and viscosity are similar because the viscosity of a polymer solution is scaled to its molecular weight (Florence and Attwood, 1988). The general influence of molecular weight on bioadhesion has been discussed at length in section 1.5.1.

The proportion of mannuronate and guluronate residues in the alginates was also different, with LFR5/60, SF120 and SF/LF having relatively high guluronate content (>63%) compared to LF120 (44.4%) (table 2.2). Rotation about the diaxial glycosidic

linkages in polyguluronate blocks is sterically hindered (Pronova), which affects the flexibility of the alginate chains (Mitchell and Blanshard, 1976, and Smidsrod and Draget, 1996). Subsequently, the ability of alginate chains to interpenetrate and entangle with mucus gel network may be affected. Differences in the flexibility of alginate chains may also partly account for differences in the solution viscosity.

Analysis of the high G alginates (LFR5/60, SF120 and SF/LF) revealed that the average polyguluronate block length ($N_{G>1}$) of LFR5/60 and SL/LF were similar, but the $\bar{N}_{G>1}$ value of SF120 was considerably lower (table 2.2). The $\bar{N}_{G>1}$ value of LF120 is predictably lower than $\bar{N}_{G>1}$ of the high G alginates. The average length of polyguluronate may also influence the flexibility of alginate chains, with longer polyguluronate blocks being less flexible than shorter polyguluronate blocks. This may influence their ability to interpenetrate the mucus gel network.

The particle size distributions of the alginates were also different (table 2.4), with SF/LF having the widest distribution and SF120 having the narrowest distribution. The shapes of the particles were also different. Particle size and shape are known to influence the hydration kinetics of hydrophilic polymers and matrices, with larger particles hydrating more slowly than smaller particles (Alderman, 1984). These differences may influence the degree to which the alginate matrices hydrate and may also influence their ability to dehydrate the mucus layer. Dehydration of the mucus gel layer as a result of polymer hydration has been suggested as a possible mechanism of bioadhesion (Mortazavi and Smart, 1993).

Furthermore, the chains of hydrated alginate may be more flexible than chains of dry alginate, thus facilitating interpenetration into mucus gel network. Also, more adhesive chemical groups will be exposed on hydrated polymer chains than on dry polymer chains, increasing the bioadhesive interaction between polymer and mucus (Ahuja *et al*, 1997).

Consequently, 90-125 μm particles of LFR5/60, SF120, and SF/LF were used to study the influence of molecular weight on the bioadhesion of sodium alginate. Likewise, 90-125 μm particles of SF120 and LF120 were used to study the effect of M:G ratio on alginate bioadhesion. The 63-90 μm, 90-125 μm and 125-180 μm particle size fractions

of LF120 were used to study how particle size influences the bioadhesive bond strength of alginates.

The sodium alginates used in this project are commercially available, although the range used here is not comprehensive. Higher molecular weight alginates (for example, Protanal HF (Pronova)) and lower G content alginates (for example, *Durveilla antartica* and *Ascophyllum nodosum* (Cotrell and Kovacs, 1980, and Clare, 1993)) are commercially available.

2.2.7.2. Stability of alginates

The solution viscosity of each alginate sample decreased by no more than 20% of the original viscosity of its reference alginate over 34 months (table 2.4), which suggests that molecular weight and polymer chain length of alginates decrease during the project. The general influence of polymer chain length and molecular weight on bioadhesive potential of polymers has been discussed previously (section 1.5.1).

This level of degradation is acceptable because the alginates still remain comparatively different throughout the duration of the project. For example, a sample of SF120 at 34 months would still have a considerably higher molecular weight than a sample of LFR5/60 at 0 month. The level of alginate degradation also satisfies stability criteria supplied by Pronova Biopolymer. This states that the solution viscosity of alginate must decrease by no more than 25% of its original value.

Alginates are regularly removed from storage at 4°C and equilibrated to room temperature (≈22°C) before they are used. Condensation as they are equilibrated to room temperature may increase the rate of alginate hydrolysis and affect alginate degradation. However, the water contents of reference and sample alginates were not different (table 2.3), suggesting that condensation during equilibration did not influence alginate degradation.

2.2.7.3. Characterisation of dry and hydrated alginate matrices

The SEM micrographs of alginate matrix surfaces showed that alginate matrices were porous and suggested that the matrices may have different porosities (figures 2.3 and 2.4). Generally, matrices of LFR5/60, SF120 and LF120 alginates tend to reflect the granular and spheriodal shape of the particles (figure 2.1), resulting in large intragranular pores. In comparison, particles of SF/LF tend to be fibrous (figure 2.1), resulting in matrices with a large number of small intra- and intergranular pores. The porosity of an alginate matrix may influence the hydration properties of an alginate matrix and may influence ability of alginate matrices to dehydrate the mucus layer.

The SEM micrographs also showed that LF120 matrices appeared to contain a number of fines, which may have been produced during sieving or may be residues from the alginate manufacturing process. These fines are also present in the alginate powders (figure 2.1). The fines may influence the hydration properties of the alginate matrices and their ability to dehydrate the mucus gel layer. Wan *et al*, 1986 carried out a study to show that 50% w/w fines in rapidly disintegrating Phenacetin tablets interfered with the uptake of hydrating fluid. However, rapidly disintegrating tablets and hydrophilic matrices are dissimilar.

Micrographs of prehydrated matrices (figure 2.5) did not show any significant differences between different alginates. Little morphology was revealed except that micrographs showed extensive ice crystal formation in the outer gel layer, indicating high levels of hydration. In comparison, the alginate gel next to the dry core appeared to be less hydrated. The general structure of the viscous gel layers was similar to that of SIF hydrated alginate matrices, as previously reported by Hodson *et al*, 1995.

The extensive hydration suggests that the alginate structure in the outer gel layer will be highly expanded and may facilitate polymer interpenetration. In contrast, the extensive hydration of the outer region may have reduced the cohesiveness of the alginate gel, resulting in the formation of a slippery mucilage, which may be easily sheared.

2.2.8. Conclusions

The range of alginates used in this study had different molecular weights, M:G ratios and particle size distributions. The molecular weight and M:G ratio may influence the ability of alginate molecules to interpenetrate and chemically interact with the mucus gel network. Particle size may influence the hydration kinetics of alginates and of the matrices, which may affect the matrices' ability to dehydrate the mucus gel.

Subsequently, 90-125 μm particles of LFR5/60, SF120 and SF/LF were used to study the relationship between molecular weight and bioadhesion and 90-125 μm particles of SF120 and LF120 were used to study the influence of M:G ratio on bioadhesion. The 63-90 μm, 90-125 μm and 125-180 μm particles of LF120 were used to study how particle size affects alginate bioadhesion.

SEM micrographs showed that the dry alginate matrices were porous and that the matrices may have different porosities. This may influence the hydration kinetics of the matrices, which may in turn influence their ability to dehydrate the mucus gel. SEM micrographs of hydrated alginate matrices showed little difference between the matrices. The alginate structure in the outer gel layer is highly expanded, suggesting that polymer interpenetration may be a possible bioadhesive mechanism.

2.4. Characterisation of pig gastric mucus

2.4.1. Rationale

Studies have shown that mucin can significantly influence the bioadhesion of some polymers (Rossi *et al*, 1995). Other studies (Kocevar-Nared *et al*, 1997, and Madsen *et al*, 1996) have shown that the properties of commercially available mucins, for example Sigma mucins, show little similarity to the properties of native mucus. The handling and treatment of mucus have also been shown to affect the rheological properties of mucus (Madsen *et al*, 1996) and the bioadhesive potential of polymers (Rossi *et al*, 1995). Therefore, the aim of this section was to characterise the properties of mucus used in this project.

2.4.2. Method to harvest and solubilise pig gastric mucus

Freshly slaughtered pig stomachs were opened, contents evacuated and the mucus surfaces gently rinsed with cold water to remove embedded debris. Gel layers were carefully scraped from mucosae using a microscope slide and collected in ice-cooled aqueous proteinase inhibitor buffer. The contents of the buffer are listed in table 2.5. The buffered scrapings were homogenised for one minute at full speed in a Waring B10 blender. The time between collection and solubilisation of native mucus in proteinase inhibitor buffer was maximally one hour.

The resultant mucus 'soup' was centrifuged at $6x10^3$ g at 4°C for 60 mins and the clear yellow-brown soluble mucus solution was decanted over glass wool to remove tissue debris and insoluble material. This was stored at 4°C prior to further purification.

Table 2.5 Contents of aqueous proteinase inhibitor buffer

Chemical	Quantity	Inhibitory action/use
Sodium hydrogenphosphate	67 mM	pH buffer, pepsin
Potassium hydrogenphosphate	67 mM	pH buffer, pepsin
α-aminocaproic acid	100 mM	Plasminogen → plasmin
EDTA	10 mM	Metal dependent proteinases
Iodoacetamide	1 mM	Thiol dependent proteinases e.g. cathepsin B
Benzamidine hydrochloride	5 mM	Trypsin and trypsin-like enzymes
N-ethylmaleiamide	10 mM	Endonucleases and dehydrogenases
Phenylmethylsulphonylfluoride	3 mM	Serine proteases e.g. elastase

2.4.3. Method to purify mucus glycoprotein using a caesium chloride equilibrium density gradient

The mucus solution obtained in section 2.4.2 was adjusted to a density of 1.42 g ml^{-1}, by adding either solid caesium chloride or deionised and distilled water. The mucus solution was then ultra-centrifuged in 35 ml capacity polyallomer tubes at $1.5x10^5$ g at

4°C for 48 hours. The density gradients were separated into nine equal volume fractions, which were then pooled. The concentrations of protein, amino acids and glycoprotein in each pooled fraction were determined. The fractions containing high concentrations of glycoprotein and low concentrations of nucleic acid and protein (typically fractions 4 to 8) were collectively pooled for further purification (Allen, 1998).

Fractions containing mucin tend to have densities between 1.4 g ml^{-1} and 1.6 g ml^{-1}. Those fractions containing soluble proteins tend to have densities below 1.3 g ml^{-1}, whilst those containing nucleic acids tend to have densities greater than 1.6 g ml^{-1} (Knight, 1997, and Harding, 1989).

Mucins also have a low conjugated amino acid content and as a result 280 nm absorbance measurements can be used to determine the concentration of protein with little interference from glycoprotein (Hutton, 1991, and Mantle and Allen, 1978). The concentration of nucleic acids can be determined by ratioing the absorbances at 280 nm and 260 nm (Warburg and Christian, 1942).

Each pooled fraction was also exhaustively dialysed against distilled and deionised water to remove caesium chloride and then assayed, using a periodic acid-Schiff's base (PAS) assay to determine mucin content (Mantle and Allen, 1978).

2.4.3.1. Results

Figure 2.6a shows that fractions 4 to 9 had densities between 1.4g ml^{-1} and 1.6g ml^{-1}, indicating a high glycoprotein content. The PAS assay for mucus glycoprotein (shown in figure 2.7b) revealed that fractions 4 to 8 have at least 372 mg glycoprotein per fraction compared with up to 131 mg glycoprotein per fraction in fractions 1, 2, 3 and 9. Figure 2.6b shows that fractions 1, 2, 3, 4 and 9 have higher concentrations of protein and nucleic acid than fractions 5-8. Protein and nucleic acids may interfere with gel formation and the network structure of mucin. These results are typical of partially purified pig gastric mucus.

(a)

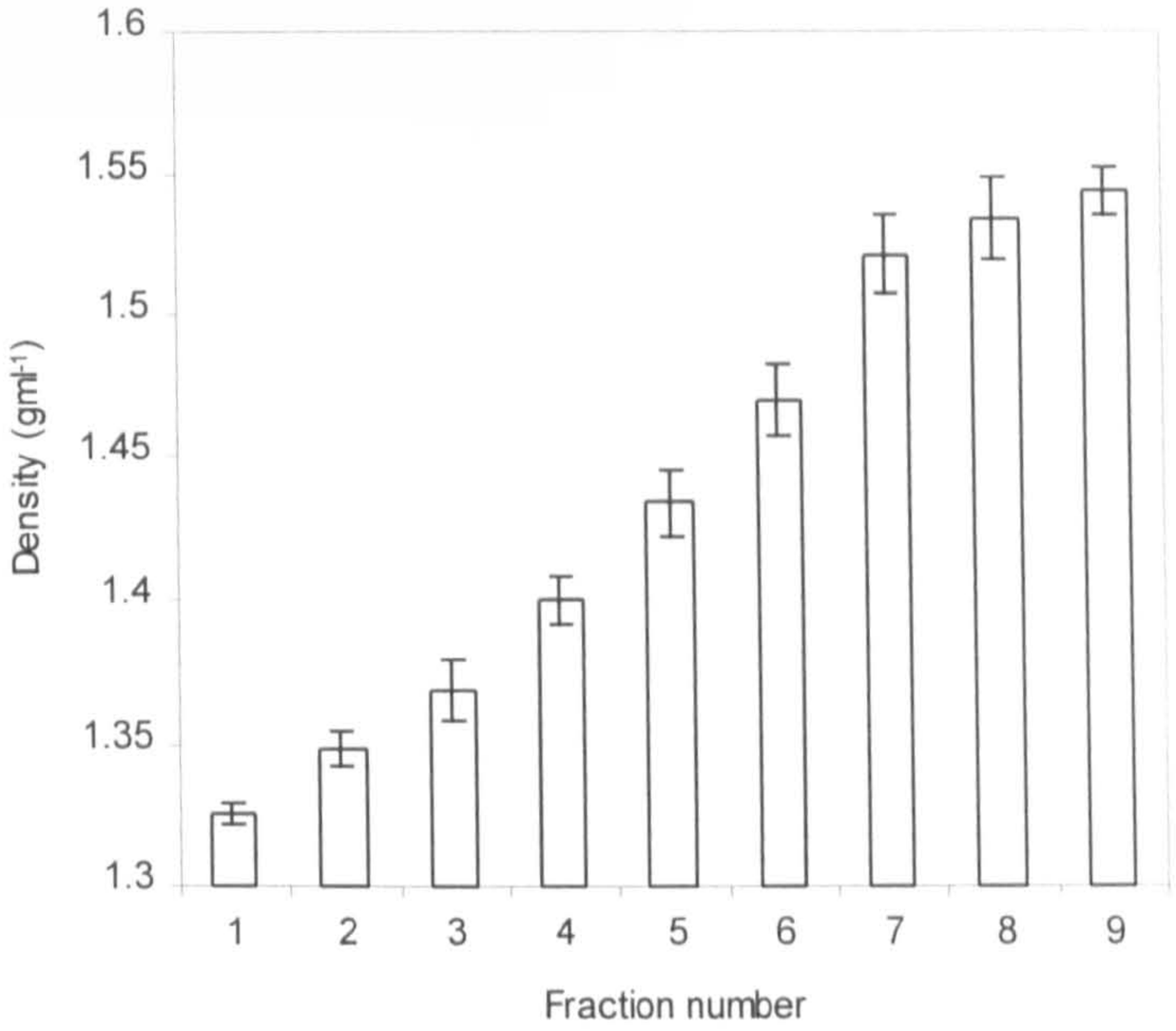

(b)

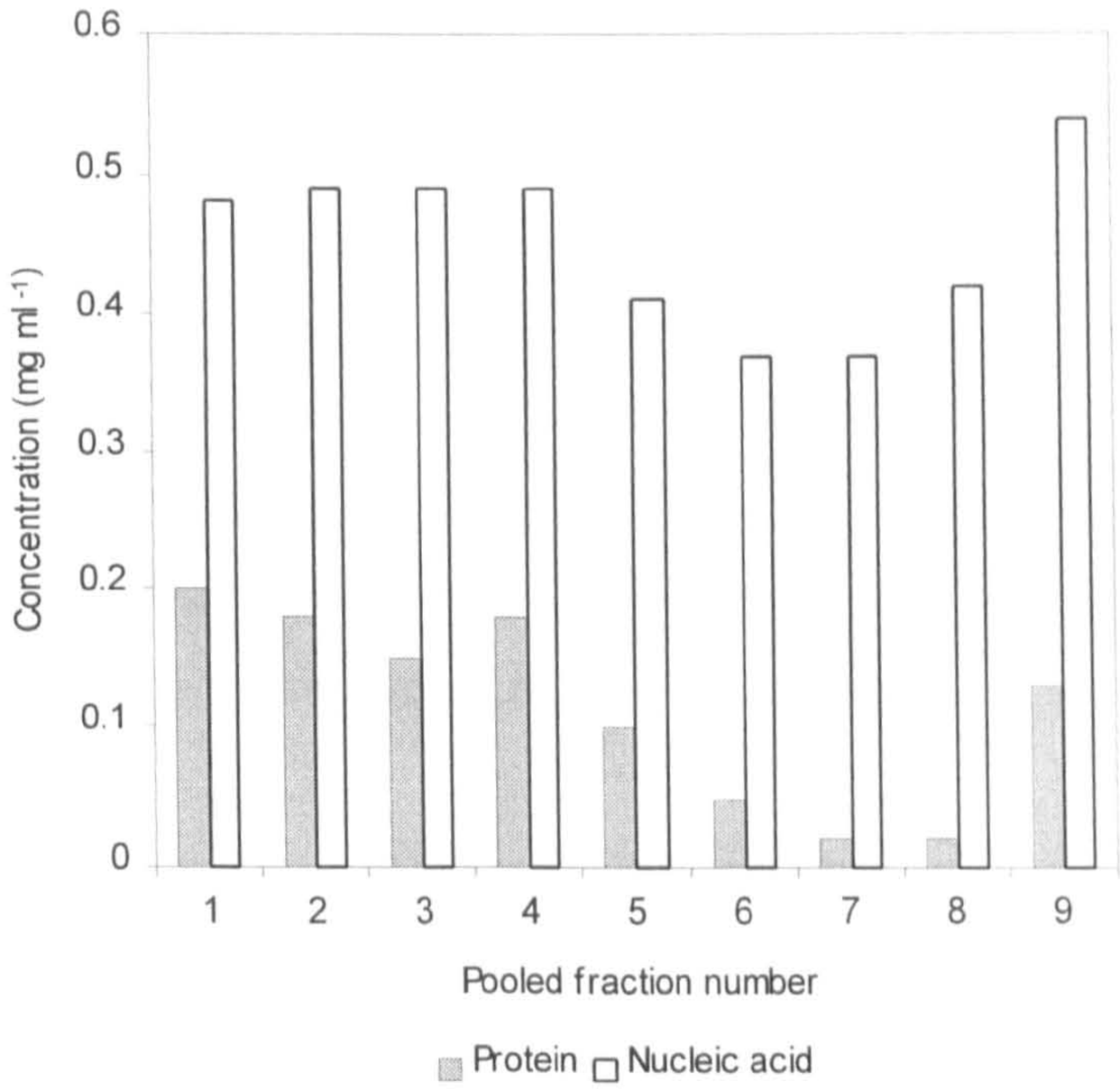

Figure 2.6 (a) Density of the pooled fractions of soluble mucus (mean, n=3, ±1 SD). (b) Concentration of protein and nucleic acid in the pooled fractions of soluble mucus (n=1).

From these results, fractions 4 to 8 were pooled for further purification. These fractions contained the highest content of glycoprotein and the lowest concentration of protein and nucleic acid.

2.4.4. Method to produce mucus gel using vacuum dialysis

The pooled glycoprotein solution obtained in section 2.4.3 was exhaustively dialysed against physiological saline for 24 hr and then vacuum dialysed using a 14 kDa membrane to obtain ≈50 mg ml^{-1} glycoprotein gel (Bell, 1983). The mucus gel was stored at minus 20°C in an airtight container and defrosted overnight at 4°C and equilibrated to room temperature for at least 2 hours before use.

2.4.5. Method to prepare Sigma mucin solution

Freeze-dried partially purified pig gastric mucin (Sigma type III mucin) was slowly dissolved in physiological saline at 4°C to obtain a 190 mg ml^{-1} homogenous solution. Solutions of this concentration appeared to be visually similar to purified gastric mucus.

In FRAP studies, FITC-dextrans were dissolved in the mucin solution to obtain a FITC concentration equivalent to 0.01% w/v sodium fluorescein. Sigma mucin solutions were stored and treated in the same way as purified pig mucus.

2.4.6. Characterisation of purified pig gastric mucus and Sigma mucin solution

2.4.6.1. Method to measure glycoprotein content

A modified periodic acid-Schiff's base (PAS) assay was used to determine the glycoprotein content of purified pig mucus (Mantle and Allen, 1978). Schiff's reagent was prepared by adding 1 g of basic fuchsin to 100 ml of boiling water and cooling to 50°C. 20 ml of 1M hydrochloric acid was added and the solution decolourised with 2 x 300 mg activated charcoal. The mixture was filtered through a celite pad to remove charcoal and produce a deep red solution, which was stored in the dark. Prior to use, 0.1 g of sodium metabisulphite was added to every 6 ml of Schiff's reagent required and

incubated at 37°C for 90 mins until the solution turned pale yellow. A 1% w/v periodic acid solution was prepared by adding 10 µl of 50% w/v periodic acid solution to 10 ml of 7% w/v acetic acid.

0.2 ml aliquots of freshly prepared 1% w/v periodic acid solution were added to dilute mucin solutions in 0.2M sodium chloride and 0.02% w/v sodium azide. Periodate-mucin solutions were then incubated for 60 mins before 0.2 ml aliquots of Schiff's reagent were added. The solutions were allowed to stand at room temperature for 30 mins before the absorbance at 555 nm was measured.

2.4.6.2. Method to determine the concentration:absorbance plot for PAS stained mucus glycoprotein

Standard mucin solutions were used to obtain a concentration:absorbance plot for the PAS stained mucin. A stock glycoprotein solution was prepared by mixing a 1:100 w/w ratio of papain/Sigma type III mucin for 48 hours at 60°C in a buffer containing 67 mM sodium phosphate, 5 mM cysteine hydrochloride and 5 mM EDTA. This ensured complete proteolytic digestion of the mucin. Standard solutions were prepared by appropriately diluting the stock mucin solution and were then PAS stained according to section 2.4.6.1.

2.4.6.2.1. Results

A concentration:absorbance plot for PAS stained mucus glycoprotein is shown in figure 2.7a. This was used as a calibration curve for the PAS assay.

2.4.6.3. Method to determine the content of polymeric glycoprotein by size exclusion chromatography.

A 400 x 15 mm glass column was filled with Sepharose 2B gel to produce a 250 x 15 mm gel column. The flow characteristics, excluded and included volumes were determined using a calibration solution containing 0.1% w/v dextran blue (measures the

(a)

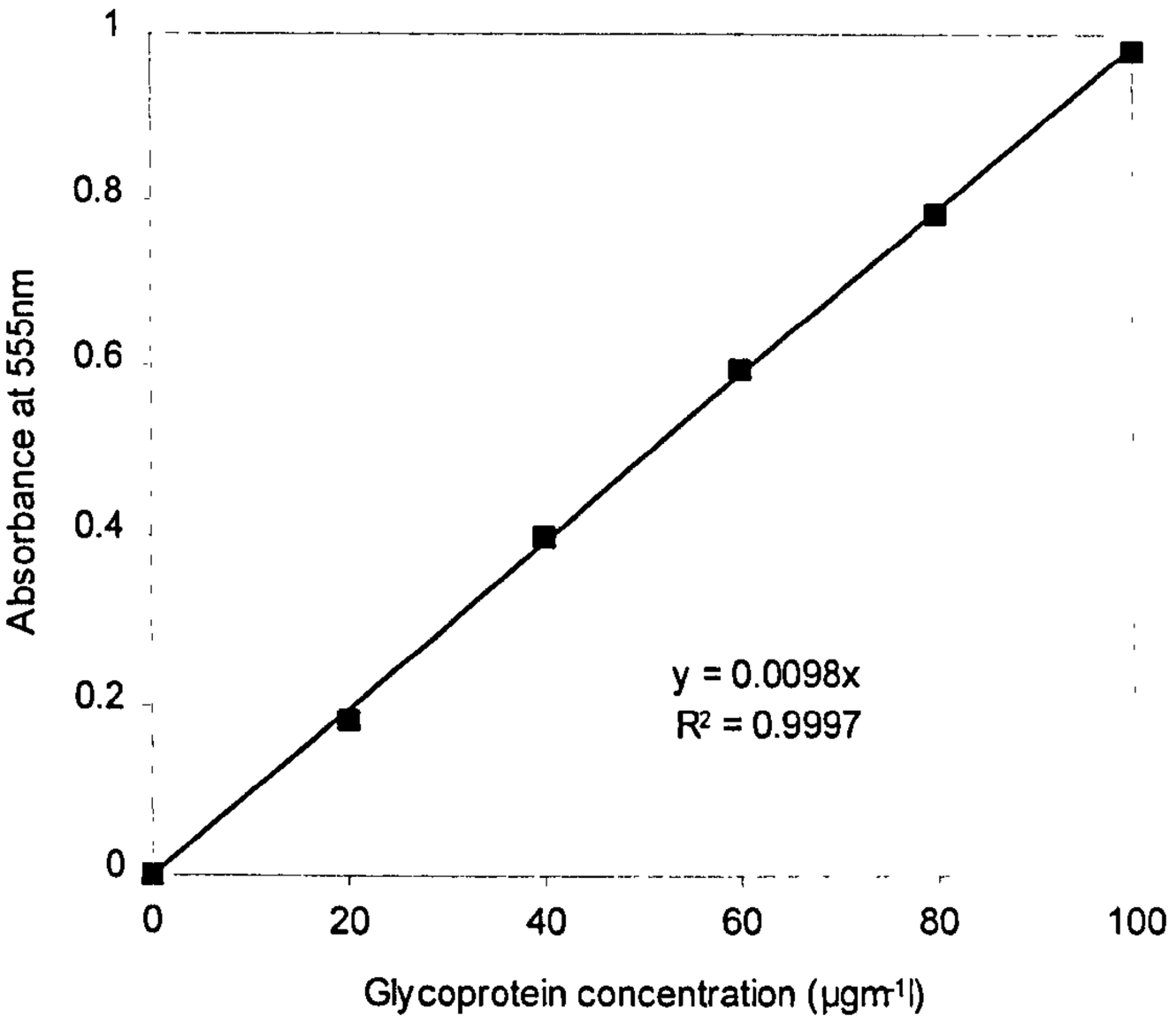

(b)

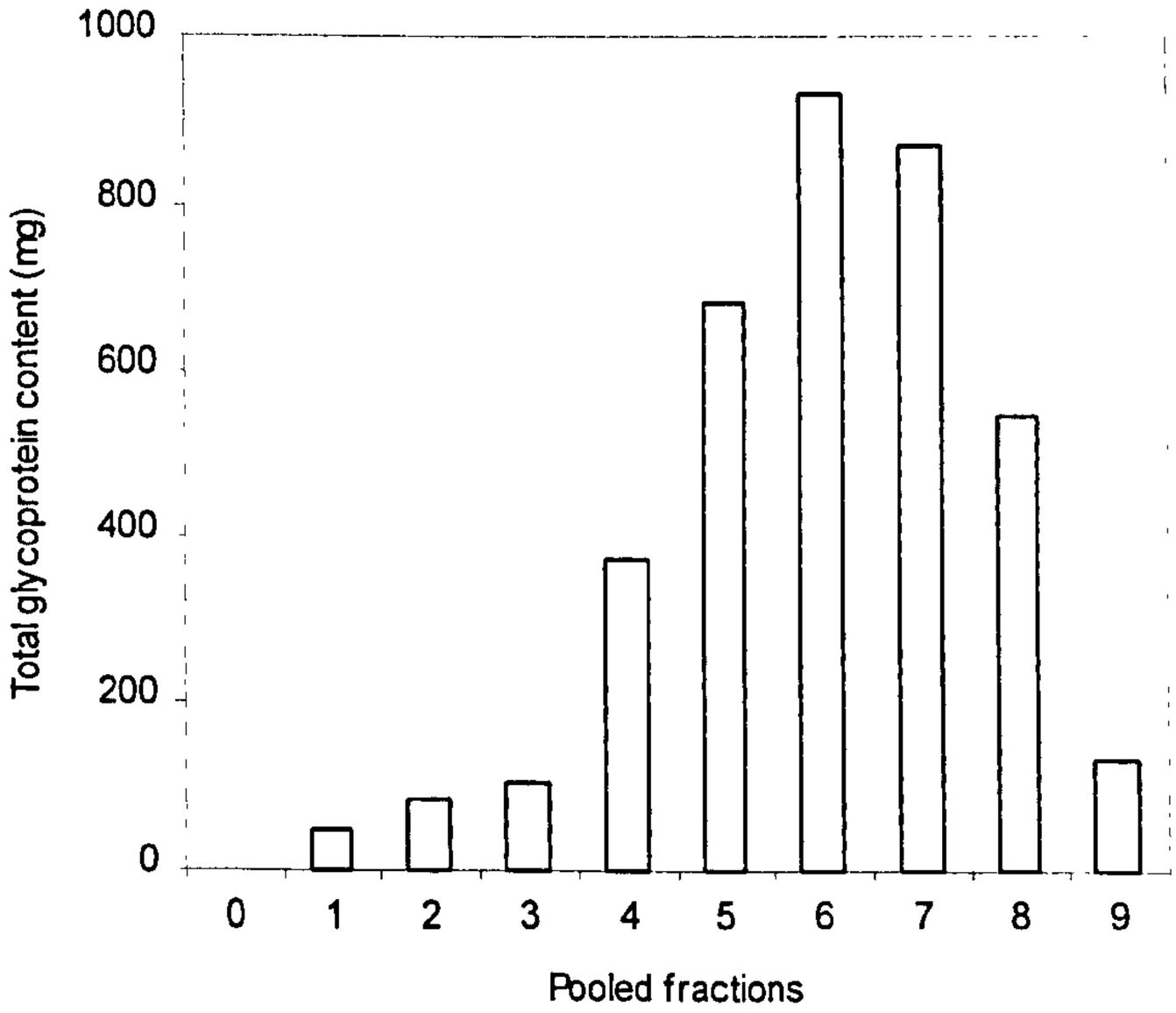

Figure 2.7 (a) Concentration:absorbance plot of PAS stained mucus glycoprotein. (b) Content of PAS stained mucus glycoprotein in the pooled fractions of soluble mucus (n=1)

excluded volume) and 0.05% w/v methyl orange (measures the included volume) (Bell, 1983). This work was carried out by J. Knight, University of Newcastle.

Approximately 2 mg of glycoprotein in 2 ml of 0.2M sodium chloride and 0.02% w/v sodium azide was carefully pipetted onto the column. The column was eluted with 0.2M sodium chloride and 0.02% w/v sodium azide solution at 20 ml hr^{-1} using gravity feed. 1.00 ml fractions were collected and subsequently PAS assayed for glycoprotein content (section 2.4.6.1). A concentration:absorbance plot (figure 2.7a) was used to convert absorbance measurements into glycoprotein concentrations.

2.4.6.3.1. Results

Figure 2.8 shows the size exclusion chromatogram for purified pig gastric mucus used in MRI studies.

The large sharp peak showed the elution of high molecular weight material and represents the polymer form of mucin. The rest of the chromatogram was the elution of lower molecular weight material, corresponding to degraded mucin monomers and sub-units (figure 2.8). Integration of the chromatogram revealed that the purified pig gastric mucus contained 46.3% of mucin polymer. This was typical of mucus glycoprotein purified using the protocol described above. The pig gastric mucin purified in this section used in the MRI studies of chapters 7,8 and 9.

2.4.6.4. Method to determine the rheological characteristics of mucus

The rheological characteristics of different mucus samples were measured at 37±1°C using a Bohlin CVO controlled stress rheometer, fitted with a 4°/40 mm cone and plate geometry and operated in the oscillation mode (table 2.5). An amplitude sweep of the sample was used to determine the linear viscoelastic region (LVER). The median strain of the LVER was used as the target strain in the frequency sweep, which determined the rheological profile of the mucus sample. Unless stated, experiments were conducted using the parameters listed below. Some of the evaluations were carried out by P. Dickson, Reckitt and Colman Products, Hull.

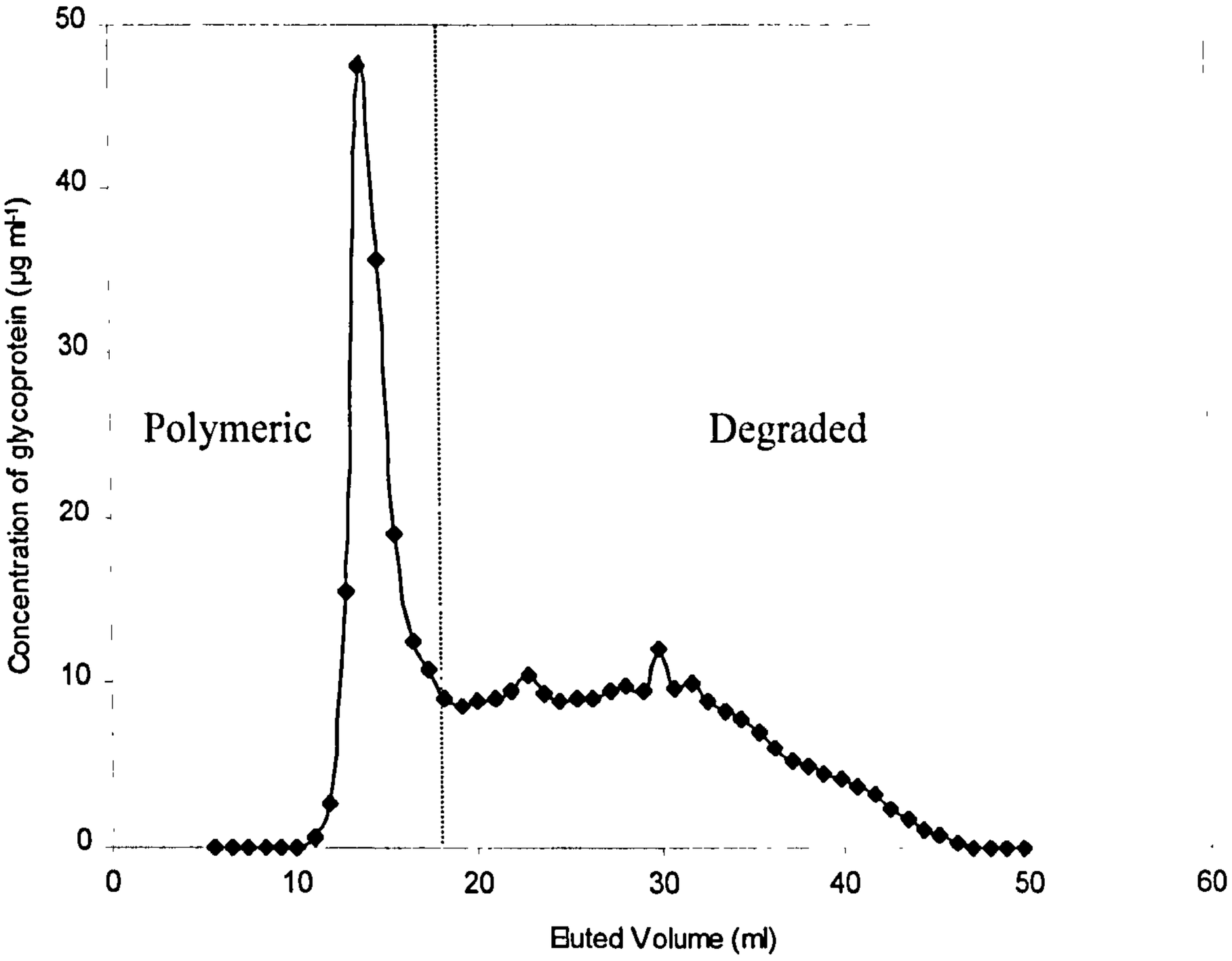

Figure 2.8 A chromatogram of the purified pig gastric mucus used in MRI studies.

The polymer and degraded mucin were separated using size exclusion chromatography. The fractions were PAS stained and the absorbance at 555 nm measured. These were then converted into glycoprotein concentrations using the concentration:absorbance plot illustrated in figure 3.7a (n=1).

Table 2.5 Bohlin CVO parameters used in determining the rheological profile of mucus samples

Amplitude sweep		**Frequency sweep**	
Frequency	1 Hz	Sweep type	step
Start stress	0.05 Pa	Start frequency	0.01 Hz
End stress	500 Pa	End frequency	100 Hz
Ramp direction	Up	Ramp direction	down
Temperature	37±1°C	Temperature	37±1°C

Freshly slaughtered pig stomachs were opened, contents evacuated and the surfaces gently rinsed with cold water to remove embedded debris. The gel layers of 10 stomachs were carefully scraped from the mucosa using a microscope slide, collected in separate glass vials and stored at minus 20°C. The time between the collection and freezing of native mucus was maximally one hour. Frozen mucus samples were defrosted overnight at 4°C and equilibrated to room temperature for at least 2 hours before being tested.

2.4.6.4.1. Results

Table 2.6 Initial and target stresses for the amplitude sweep of native mucus, purified pig gastric mucin and Sigma mucin.

Pig gastric mucus	**n**	**Mean initial stress value (Pa)**	**Mean target stress (Pa)**		
			Mean	**±SD**	**Range**
Native	10	0.05	0.015	0.01	0.002-0.045
Purified	3	0.03	0.024	0.02	0.006-0.045
Sigma	1	0.03	0.010	-	-

Table 2.7 Rheological characteristics of native and purified pig gastric mucus.

Pig gastric mucus	n	Mean storage modulus (0.01 Hz) (Pa)			Median tan δ value
		Mean	±SD	Range	
Native	10	9.57	9.9	1.5-32.1	0.22
Purified	3	1.77	0.3	1.4-2.0	0.90
Sigma	1	0.38	-	-	1.54

For the purposes of this project, elastic gels were defined as having tan $\delta<1$ and viscous solutions were defined as having tan $\delta>1$.

Table 2.7 shows that native and purified mucus had tan δ values indicative of elastic gels. The mean G' of native pig gastric mucus was considerably lower than purified pig gastric mucus, indicating that native mucus has a stronger, more elastic gel-like structure than that of purified mucin. In contrast to purified and native pig gastric mucus, Sigma mucins had tan δ values indicative of viscous solutions (table 2.7).

2.4.7. Discussion

The purified pig gastric mucin obtained using the above method had a mucin polymer concentration of 46.3%. The remainder of the mucin was partly degraded polymer and mucin sub-units. The polymeric and degraded mucin molecules in the mucus could have been separated using size exclusion chromatography (Bell et al, 1984 and 1985). This was not done since mucus gels with high concentrations of mucin polymer were thought not to be representative of the *in vivo* composition and state of mucus.

The purified pig gastric mucin used in this study had an elastic gel-like structure (tan $\delta<1$)(table 2.7). The studies of Bell *et al*, 1984 and Madsen *et al*, 1996, also found that purified mucin had an elastic gel-like structure. However, the tan δ values reported in these studies were considerably lower than the tan δ value found in this study, suggesting a more gel-like structure. This may result from the three studies using different purification procedures. Bell *et al*, 1984, used a procedure similar to the one used in this study but then used size exclusion chromatography to separate the mucin

polymer from degraded mucin. Madsen *et al*, 1996, used a series of homogenisation and centrifugation steps to separate the mucin polymer from degraded mucin. This suggests that the degraded mucins in the purified mucus of this study may interfere with the gel forming properties of the polymeric mucins.

Native pig gastric mucus also had an elastic gel-like structure (tan $\delta<1$)(table 2.7). This agreed with previous findings of Bell *et al*, 1984 and Kocevar-Nared *et al*, 1997. In contrast, Madsen *et al*, 1996, found that native mucus had a liquid-like rheological character (tan $\delta=1.47$), but this was attributed to the mucus gel being diluted during sample preparation. It may also be due to the polymer degrading due to an absence of enzyme or microbacterial inhibitors.

The storage moduli of native mucus and purified mucin indicate that native mucus had a more gel-like structure than purified mucus (table 2.7). This suggests that the mucin polymer may have degraded during the purification process, reducing the ability of purified mucin to form an elastic gel structure. The purification of native mucus may also remove certain components, which may contribute to the gel forming ability of mucin. A similar but opposite phenomenon is seen in small intestinal mucus on removal of protein (Sellars *et al*, 1991).

Sigma partially purified pig gastric (type III) mucin had a viscous liquid-like structure (tan $\delta>1$) suggesting that the polymer structure was entirely dissimilar to either purified or native pig gastric mucus (table 2.9). This agrees with work previously carried out by Madsen *et al*, 1996, who used a 150 mg ml^{-1} solution of Sigma type III mucin. This suggests that the manufacturing process of Sigma mucin caused considerable degradation of the mucin polymer, affecting its ability to form an elastic gels Also, freeze-drying the mucin may also affect its gel-forming properties.

These studies suggest that the type of mucin used in bioadhesive studies may have a considerable influence on the underlying mechanisms of bioadhesion and the observed bioadhesive bond strength of alginates. This is especially so if alginate bioadhesion involves mechanisms that depend on the polymer structure of mucus, for example, polymer interpenetration or mucus dehydration.

2.4.7.1. Discussion on the mucus used in the project

The process used in this study to purify pig gastric mucin from native mucus was extremely time-consuming and produced relatively small yields. A typical purification run would take ≈5-6 weeks to produce ≈5-10 ml of purified pig gastric mucus from ≈60 pig stomachs. Therefore, purified pig gastric mucin was used selectively.

The MRI technique used ≈50 µl of mucus per experiment compared to ≈ 0.5 ml of mucus per experiment in the FRAP technique. Subsequently, it was impractical to use purified pig gastric mucus for both MRI and FRAP studies. Therefore, purified pig gastric mucin was used in the MRI studies investigating the bioadhesion of alginate matrices and the characterisation of this mucin has been presented in this chapter. Sigma partially purified pig gastric mucin was used in the FRAP studies investigating the bioadhesion of alginate matrices because it is readily available in large quantities, even though it was dissimilar to native or purified mucus.

2.5.2. Conclusions

The purified mucin gel used in the MRI studies (chapter 6) contained 43.6% of mucin polymer. Native and purified pig gastric mucus had elastic gel-like structures, which agreed with previously published data. In contrast, Sigma partially purified pig gastric mucin had a viscous liquid-like structure, which was entirely dissimilar to either native or purified pig gastric mucus. This also agreed with previously published data. The type of mucin may influence the bioadhesion of alginate matrices, particularly if the underlying mechanisms are dependent on the structure of the mucin polymer network.

List of materials

Material	Manufacturer	Batch number
α-amino-n-caproic acid	Sigma Chemical	86H07821
Agarose (low melting point)	Nycomed Amersham	1190300
Benzamidine HCl	Sigma Chemical	67H0769
Cysteine hydrochloride	Sigma Chemical	72F06201
EDTA	Sigma Chemical	85H00082
FITC-dextran (12 kDa)	Sigma Chemical	66H5035
FITC-dextran (580 kDa)	Sigma Chemical	74H5012
FITC-dextran (2000 kDa)	Sigma Chemical	27H5043
FITC-dextran (71.2 kDa)	Sigma Chemical	25H5023
FITC-dextran (19.6 kDa)	Sigma Chemical	1545044
FITC-dextran (167 kDa)	Sigma Chemical	86H5004
Fluorescein sodium	BDH	2239810
Glass beads (212-300 μm)	Sigma Chemical	127F-0781
Mucin type III	Sigma Chemical	47H7086
N-ethylmaleimide	Sigma Chemical	126H1197
Papain	Sigma Chemical	91H9816
Phenylmethylsulphonylfluoride	Sigma Chemical	89F4207
Silica gel (Type III)	Sigma Chemical	203971
Sodium alginate	Pronova Biopolymer	477021
Sodium alginate	Pronova Biopolymer	907788
Sodium alginate	Pronova Biopolymer	911846
Sodium alginate	Pronova Biopolymer	511246
Sodium chloride	Thorton & Ross	12 BY
Tetrahydrofuran	BDH	13717
Water	USF ELGA	-
White soft paraffin BP	Boots	IP59

List of suppliers

Supplier	Address
BioRad Microscience	Microscience Division, BioRad House, Maylands Avenue, Hemel Hempstead, Hertfordshire, HP2 7TD.
Boots (Knoll-BASF)	Castle Quay, Castle Boulevard, Nottingham, NG7 1FW, UK.
BDH Laboratory Chemicals	Poole, Dorset, BH15 1TD, UK.
G. Wood & Sons Wholesale Butchers	Clipstone, Nottingham, UK.
Nycomed Amersham	Amersham Place, Little Chalfont, Buckinghamshire, HP7 9NA, UK.
Pronova Biopolymer	P.O. Box 494, N-3002 Drammen, Norway.
Reckitt & Colman Products	Dansom Lane, Hull, UK.
Sigma Chemicals	Sigma Chemical Co., Fancy Road, Poole, Dorset, BH17 7BR, UK.
Stable MicroSystems	Blackdown Rural Industries, Haste Hill, Haslemere, Surrey, GU27 3AY, UK.
Thorton & Ross Ltd	Linthwaite Laboratories, Huddersfield, HD7 5QH, UK.
USF ELGA	High Street, Lane End, High Wycombe, Buckinghamshire, HP14 3JH, UK.

Chapter 3

Development of a test to measure the bioadhesive bond strength of sodium alginate matrices

3.1. Introduction

A detachment force test provides a simple and quick way to measure the strength of a bioadhesive bond formed between a matrix dosage form and mucus. Chapter 1 indicated that various experimental factors and conditions might influence the observed bioadhesive bond strength of a polymer. Therefore, the aim of this chapter was to study how such factors influence the observed bioadhesive bond strength of alginate matrices determined using a detachment force test.

3.2. Detachment force tests

Detachment force tests assume the force required to remove a polymer from the mucosal tissue is opposite to the bioadhesive bond strength. The underlying principles of this type of test have been fully discussed in section 1.6.1.1. Detachment force tests are usually conducted on tensile test apparatuses. In situations where the substrates are inflexible, e.g. when the mucosal tissue has been adhered to a microscope slide (e.g. Ponchel *et al*, 1987), the predominant mechanism of removal is tensile fracture. In cases where the stress is applied perpendicular to the mucosal surface, the predominant mechanism is shear fracture (Smart *et al*, 1984 and Sam *et al*, 1992). If one of the substrates is flexible, e.g. when mucosal tissue is clamped in an O-ring (e.g. Tobyn *et al*, 1995), the actual mechanism of removal is a peeling action rather than tensile or shear fracture (Jacques and Buri, 1992).

The majority of tensile test apparatuses used in bioadhesive research are in-house custom-built designs or are based on the commercially available Instron type tensile test machine. An example of the latter type is the TA-XT2 texture analyser (Stable MicroSystems, Cambridge), which can apply a variable pre-load to aid formation of the bioadhesive bond. Several studies have shown that the TA-XT2 texture analyser can rapidly and precisely determine the strength of bioadhesive bonds formed by a range of cellulose ethers (HPMC, HPC, CMC) and carbomer polymers (Maggi *et al*, 1994 and Tobyn *et al*, 1995).

Several characteristic parameters have been used to quantify the strength of a bioadhesive bond (Ponchel *et al*, 1987). The maximum detachment force (F_{max}) and

work of adhesion (W_a) are the most easily determined and most frequently reported parameters of bioadhesive bond strength. The F_{max} is defined as the maximum force required to fracture the bioadhesive bond and is a static, tensile measurement of the bond strength. In comparison, W_a is defined as the energy required to fracture the bioadhesive bond and is a dynamic measurement of bond strength. The W_a has been reported to be a more sensitive indicator of bioadhesive bond strength than F_{max} (Tobyn, 1994). However, it is the latter that remains the most frequently reported parameter in bioadhesion studies.

3.3. Development of a method to measure the strength of a bioadhesive bond

3.3.1. Introduction

The detachment test used in this work was first developed by Tobyn *et al*, 1995, in order to study the influence of molecular weight, cross-linking, monovalent/divalent ions and addition of PVP on the bioadhesive bond strength of carbomer, carboxymethylcellulose and xanthan gum polymers (Tobyn *et al*, 1996a and 1996b). Chapter 1 has discussed how some test parameters may significantly influence the observed bioadhesive bond strength of a polymer. Therefore, the aim of this section was to study the influence of some test parameters on the observed bioadhesive bond strength of alginate matrices.

3.3.2. Method to manufacture alginate matrices

200±20 mg quantities of 90-125 μm SF120 sodium alginate were compressed into 10 mm diameter, circular flat face matrices on a Manesty F3 tablet press, fitted with a tablet compression monitor model TCM1 (Copley Instruments Ltd, Nottingham) using an upper punch pressure of 400-410 mPa. Matrices were stored in sealed containers at 4°C over silica gel and warmed to room temperature for one hour before use.

3.3.3. Method to prepare physiological saline

Physiological saline was prepared by dissolving 0.9 g of sodium chloride in 100 ml of deionised and distilled water.

3.3.4. Method to measure the strength of a bioadhesive bond

3.3.4.1. Preparation of pig gastric mucosa for detachment force analysis

Freshly slaughtered pig stomachs were obtained from the abattoir, opened and the contents evacuated. The mucus surface was then gently rinsed with cold water to remove any embedded debris. The quality of the mucus surface was visually examined and those stomachs that appeared diseased were rejected. The cardiac mucosa of each stomach was separated from the muscle layer and dissected into 25 mm thick strips. These strips were folded in half to protect the mucus surface and stored at minus 20°C. The time between collection and freezing was maximally one hour.

3.3.4.2. Detachment force test

A TA-XT2 texture analyser, fitted with a 5 kg load cell, was used to measure the bioadhesive bond strength (figure 3.1). Pig gastric mucus was defrosted overnight at 4°C and equilibrated to room temperature for at least two hours. A 25 x 25 mm square of tissue was clamped in the sample cell using a perspex O-ring (figure 3.2) and allowed to equilibrate in 400 ml of physiological saline at 37±1°C for at least 20 mins. The lower surface of an alginate matrix was attached to a 80 x 9.6 mm circular perspex probe using double-sided adhesive tape and hydrated in physiological saline at 37±1°C for a predetermined length of time. The experimental parameters used in the detachment force test are shown in table 3.1. Mucosa from the same stomach was used to compare different alginates.

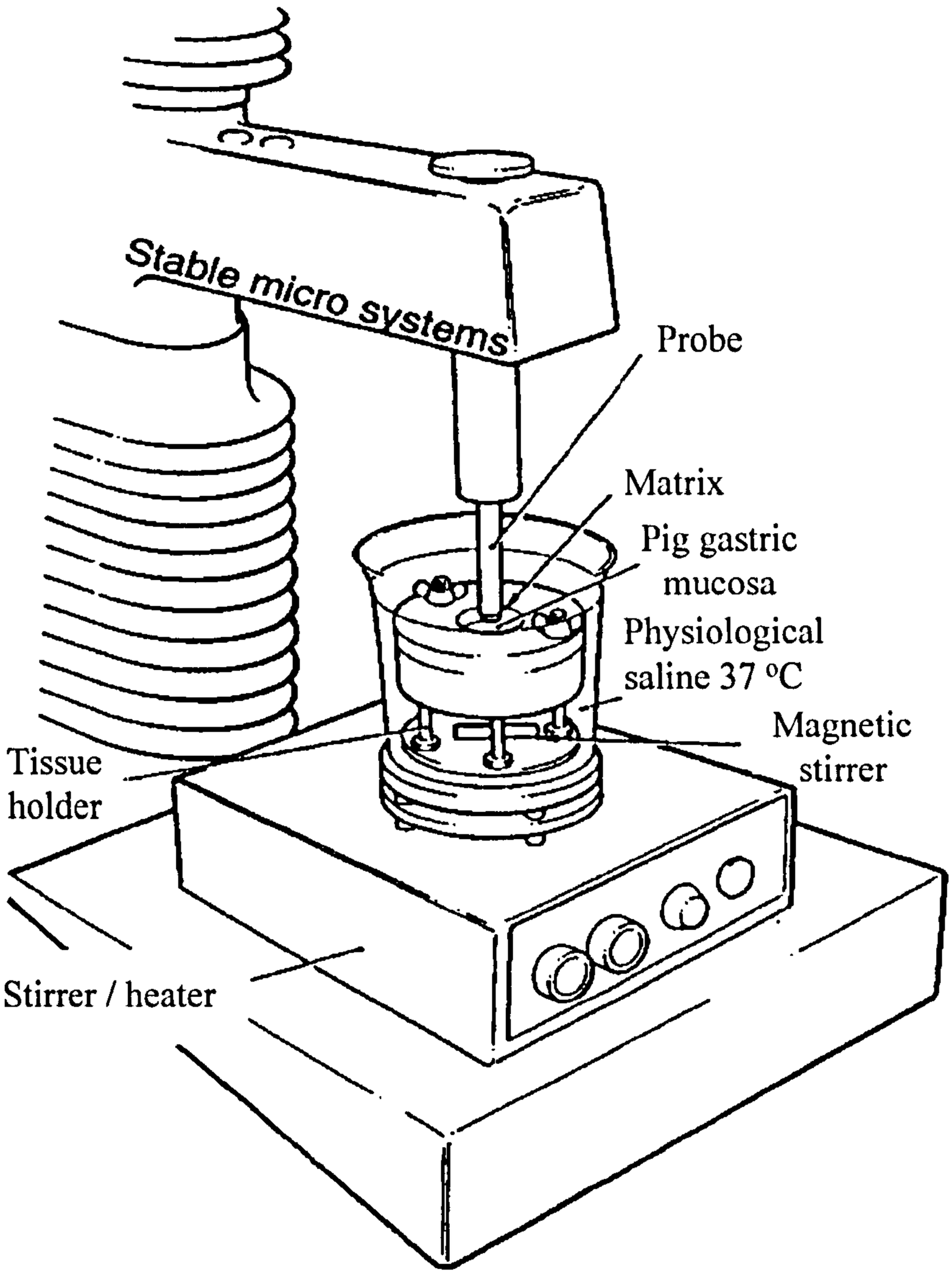

Figure 3.1 Sample cell geometry used in the detachment force test (taken from Tobyn *et al*, 1995)

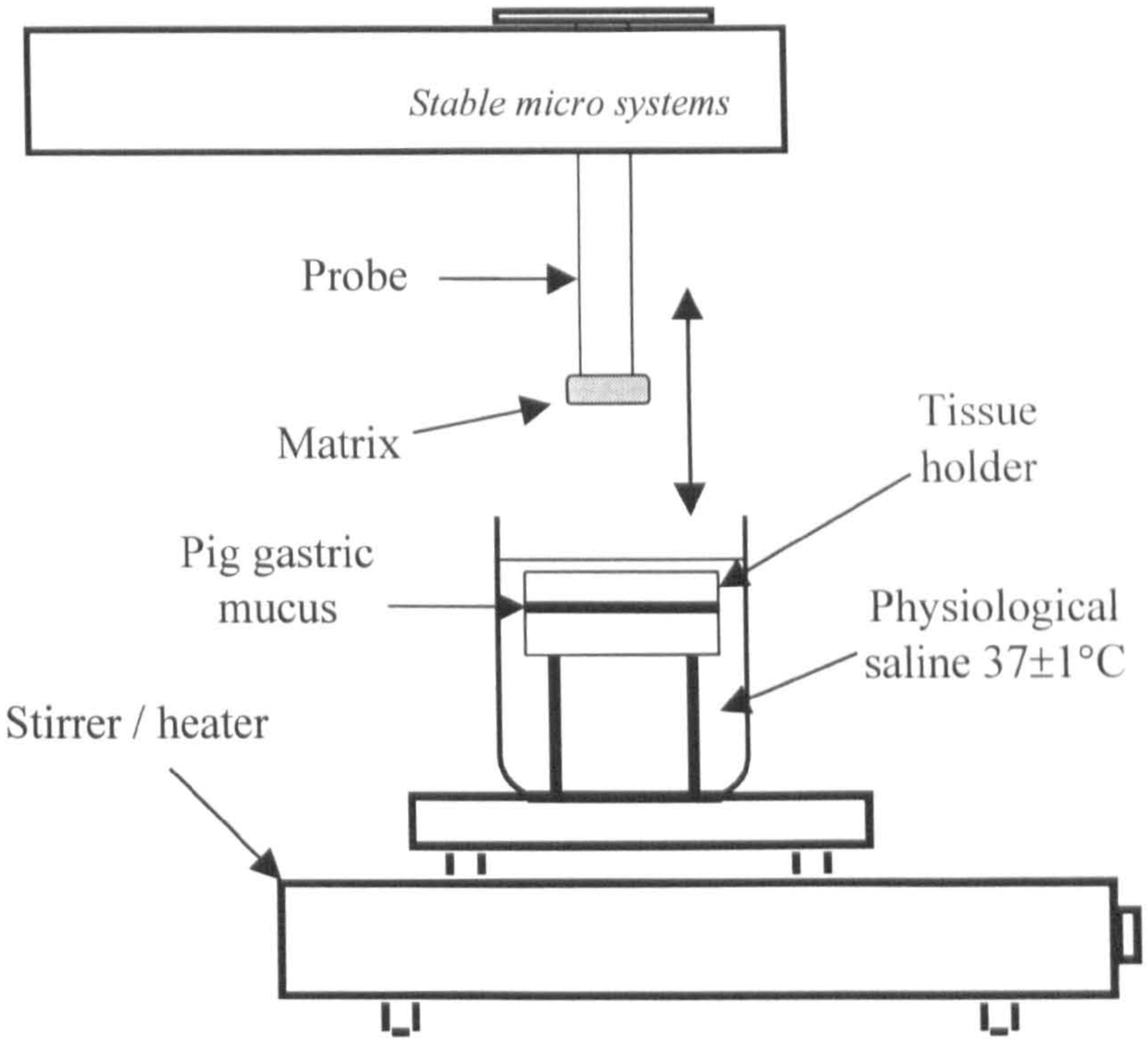

Figure 3.2 Detail of sample cell geometry used in the detachment force test.

Table 3.1 A summary of the experimental parameters used in the detachment test

Tissue parameters	
Tissue section	Pig gastric tissue, cardiac region
State	Frozen and thawed
Bathing medium	Physiological saline at 37±1°C
Equilibration time	≥ 20 mins
Instrument parameters	
Bond formation force	See section 3.3.6
Bond formation time	See section 3.3.5
Probe withdrawal speed	0.1 mm s^{-1}
Prehydration of matrix	See section 3.3.6
Withdrawal distance	30 mm
Points per second	50
Tablet parameters	
Matrix weight	200±20 mg
Compaction pressure	400-410 mPa
Bioadhesive bond strength parameters measured	
Main parameter	Work of adhesion
Other parameters	Maximum detachment force

3.3.4.3. Calculation of the maximum detachment force and work of adhesion

The F_{max} and the area under the force-time profile (AUC_{FT}) can be directly determined from the force-time profile (figure 3.3). The W_a can be calculated using equation 3.1.

$$W_a = \frac{AUC_{FT} x D}{(T_1 - T_2)} \quad (3.1)$$

AUC_{FT} is area under a force-time profile, D is distance between intersections of the profile with the x-axis, T_1 and T_2 refer to the times when the profile passes through the x-axis.

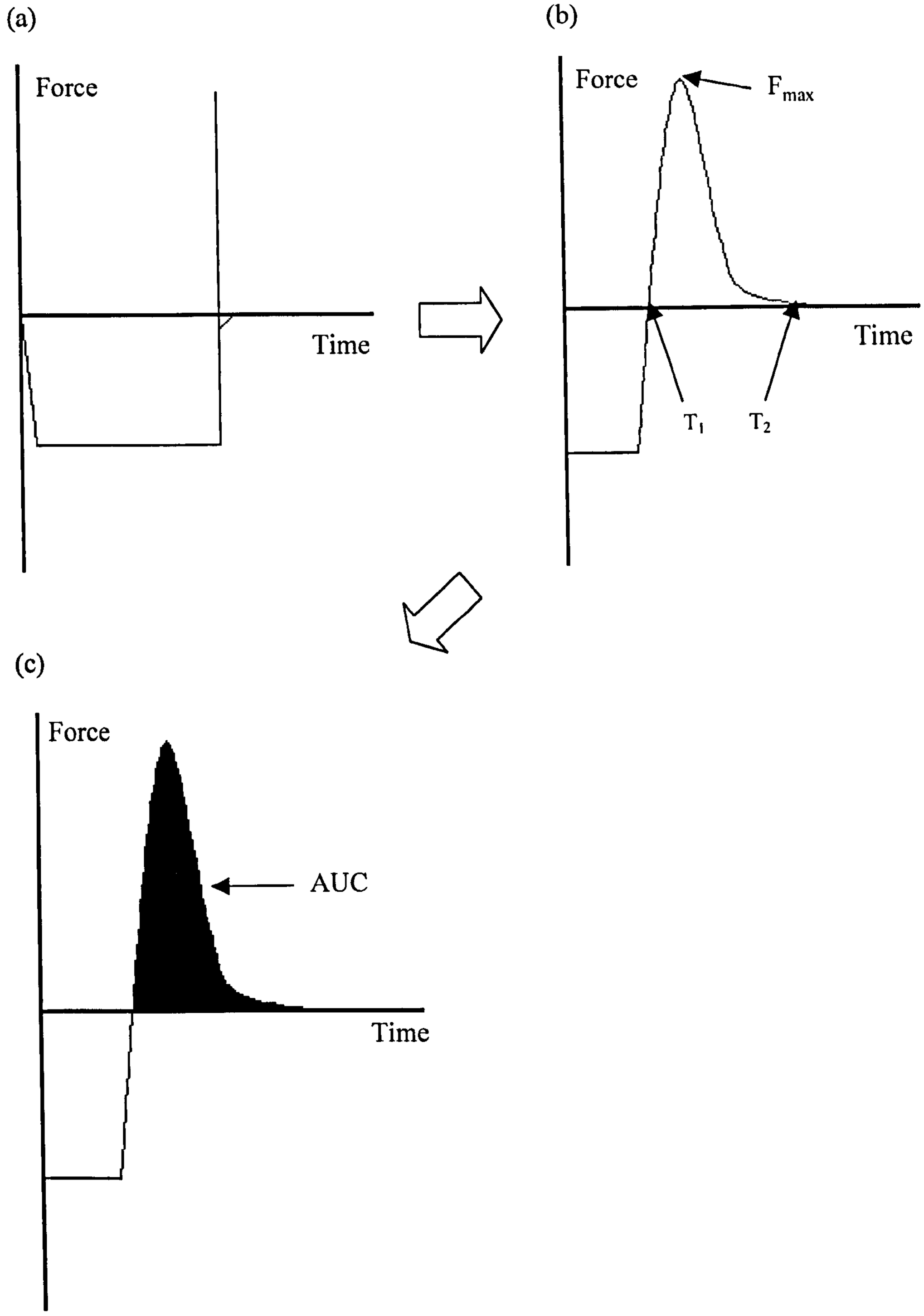

Figure 3.3 Force-time profiles generated by the detachment force test

(a) Actual representation of a force-time profile, (b) the enlarged section of the profile showing the F_{max} and the x-axis intersections (T_1 and T_2) and (c) the area under curve (AUC) (shaded).

3.3.5. Influence of bond formation time on the bioadhesive bond strength of alginate matrices

The aim of this section was to carry out a preliminary study on the influence of bond formation time on the bioadhesive bond strength of alginate matrices. In Tobyn's standard detachment test (Tobyn *et al*, 1995), a bioadhesive bond was formed using a 0.5 N force applied for 600 secs. This was used as a starting point for this work.

3.3.5.1. Method

Sodium alginate matrices were prehydrated in physiological saline at 37±1°C for 30 sec and a force of 0.5 N was applied to form a bioadhesive bond. The test was then conducted in the standard way (section 3.3.4).

3.3.5.2. Results

Table 3.2 Influence of bond formation time on W_a and F_{max} values

Contact time (sec)	n	W_a (mJ)	±SD	F_{max} (N)	±SD
600	6	-	-	-	-
300	6	0.0135	0.021	0.435	0.30

In studies where the contact force was applied for 600 sec, the bioadhesive bond was so strong that the alginate matrices could not be removed from the tissue. Subsequently, neither W_a nor F_{max} could be determined. Following this, the bond formation time was decreased from 600 sec to 300 sec, which produced bioadhesive bonds with measurable W_a and F_{max} values. Therefore, future studies used a bond formation time of 300 sec.

3.3.6. Influence of prehydration time and bond formation force on the bioadhesive bond strength of alginate matrices

Several studies have shown that the strength of the bioadhesive bond may be influenced by the hydration state of an adhesive and the force applied to form the bond. The

underlying mechanisms are fully explained in sections 1.5.3.2 and 1.5.3.3. Thus, the aim of this section was to study how these factors influence the strength of bioadhesive bonds formed by alginate matrices.

3.3.6.1. Method

Alginate matrices were prehydrated in physiological saline at 37±1°C for 0, 30, 60, 300, 600, 900 or 1200 sec and a force of either a 0.5 N or 0.25 N was applied for 300 sec to form the bioadhesive bond. The test was then conducted in the standard way (section 3.3.4).

3.3.6.2. Results

Figure 3.4 shows the influence of prehydration time and bond formation force on the W_a and F_{max} of bioadhesive bonds formed by alginate matrices.

The bond formation force did not influence the F_{max} or W_a values of bioadhesive bonds formed between alginate matrices and pig gastric mucus. Likewise, prehydration time did not influence either F_{max} or W_a. However, at prehydration times of 600 sec and 900 sec, the bond formation force appeared to affect the variability of W_a. When matrices were prehydrated for 600 sec, the variability of W_a increased as the bond formation force increased. In contrast, when matrices were prehydrated for 900 sec, the variability of W_a decreased as the bond formation force increased.

Therefore, future studies using prehydrated alginate matrices used a prehydration time of 600 secs and a bond formation force of 0.25 N.

3.3.7. Influence of mucus surface treatment on the bioadhesive bond strength

The normal cycle of mucus turnover in the stomach results in the lumenal surface of the mucus layer being composed of a high proportion of degraded mucins, which are equally likely as polymeric mucin to interact with the alginate. This may influence the observed bioadhesive bond strength since the degraded mucins may not contribute

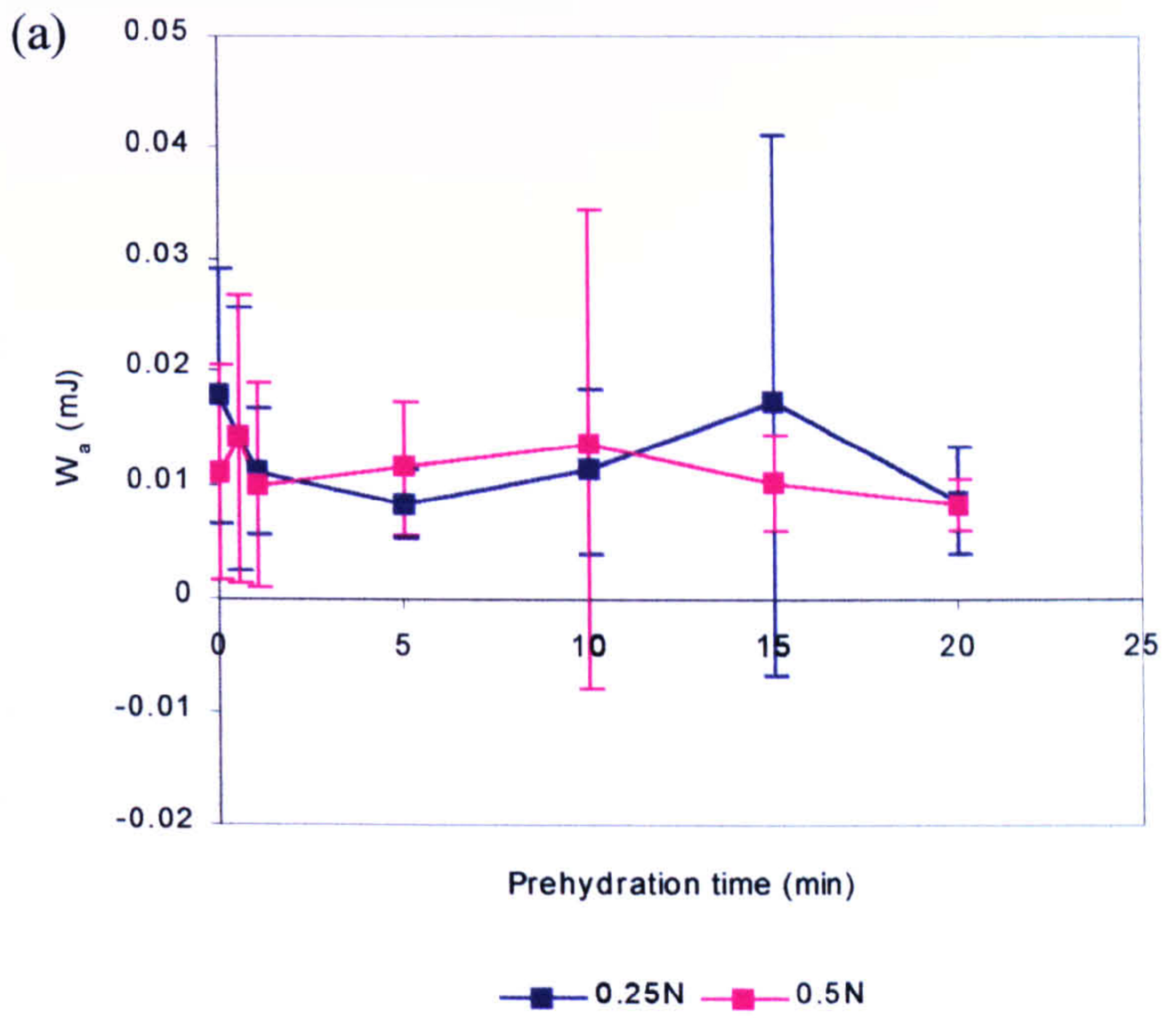

Figure 3.4 The influence of prehydration time on the W_a and F_{max} of bioadhesive bonds formed with different bond formation forces.

(a) W_a and (b) F_{max} of bioadhesive bonds formed by SF120 alginate matrices, prehydrated in physiological saline at 37±1°C, using different bond formation forces (mean, n=6, ±1 SD).

towards the cohesion of the mucus gel layer (Bell *et al*, 1985) and may also prevent the polymer from interacting with polymeric mucin. Therefore, the aim of this section was to evaluate ways of removing this surface layer of degraded mucin.

3.3.7.1 Method

Mucus surfaces were either scraped or blotted before the mucus layer was equilibrated in physiological saline. Scraping of the mucus surface involved gently dragging a microscope slide across the mucus surface and blotting of the surface involved placing Whatman No 1 filter paper on the mucus surface for 15 sec. The standard test (section 3.3.4) was applied to determine the bioadhesive bond strength of matrices prehydrated in physiological saline for 10 mins.

3.3.7.2. Results

Table 3.3 Influence of mucus surface treatment on W_a and F_{max}

Surface treatment	**n**	**W_a (mJ)**	**±SD**	**F_{max} (N)**	**±SD**
No treatment	16	0.0058	0.002	0.4842	0.194
Blotted	16	0.0070	0.004	0.5409	0.251
Scraped	16	0.0079	0.004	0.5661	0.251

The W_a and F_{max} of bioadhesive bonds formed with either 'scraped' or 'blotted' pig gastric mucus were stronger than those formed with untreated mucus. However, there was no evidence to suggest that the W_a and F_{max} values were statistically significant ($p>0.05$). The surface treatments did however increase the variability of W_a and F_{max}, suggesting a decrease in the reproducibility of the test. Therefore, future studies did not pre-treat the surface of the mucus.

3.3.8. Discussion

3.3.8.1. Effect of the bond formation time on bioadhesive bond strength

The W_a and F_{max} of bioadhesive bonds decreased as the bond formation time decreased (table 3.2), which suggests that the mechanisms underlying the bioadhesive interaction between alginate and mucus are time dependent. A study using the same apparatus also found that the W_a of bioadhesive bonds formed between Carbopol 934P and pig gastric mucus was time dependent (Tobyn *et al*, 1995). Other studies have shown that F_{max} is dependent on bond formation time (Smart, 1991, Blanco-Fuente *et al*, 1996, Smart *et al*, 1984, Leung and Robinson, 1990). In contrast, Woolfson *et al* in 1992 found no discernible relationship between bond formation time and F_{max} of bioadhesive bonds formed between sodium carbopol/sodium CMC polymer films and human cervical tissue.

3.3.8.2. Effect of the prehydration time on bioadhesive bond strength

The prehydration time of the matrices did not seem to influence the W_a and F_{max} of bioadhesive bonds formed by alginate matrices (figure 3.4), which is in contrast to other polymers. Ponchel *et al*, 1987, found that polyacrylic acid:HPMC matrices exhibited maximum bioadhesive strength when prehydrated for 10 mins. Other studies have shown that the F_{max} of bonds formed by sodium Carbopol/sodium CMC polymer films (Woolfson *et al*, 1992) and the W_a of polyacrylic acid matrices (Tobyn *et al*, 1995) are inversely related to prehydration time. However, in the same study carried out by Tobyn *et al*, 1995, the W_a seemed to become independent of prehydration times longer than 120 secs in cases where the bond formation time was short (1 min).

The relationship between prehydration time and bioadhesive bond strength depends on the underlying mechanisms of bioadhesion. For example, hydration of the polyacrylic acid polymer causes the polymer to swell and expose more carboxylic acid groups, which may hydrogen bond with mucin. Hydration of a polymer also increases the mobility of the polymer chains, which may facilitate polymer interpenetration. Also, some polymers may be bioadhesive as a result of their ability to dehydrate the mucus layer (Mortazavi and Smart, 1993). However, over hydration of the polymer may

produce a slippery mucilage with low cohesive strength that can be easily sheared (Smart *et al*, 1984, and Woolfson, 1992).

3.3.8.2. Effect of the bond formation force on bioadhesive bond strength

In this study, the bond formation force did not influence either W_a or F_{max} (figure 3.4). The F_{max} of bioadhesive bonds formed by sodium CMC/sodium Carbopol films are also not affected by the bond formation force (Woolfson *et al*, 1992). Sodium CMC is structurally very similar to sodium alginate.

In contrast, other studies have shown the W_a and F_{max} of bioadhesive bonds formed by other polymers are dependent on the bond formation force, for example polycarbophil, divinylbenzene cross-linked PMA and PHEMA films (Park and Robinson, 1985), Carbopol matrices (Tobyn *et al*, 1995, and Blanco-Fuente, 1996). It is thought that increasing the bond formation force improves wetting and interpenetration of the polymer.

Although the mean W_a was not dependent on either prehydration time or bond formation force, the variability of W_a appeared to be influenced by these parameters, especially in matrices prehydrated at intermediate times: 600 sec for the 0.5 N bond formation force and 900 sec for the 0.25 N bond formation force (figure 3.4). The variability of F_{max} was not influenced by prehydration time.

It was thought that variability in the W_a values might be related to the viscous alginate gel layer reaching a stage of hydration in which it has a varying degree of cohesiveness. Alternatively, it may be due to the W_a being a more sensitive parameter of bioadhesive bond strength than F_{max}, as indicated previously by Tobyn *et al*, 1994.

A bioadhesive test may be sensitive to some of the test parameters, for example the bond formation time and force and the prehydration time of the polymer. Therefore, these parameters must remain constant in tests where the strengths of bioadhesive bonds formed by different polymers are compared. Likewise, the influence of these parameters on bioadhesion should be taken into account when comparing bioadhesive bond strengths measured by different tests.

3.3.8.2. Effect of treating the mucus surface on the bioadhesive bond strength

Scraping and blotting the mucus surface to remove the surface layer of degraded mucins did not influence either W_a or F_{max} of prehydrated alginate matrices (table 3.3). This suggests three possibilities. Firstly, degraded mucins did not influence the bioadhesion of prehydrated alginate matrices. Secondly the surface treatments were not successful in removing the surface layer of degraded mucins. Thirdly, the preparation of the mucosal tissue outlined in section 3.3.4.1 was sufficient to remove the degraded mucin surface layer.

3.4 Conclusions

The bond formation time influenced the W_a and F_{max} values of bioadhesive bonds formed between alginate matrices and pig gastric mucus, suggesting that the underlying mechanisms of bioadhesion were time dependent. The bond formation force and prehydration time of the matrix did not seem to affect the mean W_a and F_{max} but did seem to influence the variability of the values at certain times and forces.

The surface treatments of scraping and blotting to remove the surface layer of degraded mucins did not influence W_a or F_{max} of the bioadhesive bond but decreased the reproducibility of the test.

Chapter 4

Development of a technique to measure transport rates in a model gel using confocal microscopy

4.1. Introduction

The movement of a fluorescent solute in a polymer network can be measured using fluorescence photobleaching techniques. This chapter outlines the development of a novel photobleaching technique, which may be used to measure the mobility of fluorescent solutes inside the polymer network of a bioadhesive bond. The technique was developed on a BioRad MRC600 confocal laser scanning microscope.

4.2. Confocal laser scanning microscopy

4.2.1. Principles of confocal microscopy

Confocal microscopy is a fast, non-invasive imaging technique that can optically section translucent samples. The optical design of a confocal microscope places a pinhole aperture in the microscope axis, restricting both sample illumination and the detection of light emission to a single focal plane (figure 4.1). In essence, the confocal image is an optical section of the sample, with axial resolution that improves as the size of the pinhole aperture decreases (Dixon, 1998). Lateral resolution is also improved when the pinhole is very small, although the confocal iris blocks most of the emitted light, resulting in a reduction of sensitivity (White *et al*, 1987, Wilson, 1989 and Shuman, 1989). Confocal apertures also improve image blurring and signal to noise ratio, since the iris blocks any light scattered by the sample. Several textbooks and reviews on confocal microscopy have been published, for example, Pawley, 1990, and Melia *et al*, 1999, and the reader is referred to these for more detailed information.

Since lasers have a high degree of coherence and monochromaticity, they are usually used as the light source of choice on confocal microscopes. The laser beam is focussed to a diffraction-limited spot, which is raster scanned across the sample by either a galvanometer driven mirror or an acousto-optical modulation device. Confocal microscopes combining a laser light source with these types of optics are termed confocal laser scanning microscopes (CLSM).

(a) Epi - illumination

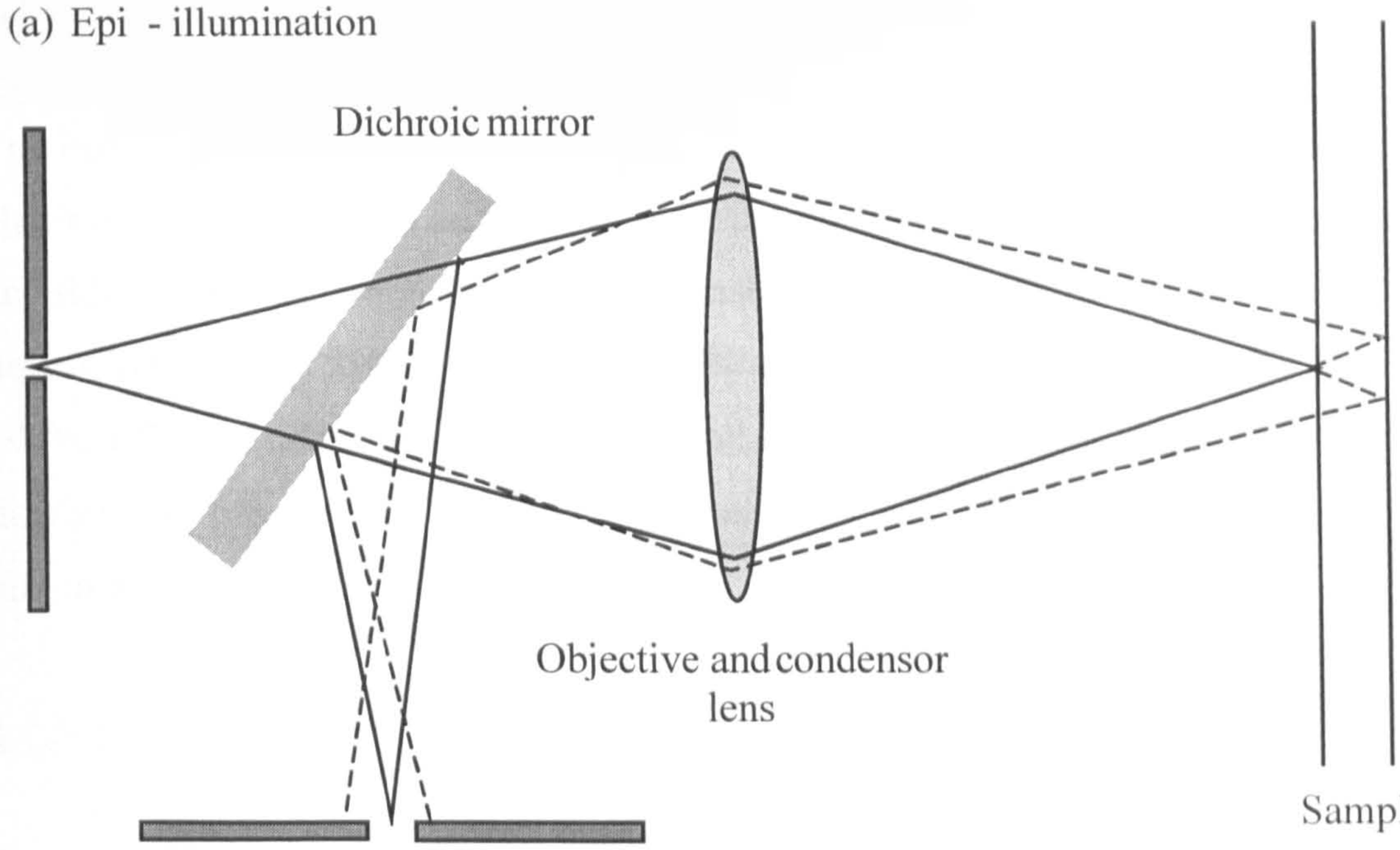

(b) Transmitted illumination

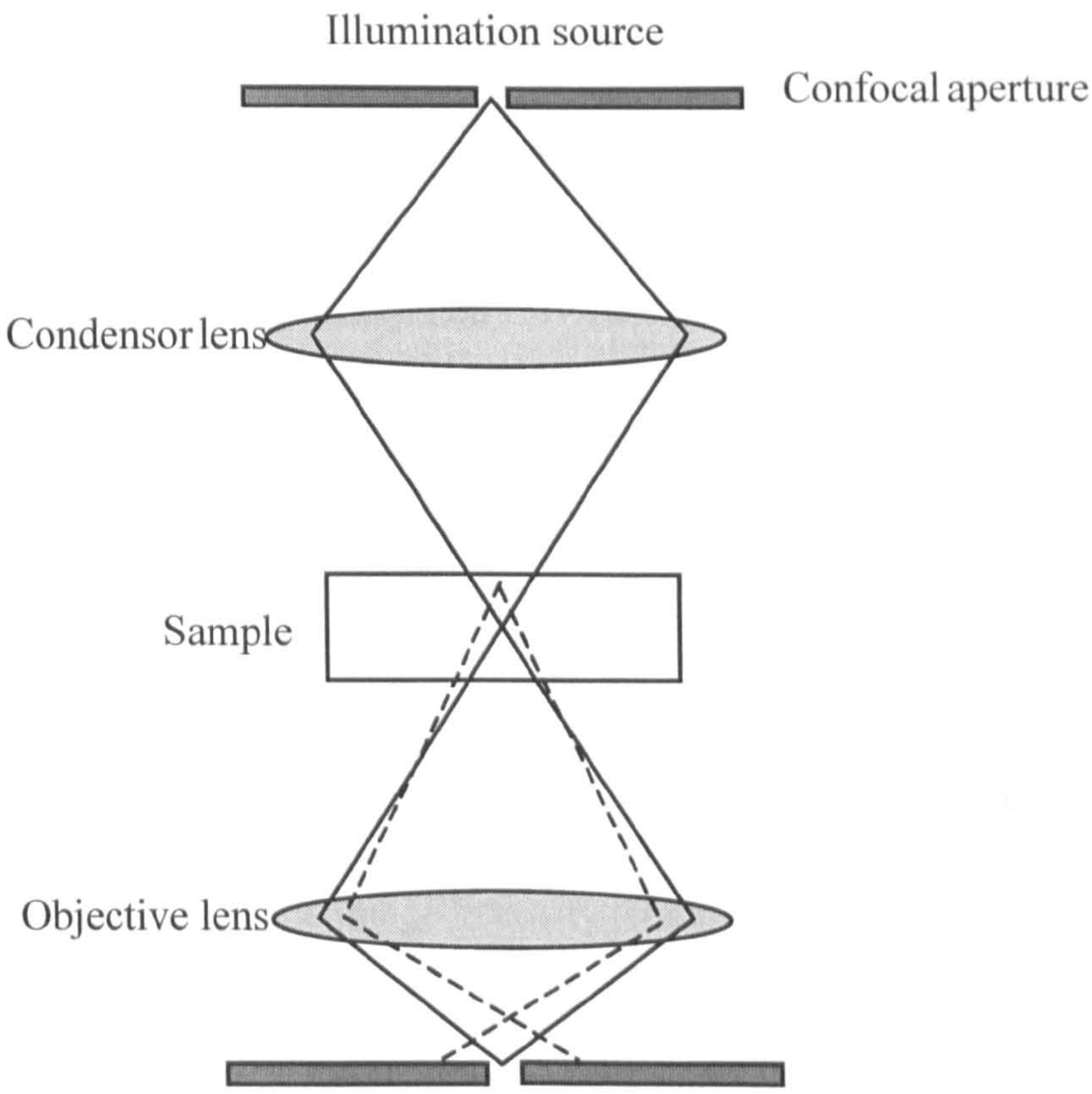

Figure 4.1 Two alternative optical arrangements of a confocal laser scanning microscope (redrawn after Pawley, 1990).

4.2.2. BioRad MRC600 confocal laser scanning microscope

The BioRad MRC600 CLSM used in this study (BioRad Microscience, Hemel Hempstead) was mounted on an upright epi-illuminating Nikon Optiphot microscope and fitted with a 15 mW Kr-Ar air-cooled laser, emitting at 488 nm, 568 nm and 647 nm and detecting at 510 nm, 585 nm and 680 nm, respectively. The MRC600 uses 100%, 10%, 3% and 1% transmission neutral density filters to attenuate the laser intensity and has a patented variable confocal aperture mechanism, ranging from 0.6 mm to 8 mm (Cutts, 1994).

4.2.3. Image distortions

Generally, CLSMs may generate either chromatic or spherical image distortions due to refraction of the laser light by the objective lens. Images are distorted more frequently in the periphery since light is refracted more by the edge of a lens than the middle. These types of image distortions may be avoided by correcting the objective lens for both spherical and chromatic aberrations (Inoue, 1990). Small vibrational disturbances may also cause extensive image distortions. This may be corrected by mounting the CLSM on an anti-vibration table and isolating the scan-head from any sources of vibration, such as the laser cooling motor. If there is a non-linearity of the scanning mechanism, the electronic detection and storage of images may also distort images (Wells *et al*, 1990). Galvanometer driven mirrors are another source of image distortions. The mirrors can distort the shape of the laser, producing similar distortions to those caused by vibration.

Excessive excitation of the fluorophore may result in the formation of a metastable triplet state, which emits energy as phosphorescence rather than fluorescence, resulting in an apparent decrease in the image intensity (Haugland, 1992). Fluorescence quenching, which occurs at high fluorophore concentrations, may also cause an apparent decrease in fluorescence. Opaque occlusions and the absorption of emission light by the sample may affect an image. These types of image aberrations can be minimised by using a low concentration of fluorophore and an excitation light of low intensity.

4.3. Fluorescence recovery after photobleaching (FRAP)

4.3.1. Principles of photobleaching techniques

The underlying principle of this technique is that a high intensity light pulse is used to irreversibly photobleach a localised area in a fluorescent sample, resulting in a decrease in the emission of fluorescence. A lower intensity light source is then used to monitor the subsequent recovery of fluorescence (figure 4.2), which is a function of the mobility of the fluorescent species. This technique assumes that there is a linear relationship between fluorescence and concentration of fluorophore, which exists with low light intensity excitation and low fluorophore concentration.

4.3.1.1. Fluorescence and photobleaching

At this point it is worthwhile to briefly explain the underlying mechanisms of fluorescence and photobleaching. In fluorophores, electrons can exist in different energy levels, each having their own rotational and vibrational states. Most electrons exist in the ground state (S_0) and can be promoted to higher energy states (S_1) by absorbing a quantum of light energy. Excited electrons may then lose vibrational energy and relax to the lowest vibrational level of S_1. Eventually, electrons return to S_0 by losing energy as fluorescence usually within 10^{-12}-10^{-9} sec. The emission of fluorescence always occurs at a longer wavelength than the excitation light and this phenomenon is termed the Stokes shift (Hall *et al*, 1991).

Excited electrons may also lose energy through internal conversions or through inter-system crossings. The latter is spin-forbidden and results in the production of long-lived triplet-states, T_1 (>100 ns), which eventually relax through the emission of phosphorescence. Since the decay of triplet states is relatively slow, electrons can become trapped (Wells *et al*, 1990), resulting in a transient apparent decrease in fluorescence. This effect can be mistaken for either a decrease in fluorophore concentration or fluorophore photodestruction. Subsequently, triplet states may affect any method that quantitatively analyses fluorescence and relates it to the concentration of a fluorescent molecule.

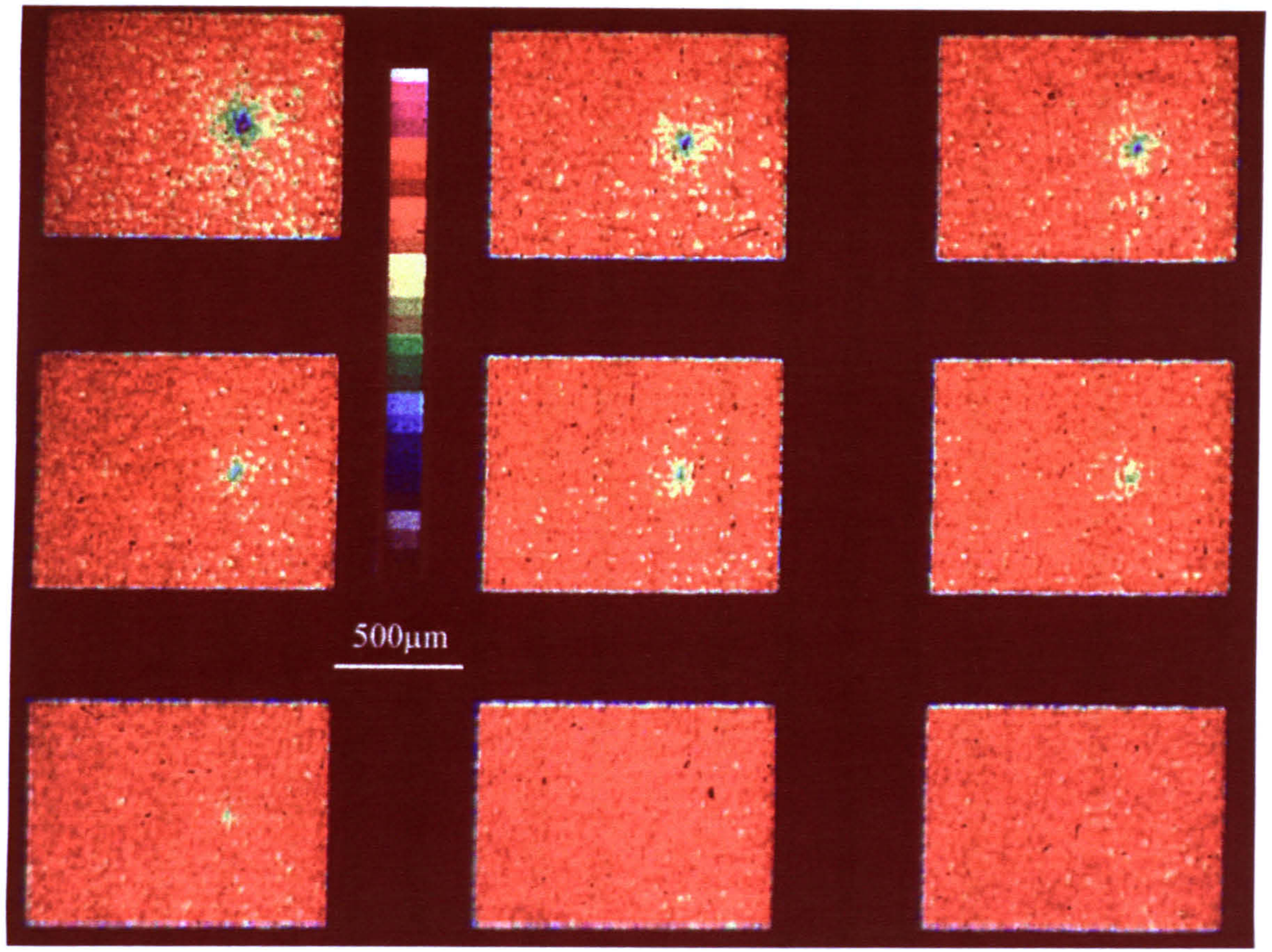

Figure 4.2 The movement of fluorescent molecules into a photobleached area causing a recovery in the fluorescence intensity

(taken from Cutts, 1994)

In 1995 and 1996, Song *et al* showed that photobleaching may involve polymolecular triplet state reactions, having poly-exponential reaction rates. This is in stark contrast to what the majority of FRAP mathematical models assume photobleaching to be. FRAP models generally assume photobleaching to be a unimolecular reaction, having a first order reaction rate. However, these conditions only exist under certain circumstances, for example, when fluorophore concentration is low (Song *et al*, 1995).

4.3.2. The development of photobleaching methods

4.3.2.1. The initial development of FRAP mathematical models

In one of the first FRAP experiments, Peters *et al*, 1974, photobleached one half of a fluorescently labelled erythrocyte ghost and mathematically analysed the subsequent fluorescence recovery to determine the membrane mobility. The introduction of laser light sources prompted the development of new mathematical models, which could analyse fluorescence recovery in an area irradiated by a laser.

Using a model first reported by Elson and Magde, 1974, Axelrod *et al*, 1976, developed a mathematical model to analyse FRAP data generated using a single stationary focussed laser beam. Since the cross-sectional profile of a laser can vary between a Gaussian profile and a uniform intensity, circular disk profile, the model accounted for fluorescence recovery in an area spot photobleached by a light source with either profile. The mathematical analyses also considered the type of transport process, accounting for both uniform flow and simple diffusion. However, the Axelrod model is restricted by several assumptions. The photobleaching of the fluorophore must follow first order reaction kinetics and must be short compared to the characteristic diffusion time. Also, the bleached profiles must be circularly symmetrical and fluorescence recovery should only be a consequence of pure two-dimensional Fickian diffusion.

For a Gaussian profile laser beam, the model can be summarised by equations 4.1 and 4.2 (Blonk *et al*, 1993). Equation 4.1 describes the normalised recovery curve.

$$f(t) = \frac{\sum_{n=0}^{\infty} \frac{-\kappa^n}{n!}}{1 + n\left[1 + \left(\frac{2t}{\tau_D}\right)\right]} \qquad (4.1)$$

Equation 4.1 is related to the diffusion coefficient by equation 4.2

$$\tau_D = \frac{\omega^2}{4D} \qquad (4.2)$$

f(t) is the normalised fluorescence recovery, κ is the bleach rate constant, τ_D is the characteristic diffusion time, ω is half width of the Gaussian profile at e^{-2} height of the profile, t is time and D is the diffusion coefficient.

Axelrod's mathematical analysis for a uniform intensity, circular disk profile has been severely criticised and subsequently has been adapted by several investigators. At recovery times, which are short compared to the characteristic diffusion time ($t/\tau_D<0.3$), the fluorescence recovery model encounters considerable computational problems. Using a different set of theoretical concepts, Lardner, in 1977, proposed a range of equations that calculated diffusion coefficients for $t/\tau_D<0.05$. In 1983, Sompasis used a similar theoretical approach to Axelrod, but with a different mathematical derivation, to extend the calculation of diffusion coefficients down to $t/\tau_D=0.05$. Finally, in 1988, Lopez *et al* combined the models of Lardner and Sompasis to produce a set of mathematical expressions to calculate diffusion coefficients at all values of t/τ_D.

4.3.3. Different photobleaching methods

4.3.3.1. Pattern photobleaching and multipoint analysis

Several other alternative approaches to Axelrod's FRAP model have also been developed. In 1978, Smith and McConnell developed periodic pattern photobleaching (FRAPP). This method passes a stationary laser beam through a Ronchi ruling to photobleach parallel stripes onto a fluorescent sample, which results in a periodic variation of fluorescence intensity. The mathematical model analyses the decay of the spatial frequency and amplitude of the periodic pattern to determine the diffusion coefficient. Others models based on FRAPP have been developed. For example, Munnelly *et al*, 1998, used the interferometric fringe pattern of two intersecting laser beams to pattern photobleach a fluorescent sample. This technique is able to bleach whole cell surfaces.

In 1979, Koppel developed multipoint analysis FRAP. This method uses a stationary laser to spot bleach a fluorescent sample. Fluorescence recovery is measured by using a movable focussed attenuated laser beam that can be sequentially positioned at up to twelve locations in and adjacent to the bleached area. The method can also monitor fluorescence recovery by line scanning. The methods of FRAPP and multipoint analysis FRAP are more sensitive to identifying directional flows and diffusion processes than Axelrod's model.

4.3.3.2. Total internal reflectance FRAP

Thompson *et al*, 1981, developed a FRAP technique using total internal reflectance fluorescence (TIR-FRAP). At certain incidence angles, a laser beam is totally internally reflected at the solid-liquid interface, generating an evanescent field at the reflectance point that can be used for photolysis and fluorescence imaging. Since the evanescent field decays exponentially from the interface and the beam spot is much wider than the photobleaching depth, fluorescence recovery can be modelled one-dimensionally, which potentially simplifies the mathematical analysis of the data (Swaminathan *et al*, 1996).

4.3.3.3. Continuous and discontinuous photobleaching techniques

FRAP techniques can be described as either discontinuous or continuous. Discontinuous techniques use an intense laser pulse of short duration in comparison to the characteristic diffusion time so that the diffusion of fluorescent molecules during photolysis is negligible. For example, in Axelrod's model, the duration of the pulse must be less than 10 % of the characteristic diffusion time (Axelrod *et al*, 1976). Recovery of fluorescence is then monitored using an attenuated laser. In contrast, continuous techniques measure fluorescence recovery whilst continually bleaching the sample. In fundamental terms, discontinuous techniques separate diffusion and photolysis while continuous techniques account for diffusion occurring during the photobleaching.

The first continuous technique, continuous fluorescence microphotolysis (CFM), was developed by Peters *et al* in 1981. CFM determines a diffusion coefficient from the fluorescence decay profile, which has been generated using a light source with a cross-sectional profile of a uniform intensity, circular disk. This technique accounts for diffusion occurring during photolysis and tends to be experimentally simpler than the discontinuous methods, although the analysis of experimental data requires detailed knowledge of the photobleaching kinetics.

4.3.3.4. Photobleaching techniques using confocal microscopes

Confocal microscopes combine the advantages described in section 4.2.1 with an ability to increase the amount of spatial information available for analysis. CLSMs possess all the instrumental components required for FRAP studies, except for a fast laser intensity modulation device, which may be custom fitted. In 1993, Blonk *et al* developed a discontinuous FRAP technique on a CLSM, which is similar to Koppel's multipoint analysis FRAP method.

In the same study, Blonk *et al* also proposed three different mathematical models, which were developed specifically to analyse FRAP data generated using CLSM. The first model is able to analyse data generated by a CLSM with a scanning laser beam and a closed confocal aperture. Essentially, this model accounts for three-dimensional

fluorescence recovery, but requires a detailed knowledge of both the axial resolution and the size of the confocal aperture. The second model is similar to the first model, except that the confocal aperture is fully open. The third model is similar to the second model, but the laser beam is stationary. The latter model is analogous to Axelrod's Gaussian profile model. The last two models assume that diffusion is two-dimensional and therefore, the CLSM must use low magnification and low numerical aperture objective lens in order to satisfy this assumption.

In 1994, Wedekind *et al* and Kubitscheck *et al*, 1994a, developed scanning microphotolysis (SCAMP), which uses a fast switching device to modulate laser intensity during scanning. As a result, SCAMP can photobleach and measure the recovery of fluorescence in different shapes. Kubitscheck *et al*, 1994b, proposed three different models to analyse fluorescence recovery data generated using SCAMP. In the first model, single time-point fluorescence profiles are used to determine individual diffusion coefficients, which are then used to calculate an average diffusion coefficient. The second model uses the linear relationship between variance of fluorescence intensity and time to determine the diffusion coefficient and the mobile fraction of fluorophore. The third model is analogous to Axelrod's model. Recently, Wedekind *et al*, 1996, have combined a high-resolution version of SCAMP and Blonk's model to develop line scanning microphotolysis (LINESCAMP)

4.3.3.5. Continuous photobleaching techniques using confocal microscopes

Continuous fluorescence multipoint microphotolysis (CFMM) was one of the first continuous photobleaching methods developed specifically for CLSM (Cutts *et al*, 1995). Using an analytical solution first derived by Brunger *et al* in 1985, CFMM accounts for diffusion occurring during photolysis. Equation 4.3 describes the initial post-bleach fluorescence profile across the photobleached spot.

$$\frac{\partial C(r,t)}{\partial t} = D\left[\frac{1}{r}\frac{\partial}{\partial r}\left(r\frac{\partial C(r,t)}{\partial r}\right)\right] - 2k_0 \exp\left[\frac{-2r^2}{\omega^2}\right]C(r,t) \qquad (4.3)$$

D is the diffusion coefficient, r is the radius of the bleached spot, t is time from the start of bleaching, k_0 is the photolysis rate constant and ω is half width of the Gaussian profile at e^{-2} height profile.

The fluorescence intensity is related to fluorophore concentration by equation 4.4

$$F(\Delta r,t) = \Pi\alpha\int_{-\infty}^{\infty} C(r,t)k(r-\Delta r)rdr \qquad (4.4)$$

F is fluorescence intensity.

CFMM uses equations 4.3 and 4.4 to determine diffusion coefficients from a single post-photobleached image. The experimental simplicity of this technique is counter-balanced by complicated mathematical analysis.

4.3.3.6. Photobleaching techniques using two-photon confocal microscopy

Two-photon confocal microscopy is a highly spatially selective imaging technique that is capable of higher resolution than single-photon confocal microscopy (up to 500% increased lateral resolution, (Kubitscheck *et al*, 1996)). Kubitscheck *et al*, 1996, combined the techniques of SCAMP and two-photon confocal microscopy to develop a three-dimensional SCAMP technique, in which the rate of fluorescence influx is used as a measure of fluorophore mobility.

4.3.3.7. FRAP models accounting for anomalous diffusion

The majority of FRAP models assume the diffusion of fluorescent molecules is due to Brownian motion and that a fraction of the fluorescent molecules are immobile. In this case, the diffusion coefficient is independent of time but dependent on the structure of

the medium. However, several studies tracking cell surface receptors have indicated that diffusion may occur by other mechanisms, such as anomalous or restricted diffusion. In these cases, the diffusion coefficient is dependent on both time and the structure of the medium. Several investigators have adapted Axelrod's model to account for diffusion coefficients being time dependent (Feder *et al*, 1996 and Perisamy *et al*, 1998) and for multiple diffusing species that may undergo either simple Brownian diffusion or anomalous diffusion (Perisamy *et al*, 1996 and 1998).

4.4. Development of a technique to measure the mobility of a fluorescent solute in a model gel system

4.4.1. Rationale

The bioadhesion of hydrophilic matrices may involve mechanisms, for example polymer interpenetration and mucus dehydration, that can affect the structure and diffusion retarding properties of the polymer and mucus networks. Consequently, solute mobility may be used to indirectly monitor changes in the structure of the polymer and mucus networks. Fluorescence photobleaching is one method that can determine the localised rate of transport of a solute in the microscopic environment of a polymer network.

4.4.2. The mathematical model

The recovery of fluorescence in a photobleached hole is described by equation 4.5 (Grebenkamper and Galla, 1994).

$$\frac{[F(t)-F(\infty)]}{[F(0)-F(\infty)]}=\exp\left(-\frac{t}{\tau}\right) \qquad (4.5)$$

F(t) is the fluorescence intensity at time t, F(0) is the fluorescence intensity immediately after bleaching, F(∞) is the fluorescence intensity at very long times after photobleaching and τ is the characteristic fluorescence recovery time.

The characteristic fluorescence recovery time (τ) is related to the rate of transport (R_T) by equation (4.6).

$$R_T \approx \frac{A^2}{\tau} \tag{4.6}$$

R_T is lateral rate of transport and A^2 is area of the bleached spot.

4.4.3. The relationship between fluorescence and fluorophore concentration

An essential assumption of all fluorescence photobleaching techniques is that the relationship between fluorescence intensity and fluorophore concentration is linear. Therefore, the aim of this section was to determine the range of sodium fluorescein concentrations having a linear relationship with fluorescence.

4.4.3.1. Method

100 mg of sodium fluorescein was dissolved in 100 ml of physiological saline to give a 0.1% w/v stock sodium fluorescein solution, which was diluted with physiological saline to give a range of dilute solutions. The solutions were excited at 0.015 mW laser power using the 488 nm laser line of the CLSM and fluorescence was detected at 510 nm.

4.4.3.2. Results

A fluorescence:concentration plot of sodium fluorescein is shown in figure 4.3. This shows that sodium fluorescein concentrations up to 0.01% w/v have a linear relationship with fluorescence intensity. This agrees with previous work carried out on the same instrument by Cutts *et al*, 1995. Therefore, future experiments used fluorescent markers at concentrations equivalent to 0.01% w/v sodium fluorescein.

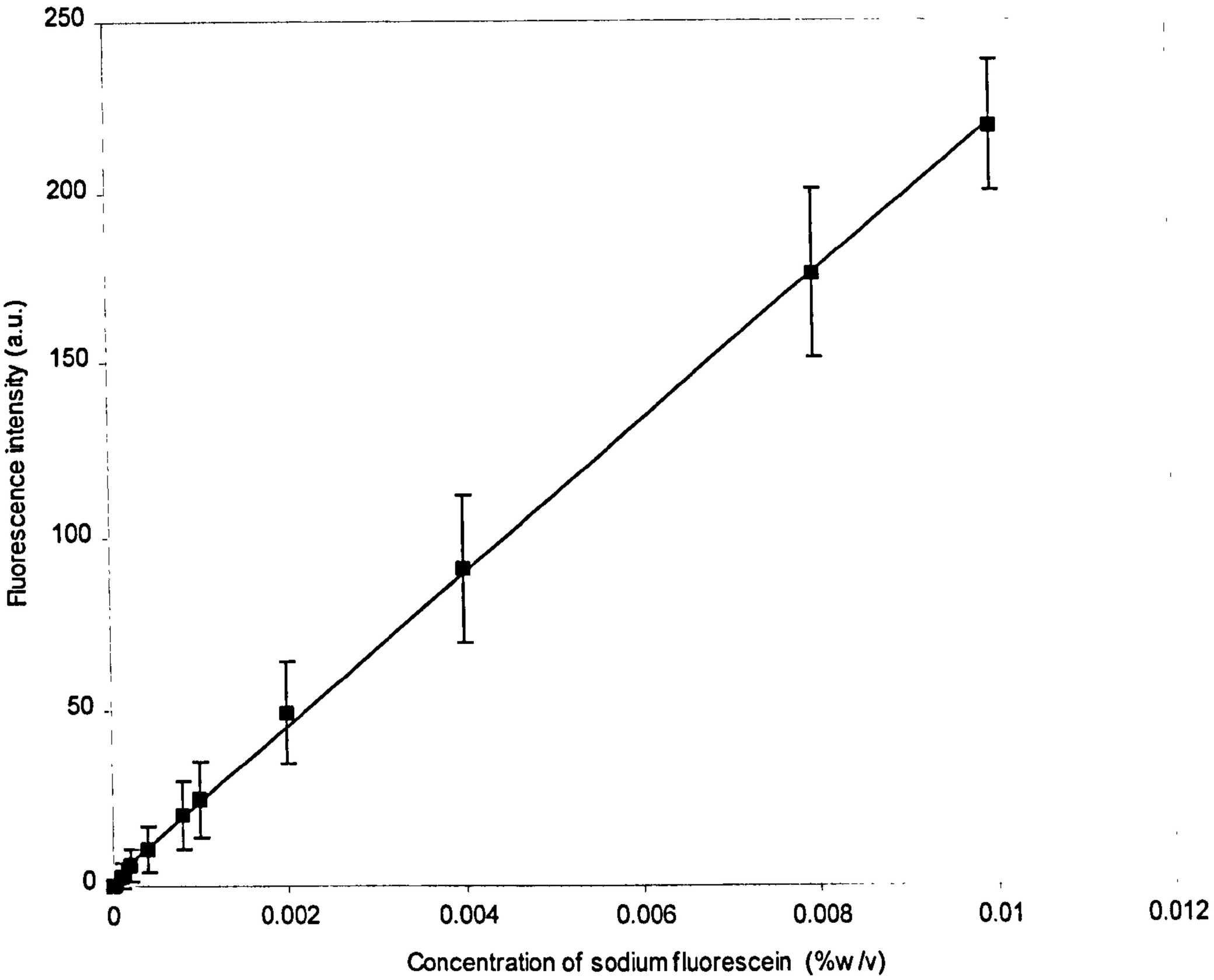

Figure 4.3 The relationship between fluorescence intensity and the concentration of sodium fluorescein

A fluorescence:concentration plot of sodium fluorescein in physiological saline, determined at 25±1°C, using a BioRad MRC600 CLSM fitted with a Nikon x10 (NA 0.13) objective, exciting at 488 nm and detecting at 510 nm (mean, n=3, ±1 SD).

4.4.4. Calibration of the time between recovery images

The mathematical model used in this study (section 4.4.2) requires the exact time between fluorescence recovery images to be known in order to accurately and precisely calculate the rate of transport. Therefore, the aim of this section was to measure the exact times between the recovery images acquired using the BioRad MRC600 CLSM.

4.4.4.1. Method

The laser beam of the CLSM was focussed onto a photodiode cell, which was connected to an oscilloscope. The photodiode can detect the scanning of the laser beam and produce a trace on the oscilloscope. The photobleaching program, JPROGBLCH, was run and the input time (T_i) between the images was varied. The actual time (T_a) between the scanning traces of the recovery images was measured on the oscilloscope. The input time (T_i) was defined as the desired time between each recovery image and the actual time (T_a) was defined as the exact time between recovery images.

4.4.4.2. Results

Table 4.1 The exact time (T_a) between recovery images acquired using the bleaching program, JPROGBLCH (n=3).

T_i (sec)	T_a (sec)	±SD	$\lvert T_a - T_i \rvert$ (sec)
1	3.55	0.13	2.55
2	3.58	0.31	1.58
3	3.55	0.15	0.55
4	4.13	0.93	0.13
5	5.14	0.07	0.14
7	7.13	0.07	0.13
10	10.15	0.02	0.15
12	12.17	0.15	0.17
15	15.19	0.07	0.19
20	20.20	0.07	0.20
25	25.20	0.07	0.20
30	30.19	0.06	0.19

Table 4.1 lists the actual times between recovery images. The results show that for T_i<3 secs, T_a≈3.55 sec and for T_i>3 sec (T_i+0.13)<T_a<(T_i+0.20) secs. The shortest possible time between recovery images that can be measured using this experimental set-up was ≈3.55 sec. Therefore, this indicates that highly diffusable species cannot be measured, limiting the range of measurable transport rates.

This 'lag time' between T_a and T_i when T_i<3 secs may be due to a combination of slow operation of the laser shutters and the galvanometer-driven mirrors by the computer. Using a computer with a faster processor and more memory may reduce the 'lag time'.

4.4.5. General method for photobleaching and imaging recovery of fluorescence

Fluorescent samples were photobleached at 5 mW laser power and fluorescence recovery was imaged at 0.15 mW laser power using the 488 nm laser line and detecting at 510 nm. Figure 4.2 illustrates a typical example of fluorescence recovery in a photobleached fluorescent sample. The program JPROGBLCH (Cutts, 1994), written by J. Adler, University of Nottingham, automated the procedures involved in photobleaching and imaging the samples.

Semper 6.4 (Synoptics, Cambridge) image analysis software was used to locally average the recovery images over a 3 x 3 pixel square. Each recovery image was divided by the pre-bleach image in order to remove image artefacts and improve the signal-to-noise ratio. The radial fluorescence intensity profiles (F_P) across the bleached holes were measured and output in ASCII format. Figure 4.4a shows a typical set of radial profiles showing fluorescence recovery. The Semper program, FRAP5, was written to automate the image analysis procedures.

The photobleached area (A^2) was determined from the initial post-bleached image. This area was defined as the area of the sample in which fluorescence had decreased by more than 10% of the original value. The 10% decrease in fluorescence was considerably greater than that induced by the normal imaging of the sample. The Semper program, AREA1, was written to automate this procedure.

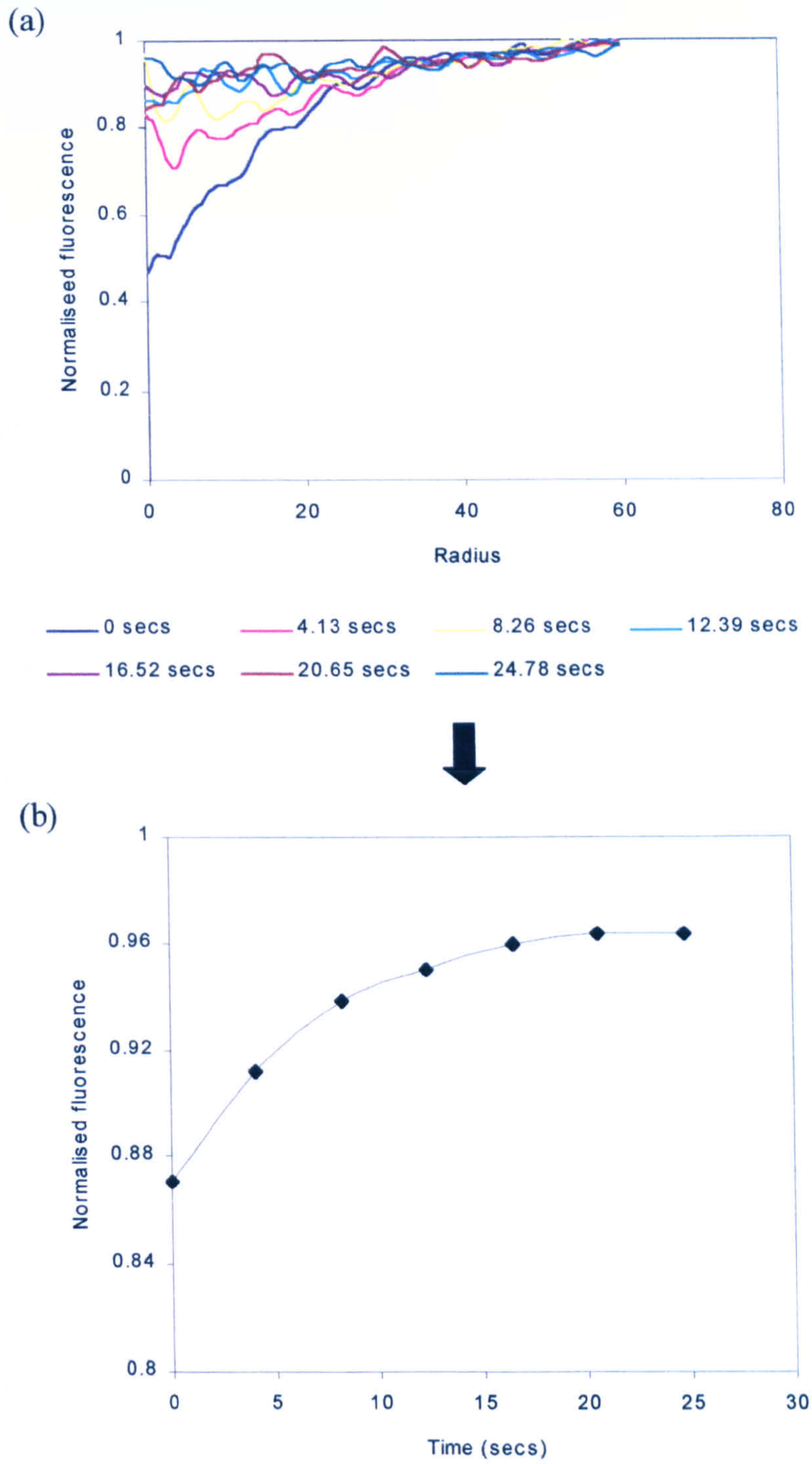

Figure 4.4 Examples of (a) fluorescence intensity profiles (F_P) and (b) the fluorescence recovery profile (R_P) of a photobleached area.

The fluorescence recovery profile (R_P) was determined by integrating the fluorescence intensity profiles (F_P), which were obtained by photobleaching a 580 kDa FITC-dextran for 4 sec and imaging fluorescence recovery every 4.13 sec.

In order to determine the characteristic fluorescence recovery time (τ), the fluorescence profiles (F_P) were integrated and plotted against time to produce a fluorescence recovery profile (R_P) (figure 4.4b), which was then fitted to a range of theoretical fluorescence recovery profiles, calculated using equation 4.5. The diffusion programs, FRMK1, FRMK3 and FRMK6, written by J. Holden, University of Nottingham, automated the calculation of τ. The rates of transport (R_T) were calculated using equation 4.6. The diffusion programs differed in respect to the type of algorithm used to calculate τ. The critical parameters of each type of algorithm are listed in table 4.2.

Table 4.2 The diffusion programs used to calculate the rate of transport

Parameter	**Diffusion program**		
	FRMK1	**FRMK3**	**FRMK6**
F(0)	Constant	Constant	Constant
F(∞)	Constant	Constant	Varied
Integration method	Radial[a]	Circular[b]	Radial[a]
Fitting procedure	Least sum of squares	Pearson's r^2 value	Least sum of squares

[a] Radial integration calculates the integral as area under F_P, i.e. $\int_0^R f(r)\,dr$

[b] Circular integration calculates the integral as a function of radius and area under F_P, i.e. $\int_0^R 2\Pi r\, f(r)\,dr$

4.4.6. Method for manufacturing an agar gel permeated with FITC-dextrans

Low melting point agarose was dissolved in physiological saline at 40°C to produce a 1% w/v agar solution. FITC-dextran was added and stirred to produce a homogeneously mixed solution. Agar gel slabs were prepared by filling a white soft paraffin cavity, lined with 212-300 μm diameter glass beads, with molten agar and sealing with a cover slip. The molten agar was allowed to cool and set at room temperature for 30 mins before being used.

4.4.7. Influence of the number and the radius of fluorescence intensity profiles on the rate of transport

The number and radius of the fluorescence profiles (F_P) used by the diffusion programs to calculate R_T values can be varied. Therefore, the aim of this section was to study the relationship between the number and radius of F_P used by the diffusion programs and the rate of transport (R_T).

4.4.7.1. Method

Agar gel slabs permeated with 71.2 kDa FITC-dextran were prepared according to the method in section 4.4.6. The slabs were equilibrated at 25±1°C for 15 mins before being photobleached for 5 sec and fluorescence recovery monitored every 15.9 sec after photobleaching. Ten sets of profiles measuring fluorescence recovery were obtained and these were used as 'standards' for the diffusion programs FRMK1, FRMK3 and FRMK6 to calculate R_T. In the study investigating the influence of the number of fluorescence profiles on R_T, 74 μm long profiles were used to calculate R_T. In the study investigating the influence of F_P radius on R_T, nine fluorescence profiles were used to calculate R_T.

4.4.7.2. Results

Figure 4.5a shows how the number of fluorescence profiles (F_P) used by the diffusion programs influences the R_T values. Figure 4.5b shows how the radius of the fluorescence profiles (F_P) affects the R_T values.

The R_T values calculated by FRMK1 and FRMK6 decreased as the number of fluorescence profiles increased, although the relationship was not linear. In contrast, the R_T values calculated by FRMK3 appeared to slightly increase when $F_P \leq 5$, but was approximately constant $F_P \geq 6$. The diffusion program FRMK6 calculated R_T values at least three times faster than FRMK1 and at least twelve times faster than FRMK3.

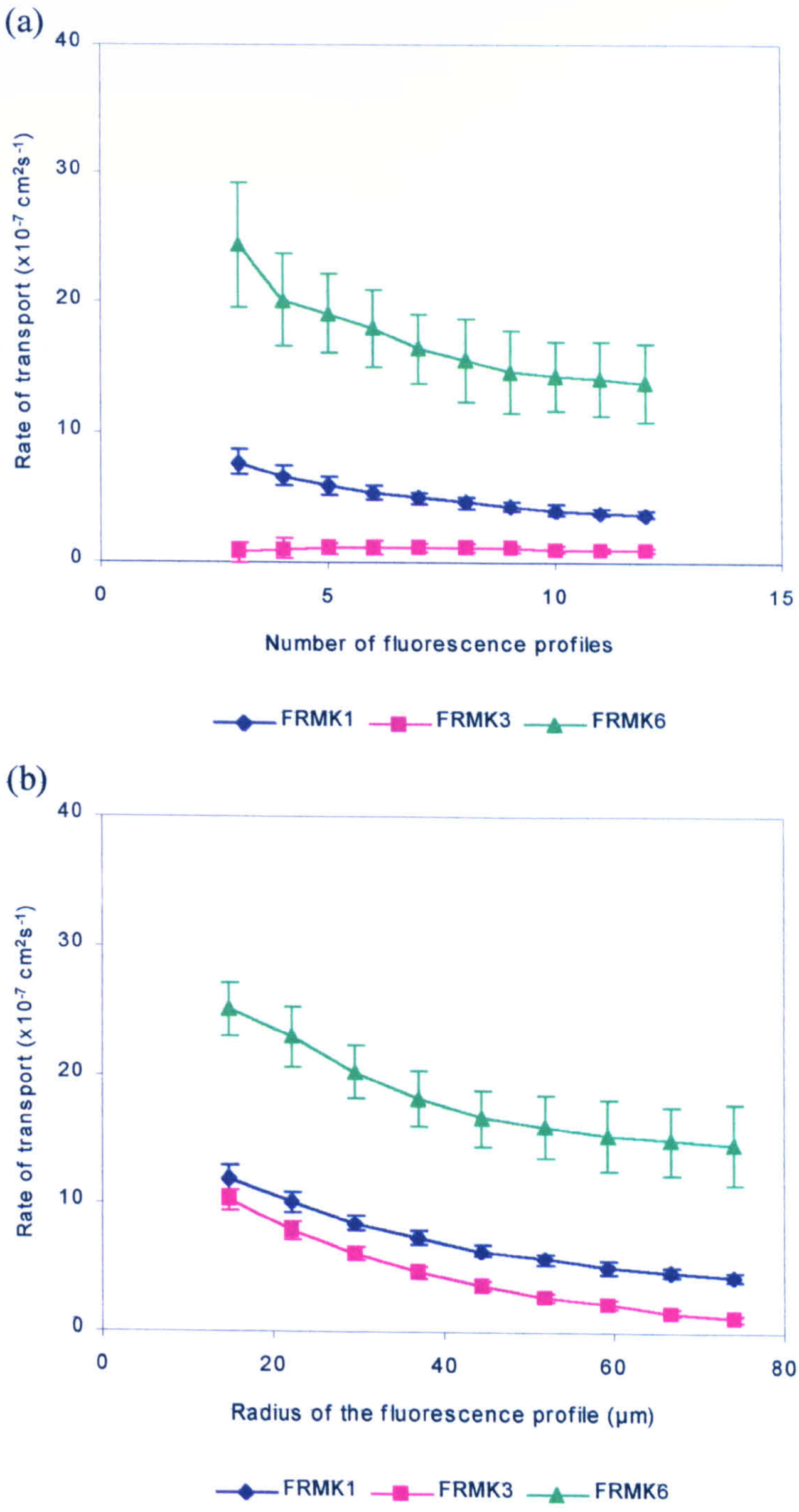

Figure 4.5 Influence of (a) the number and (b) the radius of the fluorescence intensity profiles (F_P) on the rate of transport (R_T).

The R_T values were determined using a set of fluorescence profiles (F_P) generated by photobleaching agar gel slabs, permeated with 71.2 kDa FITC-dextran at 25±1°C, for 5 sec and monitoring fluorescence recovery every 15.9 sec (mean, n=10, ±1 SD).

The R_T values calculated by all three diffusion programs decreased as the F_P radius increased. The diffusion program FRMK6 calculated R_T values at least three times faster than FRMK1 and at least five times faster than FRMK3.

4.4.7.3. Discussion

The R_T values determined by the diffusion programs, FRMK1 and FRMK6, were influenced by the number of fluorescence profiles used to calculate R_T. The R_T values were inversely related to the number of profiles, although this relationship was not linear (figure 4.5a).

The number of F_P used by the diffusion programs to calculate R_T relates to the length of time that fluorescence recovery has been monitored and in this case, recovery images were acquired every 15.9 secs. The shape of the recovery profiles (figure 4.4b) suggests that fluorescence recovery is rapid in the early stages but slows down at later times. Therefore, the early part of the recovery profile may give higher R_T than the profile at later times.

The R_T values in figure 4.5a seem to be approaching equilibrium as the number of profiles increase and consequently as more fluorescence recovery is monitored. This type of relationship is inferred by the Axelrod model, which states that at least 80% of the complete fluorescence recovery data must be used to determine diffusion coefficients (Axelrod *et al*, 1976). Therefore, it seems rather than a using a set minimum number of profiles to calculate R_T, the minimum number of profiles used should monitor most of the fluorescence recovery.

In the case of the diffusion program FRMK3, the independence of R_T on number of fluorescence profiles (F_P) when $F_P \geq 6$ seemed to be desirable (figure 4.5a). However, close examination of the algorithm used by FRMK3 revealed that it 'weights' the integral of the F_P at large radial distances. This may distort the recovery profile (R_P) and distort the calculation of R_T values. Therefore, FRMK3 was not developed further since this 'radial weighting' may result in the diffusion program not being sensitive to small differences in R_T values.

The R_T values calculated by all three diffusion programs also seemed to be influenced by the F_P radius, with the value of R_T decreasing as the F_P radius increased (figure 4.5b). The recovery profiles (R_P) calculated using fluorescence profiles (F_P) of different radius have different shapes. This is seen in figures 4.6a and 4.6b. The recovery profiles calculated from short radius fluorescence profiles had greater slopes than recovery profiles calculated from longer radius fluorescence profiles and consequently have faster R_T values.

Other fluorescence photobleaching methods stipulate that the radius of the fluorescence profile (F_P) must be considerably greater than the radius of the bleached hole, for example Kubitscheck *et al*, 1994b and Gribbon and Harding, 1998 specify that the radius of F_P must be at least three times longer than the bleached hole radius.

4.4.7.4. Conclusion

The number and radius of the fluorescence profiles (F_P) may influence the calculated values of R_T. These parameters must remain constant when measuring the R_T values in different samples. It seems that the number of fluorescence profiles used to calculate R_T must monitor most of the fluorescence recovery. The radius of the profiles should be larger than the radius of the bleached hole.

4.4.8. Influence of photobleaching time and time between recovery images on rate of transport

In section 4.4.7, the number and radius of the F_P were shown to influence the value of R_T. The photobleaching time (T_{bl}) and the time between fluorescence recovery images (T_a) are parameters that can also be varied and may likewise influence R_T values. Therefore, the aim of this section was to study the influence of T_{bl} and T_a on R_T.

4.4.7.1. Method

Agar gel slabs permeated with either 12 kDa or 580 kDa FITC-dextrans were prepared according to the method outlined in section 4.4.6. The 580 kDa FITC-dextran was used

(a)

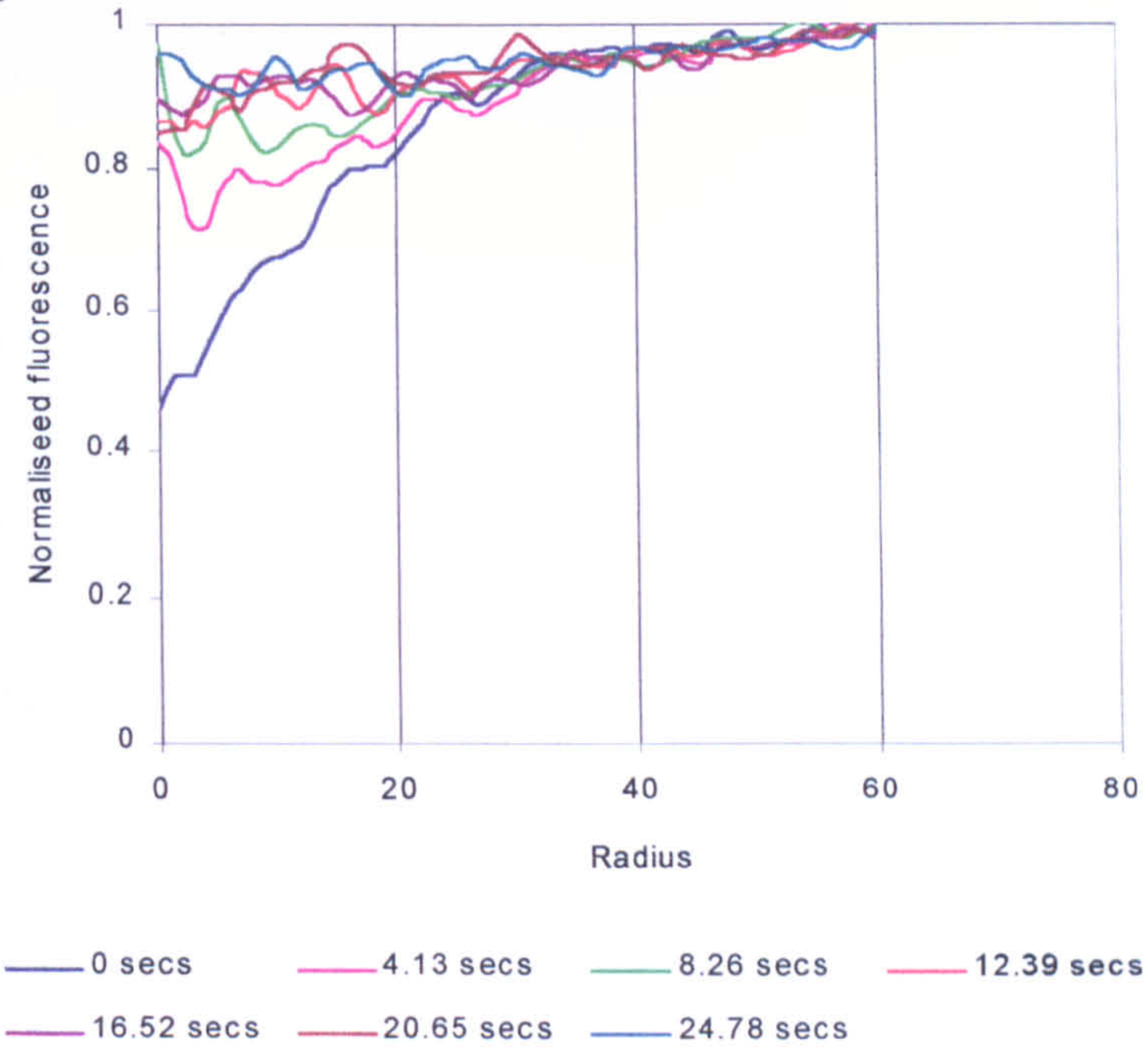

(b)

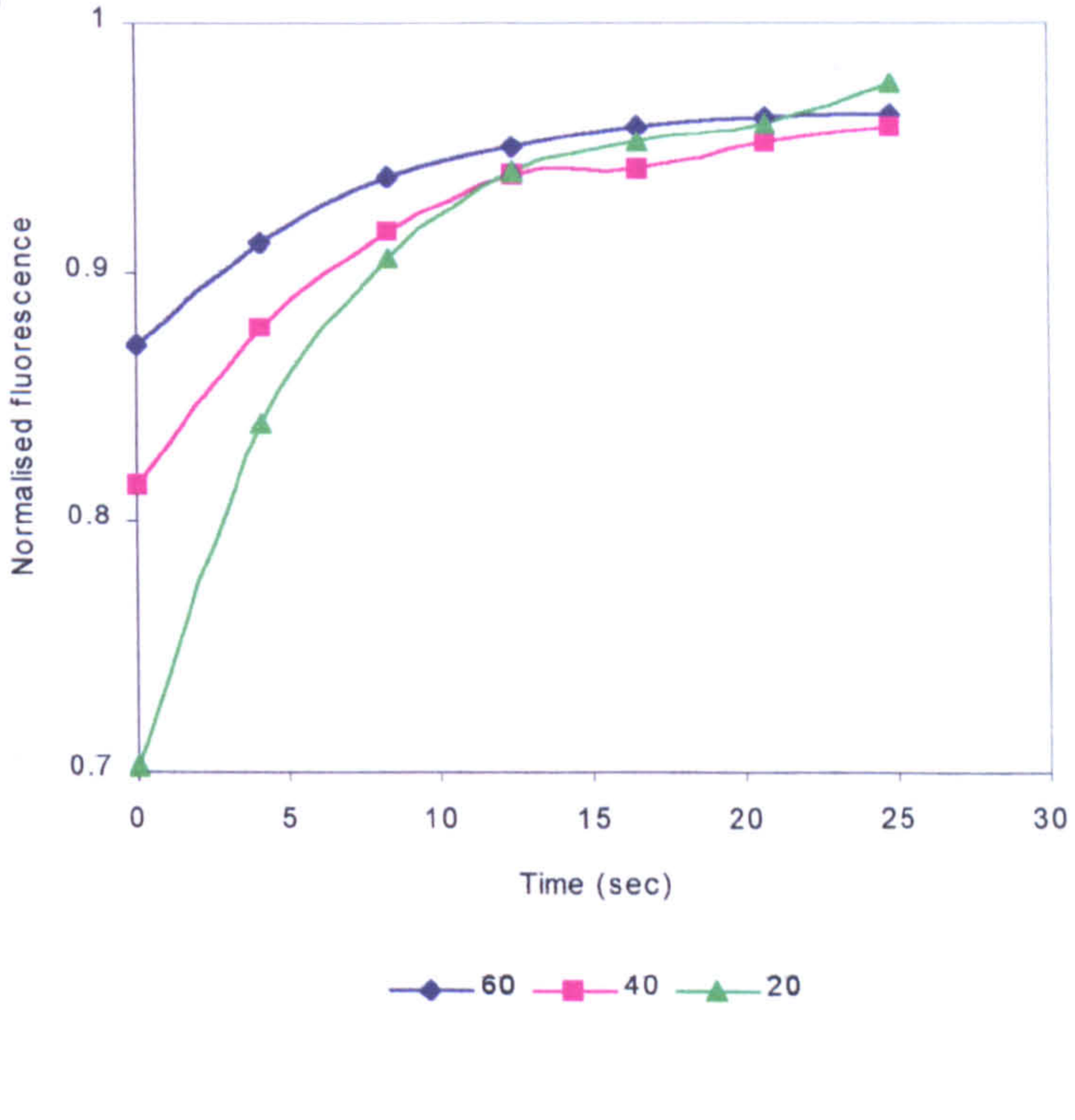

Figure 4.6 The influence of fluorescence profile radius on the fluorescence recovery profile

The recovery profiles (R_P) were calculated using fluorescence profiles (F_P) with radii of either 20, 40 or 60 pixels (see figure 4.6a).

to study the influence of T_a on R_T since it moves slowly enough to allow long T_a values to be evaluated. The 12 kDa FITC-dextran was used to study the influence of T_{bl} on R_T since its high mobility may accentuate any potential effects. The agar slabs were equilibrated at 25±1°C for 15 mins and photobleached according to the general method described in section 4.4.5. The 580 kDa FITC-dextran was photobleached for 5 sec and recovery time varied. The 12 kDa FITC-dextran was photobleached for varying times and recovery imaged every 4.18 sec. The diffusion program FRMK1 was used to calculate R_T.

4.4.7.2. Results

Figure 4.7a shows that the relationship between R_T and T_{bl} was approximately linear when $T_{bl} \leq 10$ sec, but at longer T_{bl}, R_T values decreased. The T_{bl} times of 10 secs and 20 secs produced extremely variable R_T values.

Figure 4.7b shows that the calculated R_T values decreased with increasing T_a when $T_a < 10$ sec, but were independent of T_a when $T_a \geq 10$ sec.

4.4.7.3. Discussion

The relationship between T_a and R_T values (figure 4.7b) is in essence similar to the relationship between the number of fluorescence profiles and R_T (section 4.4.7). When T_a is short (<10 sec), sufficient fluorescence recovery may not have been monitored, resulting in the calculation of erroneously high R_T values. When T_a is long (≥10 sec), most of the fluorescence recovery is monitored and the diffusion programs calculate similar R_T values.

The bleaching time (T_{bl}) has a considerable influence on the value of R_T (figure 4.7a) and the underlying reasons are unclear. The mathematical model used by Cutts *et al*, 1995, was adapted to generate sets of fluorescence profiles for a constant diffusion coefficient and for varying T_{bl} times. These profiles were then used to determine the inverse of the characteristic diffusion time (τ^{-1}), which is directly proportional to R_T (equation 4.6). It can be clearly seen from figure 4.8 that the τ^{-1} values decreased as T_{bl}

(a)

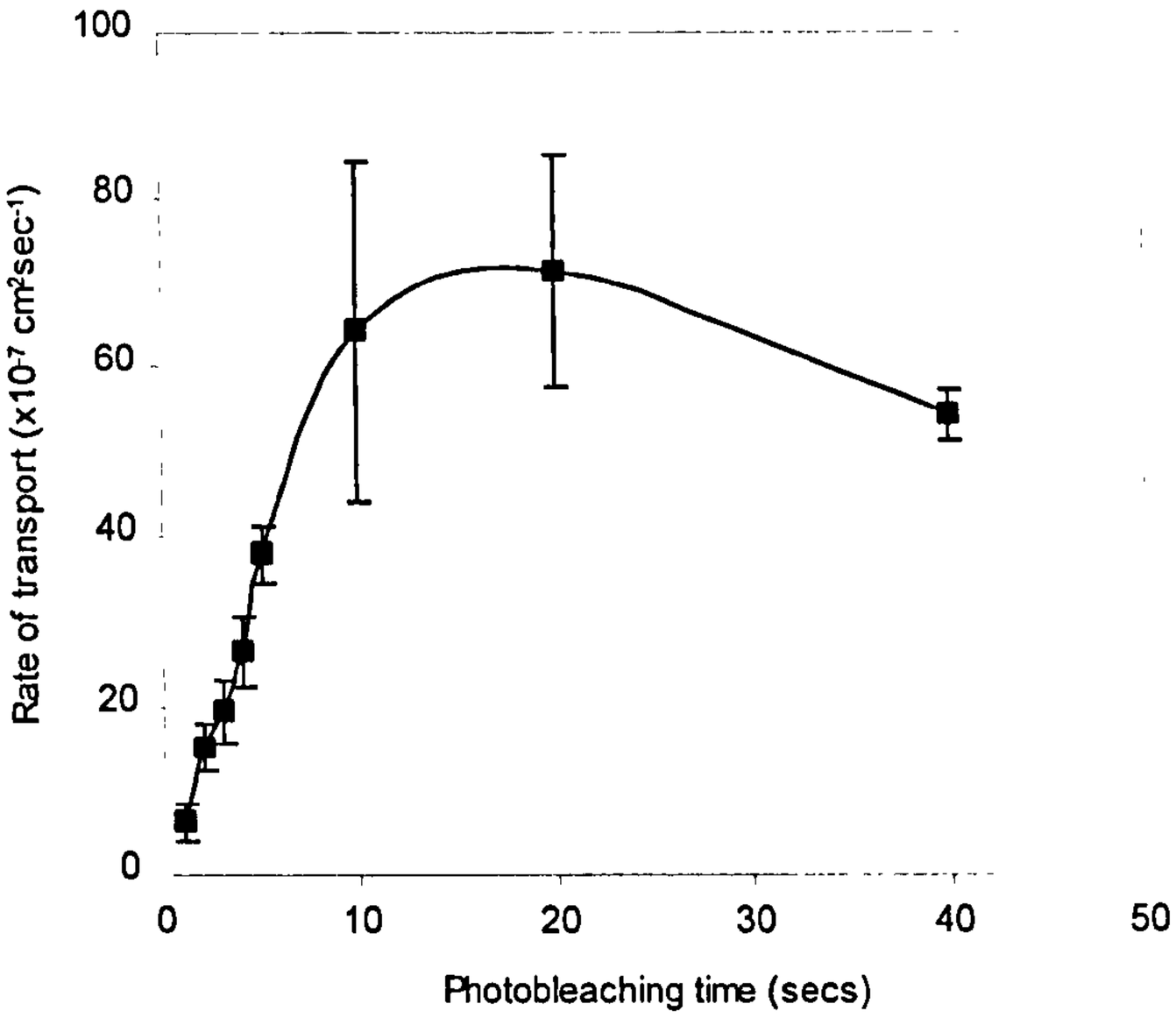

(b)

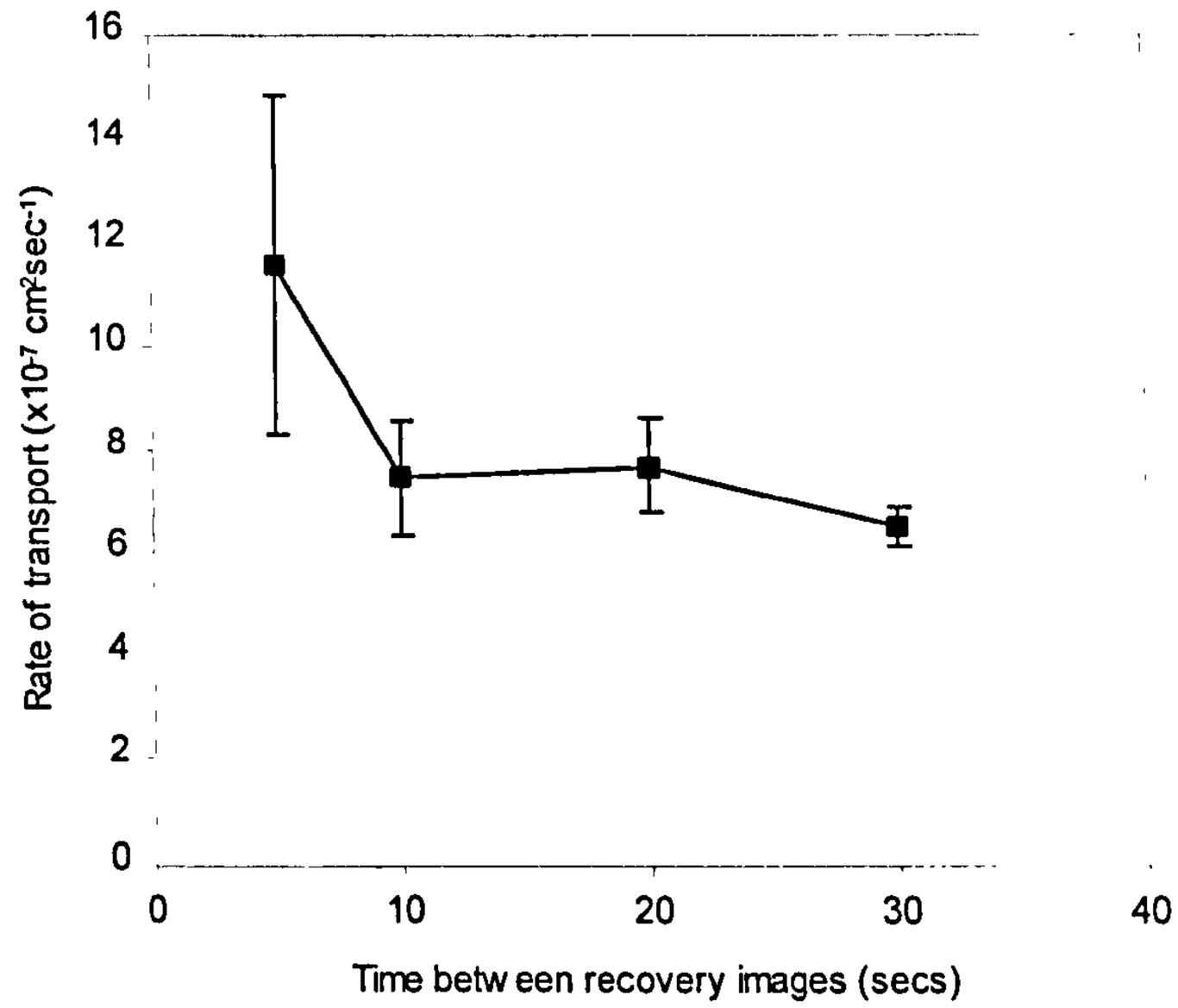

Figure 4.7 Influence of (a) photobleaching time (T_{bl}) and (b) time between recovery images (T_a) on R_T

(a) The influence of T_{bl} on R_T was determined by photobleaching 12 kDa FITC-dextran permeated agar gel slabs at 25±1°C and monitoring recovery every 4.13 sec (n=10, ±1 SD). (b) The influence of T_a on R_T was determined by photobleaching 580 kDa FITC-dextran permeated agar gel slabs at 25±1°C for 5 sec and monitoring recovery (n=10, ±1 SD).

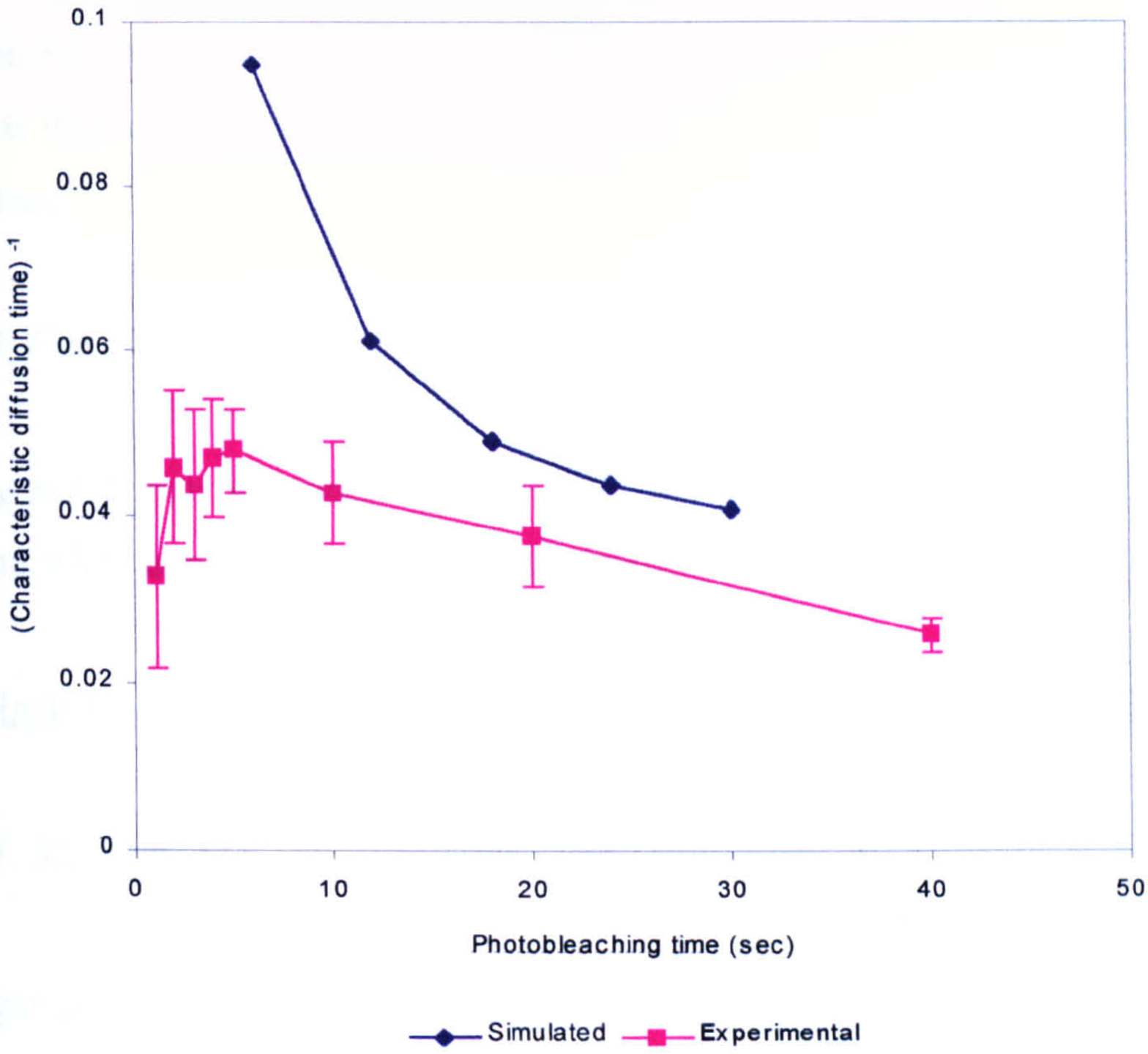

Figure 4.8 Influence of photobleaching time on the characteristic diffusion time

Experimental τ^{-1} values were determined by measuring the mobility of 12,000 Da FITC-dextran in agar gel at 25±1°C (n=10, ±1 SD). Computer simulated τ^{-1} values represent a solute with a diffusion coefficient of 5×10^{-11} m^2 sec^{-1} (n=1).

increased, which generally agreed with the trend observed in the experimental results between 10-30 sec. Although this does not fully explain why T_{bl} influenced R_T, it suggests that the source of the influence lies with the calculation of R_T by the diffusion programs.

4.4.7.4. Conclusion

The T_{bl} and T_a may influence the calculated R_T values and therefore must remain constant when comparing the rate of transport in different samples.

4.4.8. Influence of molecular weight on rate of transport of FITC-dextrans

4.4.8.1. Method

The agar gel slabs were prepared as in section 4.4.6 and equilibrated to 25±1°C for 15 mins. The R_T values were determined by photobleaching FITC-dextrans for 5 sec and monitoring fluorescence recovery every 4.13 sec after photobleaching. The diffusion programs, FRMK1 and FRMK6, used nine 148 μm radius fluorescence profiles to calculate R_T.

4.4.8.2. Results

Figure 4.9 shows the influence of molecular weight on the mobility of FITC-dextrans in agar, determined by the diffusion programs FRMK1 and FRMK6, CFMM and a classical double diffusion cell technique

In the case of both FRMK1 and FRMK6, the calculated R_T values decreased as log[molecular weight] of the FITC-dextrans increased, but with FRMK6 the relationship was not linear. A comparison of the two sets of data showed that R_T values calculated by FRMK6 were approximately three times faster than those calculated by FRMK1. The R_T values calculated by FRMK1 were substantially more reproducible than those calculated by FRMK6.

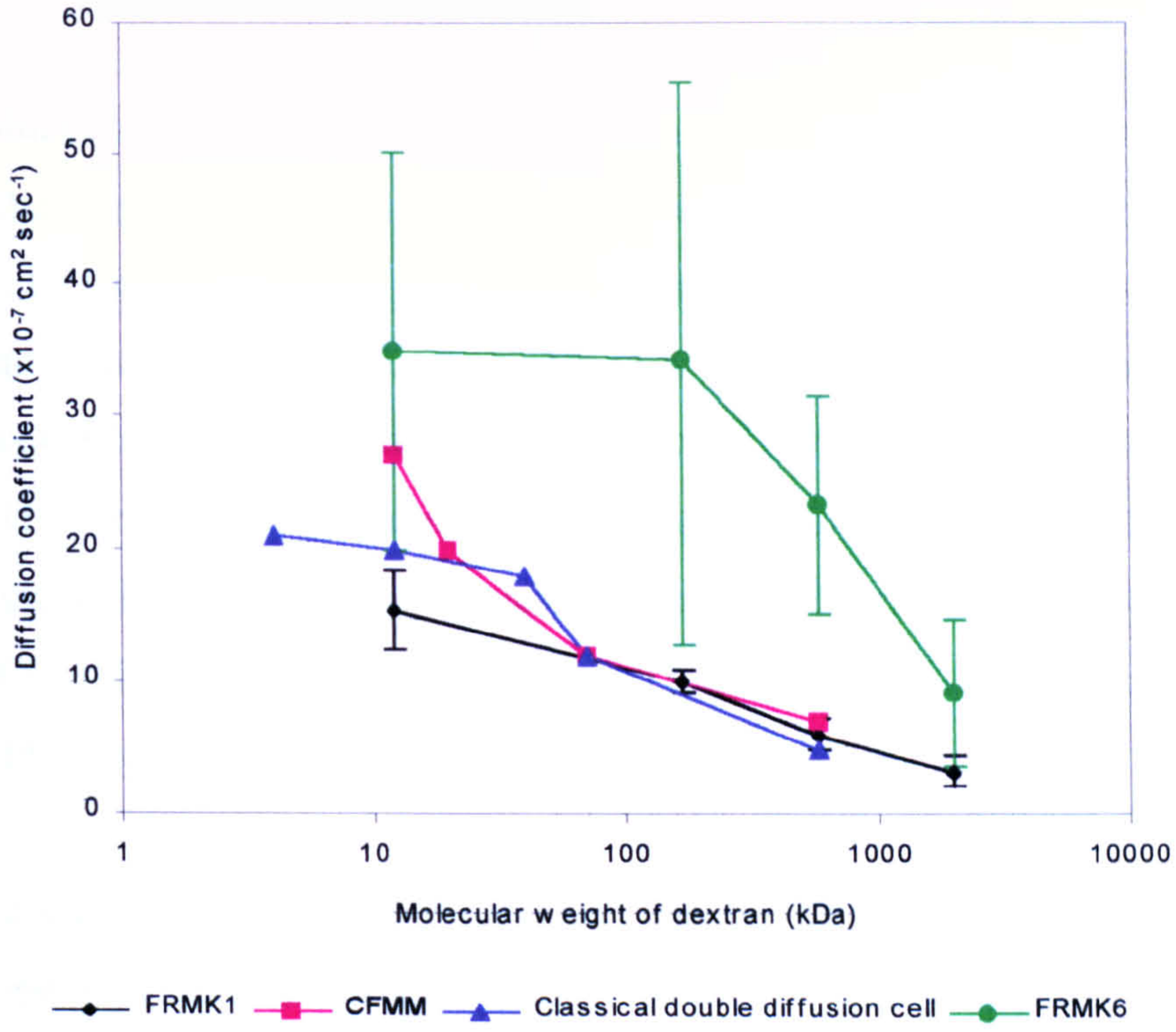

Figure 4.9 Comparison of FRMK1, FRMK6, CFMM and a classical double diffusion cell technique.

The influence of molecular weight on the mobility of FITC-dextran in agar gel was determined by FRMK1, FRMK6, CFMM and a classical double diffusion cell technique. FRMK1 and FRMK6 calculated R_T values of FITC-dextrans in agar gel at 25±1°C; the FITC-dextrans were photobleached for 5 sec and the recovery of fluorescence monitored every 4.13 sec (mean, n=10, ±1 SD). The diffusion coefficients determined using CFMM and classical double diffusion cell technique were transcribed from Cutts *et al*, 1995.

4.4.8.3. Discussion

The R_T values calculated by FRMK1 had a linear relationship with log[molecular weight]. The linearity of the relationship and the R_T values agreed with previous work carried out by Cutts *et al*, 1995, especially when molecular weight of FITC-dextran is greater than 70 kDa (figure 4.9). Cutts *et al* used CFMM and a classical double diffusion cell technique to determine diffusion coefficients of different molecular weights FITC-dextrans in the same experimental system used in this work. The R_T values calculated by FRMK6 were at least three times faster than those calculated by FRMK1, CFMM and the double diffusion cell technique and did not display a linear relationship with log[molecular weight].

Pair-wise comparisons of the R_T values were used to see whether the diffusion programs could differentiate between different molecular weight dextrans. In this analysis, R_T values of the 12 kDa dextran were compared with R_T values of the 16.7 kDa dextran. Likewise, R_T values of the 16.7 kDa dextran were compared with R_T values of the 580 kDa dextran and so forth.

The R_T values of the different molecular weight dextrans calculated by FRMK1 were statistically significantly different ($p<0.02$). In contrast, the R_T values of the 12 kDa, 16.7 kDa and 580 kDa dextrans calculated by FRMK6 were not statistically significantly different ($p>0.05$), although the R_T values of the 2000 kDa FITC-dextran were statistically significantly different ($p<0.02$).

Close examination of the algorithms of each diffusion program revealed that FRMK6 varied the value of F_∞, therefore improving the goodness of fit between theoretical and experimental recovery profiles (R_P). This suggests that FRMK6 would be the more accurate than FRMK1. However, this also suggests that FRMK6 may be more sensitive to anomalous and artefactual recovery profiles, resulting in the highly variable values of R_T seen in figure 4.9. This variability may partially explain why FRMK6 cannot differentiate between the R_T values of different molecular weight dextrans and it may restrict the practical application of FRMK6.

Therefore, the diffusion program FRMK1 was used in future experiments studying the rate of transport in bioadhesive bonds. The advantage of this method in comparison to other fluorescence photobleaching methods, especially those based on Axelrod's mathematical model, is that it is experimentally simple and the mathematical model is not restricted by the assumptions listed in section 4.3.2.1. This means that this method can measure R_T not only in homogeneous but also in heterogeneous samples, such as some pharmaceutical dosage forms and bioadhesive bonds. The disadvantage of this method is that it may be influenced by some experimental parameters. However, the majority of photobleaching methods reported in the literature do not appear to have been evaluated by the type of study outlined in this chapter. It is therefore quite possible that these models are equally influenced by similar experimental parameters.

4.5. Conclusion

The aim of this chapter was to develop a fluorescence photobleaching technique that may be used to measure the mobility of fluorescent solutes in bioadhesive bonds formed between pig gastric mucus and sodium alginate matrices. A discontinuous fluorescence photobleaching technique using the diffusion program FRMK1 has been developed that can measure the mobility of FITC-dextrans in agar gel. This technique has been characterised with respect to the experimental parameters used to measure and calculate R_T. The technique showed excellent agreement with previously published results obtained in the same experimental system using the continuous photobleaching technique of CFMM and a classical double-diffusion cell technique.

Chapter 5

Development of a technique to measure diffusion of water inside bioadhesive bonds using magnetic resonance imaging microscopy

5.1. Introduction

Several mechanisms may be involved in the formation of bioadhesive bonds. The work of Mortazavi and Smart (Mortazavi and Smart, 1993, and Smart *et al*, 1991) has suggested that the bioadhesive bond strength may be dependent on the ability of a polymer to dehydrate the mucus gel layer. The technique of MRI can non-invasively image the spatial distribution of water self-diffusion coefficient (SDC) and has been used to image complex processes occurring inside hydrating dosage forms (Rajabi-Siahboomi *et al*, 1994 and 1996). Therefore, it appears to be an ideal method to measure the diffusion of water inside a bioadhesive bond

5.1.1. Principles of magnetic resonance imaging

Some atomic nuclei, such as ^{1}H, ^{19}F, ^{31}P and ^{13}C, possess a net magnetic moment, which can align itself with (low energy) or against (high energy) an applied magnetic field (B_0). The alignment of nuclei produces a small net magnetisation, which precesses about the applied magnetic field when disturbed from equilibrium. The frequency of the precession is termed the Larmor frequency and is given by equation 5.1.

$$\nu = \frac{\gamma B_0}{2\Pi} \tag{5.1}$$

ν is the Larmor frequency, γ is the gyromagnetic constant, which is dependent on the nuclear species and B_0 is the applied field strength.

The Larmor frequency is the frequency at which nuclei maximally absorb RF energy. The absorption of RF energy causes the nuclei to attain different orientations in B_0, disturbing the net magnetisation and causing the nuclei to precess. The nuclear precession induces a small voltage in a tuned receiver coil surrounding the sample. This forms the NMR signal, which is intrinsically weak but increases in strength with increasing magnetic field and gyromagnetic constant (Melia *et al*, 1998).

The nuclei lose absorbed energy by either spin-lattice relaxation (T_1) or spin-spin relaxation (T_2) and eventually return to equilibrium. In spin-lattice relaxation, spins lose energy to the environment, causing the net magnetisation to realign with B_0. Each nucleus can also interact with other neighbouring nuclei and as a result precess at different rates, causing the net magnetisation to lose phase (Paudler, 1987). This reduces the magnitude of the transverse component of the net magnetisation and results in the decay of the NMR signal. This type of relaxation is described as spin-spin relaxation. Spin-lattice and spin-spin relaxation mechanisms can be respectively characterised by the T_1 and T_2 relaxation times. Both relaxation times are strongly environmentally sensitive and carry extra information about the sample. By applying appropriate RF pulse sequences, images may either be T_1 or T_2 weighted, as well as being dependent on ^1H density.

5.1.2. Magnetic resonance imaging microscopy

In 1973, Lauterbur (Lauterbur, 1973) and Mansfield and Grannell (Mansfield and Grannell, 1973 and 1975) demonstrated that a magnetic field gradient can be used to spatially encode NMR signals. They found that the strength of a magnetic field varies spatially within the sample in the presence of a homogenous magnetic field gradient. Since the frequency of the NMR signal is proportional to the strength of the magnetic field, the signal frequency will also vary with position. Therefore, the frequency and amplitude of the NMR signal respectively encode the spatial position and density of excited nuclei.

Generally, NMR imaging systems use magnetic gradients, which vary linearly with position in three orthogonal directions, to image the sample. The resultant signal is broken down into its constituent frequencies by Fourier transformation. The resolution of a NMR microscope is dependent on imaging time, gyromagnetic constant, imaging gradient strength and T_2 of the sample. The resolution can be approximately calculated using equation 5.2.

$$\Delta x \approx \frac{2\Pi}{\gamma G N T_2} \qquad (5.2)$$

Δx is the resolution, γ is the gyromagnetic constant, G is the imaging gradient strength, N is the number of pixels in a profile and T_2 is the spin-spin relaxation time.

The resolution is often limited practically by the need to produce images with acceptable signal to noise ratio (SNR) in an acceptable time (Melia *et al*, 1998). The SNR and image resolution can be improved by strong magnetic fields, small RF coils, small sample sizes, a large number of signal averages and increased imaging time. Also, image contrast agents, for example gadolinium, can increase the SNR and improve image resolution (Nebgen *et al*, 1995). The highest lateral resolution achieved to date is 4.5 μm, which was obtained by Bowtell *et al*, 1990, using imaging times in the order of tens of minutes. In comparison, MRI studies carried out on hydrating hydrophilic matrices have achieved typical resolutions of 100 μm (Bowtell *et al*, 1994, and Rajabi-Siahboomi *et al*, 1994). Decreasing the dimensionality of an image can dramatically reduce imaging times. One-dimensional models offer considerable advantages over two- and three-dimensional systems in MRI studies of dosage forms (Fyfe and Blazek, 1997, and Marshall *et al*, 1998), particularly so since resolution is approximately related to the sixth power of imaging time.

5.1.2.1. Image distortions

Image distortions may be caused by a number of reasons. Differences in the magnetic polarisation properties of diamagnetic substances in an external field may cause the phenomenon of susceptibility. Bowtell *et al*, 1994, reported that susceptibility at the air-

gel interface of air bubbles in gel layers of hydrophilic matrices increased the imaged size of the bubbles. Fyfe and Blazek, 1998, also noted that susceptibility at the air-gel interface of air bubbles in a gel layer may result in the erroneous lowering of local T_2 values. Frequency-field inhomogenieties of the coil can produce non-linearities in magnetic field gradients at the boundaries of large volumes, resulting in geometrical image distortions (Nebgen *et al*, 1995). In images of low resolution, pixels that straddle an interface between two components may consist of signals from both components (Nebgen *et al*, 1995). The diffusion of water molecules during image acquisition may also distort T_2 weighted (Fyfe and Blazek, 1997) as well as diffusion weighted images.

5.1.3. Measuring water mobility using MRI

The SDC of water may be determined from a NMR signal by applying a sequence of magnetic field gradients, which makes the signal dependent on the Brownian motion of the water molecule. In 1968, Tanner and Stejskal developed a modification of the steady gradient spin echo method, which had been previously used to measure SDC. This pulsed-gradient, spin-echo method was used to determine the SDC of water in a number of model systems displaying restricted diffusion. This method was able to detect much faster diffusion coefficients, more precisely than the steady gradient method.

The pulsed-gradient, spin echo method uses a 90° RF pulse to flip the net magnetisation into the transverse plane. A magnetic field gradient is then applied, making nuclei at different spatial positions precess at different rates. This results in a dephasing of the net magnetisation and the decay of signal. A 180° RF pulse is used to reverse the phase of the net magnetisation and a second field gradient is applied to produce a spin-echo. The pulse sequence is shown in figure 5.1.

Nuclei that are stationary during the experiment will experience the same magnetic field strength and as a result the second magnetic field will fully rephase the net magnetisation. However, nuclei that diffuse during the experiment will experience different magnetic field strengths, which will cause the nuclei to precess at different rates and to not be fully rephased at the end of the second magnetic gradient. The

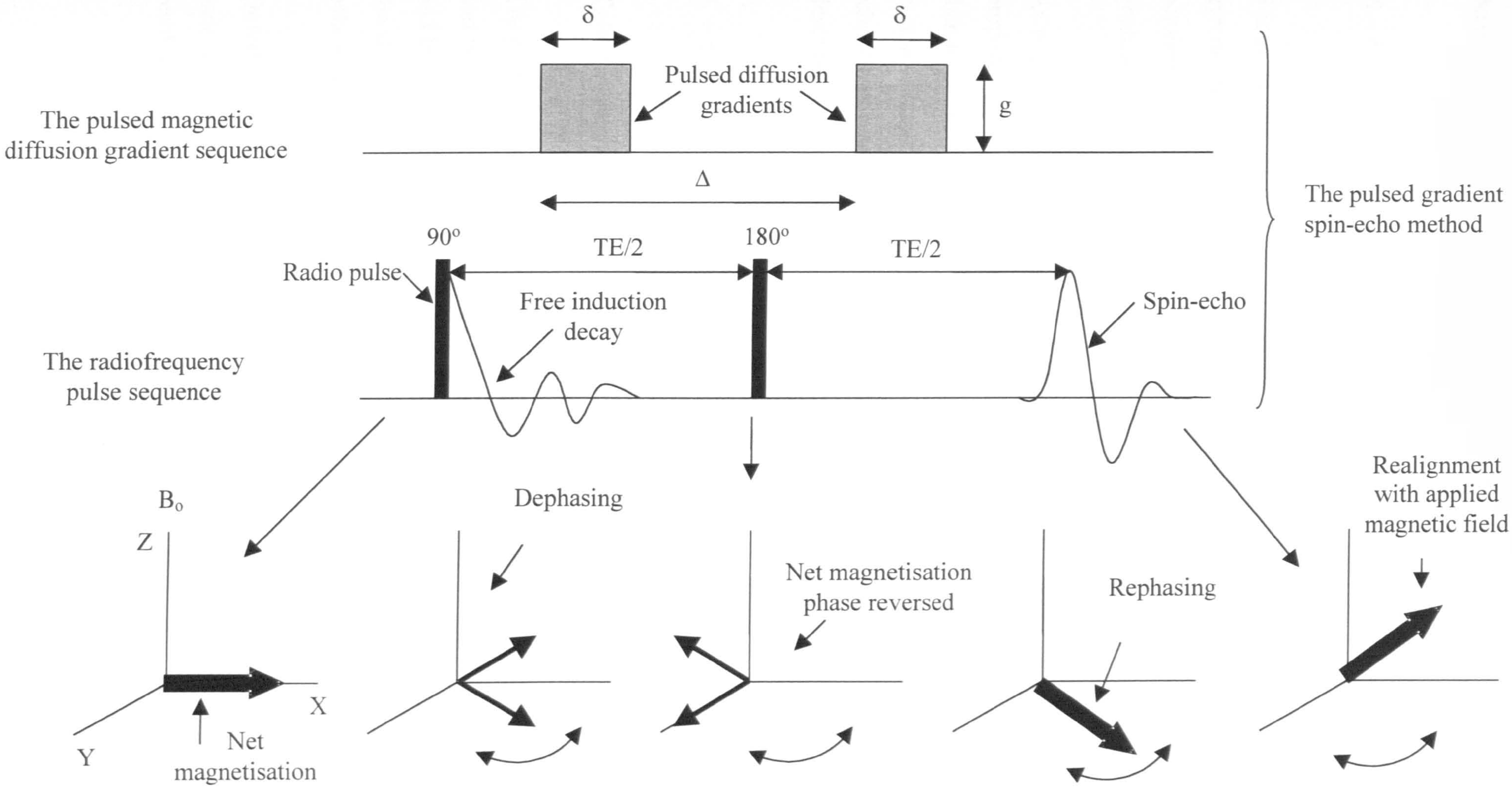

Figure 5.1 The pulsed gradient spin-echo method and the behaviour of the spins at each stage

resulting attenuation of the spin-echo is described by equation 5.3, which is used to determine the SDC (Tanner and Stejskal, 1968).

$$S = S_0 \exp\left[-\gamma^2\delta^2 g^2\left(\Delta - \frac{1}{3}\delta\right)D\right] \tag{5.3}$$

S is the attenuated NMR signal strength, S_0 is the equilibrium NMR signal, γ is the gyromagnetic constant, δ is the duration of the magnetic gradient, Δ is the time interval between the start of each magnetic gradient and g is the amplitude of the magnetic gradient.

As well as the SDC of water, the NMR signal can be T_2 weighted in order to study the proportion of bound and free water in a sample. Since bound water has a lower mobility than free water, bound water protons interact with each other more than free water protons interact with each other. Subsequently, bound water molecules have shorter T_2 relaxation times. Images can be T_2 weighted by varying the echo time (TE), which is described by equation 5.4.

$$S = S_0 \exp\left(\frac{-TE}{T_2}\right) \tag{5.4}$$

T_2 is spin-spin relaxation time and TE is echo time.

The pulsed gradient method only requires a low power RF pulse transmitter and a narrow band detection system since the magnetic gradients are off during the RF pulses and the spin echo. Gradients between 10 and 100 times larger than those feasible with the steady gradient method can be used, since changing the gradient does not change the echo shape

However, the practical applications of MRI are currently limited to imaging liquid state samples. This is because solid state samples have extremely short T_2 relaxation times, resulting in a rapid decay of the NMR signal. To date, conventional NMR microscopes

are not able to detect rapidly decaying NMR signals, such as those of solid state samples.

5.1.4. Applications of MRI microscopy

MRI microscopy has been used in food sciences to image the structure (Duce and Hall, 1995, and Duce *et al*, 1995) and manufacturing processes of food (Hills, 1995). The technique has also been used to image the structure inside some hydrating pharmaceutical dosage forms. The majority of studies in the pharmaceutical field have concentrated on imaging the dynamic processes of hydration inside hydrophilic matrices. These studies have obvious applications to the current project. This field has been extensively reviewed by Melia *et al* in 1998.

The hydration kinetics and swelling properties of polymer excipients are important factors in hydrophilic matrix technology. In one of the first studies investigating the hydration of a dosage form, Rajabi-Siahboomi *et al*, 1994, imaged the hydration and swelling of pure polymer HPMC matrices and showed that the resulting convex shaped hydrated layer resulted from the edges of the matrix hydrating more extensively than the centre of the matrix surface. This study also showed that axial swelling resulted almost equally from the growth of the hydrated gel layer and the expansion of the dry matrix core. In a further study, Rajabi-Siahboomi *et al*, 1996, discovered a water mobility gradient across gel layers of hydrated HPMC matrices and showed that the SDC and T_2 values of water in the outer parts of the gel layer approached those of free water. The same study also found water mobility inside axial gel layers was different to that inside radial gel layers and water mobility was influenced by the degree of substitution in the HPMC. Other studies have also investigated the hydration properties of HPMC compacts, relating the state of water across gel layers to polymer concentration and hydration (Fyfe and Blazek, 1997, and Madhu *et al*, 1998).

The hydration patterns inside other dosage forms have been imaged using NMR microscopy. For example, Fahie *et al*, 1997, used MRI to differentiate between different hydration mechanisms of novel biphasic matrix formulations and showed that the faster than predicted *in vitro* drug release kinetics were related to the porosity of the polymer coating. NMR microscopy has also been used to image the hydration patterns of 'fast'

and 'slow' releasing osmotic pump devices (Shapiro *et al*, 1996). Ashraf *et al*, 1994, also showed that the rate of hydration front penetration was not a rate limiting step in the release of pseudoephedrine from HPC sustained release capsule matrices.

The physicochemical properties of biodegradable monoliths composed of 50:50 poly(glycolide-co-DL-lactide) and containing the peptide drug, Goserelin, have been quantitatively and qualitatively imaged using MRI. Hyde *et al*, 1995, showed that the incorporation of a drug in a monolith changed the buffer uptake kinetics from super Case II to either Fickian or Case II depending on the region of the dosage form. Mader *et al*, 1997, used MRI and electron paramagnetic resonance (EPR) to compare *in vitro* and *in vivo* hydration, drug release and polymer erosion of a bulk eroding polymer implant (poly(glycolide-co-DL-lactide)), surface-controlled eroding polymer implants (poly(sebacic anhydride)(PSA)) and a copolymer of 1,3-bis(ρ-carboxyphenoxypropane)(CPP) and sebacic acid (SA). EPR was used to determine microviscosity of water inside the implants and the release of stable nitroxide radicals, which were incorporated into the implants as model drugs. MRI was used to monitor water content, matrix shape and the interaction with the surrounding tissue.

MRI has also been used to determine the type of transportation processes occurring inside polymer matrix systems. Valtier *et al*, 1995, used MRI to show that solvent penetration of toluene in poly(vinyl chloride) (PVC) occurs by different transport mechanisms than that of n-pentane in high density polyethylene (PEhd). In the case of PVC, the ingress of toluene was characterised by a sharp diffusion front, which is indicative of Case II transport. In comparison, the ingress of n-pentane into PEhd exhibited a smooth diffusion front, which is characteristic of Fickian (Case I) diffusion. In a joint study, Snaar and Peppas (Snaar *et al*, 1998, and Peppas *et al*, 1997) monitored the hydration of matrices manufactured from poly(vinyl alcohol) (PVA) of varying molecular weight and provided supporting evidence that phenomena such as reptation contribute towards polymer motion at the glassy-rubbery interface of polymers during dissolution, while diffusion gradually changes to Zimm type near the rubbery-solvent interface.

Other pharmaceutical applications of MRI include the non-destructive determination of porosity in matrices containing Avicel PH101 and mixtures of Avicel PH101 and acetyl salicylic acid (Nebgen *et al*, 1995). In this study, Nebgen *et al* showed that the corners of the upper axial face were highly compressed and the lower axial face was highly porous. The study also showed that plastic- or brittle-type tablets had different compaction mechanisms.

The linear relationship between alginate concentration and T_2 relaxation times has been used to determine the spatial variation of alginate concentration in heterogeneous gels (Potter *et al*, 1993a) and the pore size distribution of the gel (Potter *et al*, 1994a). The same research group has also tracked displacement of the sol/gel interface during the formation of a diffusion setting calcium alginate gel. This showed that the movement of the interface was proportional to the square root of time, indicating Fickian diffusion. It also showed that the diffusion of calcium ions was dependent on the initial concentration of calcium, the ionic strength of alginate and the pore size of the resultant gel (Potter *et al*, 1994b).

NMR microscopes have also been used to image other half spin nuclei such as ^{19}F. For example, Dinarvind *et al*, 1995, showed that the diffusion coefficient of 2,2,2-trifluoroacetamide (TFA) in thermoresponsive hydrogels at temperatures below the phase transition point was faster than at temperatures above the phase transition point. Dinarvind *et al* also showed that the swelling of the hydrogel controlled the diffusion of TFA. Christmann *et al*, 1997, used a double contrast technique to image and determine the gastrointestinal transit time of iron oxide labelled sodium alginate mini-tablets and ^{19}F labelled sodium alginate:HPMC (50:50) mini-capsules in a rat model. The double contrast technique involved using an oral contrast emulsion to highlight the gastrointestinal tract and a dosage form labelled with superparamagnetic iron oxide particles.

5.2. Development of a technique to measure the SDC of water inside a bioadhesive bond

5.2.1. Rationale

The methods used by Mortazavi and Smart (Mortazavi and Smart, 1993, and Smart *et al*, 1991) to investigate the movement of water inside a bioadhesive bond and the role of mucus dehydration in the bioadhesion of hydrophilic matrices were rudimentary. These methods could not readily determine the pattern of hydration and the diffusion of water inside a bioadhesive bond, which may considerably influence bioadhesion. Therefore, the aim of this chapter was to develop a MRI technique to measure the spatial distribution of water SDC inside a bioadhesive bond.

5.2.2. Methods

5.2.2.1. Method to manufacture sodium alginate matrices

90-125 μm particles of SF120 sodium alginate were compressed into 4.1 mm diameter, circular flat face matrices on a Manesty F3 tablet press, fitted with a tablet compression monitor model TCM1 (Copley Instruments Ltd, Nottingham) using an upper punch pressure of 400-410 mPa. The matrices were stored in sealed containers at 4°C over silica gel and warmed to room temperature for one hour before use.

5.2.2.2. Method to prepare physiological saline

Physiological saline was prepared by dissolving 0.9 g of sodium chloride in 100 ml of deionised and distilled water.

5.2.2.3. Method to prepare Sigma mucin solution

Freeze-dried partially purified pig gastric mucin (Sigma type III mucin) was slowly dissolved in physiological saline at 4°C to obtain a 190 mg ml^{-1} homogenous solution. Solutions of this concentration appeared to be visually similar to purified gastric mucus.

5.2.2.4. Method to prepare a sample for MRI studies

A dry sodium alginate matrix was placed inside a 5 mm NMR tube to make a tight fit and the tube was sealed using a nylon plug, exposing only the upper surface of the matrix. In studies using dry matrices, approximately 50 µl of Sigma mucin solution was slowly pipetted onto the matrix surface to form a sample depth of approximately 5 mm. In studies using prehydrated matrices, the matrix surface was hydrated with physiological saline at 37 ±1°C for 10 mins, which was then replaced by Sigma mucin solution as before. Figures 5.2a and 5.2b illustrate the sample cell geometries for both dry and prehydrated matrices.

5.2.2.5. Method for measuring the SDC of water inside a bioadhesive bond

The sample cell was placed in a 6 mm diameter radiofrequency saddle coil and imaging was carried out on a 11.7 T NMR microscope using a highly efficient gradient coil, capable of generating 1.73 Tm^{-1} A^{-1} (Bowtell *et al*, 1990). One-dimensional axial profiles (42.5 µm resolution), showing the variation of water concentration and self-diffusion coefficient were generated using a pulsed gradient, spin-echo sequence (repetition time [TR=5 sec], echo time [TE=2.75 ms]). Diffusion measurements were calculated using nine profiles generated with different diffusion weightings (b-values ranging from 1000 to 2.5 sec mm^2) in 1.5 mins. SDC profiles across the bond structure were obtained immediately after sample preparation and then every 5 mins for 30 mins. Samples were maintained at room temperature (20±1°C). A control sample containing distilled and deionised water (a water phantom) was used to calibrate the NMR microscope prior to the diffusion experiments.

5.2.3. Results

5.2.3.1. Water diffusion inside bioadhesive bonds formed by dry alginate matrices

The SDC profile of water inside the bioadhesive bond formed by dry alginate matrices is shown in figure 5.3a.

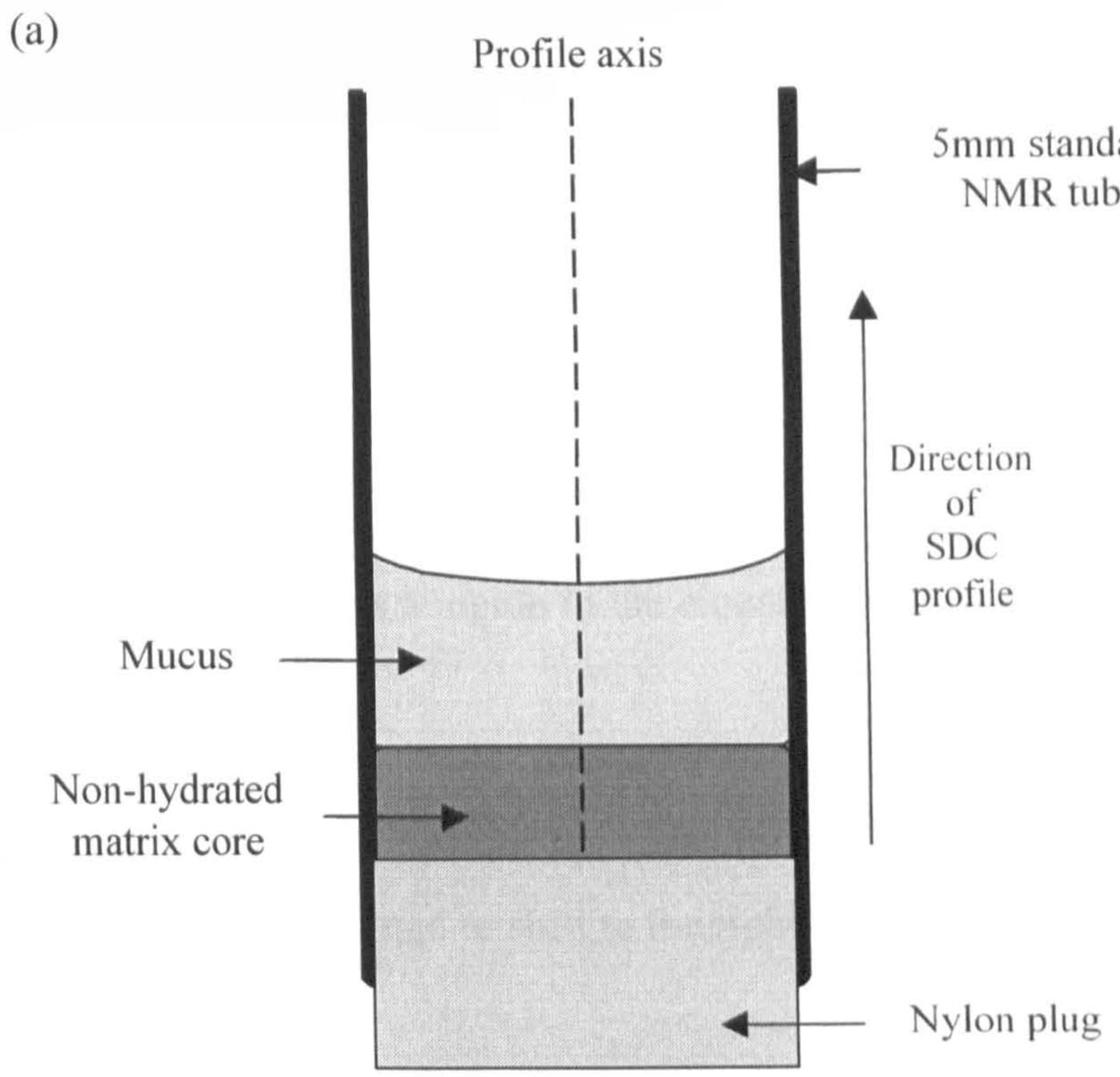

Figure 5.2 The geometry of the sample cell, which was placed inside a NMR microscope to measure the diffusion of water inside a bioadhesive bond – (a) dry matrix and (b) prehydrated matrix sample arrangement

In the region spanning from 0-850 μm, the SDC of water was either zero or non-measurable. After 1 min, the SDC of water rapidly increased between 850-1000 μm and formed the diffusion front of the SDC profile. The SDC values then formed a plateau between 1000-1250 μm before increasing to a constant SDC of $\approx 6 \times 10^{-10}$ m^2 sec^{-1}.

The gradient of the diffusion front decreased over 30 mins, indicating that diffusion of water became more Fickian-like. After 5 mins, a characteristic dip developed in the SDC profile at ≈1250-1500 μm, which seemed to increase in width and depth over time. This characteristic dip represents a region in the bioadhesive bond where the SDC of water has decreased.

The zenith and nadir points of the profile appear to be significant points in the profile. The position of these points seemed to shift to the right of their original position over time.

5.2.3.2. Water diffusion inside bioadhesive bonds formed by prehydrated alginate matrices

The SDC profile of water inside the bioadhesive bond formed by prehydrated alginate matrices is shown in figure 5.3b.

The SDC profiles seemed to be extremely noisy between 0-1000 μm. After 1 min, the SDC of water increased rapidly to a peak value of $\approx 7\text{-}8 \times 10^{-10}$ m^2 sec^{-1} between 1000-2000μm and formed the diffusion front of the SDC profile. The SDC of water then decreased to a constant SDC of $\approx 6 \times 10^{-10}$ m^2 sec^{-1}.

The gradient of the diffusion front did not seem to change over 30 mins. The SDC profile did not develop a characteristic dip, similar to that observed in the profiles of dry alginate matrices. The position of the zenith point seemed to shift to the right of its original position over time.

(a)

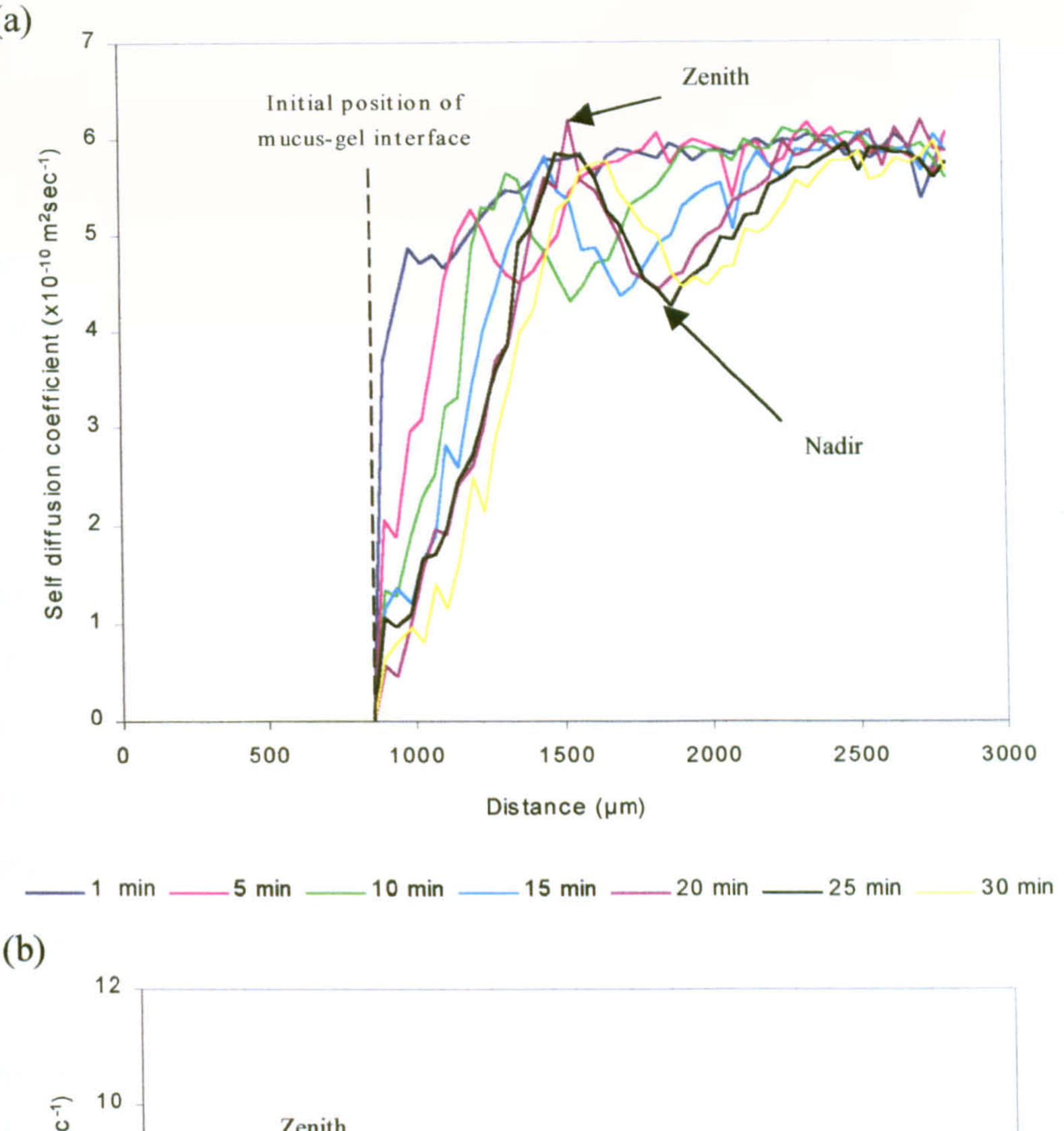

(b)

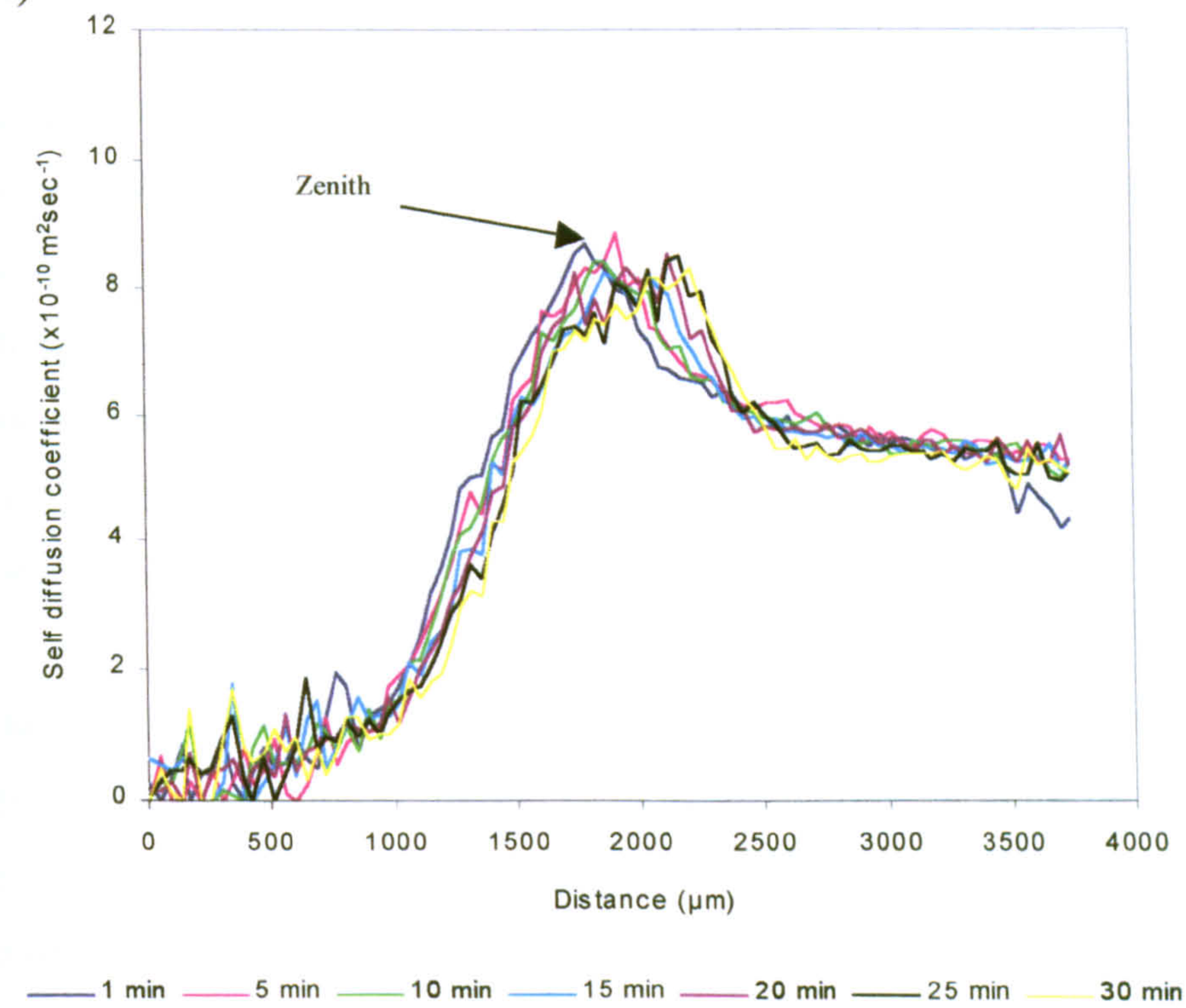

Figure 5.3 The effect of time on SDC of water inside bioadhesive bonds formed by alginate matrices

Bioadhesive bonds were formed between (a) dry (mean, n=3) and (b) prehydrated (mean, n=6) sodium alginate matrices and Sigma mucin solution at 20±1°C.

5.2.4. Discussion

In this work, MRI has been used to spatially resolve the SDC profile of water inside bioadhesive bonds formed by dry and prehydrated alginate matrices with Sigma pig gastric mucin.

5.2.4.1. The SDC profile of water in bioadhesive bonds formed by dry matrices

The SDC profile of water inside bioadhesive bonds formed between dry alginate matrices and mucus had a characteristic shape (figure 5.3a). After 1 min, the SDC profile was composed of two sections, a region in which the SDC of water seemed to be zero and a region in which the SDC values were greater than zero. This suggests that the initial region of the profile may correspond to the dry alginate matrix and the second region may correspond to the mucus.

At later times, the SDC profiles seemed to be composed of four sections. In the first section, the SDC values of water seemed to be zero and the second section was a rapid increase in SDC values to a zenith value. The third section developed a characteristic dip in the profile, indicating a region where the SDC of water had decreased, and the diffusion of water in the forth section had a constant SDC value of $\approx 6 \times 10^{-10}$ m^2 sec^{-1}. This suggests that the dry alginate matrix and mucus have interacted in some way as to influence the SDC of water.

The gradient of the diffusion front also decreased over time. The slope of the diffusion front may indicate the type of transport mechanisms involved in the diffusion of water (Valtier *et al*, 1995). A steep gradient is indicative of Case II transport, which is predominant in glassy polymers. A lower gradient is indicative of Fickian diffusion, which predominantly occurs in rubbery/viscous polymers (Valtier *et al*, 1995, and Crank, 1975). This suggests that the diffusion of water in the region relating to the diffusion front became more Fickian-like over time.

The characteristic dip in the third section of the SDC profile seemed to increase in width and depth over time. As mentioned above, the dip represents a region where the

diffusion of water has decreased. This may be due to an increase in the tortuosity of the polymer network or an increase in the proportion of bound water molecules. However, the likely mechanisms underlying the development of this characteristic dip will be fully explored in chapter 7.

The way in which the SDC profile developed over time suggests that dry alginate matrices interact with mucus in some way as to influence the diffusion of water inside the alginate matrix and the adjacent mucus. However, it is extremely difficult to accurately relate sections of the SDC profile to regions in the sample geometry (figure 5.2a). As a result, the influence of the dry alginate matrix on the diffusion of water in specific regions of the bioadhesive bond cannot be readily determined. An auxiliary technique that can effectively delimit and differentiate the SDC profiles needed to be developed.

5.2.4.2. The SDC profile of water in bioadhesive bonds formed by prehydrated matrices

The SDC profile of water inside bioadhesive bonds of prehydrated alginate matrices also had a characteristic shape, which did not seem to change over time. This suggests that the diffusion of water inside the hydrated alginate matrix and the mucus was not influenced by the interaction between hydrated alginate and mucus.

The SDC profile seemed to be composed of three sections. The SDC values in the first section were extremely noisy and the second section of the profile seemed to be the diffusion front of the profile. The shape of the diffusion front was similar to those observed in hydrating HPMC and PVA pure polymer matrices (Rajabi-Siahboomi *et al*, 1996, and Madhu *et al*, 1998) and suggests that diffusion of water occurs by either anomalous or Fickian diffusion. The third section was composed of the decrease in the SDC of water from the zenith SDC to a constant SDC value of $\approx 6 \times 10^{-10}$ m^2 sec^{-1}.

Like the SDC profiles of dry alginate matrices, it is difficult to relate sections of the profile to regions in the sample geometry (figure 5.2b), even though it seems to be composed of three regions, i.e. the dry core, the viscous alginate gel and the mucus gel layer. Therefore, an auxiliary technique, which can effectively delimit and differentiate

the SDC profiles of bioadhesive bonds formed by prehydrated alginate matrices also needed to be developed

The SDC profiles of water inside bioadhesive bonds formed by dry and prehydrated alginate had considerably different shapes. The shape of both profiles developed differently over time. This suggests that dry and prehydrated alginate matrices interact with mucus in different ways and that MRI can differentiate between the bioadhesion of dry and prehydrated alginate matrices.

5.3. Development of a technique to image the geometry of the bioadhesive bonds formed by alginate matrices

5.3.1. Rationale

Material of a biological origin is often autofluorescent (Haugland, 1992) and this may represent a possible way to differentiate the alginate and mucus regions in a bioadhesive bond. Alginate is purified from the intercellular matrix of brown seaweed and mucin is purified from native pig gastric mucus. Therefore, the aim of this section was to develop a CLSM technique that can image the alginate and mucus regions in a bioadhesive bond and delimit corresponding regions in the SDC profile.

5.3.2. Method for manufacturing square cross-section matrices

90-125 μm particles of SF120 sodium alginate were compressed into 9.6 x 9.6 mm square flat face matrices on a Manesty F3 tablet press, fitted with a tablet compression monitor model TCM1 (Copley Instruments Ltd, Nottingham) using an upper punch pressure of 400-410 mPa. The matrices were stored at 4°C over silica gel and warmed to room temperature for one hour before use.

5.3.3. Measuring the fluorescence of dry alginate, viscous alginate gel and mucus

The aim of this section was to measure the autofluorescence of a dry alginate matrix, viscous alginate gel and mucus gel layer.

5.3.3.1. Method

A dry alginate matrix, viscous alginate gel and Sigma mucin were inserted inside a 10 x 10 mm plastic cuvette and separated from each other by spacer blocks (figure 5.4a). A BioRad MRC600 CLSM, fitted with a x10 (NA 0.25) Nikon objective, imaged the sample geometry at 5 mW laser power, exciting at 488 nm and detecting fluorescence at 510 nm.

5.3.3.2. Results

Figure 5.4b shows a confocal fluorescent image of the sample cell geometry shown in figure 5.4a.

The fluorescence intensity was 254±1 for the dry alginate matrix, 70±20 for viscous alginate gel and 200±22 for Sigma mucin, using the CLSM set-up described in section 5.3.2.1. The overlap of fluorescence intensities of each sample seemed to be negligible, suggesting that the relative fluorescence intensity of the sample may be a useful way to differentiate the dry alginate core, viscous alginate gel and mucus gel regions of a bioadhesive bond.

5.3.4. Method for differentiating the dry core, viscous alginate gel and mucus in a bioadhesive bond

A BioRad MRC600 CLSM, fitted with a Nikon x10 (NA 0.25) objective, imaged the sample at 5 mW laser power, exciting at 488 nm and detecting fluorescence at 510 nm. Samples were imaged before and immediately after Sigma mucin solution was added, and then every 5 mins for 30 mins. Image ProPlus 4.0 (Media Cybernetics, Leiden, Holland) image analysis software was used to differentiate the different regions in the bioadhesive bond using fluorescence thresholds and to measure the axial movement of the interfaces. The initial position of the dry core-viscous gel interface and the start of the diffusion front in the SDC profile were used as baselines to correlate results from this method with the SDC profile.

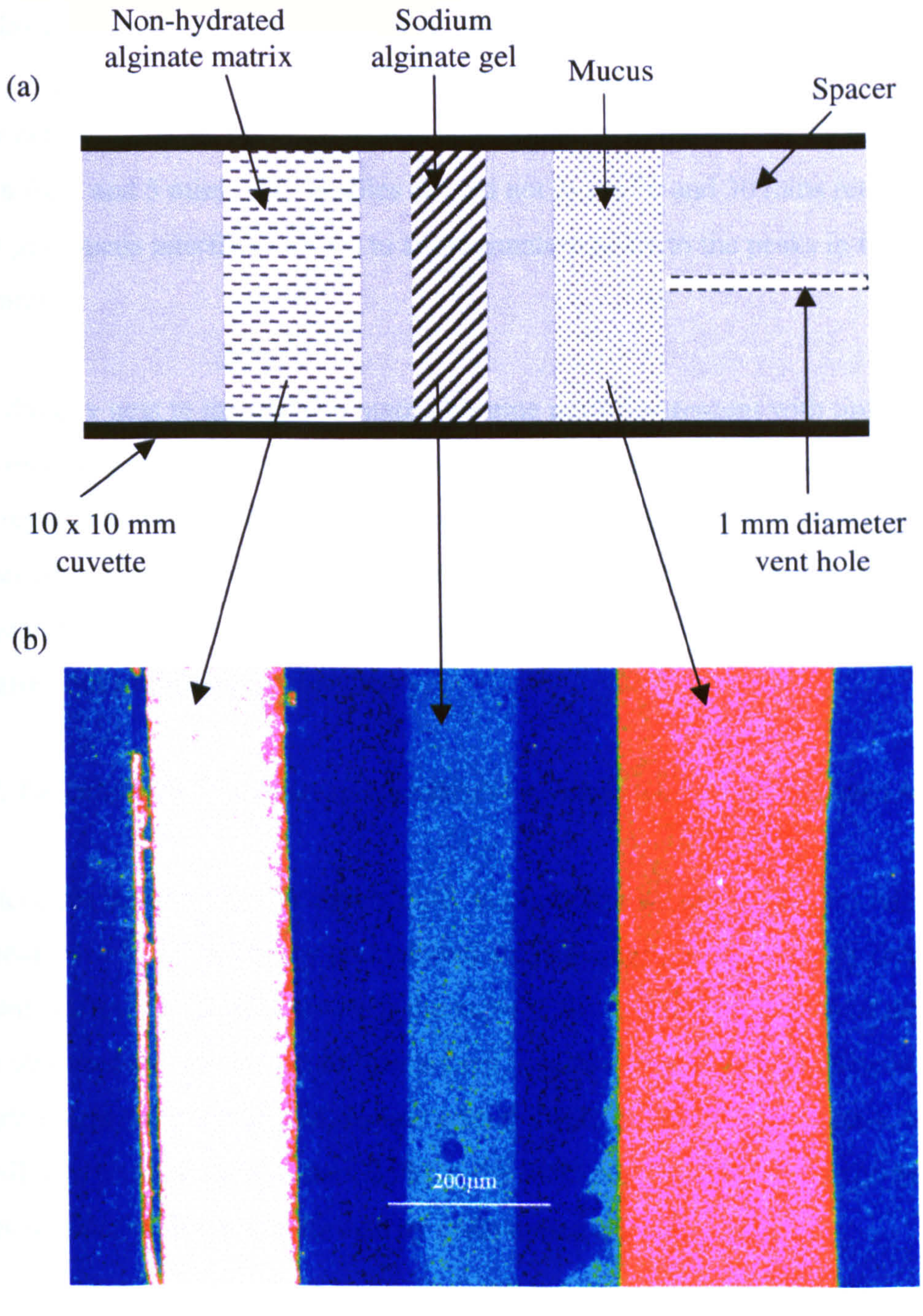

Figure 5.4 (a) The sample cell geometry used to measure the fluorescence of the dry core, viscous alginate gel and mucus gel regions of the bioadhesive bond. (b) A fluorescent image of the same sample cell geometry.

The sample cell was imaged using a BioRad MRC600 CLSM fitted with a x10 (NA 0.25) Nikon objective, exciting at 5 mW laser power using the 488 nm laser line and detecting at 510 nm.

5.3.4.1. Delimiting SDC profiles of bioadhesive bonds formed by dry matrices

Figures 5.5 shows the positions of the core-alginate gel, alginate gel-mucus and mucus-mucus interfaces marked on the dry matrix SDC profiles.

The dry core-viscous gel interface related approximately to the start of the diffusion fronts in the 1 and 5 mins SDC profiles but did not in the 20 and 30 mins profiles. The viscous gel-mucus interface seemed to approximately relate to the peaks in the profiles at all times.

Mucus directly next to the alginate matrix became more fluorescent with time. The mucus-mucus interface delimits the extent of this region and also showed that the width of this region increased with time. The mucus-mucus interface approximately related to the outer edge of the characteristic dip in the SDC profiles. It was thought that the increase in fluorescence might be related to the concentration of mucin. A further study was carried out to investigate this theory.

5.3.4.2. Delimiting SDC profiles of bioadhesive bonds formed by prehydrated matrices

The interfaces between the dry matrix core, viscous alginate gel and mucus regions in the bioadhesive bond formed by prehydrated alginate matrices were readily delimited and measured using CLSM. However, the noise in the 0-1000 μm section of the SDC profile obscured the start of the diffusion front, which was used as a baseline to correlate results from the CLSM method with the SDC profile. Consequently, it was impossible to relate data from the CLSM to the SDC profiles and delimit the SDC profiles of bioadhesive bonds formed by prehydrated alginate matrices.

(a)

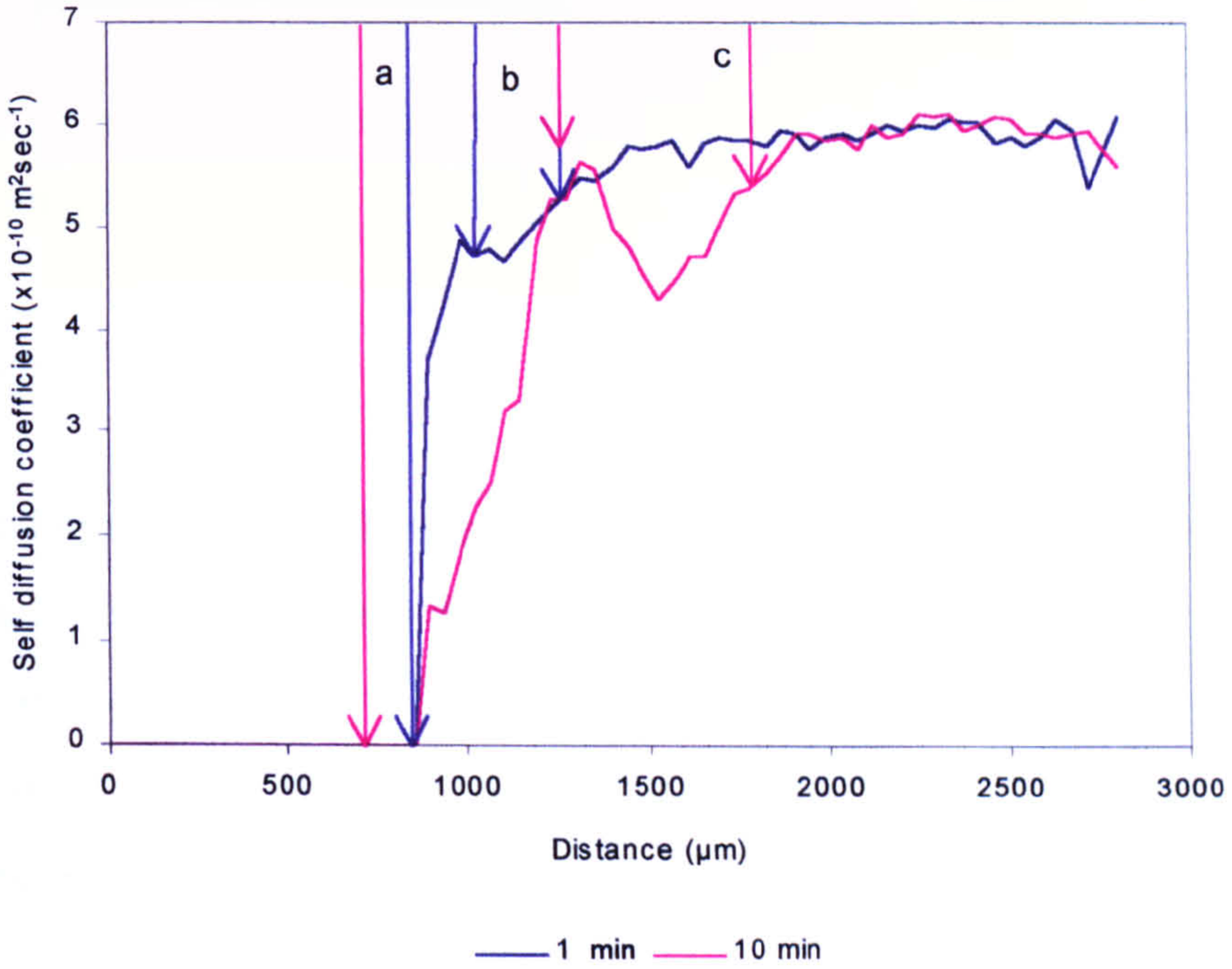

(b)

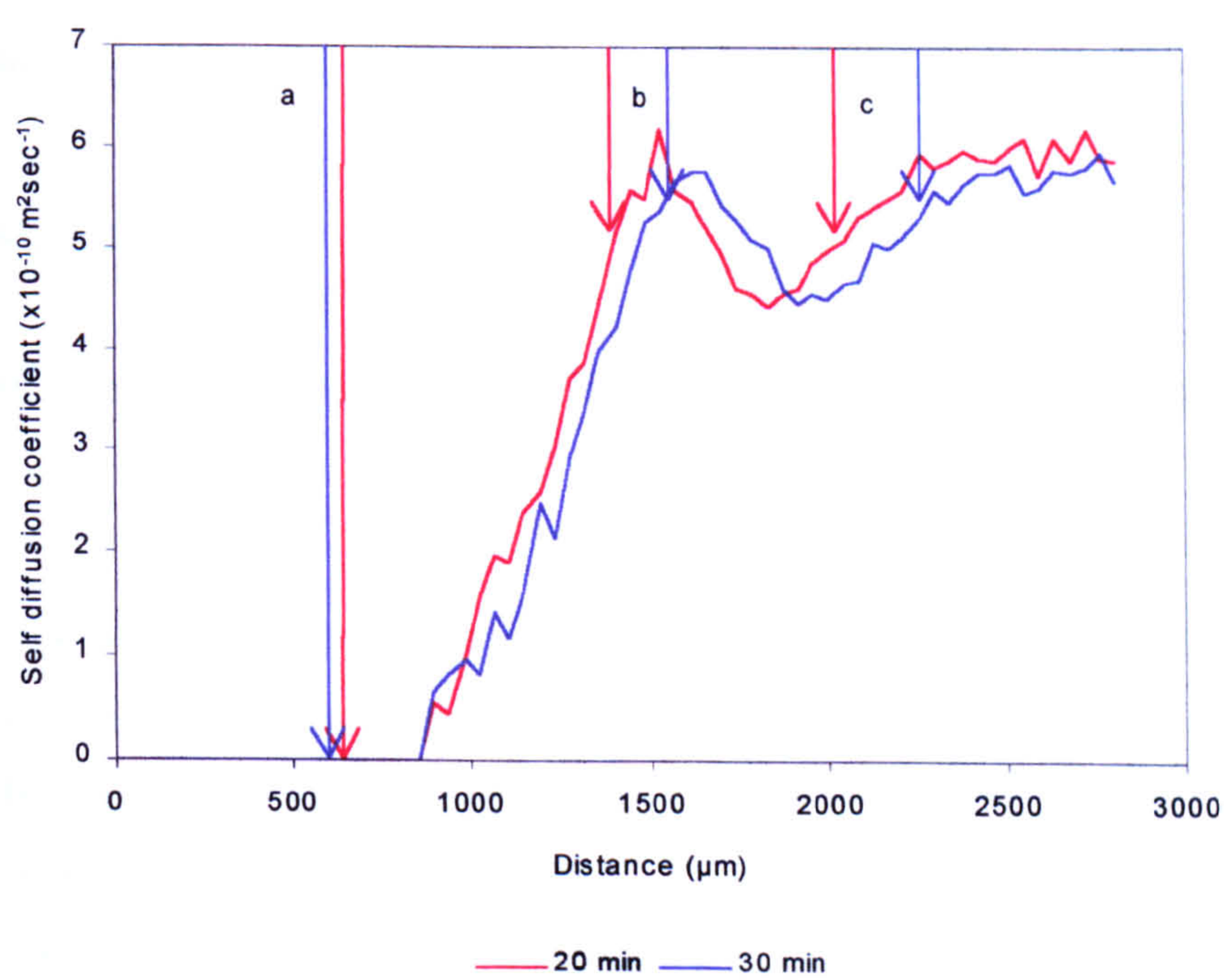

Figure 5.5 Delimited SDC profiles of water inside bioadhesive bonds of dry alginate matrices

The SDC profiles of water inside bioadhesive bonds of dry alginate matrices have been annotated with the positions of (a) the dry core-viscous gel interface, (b) the viscous gel-mucus gel interface and (c) the mucus-mucus interface.

5.3.5. The relationship between the concentration and fluorescence of mucin

The aim of this section was to determine the relationship between the fluorescence and concentration of mucin.

5.3.5.1. Method

Standard solutions of freeze-dried partially purified pig gastric mucin (Sigma type III mucin) were prepared by slowly dissolving mucin in physiological saline at 4°C to obtain a homogenous solution. The fluorescence of each solution was determined at 37±1°C using a BioRad MRC600 CLSM, fitted with a Nikon x10 (NA 0.25) objective and exciting at 5 mW laser power, using the 488 nm laser line and detecting at 510 nm.

5.3.5.2. Results

Figure 5.6 clearly showed that the fluorescence of mucin increased as the concentration of mucin increased, although this relationship was not linear.

5.3.6. Discussion

5.3.6.1. Interpreting the SDC profiles of bioadhesive bonds formed by dry alginate matrices

The fluorescence of dry alginate, viscous alginate gel and mucus gel differed in intensity and this may be used to differentiate these regions in a bioadhesive bond (figure 5.4b). However, the chemical structure of dry alginate and mucus do not contain any type of chromophore. More surprisingly, the fluorescence intensity of dry alginate decreased on hydration. It is not known what causes this phenomenon or the autofluorescence of dry alginate and mucus and requires further investigation, but this was beyond the scope of this project.

In the bioadhesive bonds of dry alginate matrices, the dry core-viscous gel interface appeared to correspond to the start of the diffusion front at early times (≤5 mins) (figure

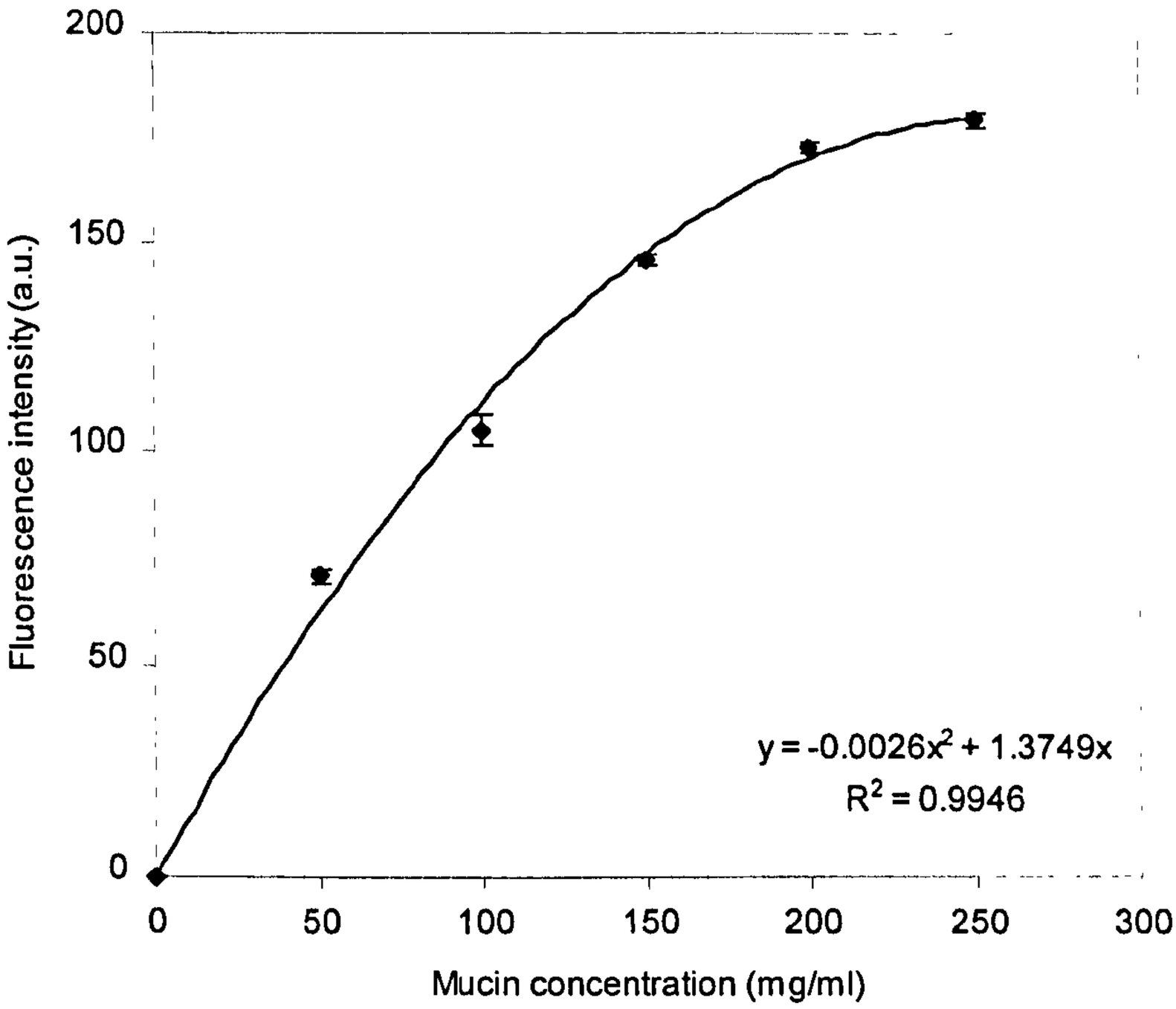

Figure 5.6 The relationship between the fluorescence and concentration of Sigma mucin

The fluorescence of mucin solutions were measured using a BioRad MRC600 CLSM fitted with a x10 (NA 0.25) Nikon objective, exciting at 488 nm and detecting at 510 nm (n=3, mean, ±1 SD).

5.5a) but did not at later times (≥ 20 mins) (figure 5.5b). The lack of a general correlation between the dry core-viscous gel interface and the diffusion front at later times may be due to the water in the viscous gel directly adjacent to the dry core diffusing too slowly to be detected by the MRI microscope.

The viscous gel-mucus interface seemed to approximately correspond with the zenith point of the SDC profiles, which suggests that the diffusion front of the SDC profiles correlates with the viscous gel layer of the alginate matrices.

Mucus directly adjacent to the alginate matrix became more fluorescent with time and the mucus-mucus interface marked the outermost limit of this region. This interface appeared to approximately relate to the outer edge of the characteristic dip in the SDC profiles (figure 5.5a and 5.5b). The fluorescence of mucus seems to be related to the concentration of mucin (figure 5.6), which indicates that the concentration of mucin may have increased in this region. This suggests that the characteristic dip in the SDC profile may be due to an increase in the tortuosity of mucin brought about by an increase in the mucin concentration. The possible mechanisms underlying the development of the characteristic dip will be fully explored in chapter 7.

There are inherent difficulties in aligning data from CLSM with the SDC profiles. For example, each point in a SDC profile represents the average of all the SDC values in a particular z-section. In comparison, the CLSM did not average all the points in a z-section. Also, the resolution of the NMR microscope is considerably less than that of the CLSM.

5.3.6.2. Interpreting the SDC profiles of bioadhesive bonds formed by prehydrated alginate matrices

The SDC profiles of bioadhesive bonds formed by prehydrated alginate matrices were not delimited since noise in the 0-1000 μm section of the profile prevented the diffusion front being used as a baseline to correlate results from the CLSM.

During the preparation of the sample, physiological saline seemed to creep between the radial face of the alginate matrix and the wall of the NMR tube. This may have hydrated the radial face of the alginate matrix and destroyed the one-dimensionality of the sample geometry. The heterogeneity of the sample in this region may have increased susceptibility in the sample, resulting in noise in the corresponding section in the SDC profile. Increasing the signal intensity threshold when calculating the SDC profile may prevent this, although this has the disadvantage of losing signal from slowly moving water molecules.

5.6. Conclusion

A MRI technique was developed to measure the SDC of water inside bioadhesive bonds formed by dry and prehydrated alginate matrices. A technique using CLSM to differentiate the dry core, viscous gel layer and mucus regions in a bioadhesive bond was also developed. This technique was used to delimit the interfaces of these regions in the SDC profiles.

The shape and development of the SDC profiles of bioadhesive bonds formed by dry alginate matrices and prehydrated alginate matrices were considerably different. This suggested that the hydration state of the alginate matrices significantly influenced the diffusion of water inside the bioadhesive bond.

Chapter 6

General methods used to study the bioadhesion of sodium alginate matrices

6.1. Introduction

This chapter describes the general methods used to study the influence of molecular weight, M:G ratio and particle size on the bioadhesion of dry and prehydrated sodium alginate matrices.

6.2. General methods used to prepare the samples

6.2.1. Method for manufacturing sodium alginate matrices

The method to manufacture alginate matrices for liquid uptake studies and detachment force tests is described in section 3.3.2. The methods to manufacture alginate matrices for MRI studies and for FRAP studies are described in sections 5.2.2.1 and section 5.3.2, respectively. The matrices were stored at 4°C over silica gel and equilibrated to room temperature for one hour before use.

6.2.2. Method to prepare physiological saline

Physiological saline was prepared by dissolving 0.9 g of sodium chloride in 100 ml of deionised and distilled water.

6.2.3. Method to prepare FITC-dextran permeated Sigma mucin solution

The method in section 2.4.5 describes the preparation of FITC-dextran permeated Sigma mucin solution.

6.2.4. Method to prepare purified pig gastric mucus

The purification and characterisation of the purified pig gastric mucus used in MRI studies are described in section 2.4.

6.3. General methods for measuring the bioadhesive bond strength of alginate matrices

The development of this method was described in chapter 3.

6.3.1. Method to prepare tissue for detachment force tests

The method in section 3.3.4.1 describes the preparation of pig gastric mucus for detachment force tests.

6.3.2. Method to measure the strength of the bioadhesive bond

The strength of a bioadhesive bond was determined by the method described in section 3.3.4.2. Matrices were either dry or prehydrated in physiological saline at 37±1°C for 10 mins. The bioadhesive bonds were formed using a 0.25 N bond formation force applied for 5 mins.

6.3.3. Method to determine the self-adhesive strength of viscous alginate gel layers

The lower surface of an alginate matrix was attached to the bottom of a 100 ml beaker using double-sided adhesive tape and the beaker clamped securely in place. The lower surface of another alginate matrix of the same type was attached to a 80 x 9.6 mm circular perspex probe using double-sided adhesive tape. The sample cell geometry is shown in figure 6.1. Both matrices were then hydrated in physiological saline at 37±1°C for 10 mins and a 0.25 N bond formation force was applied for 5 mins to produce a viscous alginate gel bond. The self-adhered matrices were pulled apart at a rate of 0.1 mm sec^{-1} to determine the W_a and F_{max}.

6.3.4. Method to determine the self-adhesive strength of mucus gel layers

A 10 x 30 mm piece of pig gastric mucosa was attached to an 80 x 9.6 mm circular perspex probe using double-sided adhesive tape and firmly secured in place. A 25 x 25 mm square of tissue was clamped in the sample cell using a perspex O-ring (figure 3.2).

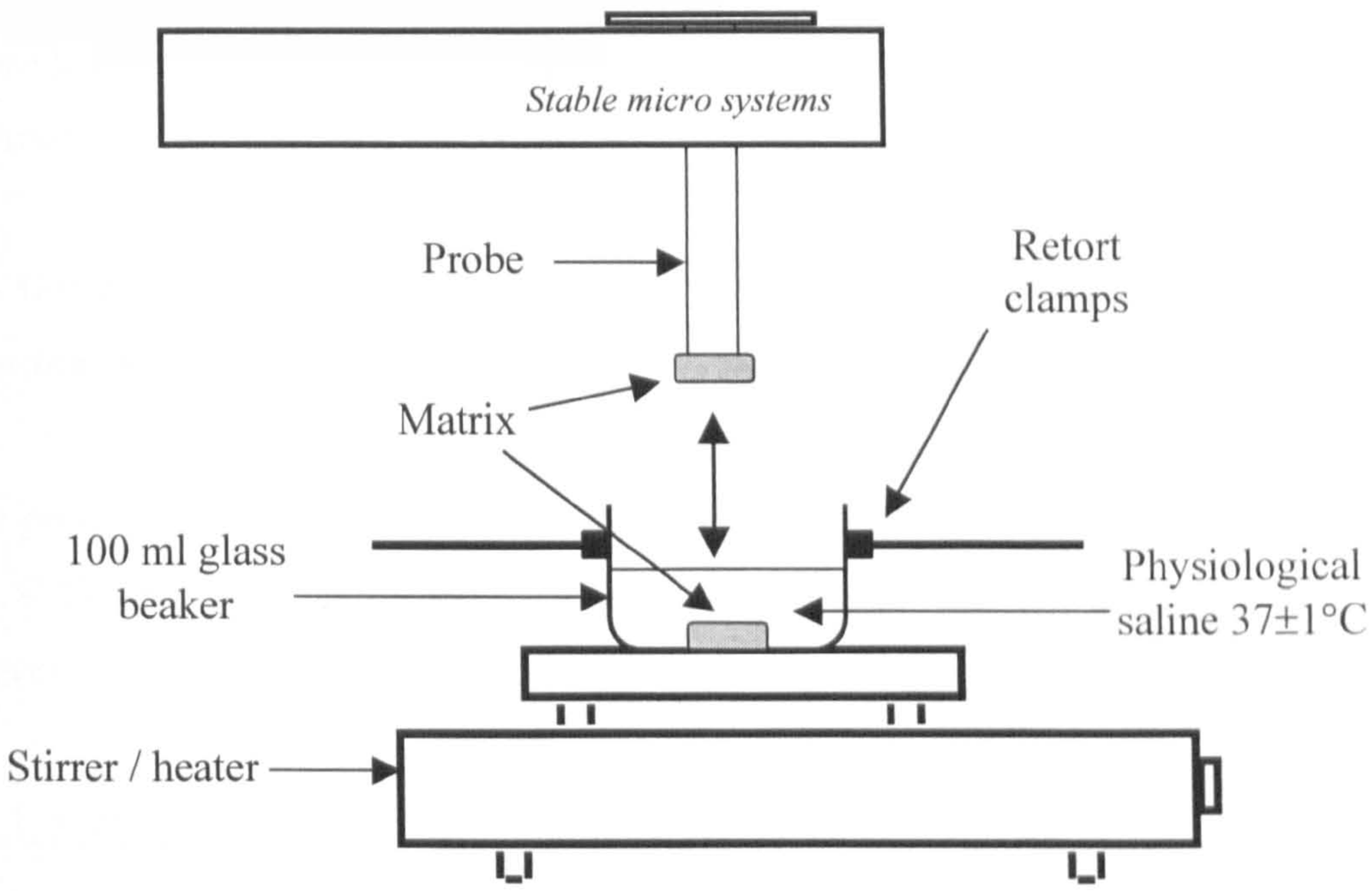

Figure 6.1 Sample cell geometry used to measure the self-adhesive strength of viscous alginate gel layers.

Both tissue samples were allowed to equilibrate in 400 ml of physiological saline at 37±1°C for at least 20 mins and a 0.25 N bond formation force was applied for 5 mins to produce a mucus gel bond.. The self-adhered mucosae were pulled apart at a rate of 0.1 mm sec^{-1} to determine the W_a and F_{max}.

6.4. General methods for measuring the mobility of fluorescent solutes inside bioadhesive bonds

The principles of fluorescence photobleaching studies and confocal microscopy (CLSM) were described in section 4.3 and 4.2, respectively. The development of the fluorescence photobleaching method used in this section was described in section 4.4.

6.4.1. Method to prepare a sample for fluorescence photobleaching

The lower surface of an alginate matrix was attached to a spacer block, using double-sided adhesive tape, and placed inside a 10 x 10 mm plastic cuvette. In studies using dry matrices, 0.5 ml of Sigma mucin solution permeated with 580 kDa FITC-dextran was slowly pipetted onto the exposed surface of the matrix. In studies using prehydrated matrices, the matrices were hydrated in physiological saline at 37±1°C for 10 mins before the mucin solution was added. A second spacer block, with a 1.0 mm diameter vent hole, was used to seal the cuvette. The sample was then maintained at 37±1°C in a heated aluminium jacket. The sample cell geometry is shown in figure 6.2.

6.4.2. Method to measure R_T of a fluorescent solute inside a bioadhesive bond

The fluorescence photobleaching experiments were carried out on a BioRad MRC600 CLSM fitted with a Nikon x10 (NA 0.25) objective and a 15 mW Kr-Ar laser. The method in section 4.4.5 describes the photobleaching process. The fluorescent samples were photobleached for 10 sec and the fluorescence recovery was imaged every 12.17 sec after photobleaching. The diffusion program, FRMK1, used nine 148 μm radius fluorescence intensity profiles (F_P) to calculate the rate of transport (R_T).

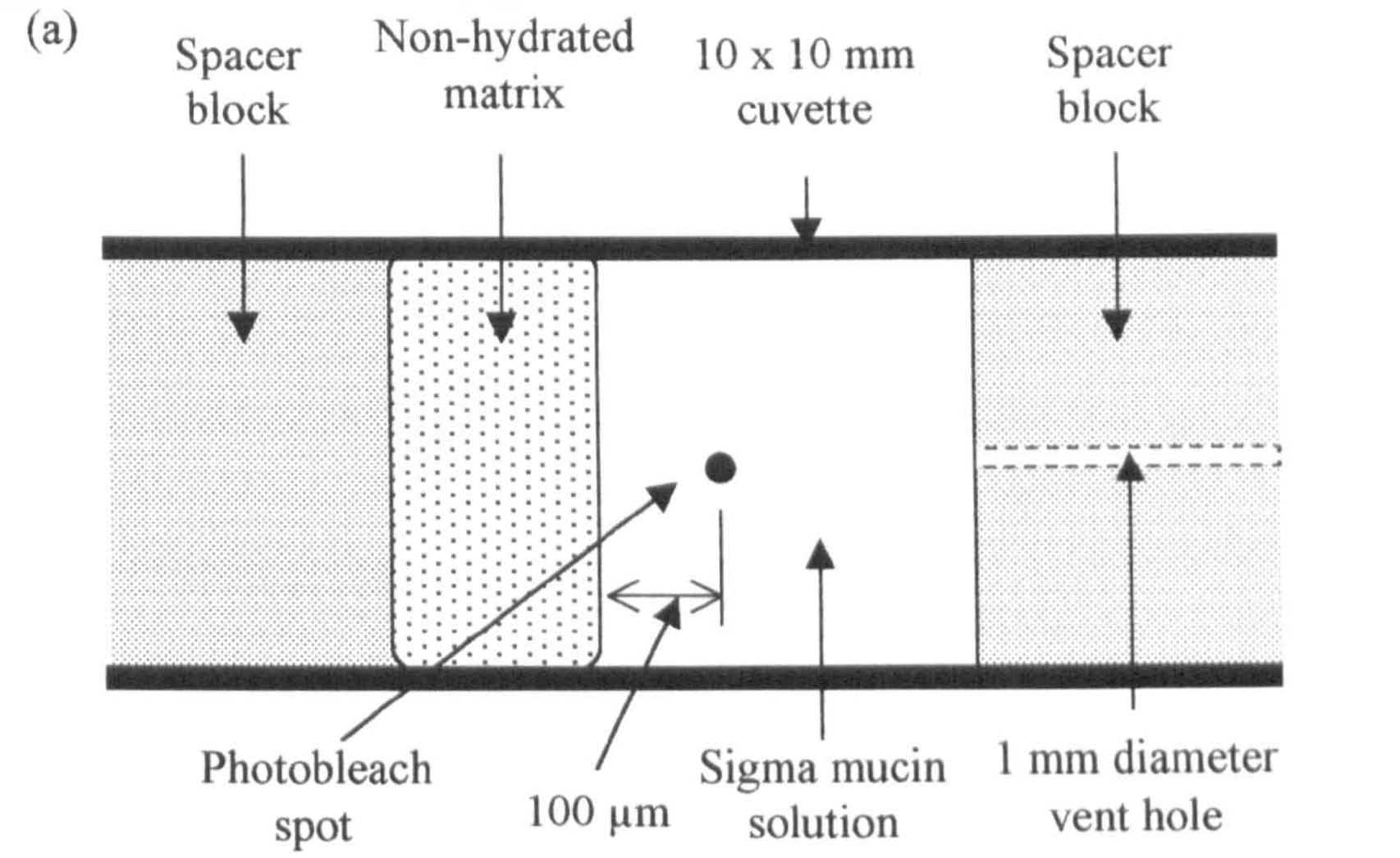

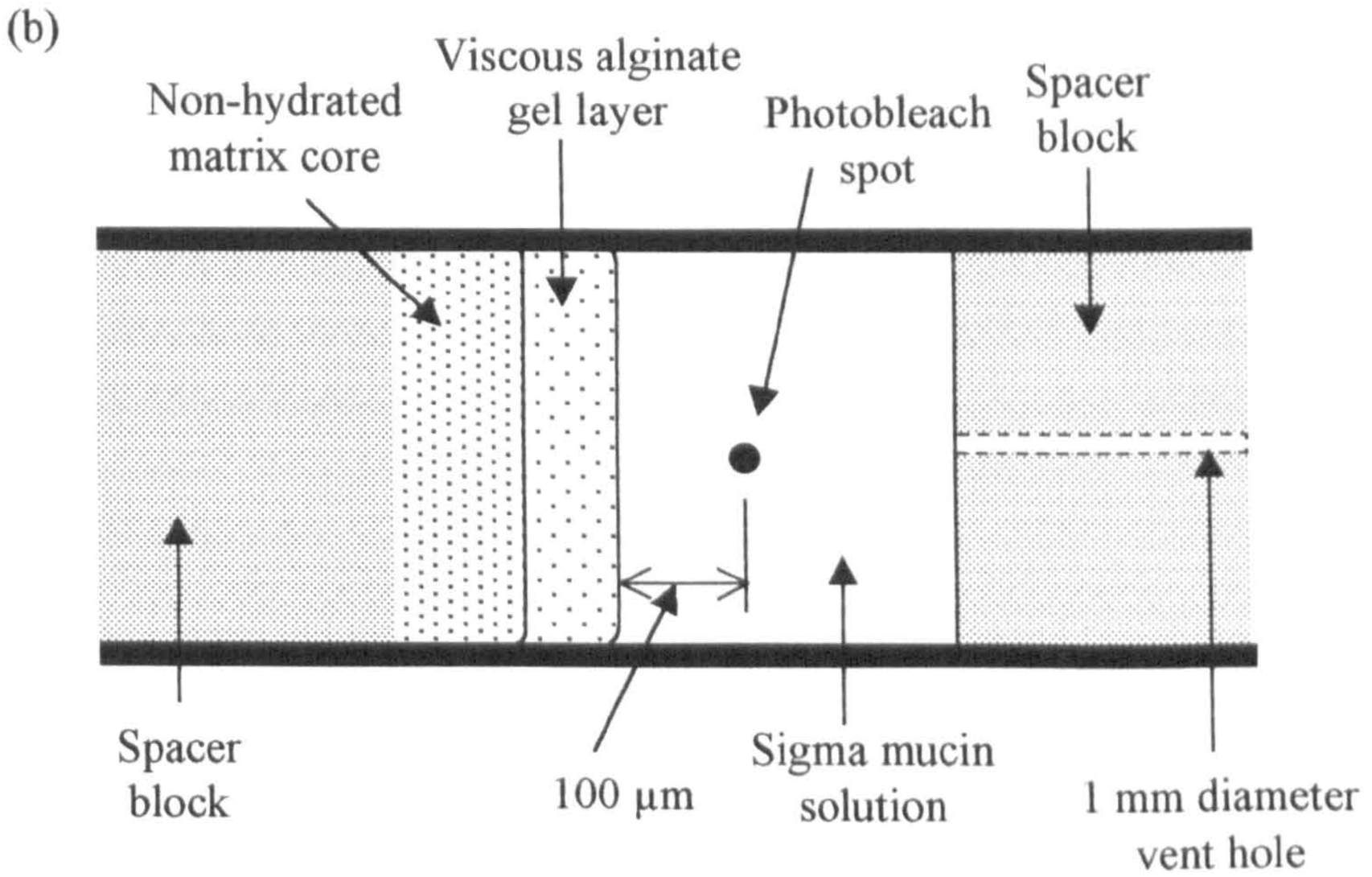

Figure 6.2 The top view of the sample cell geometry used in the FRAP studies – (a) dry matrix and (b) prehydrated matrix

6.5. General methods for measuring the SDC and concentration of water inside bioadhesive bonds

The underlying principles of magnetic resonance imaging (MRI) microscopy were described in section 5.1. The development of the method to measure SDC and concentration of water inside the bond was described in section 5.2. The development of the method to image the dry core, viscous alginate gel layer and the mucus layer regions in a bioadhesive bond were described in section 5.3.

6.5.1. Method to prepare a sample for MRI study

The samples were prepared according to the method described in section 5.2.2.4, except that purified pig gastric mucus was used instead of a Sigma mucin solution.

The development of this method was carried out using Sigma partially purified pig gastric mucin because it was more readily available in larger amounts than purified pig gastric mucin. The rheological properties of purified pig gastric mucin gel were similar to those of native pig gastric mucus. In contrast, the rheological properties of Sigma mucin were dissimilar to those of native gastric mucus and purified pig gastric mucin (section 2.4.6.4). These findings agree with other previously published studies (Madsen *et al*, 1996)

6.5.2. Method to measure the SDC and concentration of water inside a bioadhesive bond

Section 5.2.2.5 describes the method used to measure SDC and concentration of water inside a bioadhesive bond.

6.5.3. Method to image dry core, viscous gel layer and mucus regions of a MRI sample using confocal laser scanning microscopy

Samples were prepared according to the method described in section 6.5.1 and were imaged according to the method described in section 5.3.3.

6.6. General methods for measuring the ability of an alginate matrix to take up liquid

6.6.1. Introduction

Liquid uptake studies are used to measure the penetration and uptake of liquid by a dosage form. The kinetics of uptake may be analysed to reveal the underlying transport processes controlling the ingress of liquid into a dosage form. Studies of this type may provide additional information on how the alginate matrices hydrate, particularly the underlying mechanisms controlling ingress of water across the viscous alginate gel layer.

6.6.2. Background information on liquid uptake studies

Several methods have been developed to measure the ability of a dosage form to take up liquid. Some of these methods include measuring the volume of liquid (Wan *et al*, 1986 and 1987), gravimetric methods (Van Kamp *et al*, 1986), differential scanning calorimetry (Mitchell *et al*, 1993) and image analysis (Moussa *et al*, 1998 and LeNeel *et al*, 1997).

The majority of liquid uptake studies have investigated the penetration of liquid into bulk powders and tablets (Van Kamp *et al*, 1986, Ferrari *et al*, 1995, Lin *et al*, 1996) and the properties and action of excipients (Van Kamp *et al*, 1986, Gissenger *et al*, 1980, Rudnic *et al*, 1982 and Ferrari *et al*, 1988). Other studies have used liquid uptake kinetics to gain insights into the mechanisms of drug release from inert polymer matrices (Romero *et al*, 1991). The hydration dynamics of alginate matrices have also been studied using liquid uptake experiments. Hodson *et al*, 1995, showed that pH of the hydrating fluid influenced the uptake of liquid by sodium alginate matrices, with matrices hydrating in SGF taking up more fluid than those hydrating in SIF. This was attributed to the acid gel layer being more porous and less diffusion retarding than the viscous alginate gel layer. The functional properties of other pharmaceutical products have also been characterised by liquid uptake studies, for example composite hydrocolloid dressings (Ferrari *et al*, 1994).

6.6.3. Method to measure the ability of alginate matrices to take up liquid

The study of liquid uptake by alginate matrices were carried out using the method first developed by Wan *et al* in 1986 and 1987. The apparatus (figure 6.3) was filled with physiological saline at 37±1°C, ensuring that air bubbles were not trapped. A Whatman No1 filter paper lined the sintered filter and was then covered by a PTFE O-ring, exposing 154 mm^2 of filter paper. The top of the funnel was covered to minimise evaporation. The whole apparatus was then equilibrated to 37±1°C in a water bath for 15 mins. The upper surface of a matrix was placed on the exposed filter paper. The change in position of the meniscus along the pipette was measured every 5 mins for 30 mins. The study was repeated to obtain a mean of five matrices. A 10 mm diameter circular flat face aluminium disk was used periodically to determine the volume of saline lost by evaporation and the liquid uptake data was adjusted to account for evaporation.

6.6.4. Method to determine the liquid transport kinetics

Data from liquid uptake studies were fitted to a simple exponential equation (equation 6.1) (Peppas and Sahlin, 1989), which uses a diffusional exponent to describe the transport mechanisms underlying liquid uptake (diagram 6.4a). This equation is limited to analysing the first 60% of an uptake curve (Ritger and Peppas, 1987a and 1987b).

$$V = kt^m \qquad (6.1)$$

k is the kinetic constant and m is the diffusional exponent.

In the alginate matrices used in this study, the calculated limits of the diffusional exponent were: 0.475 (Fickian diffusion); 0.475<m<0.95 (anomalous diffusion); 0.85 (Case II transport) (calculated from Peppas and Sahlin, 1989).

The Fickian diffusion and Case II transport of liquid in a polymer can be considered as additive (Peppas and Sahlin, 1989). Since Fickian diffusion is proportional to the square-root of time and Case II relaxational transport is proportional to time, equation

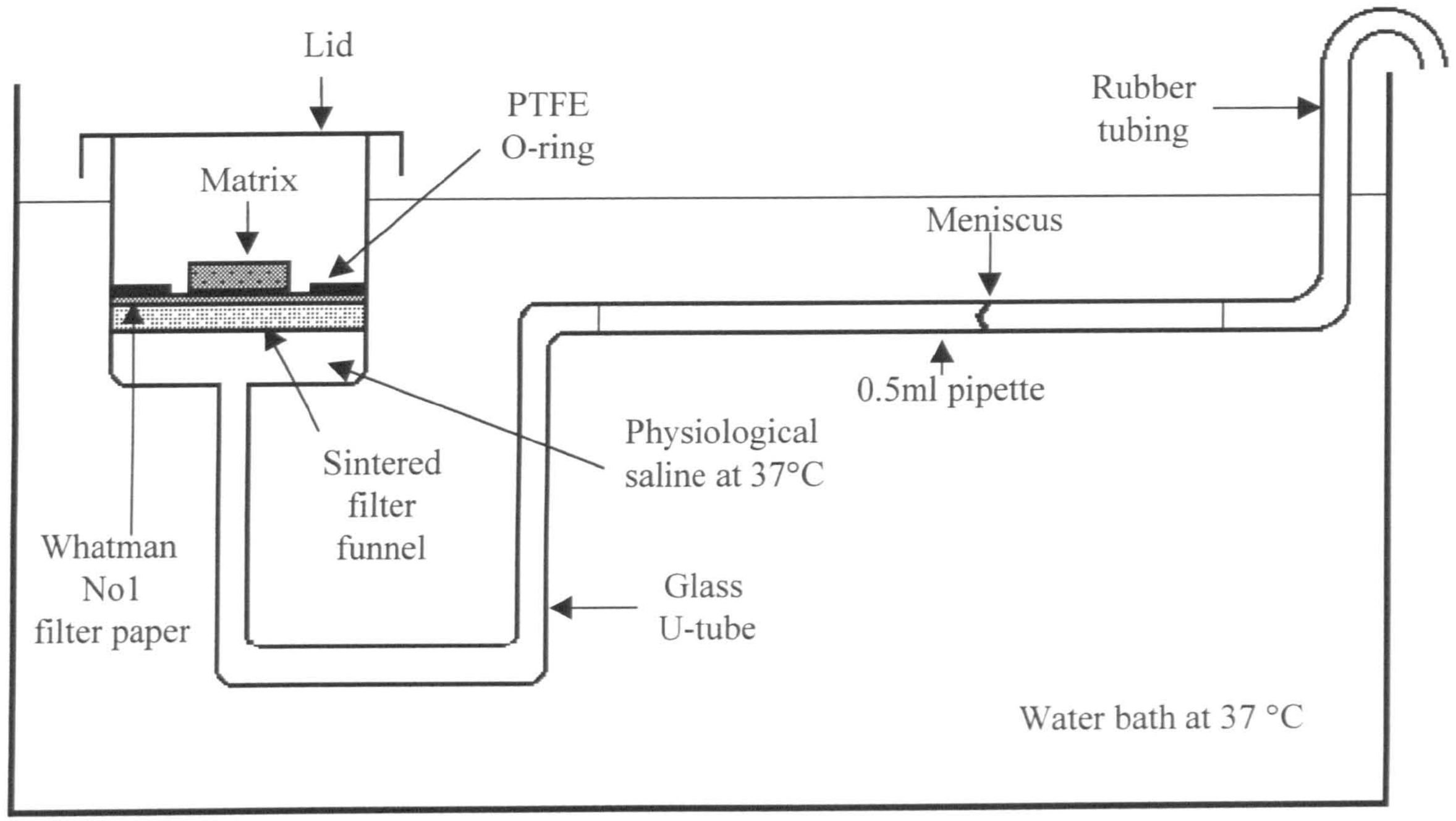

Figure 6.3 The apparatus and sample geometry used to measure the uptake of liquid by sodium alginate matrices

(a)

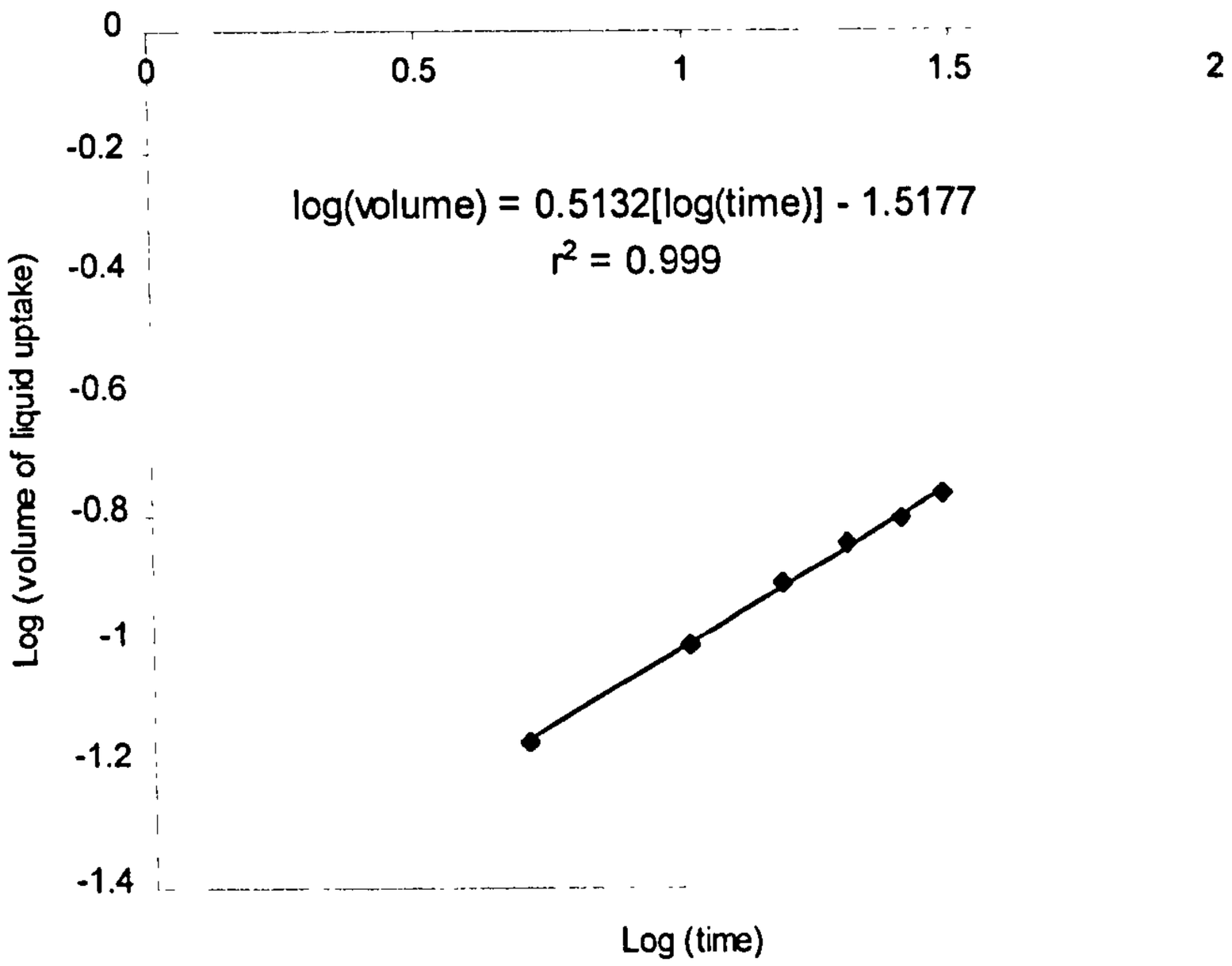

(b)

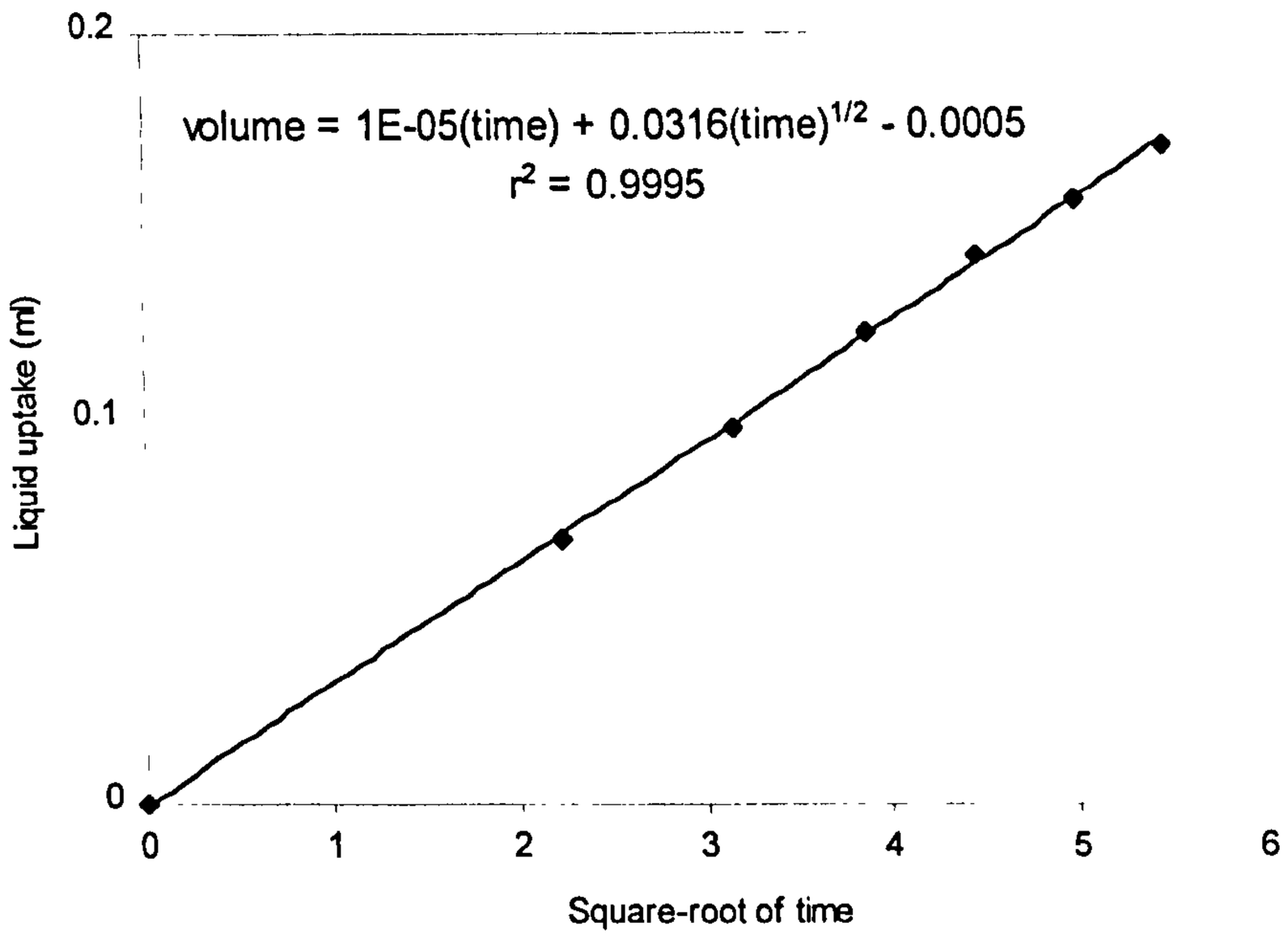

Figure 6.4 Graphs showing how transport parameters are determined from liquid uptake studies

(a) A log-log plot of liquid uptake data gives a linear relationship between volume of liquid and time, with the gradient giving the diffusional exponent. (b) The second-order polymial expression plots the volume of liquid taken up against the square-root of time. The coefficient of time represents Case II transport and the coefficient of $time^{1/2}$ represents Case I (Fickian) diffusion.

6.1 can be re-written to give a second order polynomial equation (equation 6.2). This equation was used by Wan *et al*, 1994, to analyse liquid uptake in disintegrating matrices.

$$V = \alpha t^{0.5} + \beta t + c \qquad (6.2)$$

V is the volumetric uptake, t is time, α is the coefficient of Fickian (Case I) transport, β is the coefficient of relaxational (Case II) transport and c is the kinetic constant.

The liquid uptake curves of the alginate matrices were also fitted to equation 6.2 (diagram 6.4b).

6.7. General methods for statistically analysing data

The possible combinations of alginate samples used in this project meant that result sets in which molecular weight and particle size were studied contained data from three alginate samples. In comparison, the result sets in which the M:G ratio was studied contained data from two alginate samples.

The result sets were initially tested for significant differences in data using analysis of variance (ANOVA) at a 5% significance level. In the result sets composed of three samples and where ANOVA showed statistically significant differences, a two-tailed student t-test at a 2% significance level was used to test for individual differences between the samples (a paired comparison analysis). In this situation, the 5% significance level of the ANOVA test was 'divided' between the three possible paired combinations to give a significance level of 1.667%, which was conveniently rounded up to a 2% significance level. In cases where there are only two sets of data in the result set, ANOVA is statistically equivalent to the student two-tailed t-test. The statistical analyses of results were carried out using the Analysis ToolPak statistics package in Excel97 (Microsoft Corporation, USA).

6.7.1. A worked example of the statistical analysis of a result set containing three alginates

The data were arranged in a blocked ANOVA design (table 6.1).

Table 6.1 Raw data measuring the W_a of bioadhesive bonds, arranged in a blocked ANOVA design

Experiment No.	Sodium alginate		
	35,000 Da	220,000 Da	315,000 Da
1	0.00378	0.01388	0.00521
2	0.00662	0.00288	0.01052
3	0.00108	0.00603	0.00861
4	0.00141	0.00704	0.00398
5	0.0015	0.00241	0.00325
6	0.00091	0.00299	0.0115
7	0.00232	0.00691	0.01975
8	0.00249	0.00556	0.00401
9	0.00142	0.00511	0.00659
10	0.00109	0.00997	0.01135
11	0.0069	0.00641	0.0126
12	0.00363	0.00952	0.00842
13	0.00198	0.00545	0.00518
14	0.00519	0.01471	0.01738

Data was analysed by single factor ANOVA at a 5% significance level (table 6.2).

Table 6.2 Single factor analysis of data presented in table 6.1.

ANOVA: Single Factor

Summary

Groups	Count	Sum	Average	Variance
35,000 Da	14	0.04031	0.00288	4.2E-06
220,000 Da	14	0.09888	0.00706	1.4E-05
315,000 Da	14	0.12834	0.00917	2.5E-05

ANOVA

Source of Variation	SS	Df	MS	F	P-value	F crit
Between Groups	0.00029	2	0.00014	9.79687	**0.00036**	3.2381
Within Groups	0.00057	39	1.5E-05			
Total	0.00086	41				

There was sufficient evidence to suggest that data in table 6.1 were statistically significantly different ($p<0.05$). Subsequently, a paired comparison analysis, using the student t-test at a 2% significance level, was carried out. (N.B. A paired comparison analysis was not carried out if ANOVA did not detect any significant differences in the data.)

Table 6.3 Paired comparisons of the data presented in table 6.1.

t-Test: Two-Sample Assuming Equal Variances

	35,000 Da	**220,000 Da**
Mean	0.00288	0.00706
Variance	4.2E-06	1.4E-05
Observations	14	14
Pooled Variance	9.2E-06	
Hypothesised Mean Difference	0	
Df	26	
t Stat	-3.6429	
P(T<=t) one-tail	0.00059	
t Critical one-tail	2.16203	
P(T<=t) two-tail	**0.00118**	
t Critical two-tail	2.47863	

	315,000 Da	**220,000 Da**
Mean	0.00917	0.00706
Variance	2.5E-05	1.4E-05
Observations	14	14
Pooled Variance	2E-05	
Hypothesised Mean Difference	0	
Df	26	
t Stat	1.24939	
P(T<=t) one-tail	0.11133	
t Critical one-tail	2.16203	
P(T<=t) two-tail	**0.22265**	
t Critical two-tail	2.47863	

	315,000 Da	**35,000 Da**
Mean	0.00917	0.00288
Variance	2.5E-05	4.2E-06
Observations	14	14
Pooled Variance	1.5E-05	
Hypothesised Mean Difference	0	
Df	26	
t Stat	4.31975	
P(T<=t) one-tail	0.0001	
t Critical one-tail	2.16203	
P(T<=t) two-tail	**0.0002**	
t Critical two-tail	2.47863	

Table 6.3 showed that there was sufficient evidence to suggest that the 220,000 Da and 315,000 Da alginates were statistically significantly different to the 35,000 Da alginate ($p<0.02$). However, there was insufficient evidence to suggest that the 220,000 Da and 315,000 Da alginates were statistically significantly different ($p>0.02$).

Chapter 7

Influence of molecular weight on the bioadhesion of dry and hydrated sodium alginate matrices

7.1 Introduction

Molecular weight is a known factor, which may influence the bioadhesion of polymers (Smart *et al*, 1984, Tobyn *et al*, 1996, Peppas and Buri, 1985, and Mortazavi and Smart, 1994b), and has been discussed in section 1.5.1.1. Therefore, the aim of this chapter was to study how molecular weight affects the movement of water and solutes inside bioadhesive bonds formed by alginate matrices as well as the bioadhesive bond strength. The bioadhesive bonds formed by dry and hydrated alginate matrices were considered separately since the state of hydration of the alginate may influence the underlying mechanisms of bioadhesion.

7.2. Methods

The general methods described in chapter 6 were used to test the alginate matrices. The physicochemical characteristics of the sodium alginates and the pig gastric mucus are described in chapter 3. The statistical analysis of data was carried out according to methods described in section 6.7.

7.3. Results

7.3.1. Influence of molecular weight on the water inside bioadhesive bonds formed by dry matrices

7.3.1.1. Water diffusion inside bioadhesive bonds formed by dry alginate matrices

The SDC profiles of water inside bioadhesive bonds formed by dry alginate matrices are shown in figures 7.1a, 7.1b and 7.1c.

The SDC profiles of water inside bioadhesive bonds of dry alginate matrices have a characteristic shape, which developed in a distinctive way over time, irrespective of the molecular weight of alginate.

After 1 min, the SDC profiles of all three alginate matrices rapidly increased to a value of $\approx 6.5 \times 10^{-10}$ m^2 sec^{-1} at ≈850 μm, forming a sharp diffusion front. At later times, the

(a)

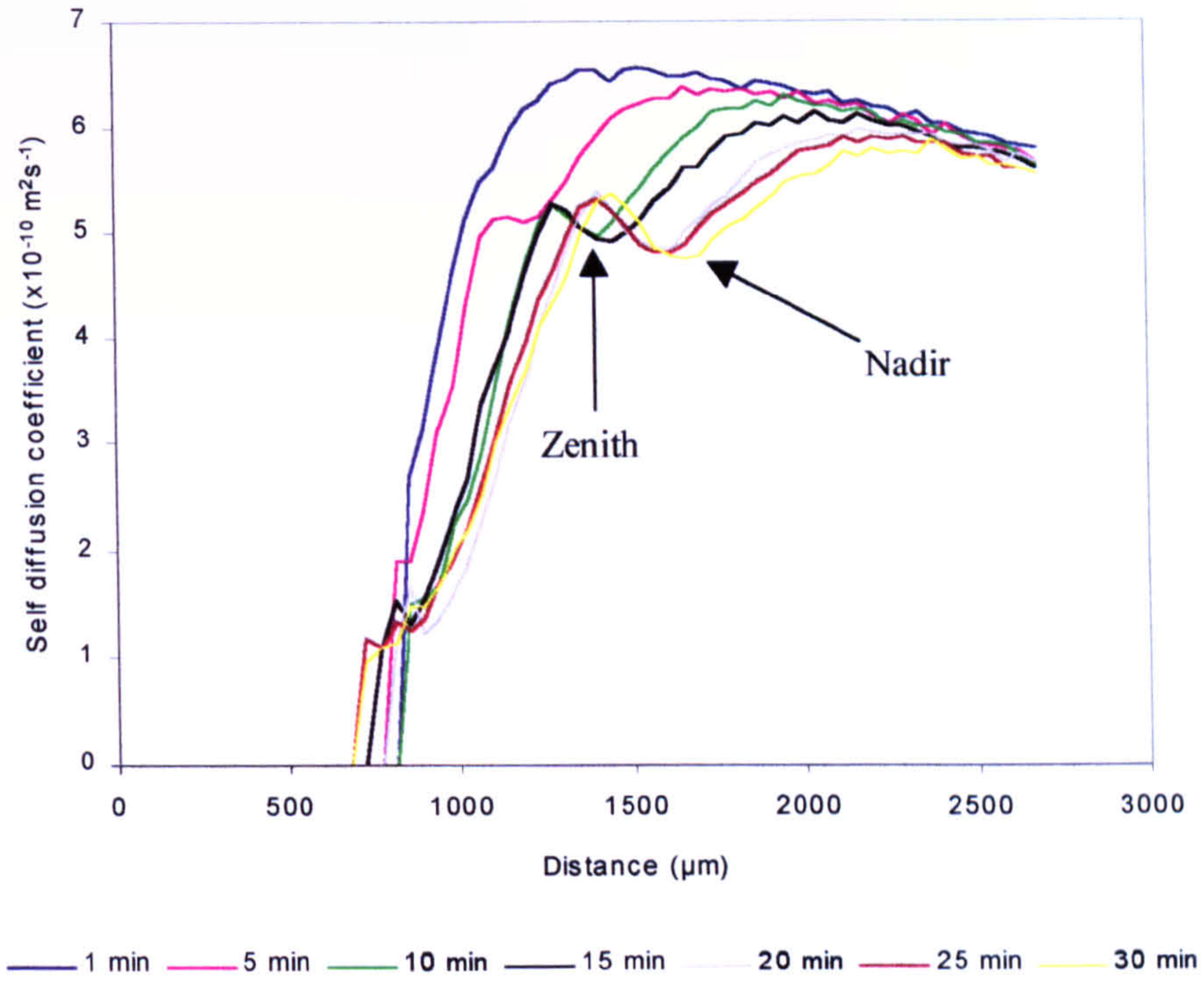

(b)

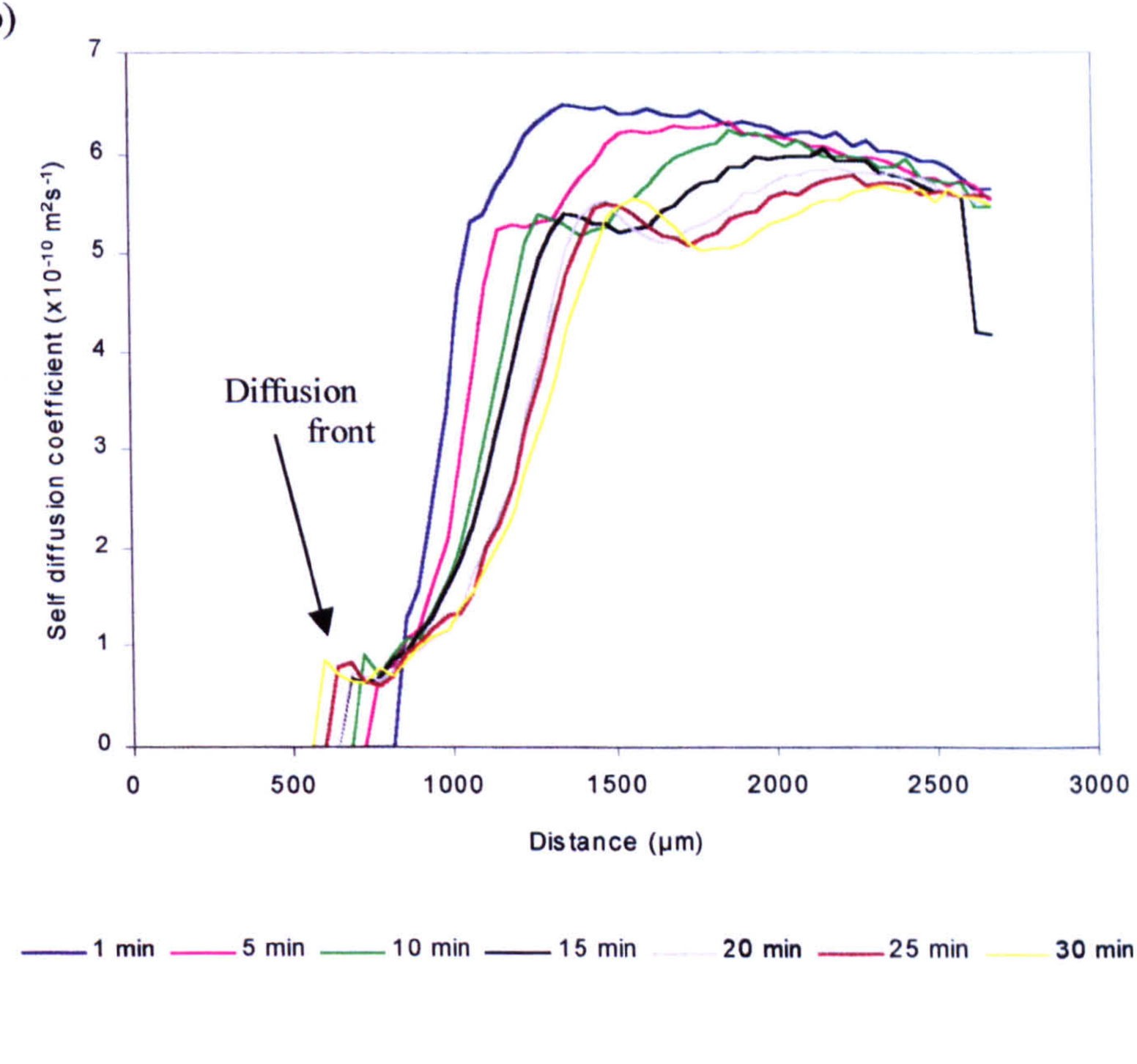

Figure 7.1 Influence of time on the SDC of water inside bioadhesive bonds - dry alginate matrices of different molecular weights

Bioadhesive bonds were formed between dry (a) 35,000 Da and (b) 220,000 Da alginate matrices and purified pig gastric mucus at 20±1°C (mean, n=4). The diffusion front, zenith and nadir points in the SDC profiles are illustrated. Standard deviation bars have been omitted for clarity.

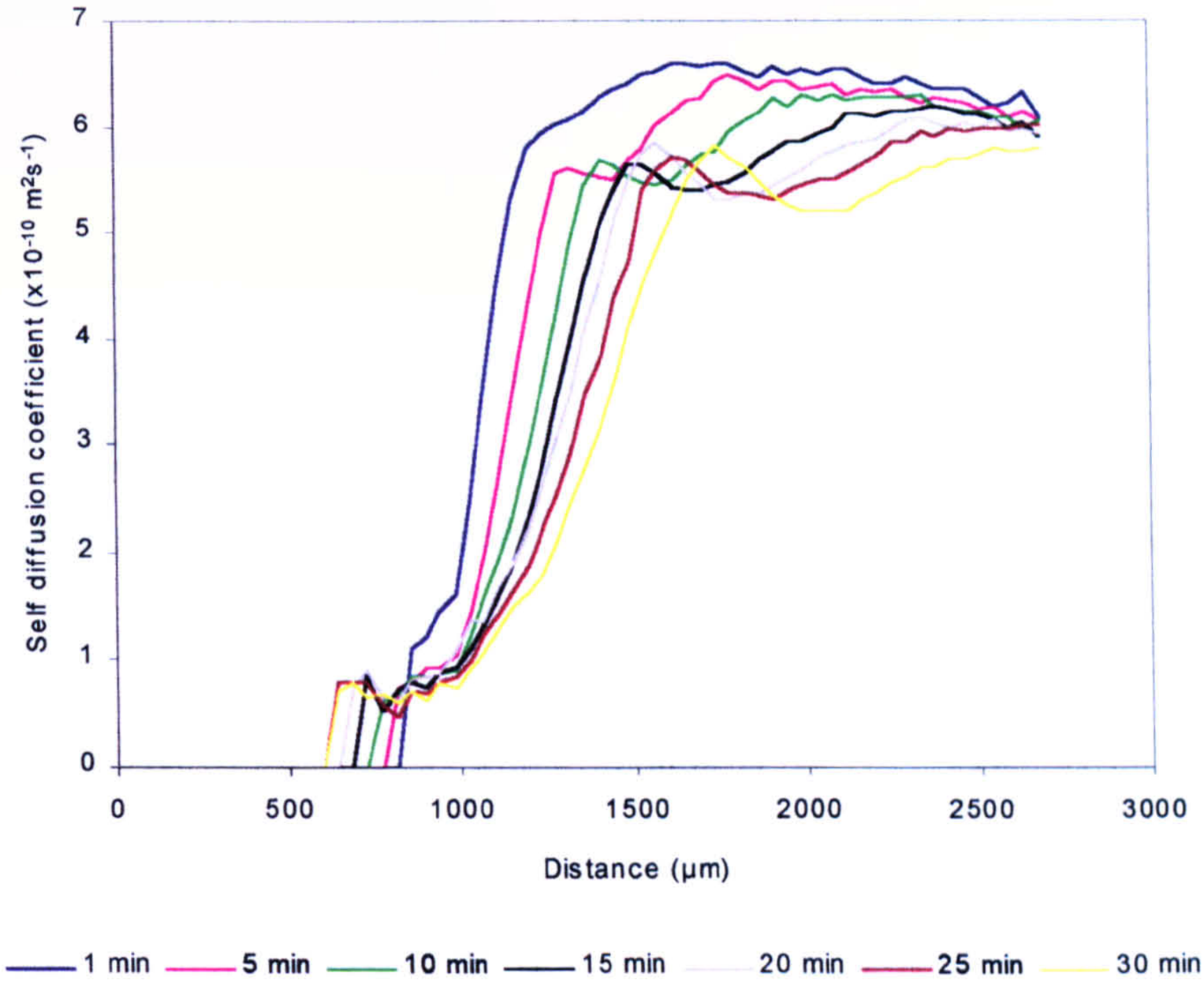

Figure 7.1c Influence of time on the SDC of water inside bioadhesive bonds - dry alginate matrices of different molecular weights

Bioadhesive bonds were formed between dry 315,000 Da alginate matrices and purified pig gastric mucus at 20±1°C (mean, n=4). Standard deviation bars have been omitted for clarity.

diffusion fronts consisted of a sharp increase in SDC, which formed a plateau before gradually increasing to a zenith SDC value. The length of the plateau seemed to increase over time and the slope of the diffusion front decreased over time.

The SDC profiles of all three alginates developed a characteristic dip at ≈1000-1500 μm after 5 mins, which increased in length and depth over time. The SDC profiles gradually decreased at >2500 μm, but it is thought that this was caused by the non-linearity of both the external magnetic field gradient and the RF coil rather than by any physical effect.

7.3.1.2. The influence of molecular weight on the SDC profiles of bioadhesive bonds formed by dry alginate matrices

Figures 7.2, 7.3 and 7.4 show the influence of molecular weight on the diffusion front, zenith and nadir points in the SDC profiles, respectively. These points were measured from the SDC profiles in figures 7.1a, 7.1b and 7.1c. The P_x value is the position of the point in the SDC profile and the SDC_x value is the SDC of water at P_x; the subscript 'x' may be 'DF', 'zen' or 'nad', denoting the diffusion front, zenith and nadir points of the profile, respectively.

The P_{DF} value suggests the innermost limit of water penetration into the alginate matrix (figures 7.5a-7.5c) and therefore a decrease in the P_{DF} value indicates the ingress of water into the dry matrix core. The P_{DF} value of the 35,000 Da alginate decreased more slowly than the P_{DF} values of the 220,000 Da and 315,000 Da alginates, which decreased at similar rates (figure 7.2a). The P_{DF} values of the 35,000 Da and 315,000 Da alginates decreased linearly with time, suggesting that the ingress of water was by Fickian diffusion (Crank, 1975). The SDC_{DF} values of all alginates decreased with time. At 1-5 mins, the SDC_{DF} value of the 35,000 Da alginate was statistically significantly faster than the SDC_{DF} values of 220,000 Da and 315,000 Da alginates ($p<0.02$). At other time points, SDC_{DF} was not significantly influenced by molecular weight ($p>0.05$) (figure 7.2b).

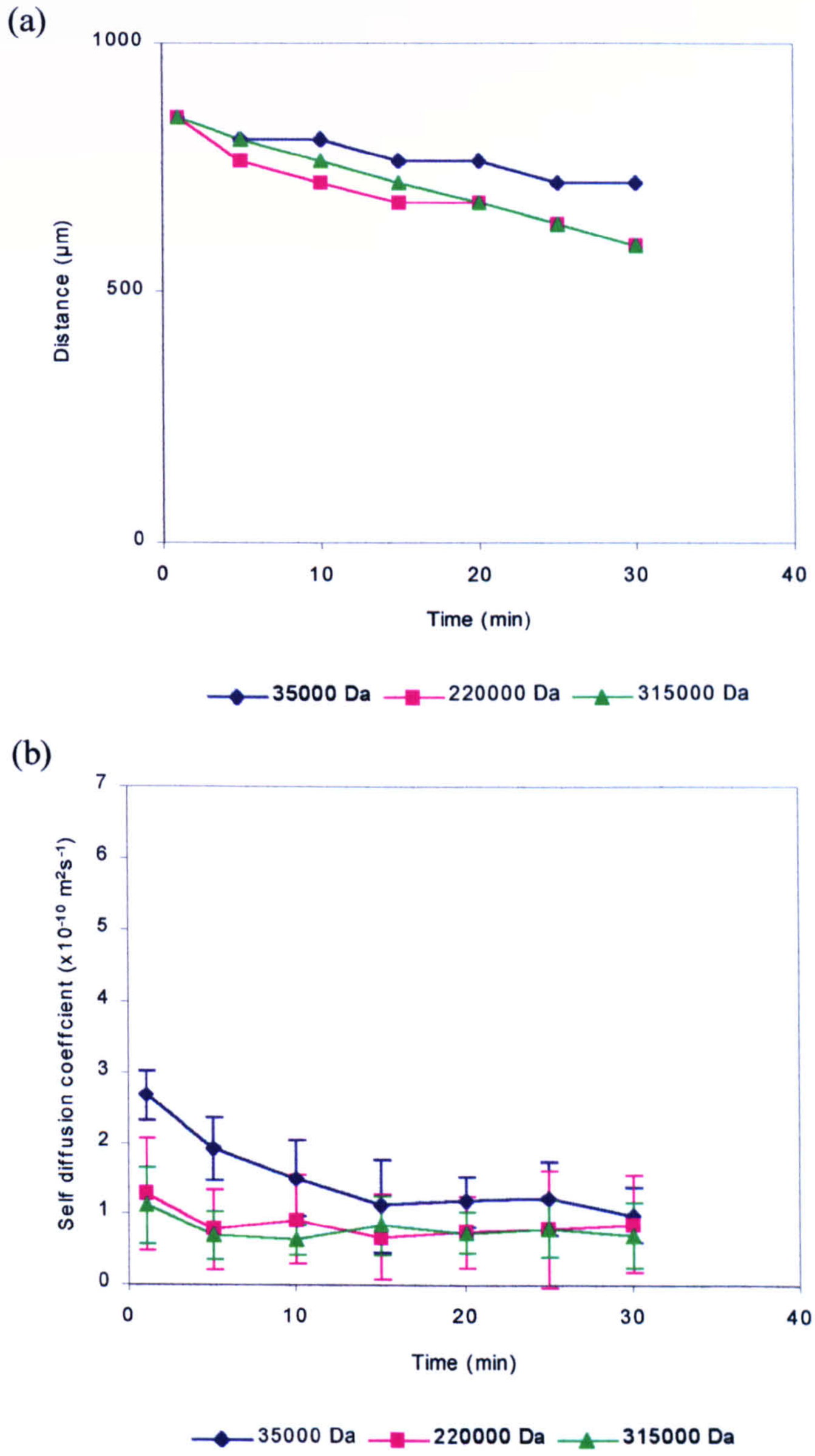

Figure 7.2 Influence of time on the diffusion front - dry alginate matrices of different molecular weights

The effect of time on (a) P_{SD} and (b) SDC_{SD} measured from the SDC profiles of water inside bioadhesive bonds formed between dry 35,000 Da, 220,000 Da and 315,000 Da alginate matrices and purified pig gastric mucus at 20±1°C (mean, n=4, ±1 SD).

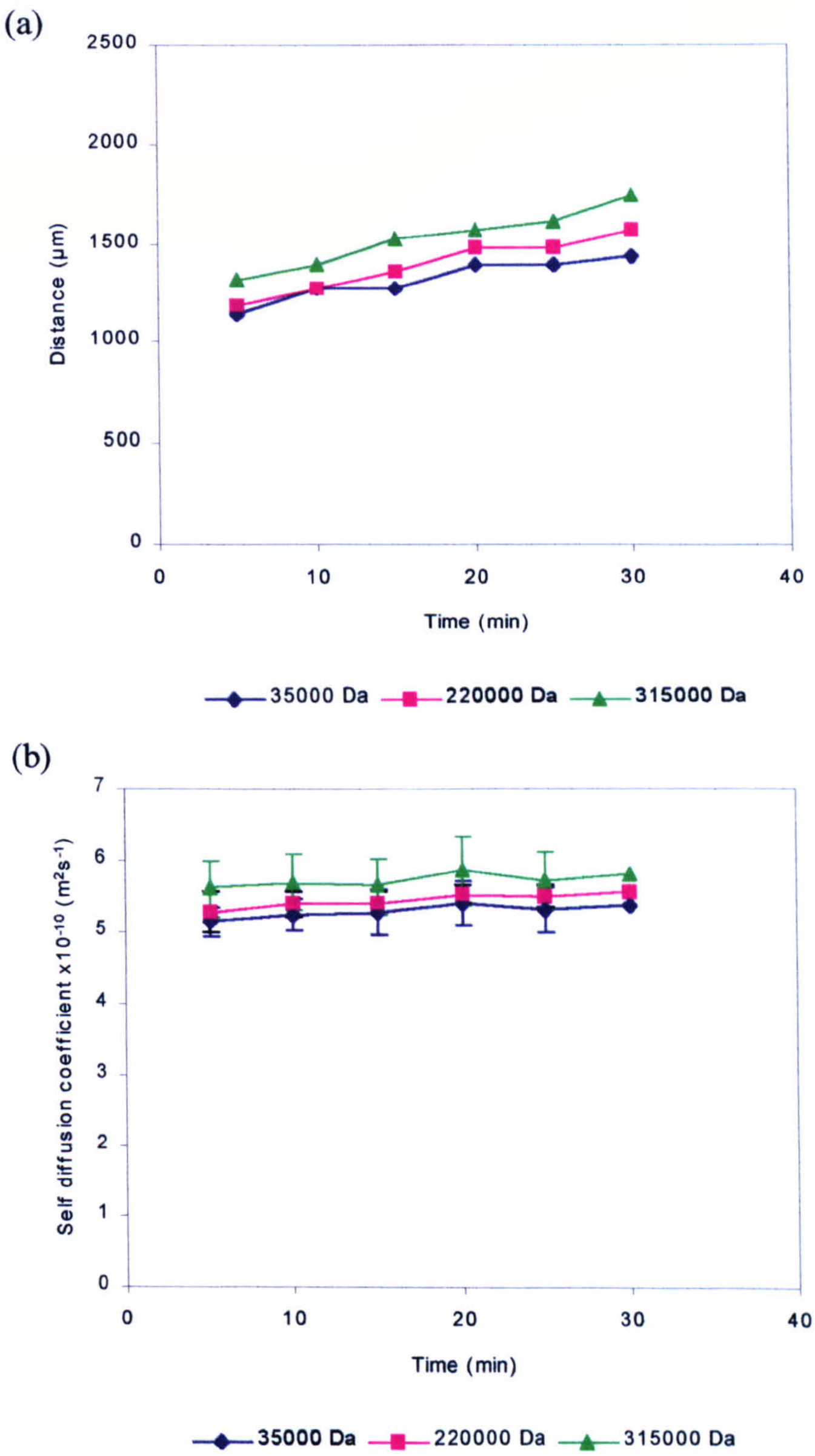

Figure 7.3 Influence of time on the zenith - dry alginate matrices of different molecular weights

The effect of time on (a) P_{zen} and (b) SDC_{zen} taken from the SDC profiles of water inside bioadhesive bonds formed between dry 35,000 Da, 220,000 Da and 315,000 Da alginate matrices and purified pig gastric mucus at 20±1°C (mean, n=4, ±1 SD).

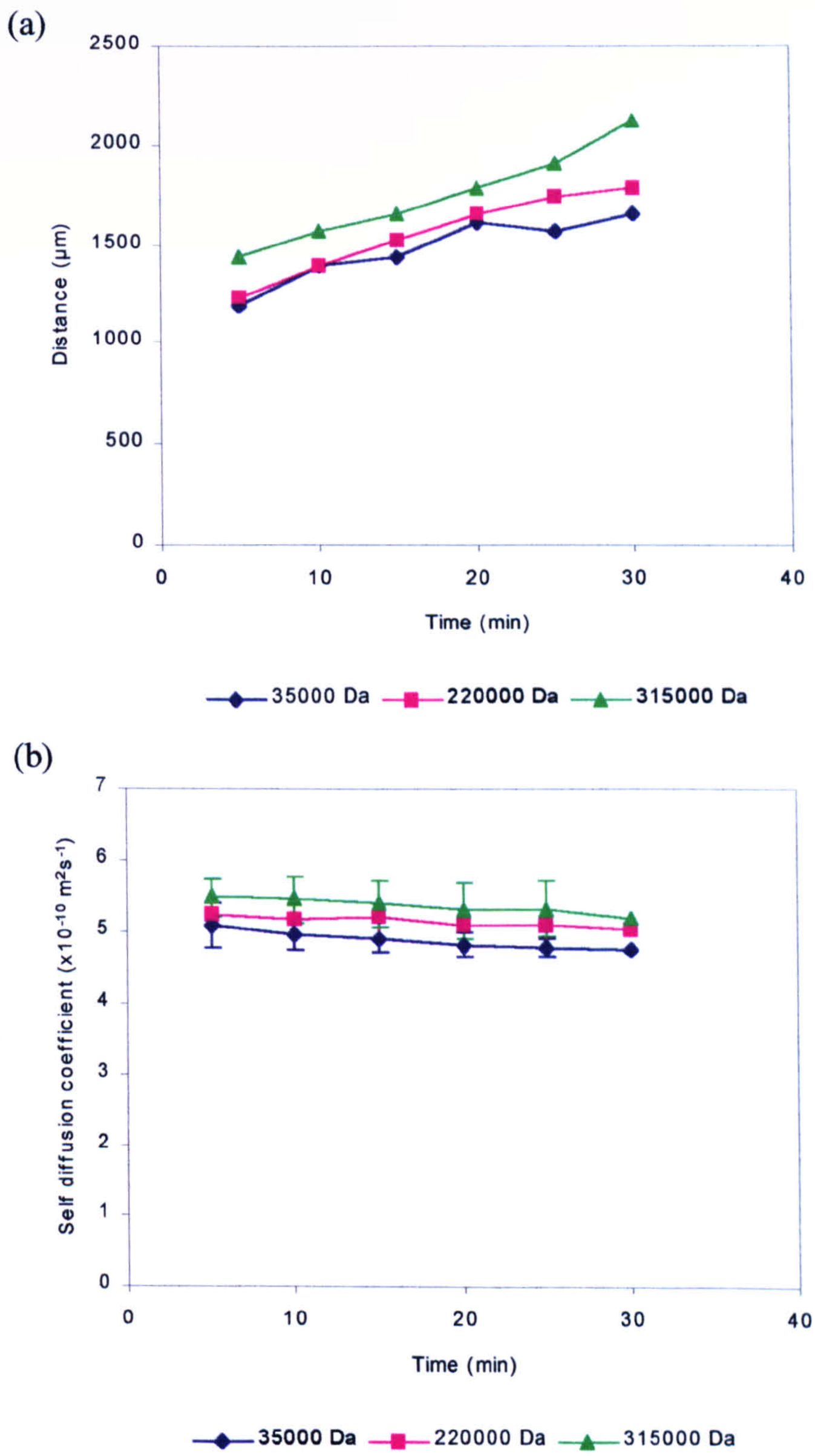

Figure 7.4 Influence of time on the nadir - dry alginate matrices of different molecular weights

The effect of time on (a) P_{nad} and (b) SDC_{nad} taken from SDC profiles of water inside bioadhesive bonds formed between dry 35,000 Da, 220,000 Da and 315,000 Da alginate matrices and purified pig gastric mucus at 20±1°C (mean, n=4, ±1 SD).

The P_{zen} and P_{nad} values of all three alginates increased with time, with the rate of movement being scaled to molecular weight (figure 7.3a and 7.4a). The P_{zen} value indicates the approximate outer limit of the viscous alginate gel layer (figures 7.5a-7.5c). The increase of P_{zen} is may be due to the matrices expanding and forming a swelling viscous alginate gel layer. The SDC_{zen} of all three alginates increased slightly with time but there were no statistically significantly differences over 30 mins ($p>0.05$) (figure 7.3b). The SDC_{nad} of all three alginates slightly decreased with time but again there were no statistically significantly differences over 30 min ($p>0.05$) (figure 7.4b).

7.3.1.3. Comparison of the SDC and concentration profiles of water inside bioadhesive bonds formed by dry matrices

The concentration and SDC profiles of water inside bioadhesive bonds formed by dry alginate matrices are shown in figures 7.5a, 7.5b and 7.5c.

The water concentration profiles of all three alginate matrices rapidly increased at ≈850 μm after 5 mins, forming a penetrant front. The gradients of the penetrant fronts decreased after 20 mins, suggesting that water penetration into the matrix became more Fickian over time (Crank, 1975, and Valtier *et al*, 1995). The water concentration profiles did not develop characteristic dips similar to those observed in the SDC profiles.

Figures 7.5a, 7.5b and 7.5c also show the approximate positions of the core-gel, mucus-gel and mucus-mucus interfaces in the concentration and SDC profiles. These positions were marked using data obtained from the CLSM method described in section 5.3. The layer of mucus gel directly next to the alginate matrices became more fluorescent over time and the mucus-mucus interface delimits the extent of this region. The diffusion and penetrant fronts approximately corresponded to the viscous alginate gel layer. The characteristic dip in the SDC profiles corresponded to the region of increasingly fluorescent mucus. The inherent difficulties and disadvantages of delimiting these profiles have been discussed in section 5.3.

(a)

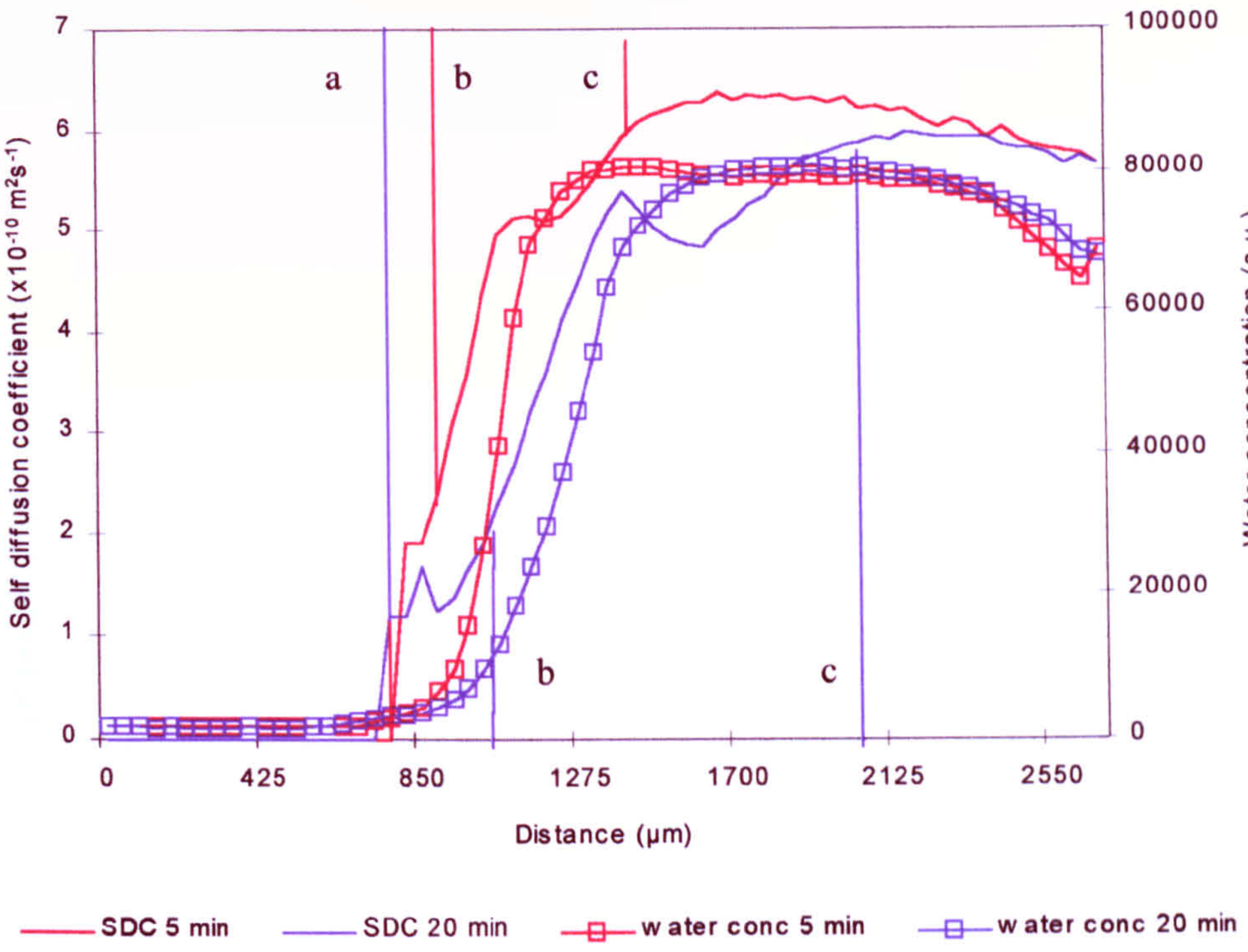

(b)

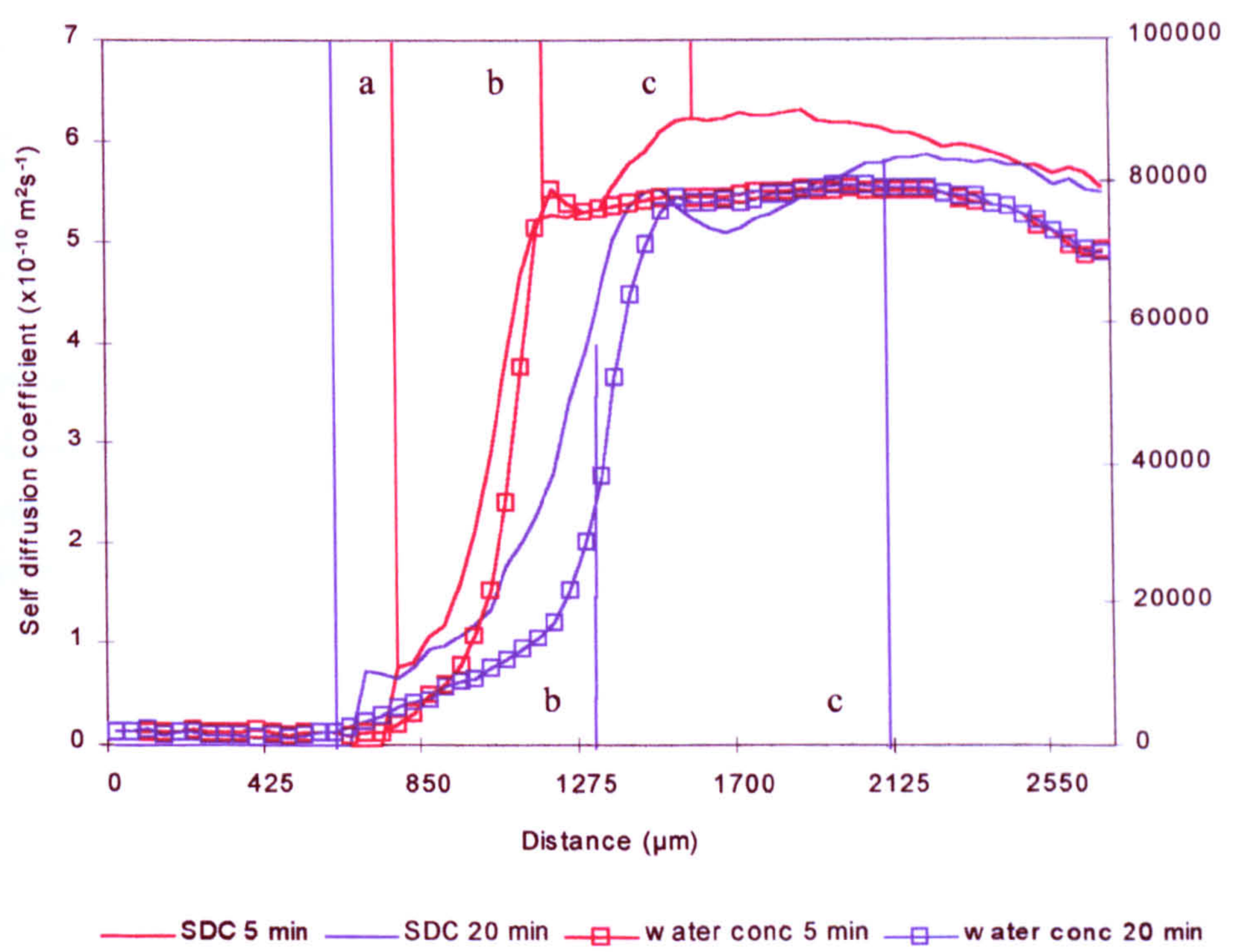

Figure 7.5 The concentration and SDC of water inside bioadhesive bonds of dry alginate matrices.

The SDC and concentration of water inside bioadhesive bonds formed between dry (a) 35,000 Da and (b) 220,000 Da alginate matrices and purified pig gastric mucus in physiological saline at 20±1°C (mean, n=4). The positions of (a) the dry core-viscous gel interface, (b) the viscous gel-mucus gel interface and (c) the mucus-mucus interface have been marked on the profiles. Standard deviation bars have been omitted for clarity.

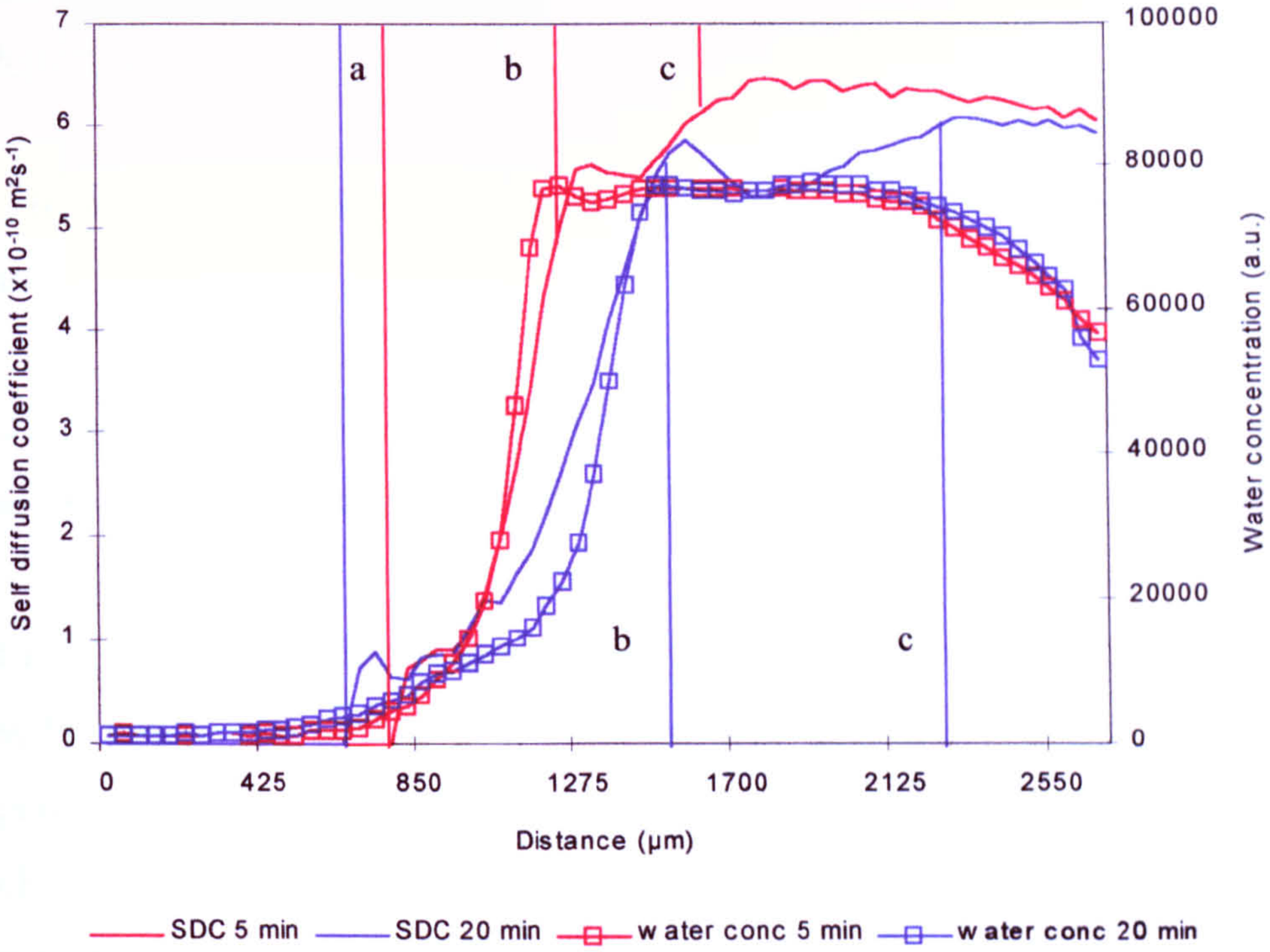

Figure 7.5c The concentration and SDC of water inside bioadhesive bonds of dry alginate matrices.

The SDC and concentration of water inside bioadhesive bonds formed between dry 315,000 Da alginate matrices and purified pig gastric mucus in physiological saline at 20±1°C (mean, n=4). The positions of (a) the dry core-viscous gel interface, (b) the viscous gel-mucus gel interface and (c) the mucus-mucus interface have been marked on the profiles. Standard deviation bars have been omitted for clarity.

7.3.2. Influence of molecular weight on water inside bioadhesive bonds formed by prehydrated matrices

7.3.2.1. Water diffusion inside bioadhesive bonds formed by prehydrated alginate matrices

The SDC profiles of water inside bioadhesive bonds formed by prehydrated alginate matrices are shown in figures 7.6a, 7.6b and 7.6c.

After 1 min, the SDC profiles of the 35,000 Da and 220,000 Da alginates rapidly increased to $\approx 9 \times 10^{-9}$ m^2 sec^{-1} at ≈850 μm, forming a diffusion front. At later times, a small plateau developed in the diffusion front at approximately 750 μm (figures 7.6a and 7.6b). The diffusion fronts are similar in shape to those observed in the SDC profiles hydrating HPMC and PVA matrix gel layers (Rajabi-Siahboomi *et al*, 1996, and Madhu *et al*, 1998).

In comparison, the diffusion front of the 315,000 Da alginate was composed of a sharp increase in SDC, which formed a plateau before increasing gradually to a zenith value (figure 7.6c). The overall shape of the diffusion front is similar to the diffusion front of the dry 315,000 Da alginate matrix (figure 7.1c). The diffusion front of the 35,000 Da alginate decreased over time but the diffusion front gradients of 220,000 Da and 315,000 Da alginates did not change over 30 mins.

The SDC profile of the 35,000 Da alginate developed a characteristic dip after 1 min, which increased in length and depth over time. This characteristic dip was similar to, but smaller than those dips observed in the SDC profiles of dry alginate matrix at a particular time (figure 7.6a). The SDC profiles of the 220,000 Da and 315,000 Da alginates did not develop similar characteristic dips (figure 7.6b and 7.6c).

Again, the SDC profiles of all three alginates gradually decreased at ≈2500 μm. This is likely to be an artefact caused by the non-linearity of the external magnetic field gradient and RF coil.

(a)

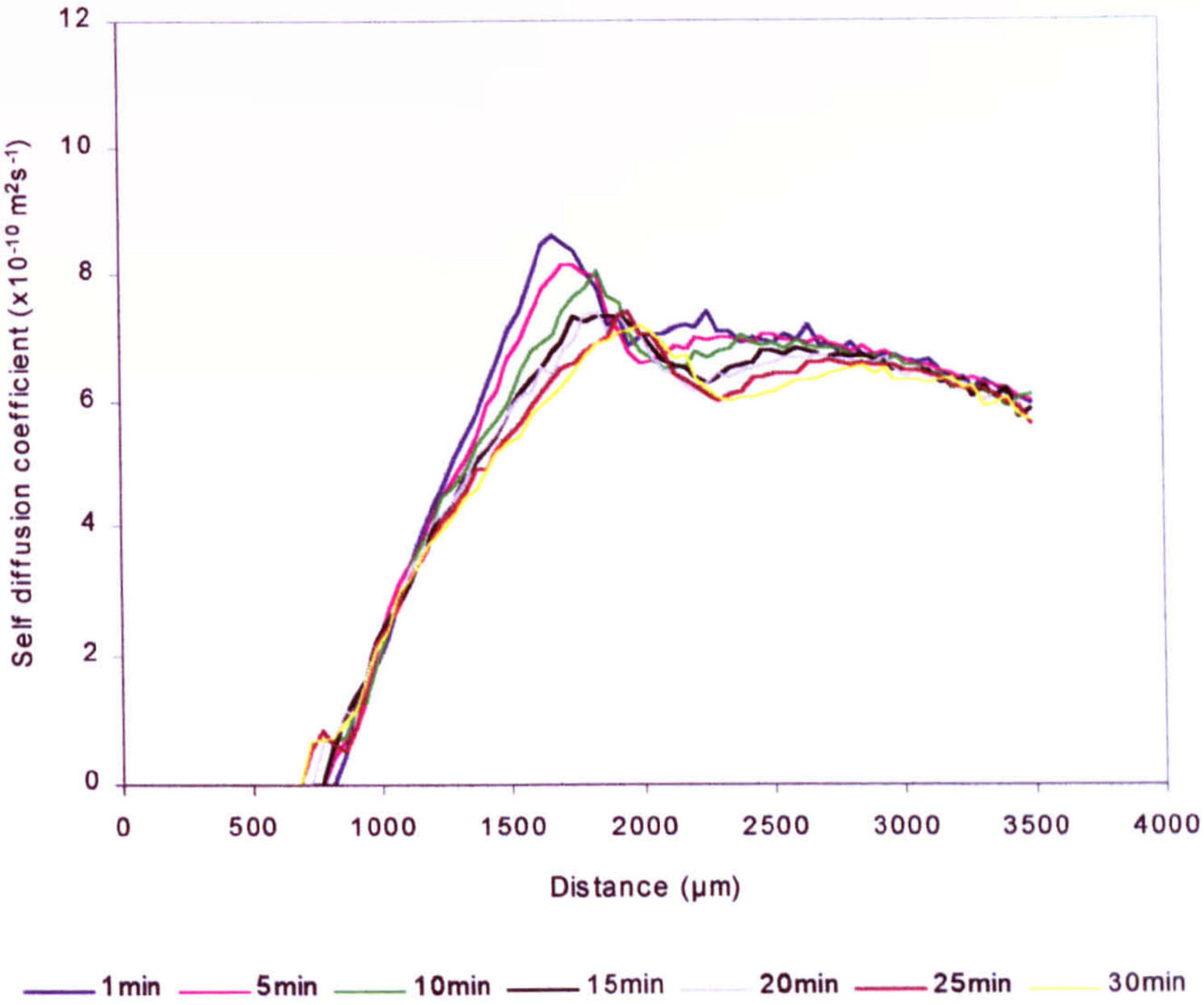

(b)

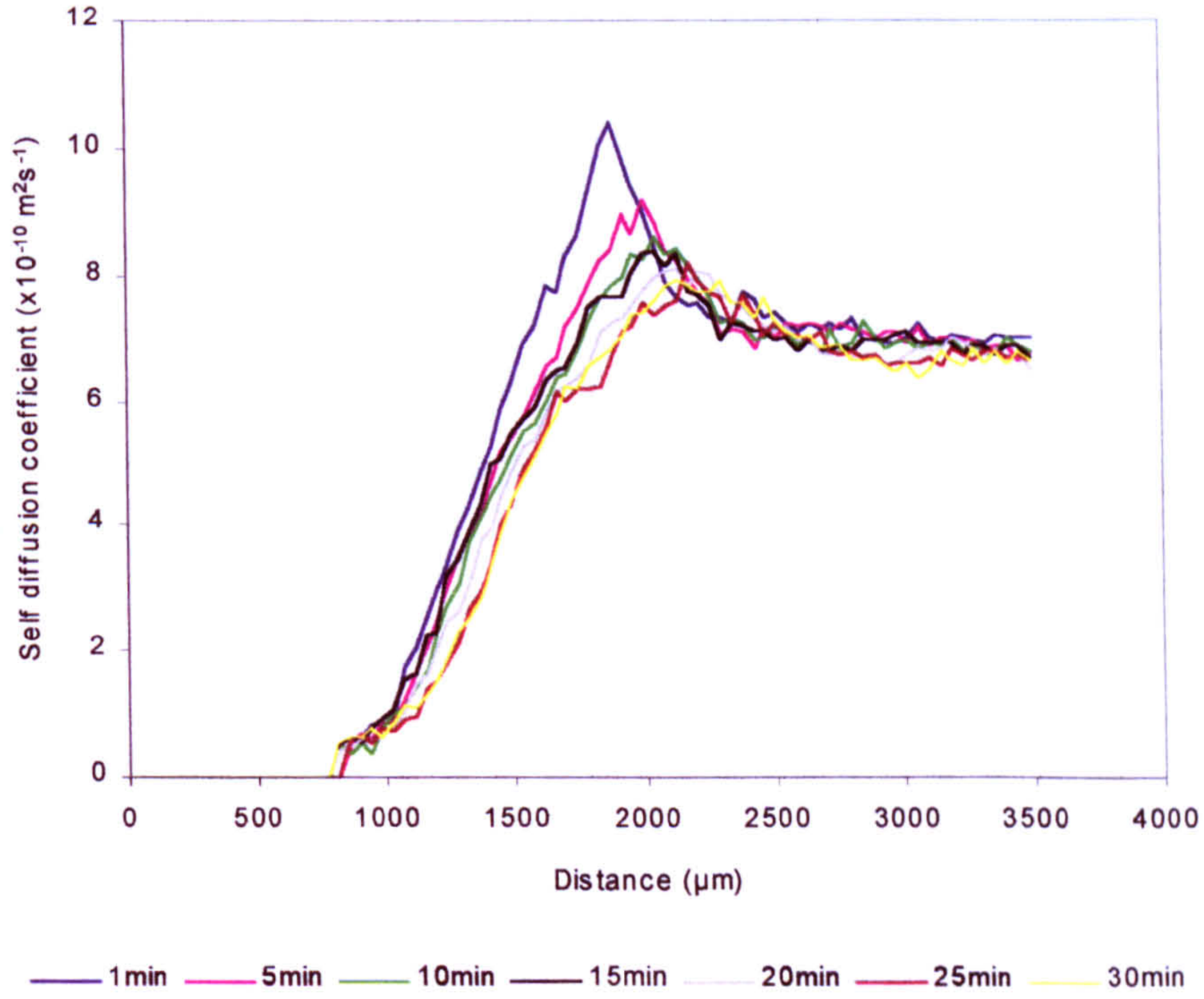

Figure 7.6 Influence of time on SDC of water inside bioadhesive bonds - prehydrated alginate matrices of different molecular weight

Bioadhesive bonds were formed between (a) 35,000 Da and (b) 220,000 Da alginate matrices, prehydrated in physiological saline for 10 mins, and purified pig gastric mucus at 20±1°C (mean, n=4). Standard deviation bars have been omitted for clarity.

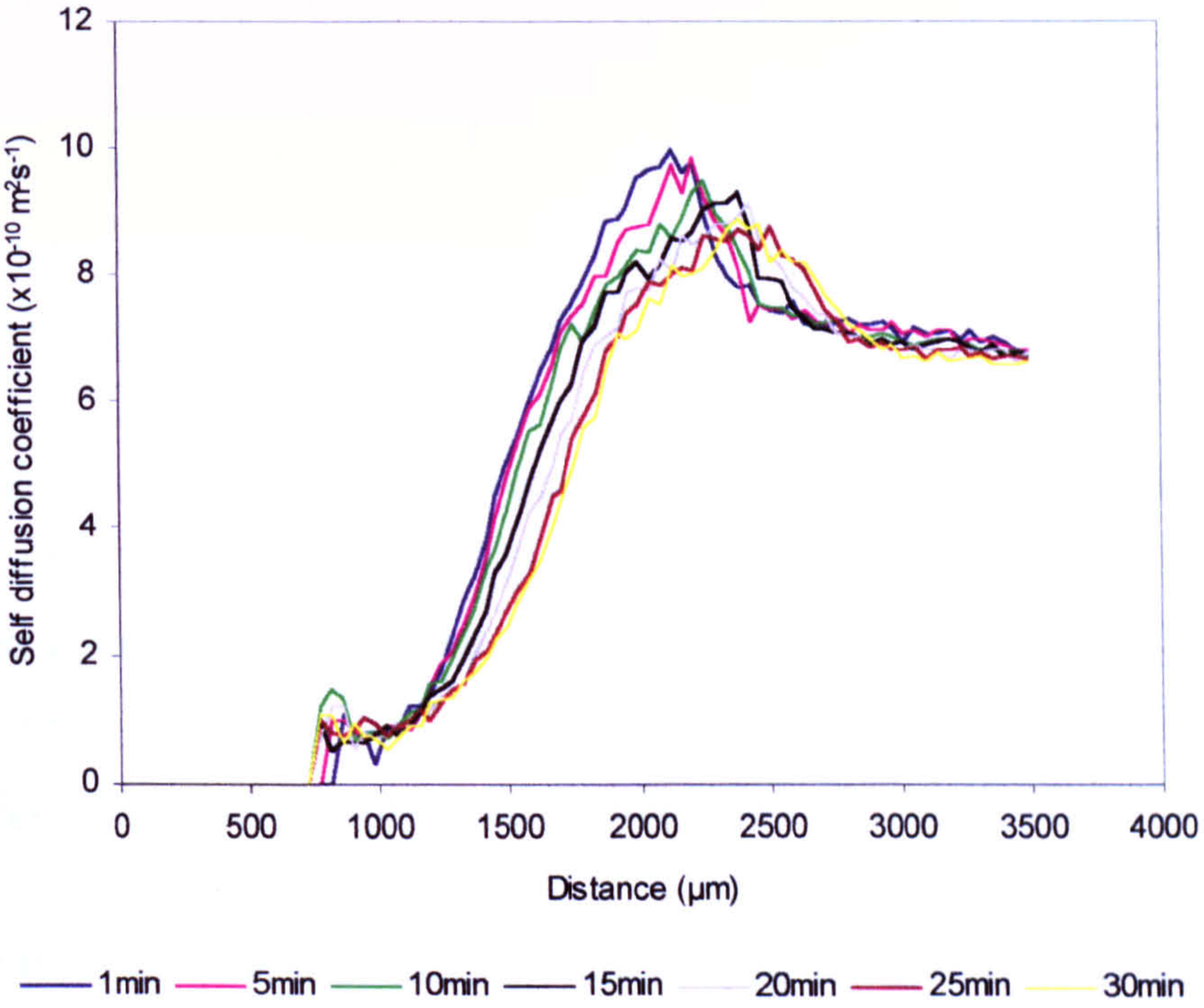

Figure 7.6c Influence of time on SDC of water inside bioadhesive bonds - prehydrated alginate matrices of different molecular weight

Bioadhesive bonds were formed between 315,000 Da alginate matrices, prehydrated in physiological saline for 10 mins, and purified pig gastric mucus at 20±1°C (mean, n=4). Standard deviation bars have been omitted for clarity.

7.3.2.2. The influence of molecular weight on the SDC profiles of bioadhesive bonds formed by prehydrated matrices

Figures 7.7, 7.8 and 7.9 show the influence of molecular weight on the diffusion front, zenith and nadir points in the SDC profiles, respectively. These points were measured from the SDC profiles in figures 7.6a, 7.6b and 7.6c.

The P_{DF} values of all three alginates decreased over time and the rate of decrease was ranked as: 220,000 Da<35,000 Da<315,000 Da (figure 7.7a). The SDC_{DF} value of the 315,000 Da alginate was significantly faster than the SDC_{DF} of the lower molecular weight alginates after 5 mins and 25 mins ($p<0.02$). At other times, the SDC_{DF} values all three alginates were not statistically significantly different ($p>0.05$) (figure 7.7b).

The initial P_{zen} values were scaled to molecular weight but increased at approximately the same rate over time (figure 7.8a). There ware no statistically significant differences in the SDC_{zen} values after 5 min ($p>0.05$). After 10 mins, the SDC_{zen} value of the 315,000 Da alginate was significantly faster than the SDC_{zen} of the 35,000 Da alginate ($p<0.02$). After 30 mins, the SDC_{zen} value of the 315,000 Da alginate was significantly faster than the SDC_{zen} of the 220,000 Da alginate ($p<0.02$), which was significantly faster than the SDC_{zen} of the 35,000 Da alginate ($p<0.02$) (figure 7.8b).

The values of P_{nad} and SDC_{nad} of the 35,000 Da alginate increased and decreased linearly with time, respectively (figure 7.9a and 7.9 b). The SDC profiles of the 220,000 Da and 315,000 Da alginates did not develop characteristic dips and subsequently did not have P_{nad} and SDC_{nad} values.

7.3.2.3. Comparison of the SDC and concentration profiles of water inside bioadhesive bonds by prehydrated matrices

The concentration and SDC profiles of water inside bioadhesive bonds formed by prehydrated matrices are compared in figures 7.10a, 7.10b and 7.10c.

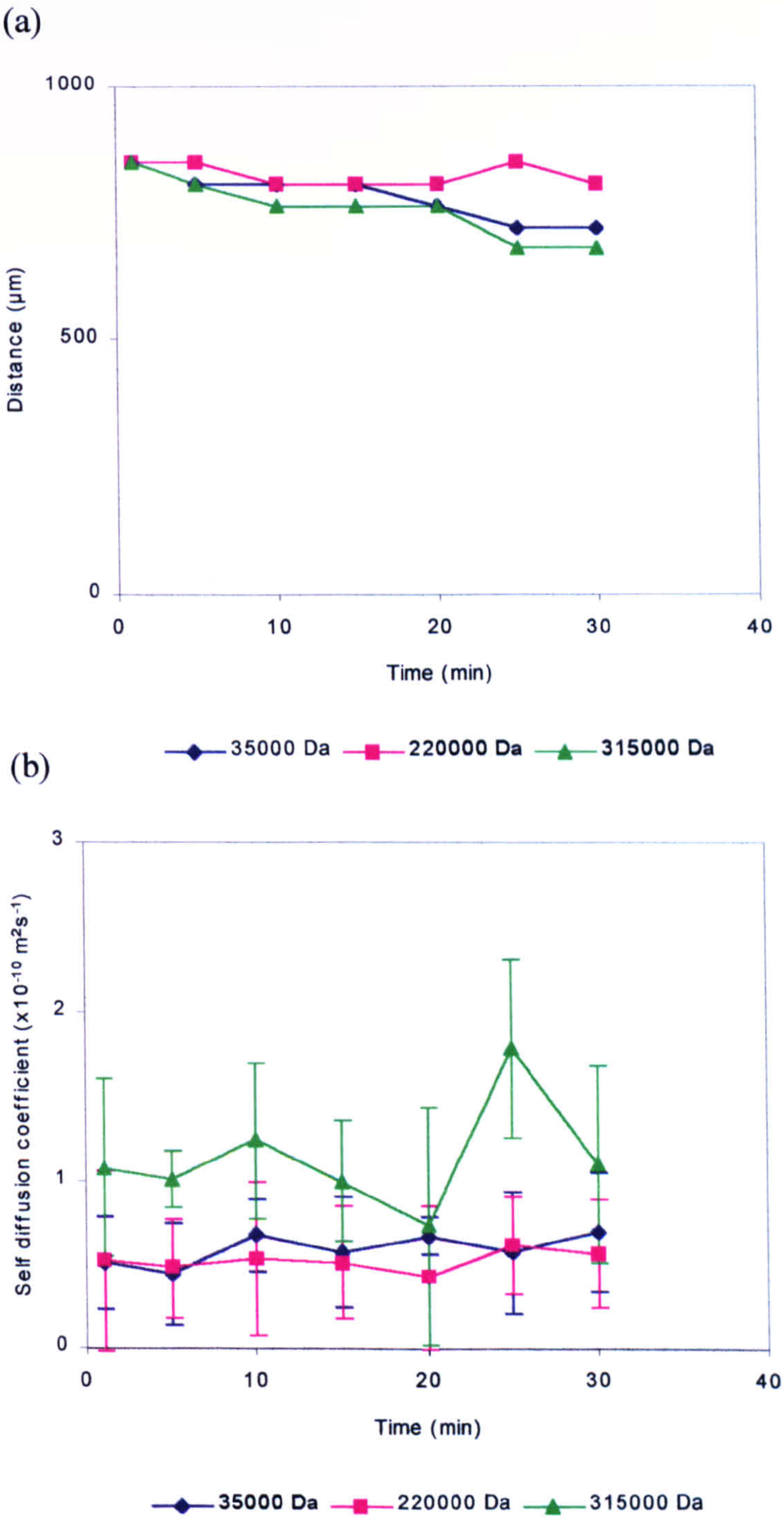

Figure 7.7 Influence of time on the diffusion front - prehydrated alginate matrices of different molecular weights

The effect of time on (a) P_{SD} and (b) SDC_{SD} taken from the SDC profiles of water inside bioadhesive bonds formed between 35,000 Da, 220,000 Da and 315,000 Da alginate matrices, prehydrated in physiological saline for 10 mins, and purified pig gastric mucus at 20±1°C (mean, n=4, ±1 SD).

(a)

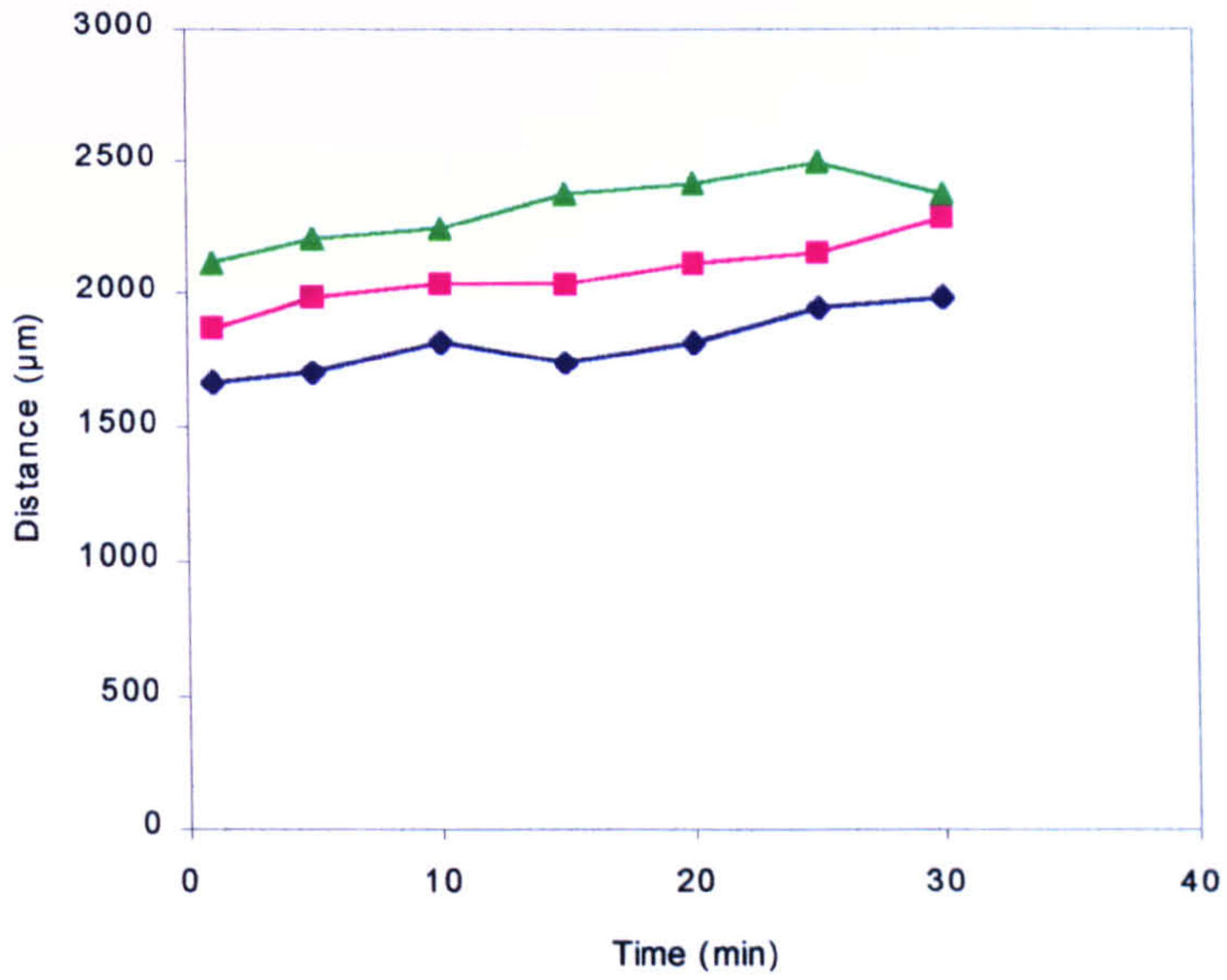

(b)

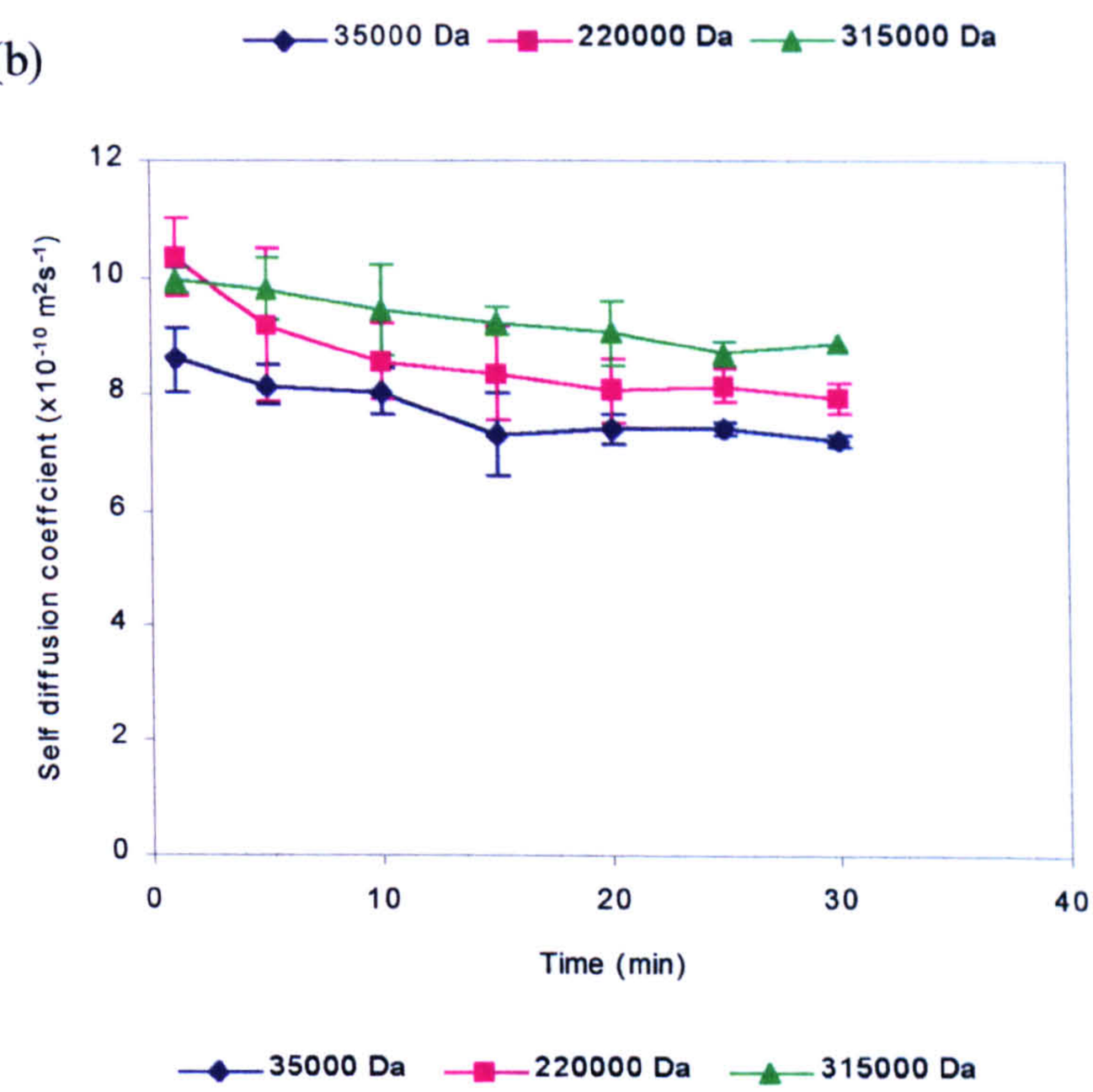

Figure 7.8 Influence of time on the zenith - prehydrated alginate matrices of different molecular weights

The effect of time on (a) P_{zen} and (b) SDC_{zen} taken from the SDC profiles of water inside bioadhesive bonds formed between 35,000 Da, 220,000 Da and 315,000 Da alginate matrices, prehydrated in physiological saline for 10 mins, and purified pig gastric mucus at 20±1°C (mean, n=4, ±1 SD).

(a)

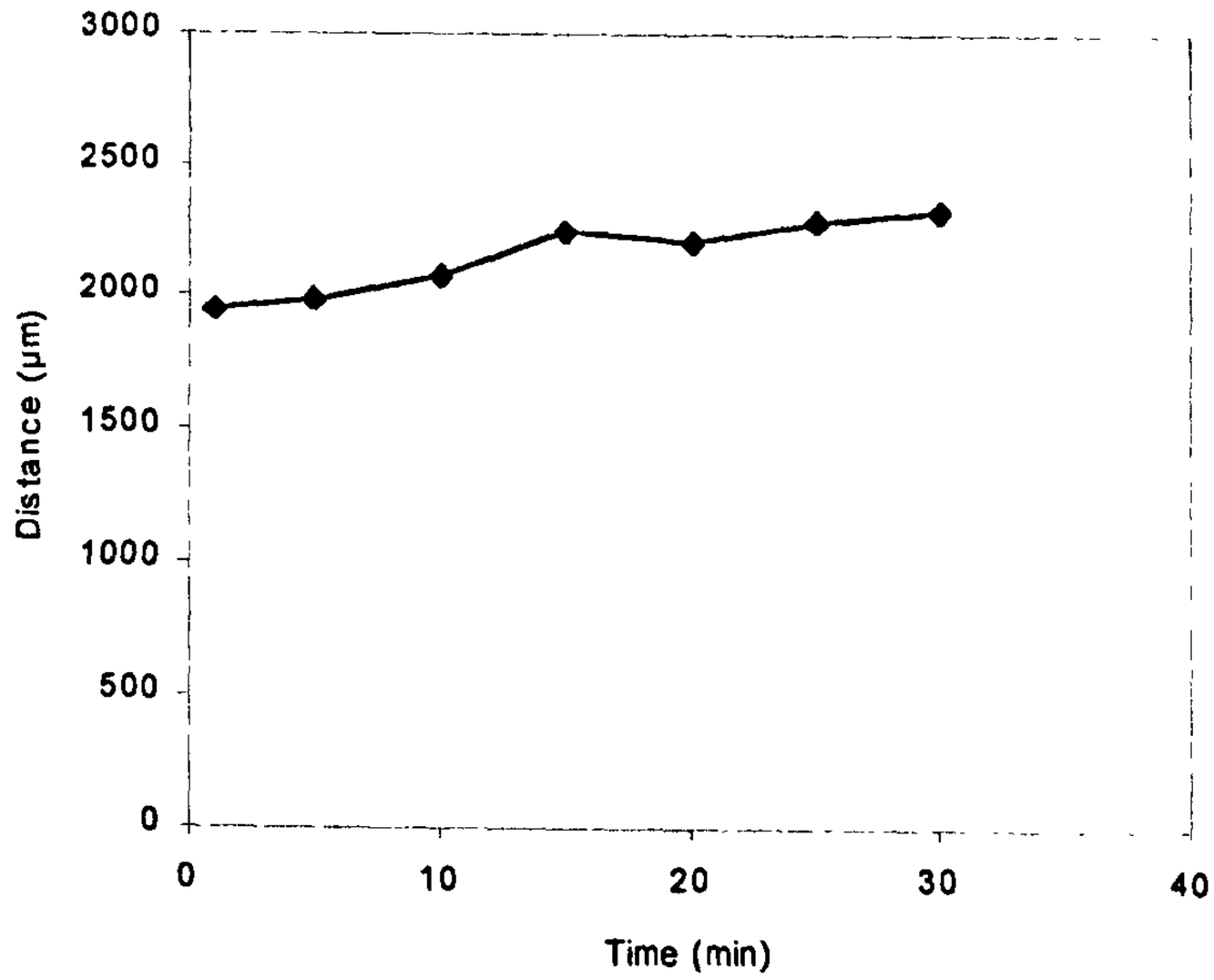

(b)

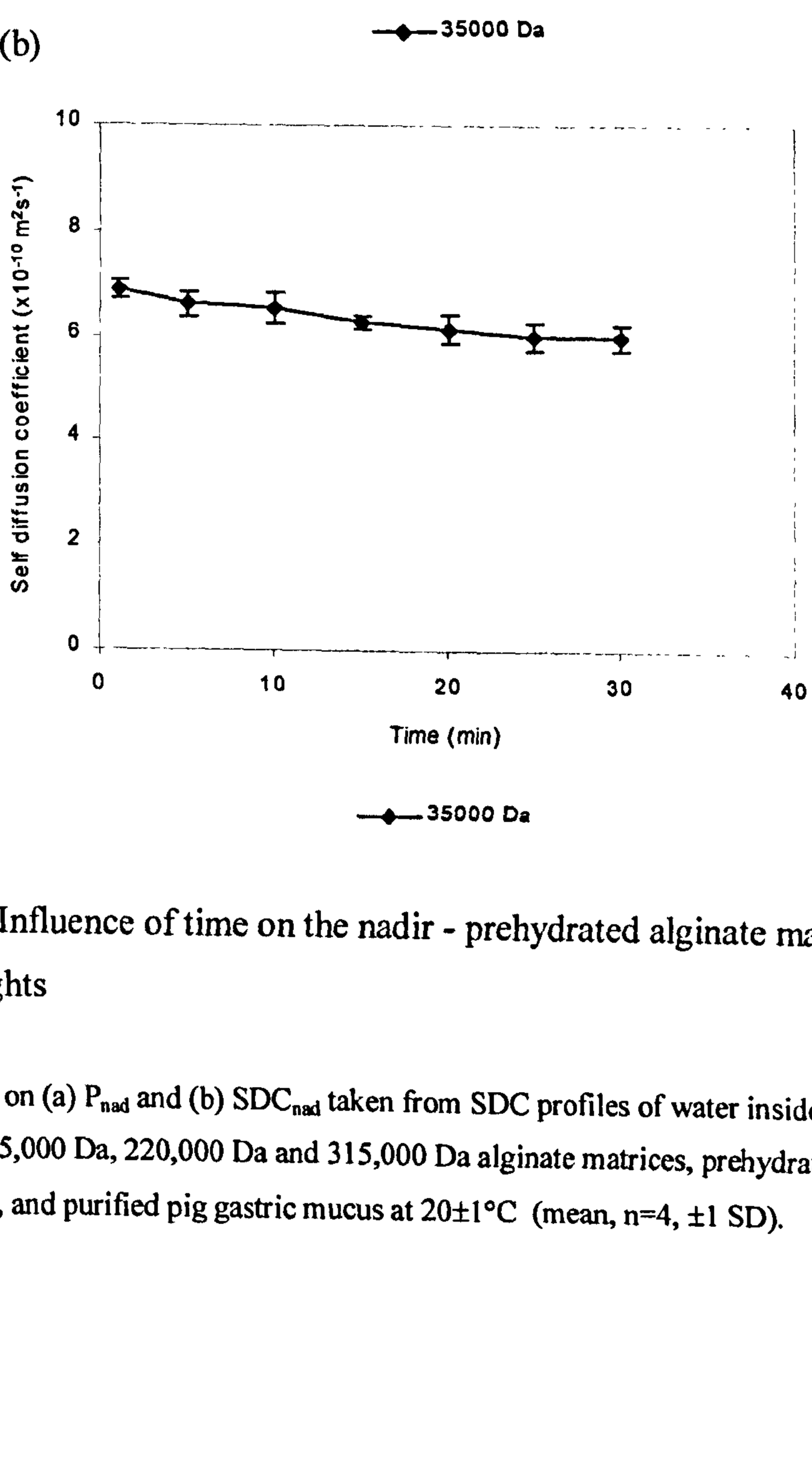

Figure 7.9 Influence of time on the nadir - prehydrated alginate matrices of different molecular weights

The effect of time on (a) P_{nad} and (b) SDC_{nad} taken from SDC profiles of water inside bioadhesive bonds formed between 35,000 Da, 220,000 Da and 315,000 Da alginate matrices, prehydrated in physiological saline for 10 mins, and purified pig gastric mucus at 20±1°C (mean, n=4, ±1 SD).

The water concentration profiles of all three alginates rapidly increased at ≈850 μm after 5 mins, forming the penetrant fronts. The gradient of these penetrant fronts decreased 20 mins, suggesting that the penetration of water into the matrices became more Fickian over time (Crank, 1975, and Valtier *et al*, 1995). The concentration profiles of 35,000 Da alginate did not develop characteristic dips, similar to those observed in the SDC profile.

Figures 7.10a, 7.10b and 7.10c also show approximate positions of the core-gel and mucus-gel interfaces on the water concentration and the water SDC profiles. The diffusion and penetrant fronts approximately corresponded to the viscous alginate gel layer.

7.3.3. Influence of molecular weight on uptake of physiological saline by alginate matrices

Figure 7.11 shows that the rate of saline uptake by the alginate matrices was rapid in the first 5 mins and then decreased over 30 mins. The shape of the graphs suggests that the alginate matrices continue to take up saline after 30 mins. There is sufficient evidence to suggest that increasing molecular weight significantly increased the volume of saline taken up by the alginate matrices over 30 min ($p<0.02$).

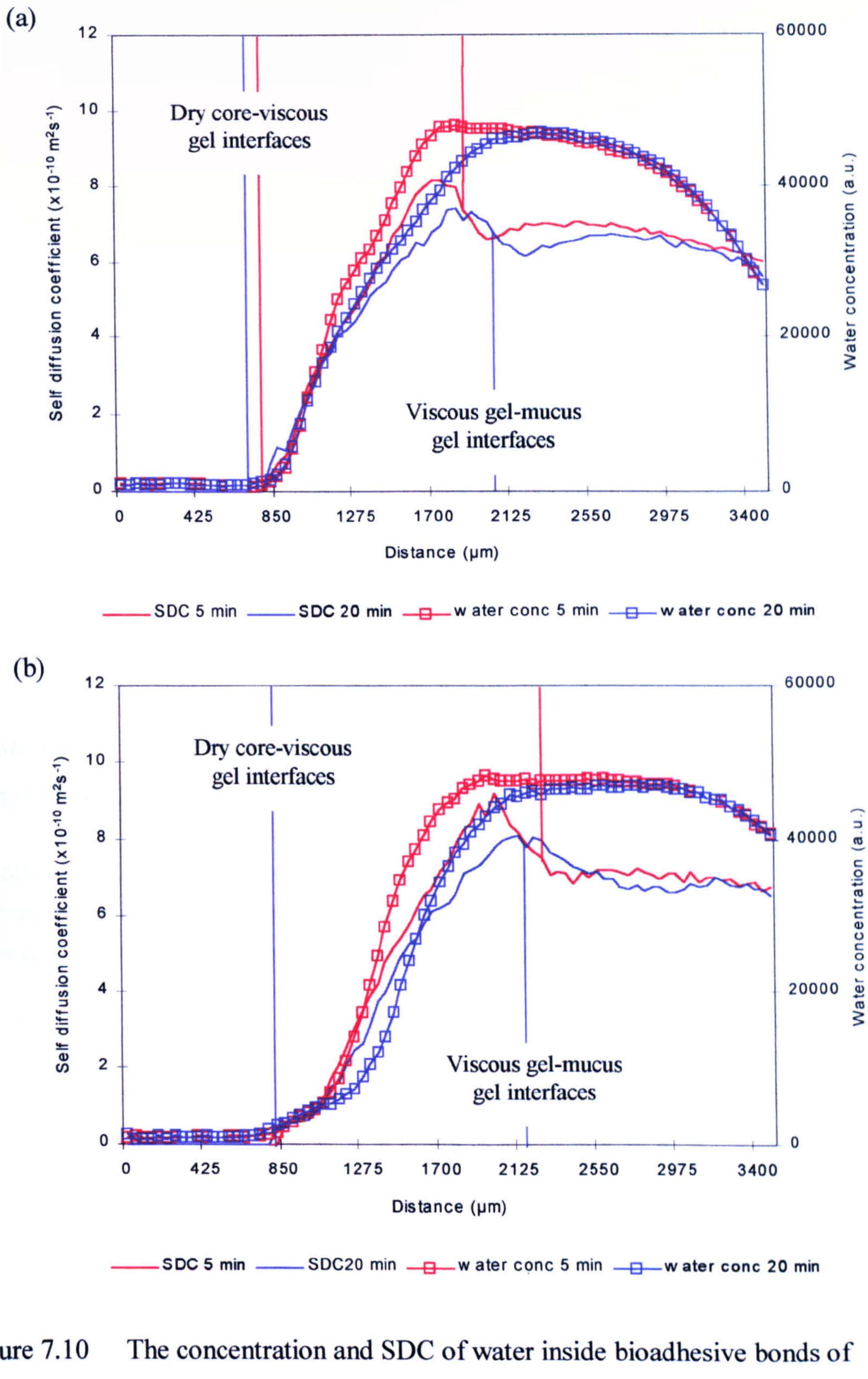

Figure 7.10 The concentration and SDC of water inside bioadhesive bonds of prehydrated alginate matrices.

The SDC and concentration of water inside bioadhesive bonds formed between (a) 35,000 Da and (b) 220,000 Da alginate matrices, prehydrated in physiological saline for 10 min, and purified pig gastric mucus in physiological saline at 20±1°C (mean, n=4). Standard deviation bars have been omitted for clarity.

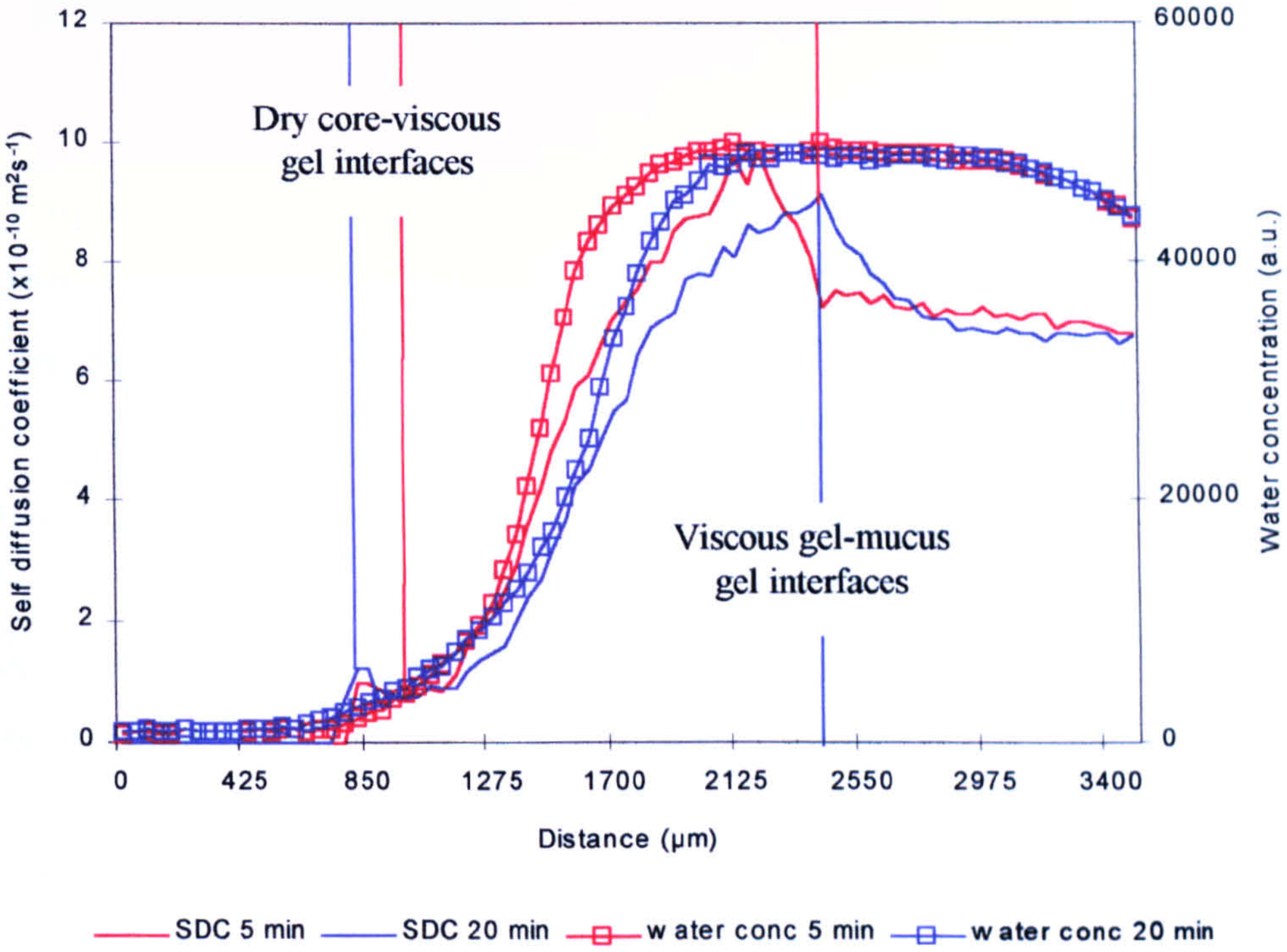

Figure 7.10c The concentration and SDC of water inside bioadhesive bonds of prehydrated alginate matrices.

The SDC and concentration of water inside bioadhesive bonds formed between 315,000 Da alginate matrices, prehydrated in physiological saline for 10 min, and purified pig gastric mucus in physiological saline at 20±1°C (mean, n=4). Standard deviation bars have been omitted for clarity.

Table 7.1 Influence of molecular weight on the saline uptake kinetics of alginate matrices.

Transport parameter	Alginate molecular weight (Da)		
	35,000	**220,000**	**315,000**
Case I (ml $min^{-0.5}$)	0.020	0.025	0.028
Case II (ml min^{-1})	0.001	0.000	0.000
Constant (ml)	0.000	0.000	0.000
r^2	0.999	0.999	1.000
Diffusional exponent	0.573	0.507	0.491
Kinetic constant	0.018	0.024	0.029
r^2	0.999	0.997	0.999

Table 7.1 shows how molecular weight influenced the Fickian and Case II transport exponents of saline uptake. Increasing molecular weight resulted in an increase in the Fickian diffusion exponent and a decrease in the Case II transport exponent. The diffusional exponents suggest that matrices of all three alginates take up saline by anomalous diffusion and that uptake became more Fickian with increasing molecular weight.

7.3.4. Influence of molecular weight on mobility of solutes inside bioadhesive bonds formed by alginate matrices

Table 7.2 The rate of transport (R_T) of FITC-dextran in the mucus adjacent to the alginate matrices

Molecular weight (Da)	n	R_T (x10^{-6} cm^2s^{-1})		±SD (x10^{-6})	
		Dry	**Prehydrated**	**Dry**	**Prehydrated**
35,000	9	6.67	6.72	6.8	4.7
220,000	7	3.39	7.99	3.5	5.1
315,000	4	3.44	6.06	2.7	1.1

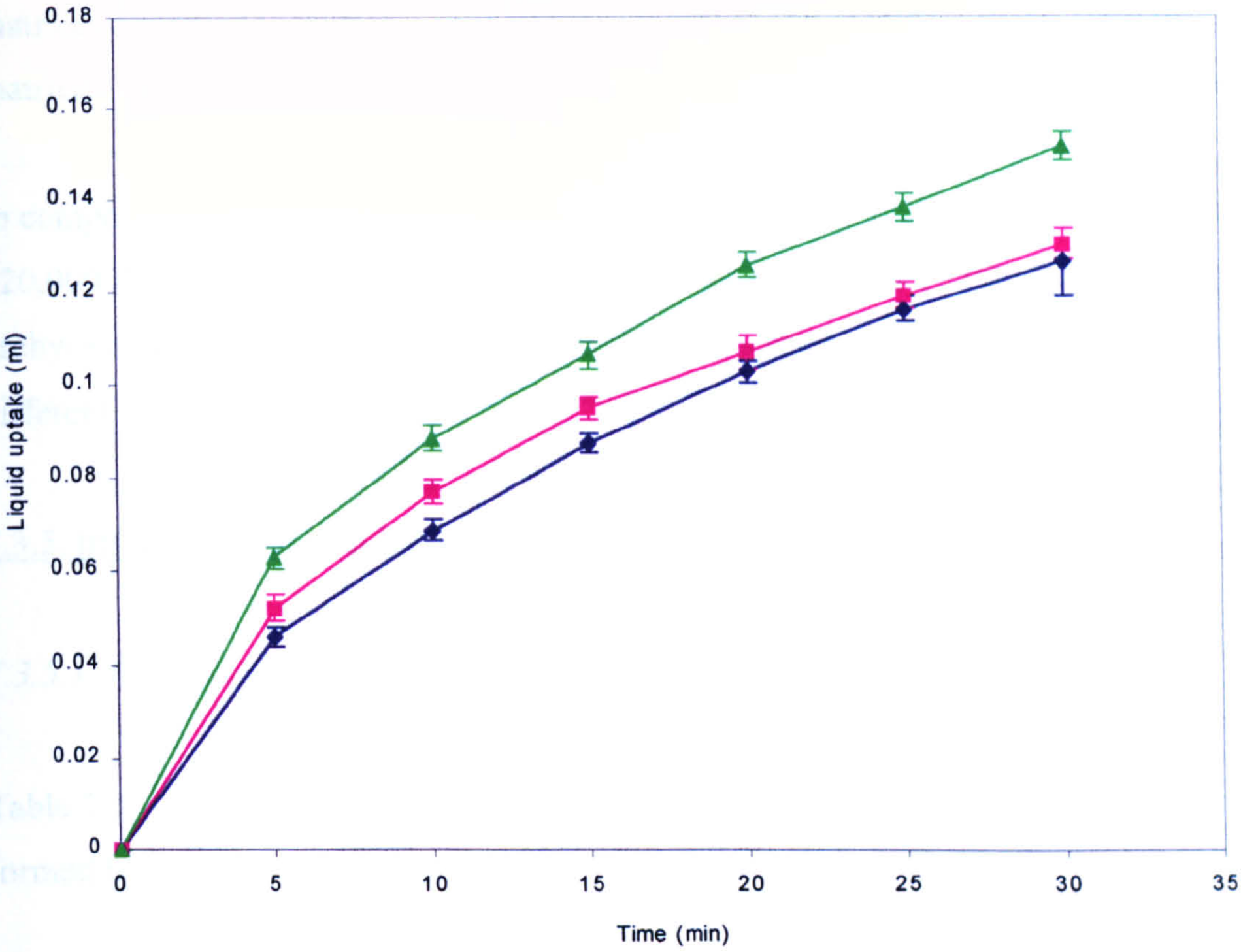

Figure 7.11 Influence of molecular weight on the volume of liquid taken up by alginate matrices.

Liquid uptake kinetics of sodium alginate matrices were determined by measuring uptake of physiological saline by 35,000 Da, 220,000 Da and 315,000 Da sodium alginate matrices at 37±1°C (mean, n=5, ±1 SD).

The R_T values in the mucus of bioadhesive bonds formed by dry 35,000 Da alginate matrices appeared to be faster than either 220,000 Da or 315,000 Da dry alginate matrices. However, the R_T values were not statistically significantly different ($p>0.05$).

In comparison, the R_T values in the mucus of bioadhesive bonds formed by prehydrated 220,000 Da alginate matrices appeared to be faster than either 35,000 Da or 315,000 Da prehydrated alginate matrices. Again, the R_T values were not statistically significantly different ($p>0.05$).

7.3.5. Influence of molecular weight on the strength of bioadhesive bonds

7.3.5.1. Bioadhesive bonds formed by dry alginate matrices

Table 7.3 Influence of molecular weight on the W_a and F_{max} of bioadhesive bonds formed by dry alginate matrices.

Molecular weight (Da)	**n**	**W_a (mJ)**	**±SD**	**F_{max} (N)**	**±SD**
35,000	14	0.0029	0.002	0.433	0.36
220,000	14	0.0071	0.004	0.693	0.47
315,000	14	0.0092	0.005	0.879	0.58

The W_a and F_{max} of bioadhesive bonds formed by dry alginate matrices appeared to increase as molecular weight increased. The W_a values of the 35,000 Da alginate matrices were statistically significantly weaker than the W_a values of 220,000 Da and 315,000 Da alginate matrices ($p<0.02$). There were no statistically significant differences between the F_{max} values ($p>0.05$).

7.3.5.2. Bioadhesive bonds formed by prehydrated alginate matrices

Table 7.4 Influence of molecular weight on W_a and F_{max} of bonds formed by prehydrated alginate matrices.

Molecular weight (Da)	**n**	**W_a (mJ)**	**±SD**	**F_{max} (N)**	**±SD**
35000	20	0.0021	0.001	0.181	0.088
220000 [(a)]	20	0.0048	0.002	0.370	0.148
220000 [(b)]	27	0.0054	0.003	0.463	0.261
315000	27	0.0043	0.002	0.434	0.237

220,000[(a)] Da sodium alginate was paired with 35,000 Da sodium alginate

220,000[(b)] Da sodium alginate was paired with 315,000 Da sodium alginate

This study was unable to use the same mucosal tissue to determine the W_a and F_{max} values of bioadhesive bonds formed by all three prehydrated alginate matrices. Section 1.7.1.1 and studies by Tobyn *et al*, 1995, and Jacques and Buri, 1992, have indicated that mucosal tissue is a major factor influencing the observed bioadhesive strength of a polymer. Therefore, the 220,000 Da alginate was used as positive control to monitor the influence of the mucosal tissue on the values of W_a and F_{max}.

The bioadhesive bonds formed by prehydrated matrices of 220,000 Da alginate had statistically significantly stronger W_a and F_{max} values than bioadhesive bonds formed by prehydrated matrices of 35,000 Da alginate ($p<0.02$). In comparison, the W_a and F_{max} values of bioadhesive bonds formed by prehydrated matrices of 315,000 Da and 220,000 Da alginates were not statistically significantly different ($p>0.05$).

The W_a and F_{max} values of bioadhesive bonds formed by both sets of 220,000 Da matrices were not statistically significantly different ($p>0.05$). This suggests that the different mucosal tissue sample were similar with respect to their influence on the bioadhesive bond. This also suggests that bioadhesive bonds formed by prehydrated matrices of 315,000 Da alginate had stronger W_a and F_{max} values than bioadhesive bonds formed by prehydrated matrices of 35,000 Da alginate.

7.3.5.3. The cohesive strength of alginate viscous gel layers

Table 7.5 The cohesive strength of self-adhered alginate viscous gel layers

Molecular weight (Da)	n	W_a (mJ)	SD	F_{max} (N)	±SD
35000	4	0.0379	0.011	3.33	0.31
220000	4	0.1802	0.060	4.28	0.10
315000	4	0.0794	0.006	4.14	0.08

Table 7.5 shows the W_a and F_{max} values of self-adhered alginate viscous gel layers were considerably stronger than W_a and F_{max} values of bioadhesive bonds formed by either dry or prehydrated alginate matrices (section 7.3.5.1 and 7.3.5.2). This suggests that the W_a and F_{max} values of bioadhesive bonds are not indicative of fractures in the viscous alginate gel layer.

7.3.5.4. The cohesive strength of native pig gastric mucus

Table 7.6 The cohesive strength of self-adhered pig gastric mucus layers

Sample	n	W_a (mJ)	±SD	F_{max} (N)	±SD
Mucus	17	0.0008	0.001	0.0686	0.027

Table 7.6 shows the W_a and F_{max} values of self-adhered pig gastric mucus layers were considerably weaker than the W_a and F_{max} values of bioadhesive bonds formed by either dry or prehydrated alginate matrices (section 7.3.5.1 and 7.3.5.2). This suggests that the W_a and F_{max} values of bioadhesive bonds are not indicative of fractures in the mucus gel layer.

7.4. Discussion

7.4.1. Influence of molecular weight on the bioadhesion of dry alginate matrices

Numerous studies have shown that molecular weight can influence the strength of a bioadhesive bond formed between polymer and mucus (Smart *et al*, 1984, Tobyn *et al*, 1996, Peppas and Buri, 1985, and Mortazavi and Smart, 1994b). Some of these studies have also indicated that there may be a certain molecular weight threshold above which the bioadhesive bond strength is maximum or that there may be an optimum molecular weight for maximum bioadhesive bond strength.

This study found that molecular weight influenced the W_a but not the F_{max} values of bioadhesive bonds formed by dry alginate matrices (table 7.3). More specifically, bioadhesive bonds formed by dry matrices of either 220,000 Da or 315,000 Da alginates had significantly stronger W_a values than bonds formed by dry matrices of 35,000 Da alginate ($p<0.02$).

It is interesting that molecular weight influences only W_a but not F_{max}. This may be due to W_a being a more sensitive indicator of bioadhesive bond strength than F_{max} (Tobyn, 1994). Alternatively, molecular weight may only influence certain properties of the bioadhesive bond formed by dry alginate matrices. Bioadhesive bonds tend to be viscoelastic in nature (Tobyn *et al*, 1995, and Smart, 1991). Their ability to flow and deform is inversely related to the rate at which stress is applied, such that the fracture becomes more tensile at faster rates of stress application, resulting in a higher breaking strength (Jacques and Buri, 1992). Therefore, the slow detachment rate (0.1 mm sec^{-1}) used in this study means that the W_a value is indicative of the bond's ability to deform and flow under an applied pressure. In comparison, the F_{max} value is a measure of the maximum tensile fracture strength of the bond (Jacques and Buri, 1992). Subsequently, this suggests that increasing molecular weight of alginate may increase the resistance of the bioadhesive bond to flow and deform under an applied stress but does not affect its tensile strength.

The long chains of the 220,000 Da and 315,000 Da alginates may form a more entangled interaction with the mucin network than the shorter chains of the 35,000 Da

alginate. The flexible, linear conformation of alginate molecules may facilitate interdiffusion and entanglement with the mucin gel network. Linear polyethylene glycol molecules (PEG) of up to 570,000 Da can interpenetrate the mucin gel network (Sahlin and Peppas, 1997). The more entangled polymer networks may take a longer time and more work to untangle and separate than less entangled networks. The relationship between molecular weight and alginate solution viscosity, which shows that viscosity is scaled to molecular weight, provides supporting evidence to suggest that alginate is capable of this type of mechanism (table 2.1). In addition, examination of the chemical structure of alginate (figure 1.2) showed that alginate molecules have a large number of –COOH groups, which may be able to H-bond to mucus glycoprotein (Tobyn *et al*, 1992). The number and density of these groups will increase with increasing molecular weight.

The increase of molecular weight from 220,000 Da to 315,000 Da did not produce a significant change in W_a values ($p>0.02$) (table 7.3). This represents a 43% increase in molecular weight compared with over 600% increase between the 35,000 Da and 220,000 Da alginates. This suggests that this relatively small increase in molecular weight (43%) was not sufficient to influence the interaction between alginate and mucin. Alternatively, alginate may have a molecular weight threshold for maximum bioadhesion, with the 220,000 Da and 315,000 Da alginates being above this threshold. However, further studies using a wider range of molecular weights need to be carried out to substantiate either theory.

The values of W_a and F_{max} are also variable, irrespective of molecular weight of alginate (table 7.3). The type of detachment force test employed in this study used a perspex O-ring to clamp the mucosal tissue, which allowed the tissue to flex and stretch during the removal of the adhered alginate matrix. The flexibility of mucosal tissue is an important factor influencing the mechanisms by which adhered polymers are removed from mucosal tissue (Jacques and Buri, 1992). In cases where the mucosal tissue is relatively inflexible, the adhesive interface is the only part of the bond which is flexible and subsequently tensile fractures tend to be predominant, resulting in a high breaking strength that may be attributed to either adhesive or cohesive failure (Sahlin and Peppas, 1996). In contrast, in cases where the polymer or mucosal tissue is flexible, the applied stresses become limited to a fine line along the adhesive interface, resulting in a peeling

mechanism being predominant and lower observed breaking strengths (Jacques and Buri, 1992). Therefore, this suggests the variability in W_a and F_{max} values may result from the alginate matrices being detached from the mucosal tissue by different types of breaking mechanisms, which are dependent on the flexibility of mucosal tissue.

The molecular weight of alginate also appeared to influence the diffusion of water inside bioadhesive bonds formed by dry matrices at first glance. Closer examination of the SDC profiles (figures 7.1a-7.1c) showed that the differences in the shape of the profiles may be due to the diffusion fronts increasing in length at different rates. The diffusion fronts correspond to the viscous alginate gel layer (figures 7.5a-7.5c), which suggests that the differences in the SDC profiles may be due to the alginate matrices having different swelling and expansion properties. This is supported by the increase in P_{zen} values over time (figure 7.3a); the P_{zen} marks the approximate position of the outer limit of the viscous alginate gel. The SDC_{DF}, SDC_{zen} and SDC_{nad} values, which are significant points in the SDC profile, were not significantly influenced by molecular weight at any time over 30 mins ($p>0.05$) (figures 7.2b, 7.3b and 7.4b). Together, this suggests that molecular weight did not actually influence the diffusion of water inside bioadhesive bonds formed by dry alginate matrices.

The SDC profiles developed characteristic dips, which increased in length and depth over time (figures 7.1a-7.1c). The size of these characteristic dips seemed to be independent of molecular weight and is supported by the SDC_{nad} values, which were not significantly influenced by molecular weight at any time over 30 mins ($p>0.05$) (figure 7.4b).

This characteristic dip in the SDC profile indicates a region where the SDC of water has decreased. The dip occurs in the section of the profile corresponding to the mucus gel layer directly adjacent to the alginate matrix (figure 7.5a-7.5b). The decrease in the SDC of water may be due to the mucin network becoming more diffusion retarding or an increase in the proportion of bound water in the mucus. The latter case may occur if the mucin becomes more able to bind water or if the proportion of free water in the mucus decreases.

Several rheological studies (e.g. Hassan and Gallo, 1990) have shown that bioadhesive polymers may increase the gel network structure of an adhesive-mucin mix by interpenetrating and entangling with mucin polymers. The result of this rheological synergism is that the tortuosity and viscosity of the gel network structure may increase, resulting in a decrease in the diffusion of water. Degim and Kellaway, 1998, have also shown that mucin reduces the diffusion of water into polyacrylic acid microspheres by forming an interfacial film at the solid liquid interface. This film may form by either adsorption onto the surface of the microsphere or by polymer interpenetration.

If interpenetration and entanglement mechanisms are considered more closely, the extent to which adhesive and mucus polymer chains interpenetrate may depend on their mutual physicochemical compatibility (Jabbari *et al*, 1993). This mutual compatibility may in turn be dependent on several physicochemical parameters. For example, polyacrylic acid and mucin are chemically compatible between pH 5-7. In this pH range, the extent to which they interpenetrate is in the order of microns. In comparison, both polymers are incompatible outside this pH range and the degree of interpenetration decreases to the order of angstroms (Jabbari *et al*, 1993). Examination of the characteristic dips show that they increase to ≈700 μm long after 30 mins, which suggests that polymer interpenetration may not a predominant factor contributing to the decrease in water SDC.

Other studies have shown that some adhesive polymers may dehydrate the adjacent mucus layer (Mortazavi and Smart, 1993, and Smart *et al*, 1991). Mucus is a viscoelastic gel, which is composed of a macromolecular cross-linked mucin network with water filled pores that functions as a barrier to diffusion (Bhat *et al*, 1995). The sialic acid and sulphate residues on the hydrated mucin molecule are negatively charged at neutral pH. The repulsion of these groups causes the mucin molecule to expand into a stretched conformation, facilitating the interpenetration and entanglement of the mucin molecules and giving rise to a meshed structure that hold water molecules inside the pores.

The diffusion retarding properties of mucus may be due to several mechanisms. The mucin network can immobilise water molecules to form the equivalent of an unstirred

water layer (Smithson *et al*, 1981). The negative charged residues on the mucin molecule may also confer some sort of electrical repulsion, which retards the diffusion of solutes, in particular, anionic solutes (Livingston *et al*, 1995). The mucin polymer network itself provides a diffusional barrier, firstly by making the diffusion pathway more tortuous and secondly by holding water molecules in a structured form, making them unavailable for free diffusion of ions through it (Williams and Turnburg, 1980).

The dehydration of mucus may remove water available for free diffusion of solutes and may also increase the concentration of mucin, making the network more tortuous and decreasing the water available for diffusion (Smith *et al*, 1986). This is observed in the diffusion of a range of small molecular weight solutes, for example butyrate (Smith *et al*, 1986), bicarbonate (Livingston *et al*, 1995), hydrogen ions (Williams and Turnberg, 1980, and Turner *et al*, 1985), tetracycline (Kearney and Marriott, 1987). Thus, these mechanisms may increase the diffusion retarding properties of the mucus gel, which may result in the observed decrease in the SDC of water. Furthermore, the removal of free water from the mucus during dehydration may increase the relative proportion of bound water and thus resulting in an observed decrease in SDC of water and the development of a characteristic dip.

Alternatively, the characteristic dip in the SDC profile may be due to an increase in the binding of water by mucin. Li *et al*, 1996, used Fourier transform pulsed field gradient spin echo ^{1}H-NMR to show that the fraction of bound water increases as the concentration of mucin increased. Smith *et al*, 1986, found that the diffusion of butyrate decreased as the concentration of mucin increased, an effect which was attributed to an increased binding of water by mucus making it unavailable for free diffusion of solutes. This also suggests that the characteristic dip in the SDC profiles was attributed to dehydration.

The mucus directly adjacent to the dry alginate matrices also increased in fluorescence over time. The fluorescence of mucus was scaled to the concentration of mucin (figure 5.6), indicating that the concentration of mucin increased over time and suggesting that mucus in this region became dehydrated. Furthermore, the region of mucus that increases in fluorescence appears to correspond to the section of the profiles containing the characteristic dip (figure 7.5a-7.5c).

Further examination of the SDC profiles (figures 7.1a-7.1c) revealed that diffusion fronts, which correspond to the viscous alginate gel layer of the matrix (figure 7.5a-7.5b), decreased over time, suggesting that diffusion in this region became more Fickian (Valtier *et al*, 1995, and Crank, 1975). Fickian diffusion is predominant in rubbery, viscous polymers (Crank, 1975), indicating that the dry alginate matrices hydrate and form viscous alginate gel layers. In the sample geometry used in this study, mucus is the only available source of water, thus, it is sensible to assume that the dry alginate matrices form viscous gel layers by dehydrating the adjacent mucus layer.

However, profiles of water concentration inside bioadhesive joints formed by dry alginate matrices (figures 7.5a-7.5c) provide evidence opposing the dehydration of mucus in the bioadhesion of dry alginate matrices. The water concentration profiles did not develop corresponding characteristic dips in their profiles.

This suggests that the characteristic dip in the SDC profiles may be due to increased binding of water by the mucin, which may have been caused by a conformational change in the mucin polymer due to the interaction with dry alginate. This induced change may then act in a 'domino effect' on the rest of the mucin, giving rise to the ≈700 μm long dip after 30 mins. Further work studying the T_2 relaxation times of water bound to mucin during bioadhesion needs to be carried out. Alternatively, this may be due to the SDC profiles being more sensitive to changes in patterns of hydration than the water concentration profiles (Bowtell, 1998).

Irrespective of the origin of the characteristic dip, this region of decreased water SDC has serious implications for the delivery of drugs from bioadhesive dosage forms. This region may decrease the local absorption of drugs across the mucosa, thus possibly negating a potential use of bioadhesive drug delivery devices. For example, the absorption of tetracycline by everted rat intestinal sacs was found to decrease as the concentration of mucin increased (Kearney and Marriott, 1987).

The R_T values of FITC-dextrans in mucus may be used to indicate the retarding of solute diffusion by the mucin network. The R_T values in mucus near the alginate gel-

mucus interface appeared to be unaffected by molecular weight after 5 mins ($p>0.05$) (table 7.2), which reflected the trend observed in the SDC profiles. However, native mucus gel severely retards diffusion of molecules greater than ≈14 kDa. It effectively acts as a molecular sieve (Desai and Vadgama, 1991, and Williams and Turnberg, 1980), although diffusion of large linear, flexible polymers may still occur by reptation. Although the mucin structure of Sigma mucin is dissimilar to the structure of native mucus, similar phenomena may occur, which may affect the R_T values and restrict the practical application of this test to bioadhesion.

Liquid uptake studies showed that the volume of saline taken up by the alginate matrices over 30 mins seemed to be related to molecular weight (figure 7.11). Electron micrographs (figures 2.3 and 2.4) show that the dry alginate matrices are porous (figure 2.1), suggesting that the rapid uptake in the first five minutes may be due to capillary suction. The hydration rate of hydrophilic polymers tends to be scaled to molecular weight (Melia, 1991, and Alderman, 1984). Consequently, matrices of low molecular weight alginate may form viscous alginate gel layers more quickly than matrices of higher molecular weight alginate. This viscous gel layer may retard diffusion of saline and slow down the uptake of saline at later times. The higher molecular weight alginates have longer chains and therefore a greater capacity to hydrate. This effect is seen in the uptake in methylcelluloses of different viscosities (Wan and Prasad, 1989). There seems to be no correlation between the saline uptake of the alginate matrices and the diffusion of water inside the bioadhesive bond. This may be that water in mucus is less freely available than water in physiological saline and consequently, the hydration and liquid uptake kinetics of the matrices are different.

Analysis of uptake kinetics (table 7.1) revealed that the ingress of saline was nearer to Case II transport in 35,000 Da alginate matrices than in higher molecular weight alginate matrices. Transport mechanisms of liquid in polymers are dependent on the rubber-glass structure of the polymer, such that Fickian diffusion is predominant in rubbery polymers and Case II transport is predominant in glassy polymers (Crank, 1973). Therefore, this suggests that the rubbery-glassy state of the alginate matrices may be important factor in their bioadhesion, with rubbery alginates having higher W_a values.

However, the liquid uptake kinetics of alginate matrices may provide a misleading insight into alginate bioadhesion. Firstly, as mentioned before, water molecules in saline are more freely available than water molecules in mucus. Secondly, the mathematical models used in this study to analyse liquid uptake kinetics assume liquid uptake to occur as a consequence of either Fickian diffusion or Case II transport. They do not account for other types of mechanisms. Thirdly, there's a range of dynamic processes, such as swelling, core relaxation, porosity, occurring at once in the alginate matrices, which are unknown and cannot be accounted for. Subsequently, the transport parameters reported in this study must be used with caution in respect to elucidating the underlying mechanisms of alginate bioadhesion.

7.4.2. Influence of molecular weight on the bioadhesion of prehydrated alginate matrices

The detachment force tests showed that molecular weight influenced both F_{max} and W_a values of bioadhesive bonds formed by prehydrated alginate matrices (table 7.4). More specifically, increasing the molecular weight of alginate from 35,000 Da to 220,000 Da produced a significant increased in W_a and F_{max} ($p<0.02$), but further increasing molecular weight from 222,000 Da to 315,000 Da did not produce a significant effect ($p>0.02$).

The relationship between molecular weight and both F_{max} and W_a values suggest that molecular weight affects both the tensile and deforming properties of bioadhesive bonds formed by prehydrated alginate matrices. This is dissimilar to the bioadhesive bonds formed by dry alginate matrices and suggests that the underlying bioadhesive mechanisms of dry and prehydrated alginate matrices may be different. The influence of molecular weight on F_{max} and W_a again suggests that prehydrated alginate matrices favoured bioadhesive mechanisms, which are dependent on molecular weight and chain length, for example hydrogen bonding between mucin and the -COOH groups of alginate and polymer interpenetration. The variability of W_a and F_{max} of bioadhesive bonds formed by prehydrated alginate matrices was again due to differences in the flexibility of mucosal tissue.

Molecular weight also influenced diffusion of water inside bioadhesive bonds of prehydrated alginate matrices. More specifically, molecular weight influenced the SDC of water in the section of the profile corresponding to the mucus gel directly adjacent to the viscous alginate gel of the matrix. The SDC profile of the 35,000 Da alginate developed a characteristic dip in this region after just 1 min. This dip increased in length and depth over time, such that it was ≈350 μm long after 30 mins. In comparison, the SDC profiles of 220,000 Da and 315,000 Da alginates did not develop characteristic dips over 30 mins.

The characteristic dip was similar to that observed in SDC profiles of dry alginate matrices (section 7.4.1), but shorter and less deep. This suggests that the prehydrated matrices of the 35,000 Da alginate dehydrated the adjacent mucus gel layer but prehydrated matrices of the 220,000 Da and 315,000 Da molecular weight alginates did not.

This may be explained by considering the properties of the viscous alginate gel layer of a prehydrated matrix. Cryogenic sections of alginate matrices after 10 mins of hydration (figure 2.5) showed two distinct regions within the viscous gel layer. The outer region was extensively and evenly hydrated and the inner region was poorly and less evenly hydrated. The hydration of the inner gel layer becomes progressively more uneven with increasing proximity to the dry alginate core.

The hydrated alginate polymers in the outer gel region will form a physically entangled mesh structure. The diffusion retarding property of hydrophilic polymers, such as alginate, is scaled to molecular weight and viscosity (Alderman, 1984). The higher molecular weight alginate chains may cause more entanglements per polymer chain and thus a mesh with smaller pores than lower molecular weight alginate chains. It is this layer that initially retards the ingress of water from the adjacent mucus gel into the hydrating alginate matrix during the formation of a bioadhesive bond.

The hydration rate of polymer in the inner gel region and dry core of hydrophilic matrices is also related to the molecular weight, with higher molecular weight polymers hydrating more slowly than lower molecular weight polymers (Alderman, 1984). This

may also influence the movement of water from the mucus across the viscous alginate gel layer and into the hydrating dry core and inner gel region. The unhydrated regions of alginate may act as barriers to the diffusion of water, in a similar fashion to glassy polymers. Together, the hydration rate of the alginate in the inner gel layer and the diffusion retarding property of the viscous alginate outer gel layer effectively reduce the 'dehydrative drive' of the prehydrated alginate matrices as molecular weight increases.

The effect of the viscous alginate gel layer on the dehydration of the adjacent mucus layer in the bioadhesive bond can be clearly seen by comparing the SDC profiles of dry and hydrated 35,000 Da alginate (figures 7.1a and 7.6a, respectively). The characteristic dip in the profile of the prehydrated alginate was shorter and less deep than the characteristic dip in the profile of the dry alginate at any one time. This suggests that dry matrices dehydrate the adjacent mucus gel layer more than prehydrated matrices, presumably because they lack a diffusion retarding viscous gel layer.

Again, molecular weight did not influence the R_T values of FITC-dextran in the mucus near to the viscous gel-mucus interface ($p>0.05$), which may be surprising at first given the influence of molecular weight on the diffusion of water in this region. However, the molecular sieve effect of the mucin network may account for the lack of a discernible trend in the diffusion of 580 kDa FITC-dextran in mucus.

The influence of molecular weight on both the bioadhesive bond strength and diffusion of water inside bioadhesive bonds suggests, although mucus dehydration can still occur depending on the molecular weight of alginate, this mechanisms may not be a major factor involved in the formation of bioadhesive bonds by prehydrated matrices.

7.5. Conclusion

The range of alginates used in this study showed that molecular weight influenced the work of adhesion measurement of bioadhesive bonds formed between dry matrices and pig gastric mucus. The same range also showed that molecular weight also influenced the maximum detachment force and the work of adhesion measurements of bioadhesive bonds formed between hydrated matrices and pig gastric mucus.

The formation of bioadhesive bonds by dry alginate matrices seemed to involve several mechanisms. There is evidence to suggest that dry alginate matrices may dehydrate the mucus gel layer and that this mechanism is independent of molecular weight. There is also evidence to suggest that molecular weight dependent mechanisms, such as polymer interpenetration and hydrogen bonding, may be involved in the formation of bioadhesive bonds.

The formation of bioadhesive bonds by prehydrated alginate matrices seemed to favour mechanisms that are dependent on molecular weight, such as polymer interpenetration and hydrogen bonding. The dehydration of the adjacent mucus by prehydrated alginate matrices may occur depending on the molecular weight of the alginate, but this may not be an influential mechanism in the bioadhesion of prehydrated alginate matrices.

Chapter 8

Influence of M:G ratio on bioadhesion of dry and hydrated sodium alginate matrices

8.1 Introduction

The proportion of guluronate and mannuronate in an alginate molecule can considerably influence its physicochemical properties (section 1.1.4) (Smidsrod and Draget, 1996) and subsequently may influence its bioadhesive potential. Therefore, the aim of this chapter was to study how the M:G ratio effects the bioadhesive bond strength and the mobility of water and solutes inside bioadhesive bonds formed by alginate matrices. In a similar fashion to chapter 7, this study was carried out on bioadhesive bonds formed by dry and hydrated alginate matrices.

8.2. Methods

The methods described in chapter 6 were used to test the alginate matrices and the physicochemical properties of sodium alginates and pig gastric mucus are described in chapter 3. The statistical analysis of data was carried out according to the method described in section 6.7.

8.3. Results

This chapter uses the term 'high G alginate' in reference to the alginate containing 69.4% guluronate and the term 'low G alginate' in reference to the alginate containing 44.4% guluronate. The two alginates used in this study do not represent extremes of M:G ratios, but only approximate 30:70 and 60:40 ratios, respectively.

8.3.1. Influence of the M:G ratio on water inside bioadhesive bonds formed by dry matrices

8.3.1.1. Water diffusion inside bioadhesive bonds formed by dry alginate matrices

The SDC profiles of water inside bioadhesive bonds formed by dry alginate matrices of differing M:G ratios are shown in figure 8.1 (figure 8.1a is a repeat of figure 7.1b but was included in this section for easy comparison).

(a)

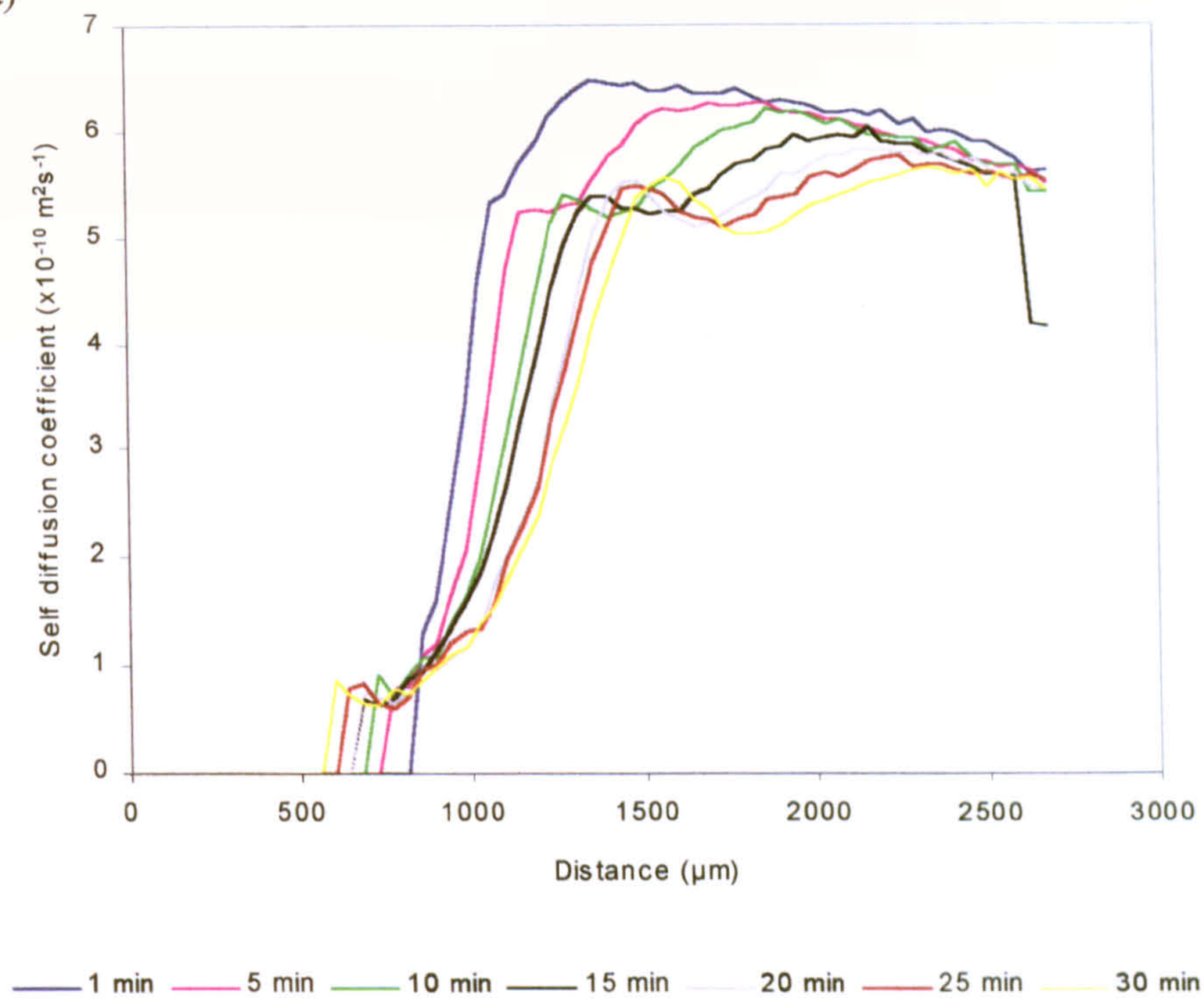

(b)

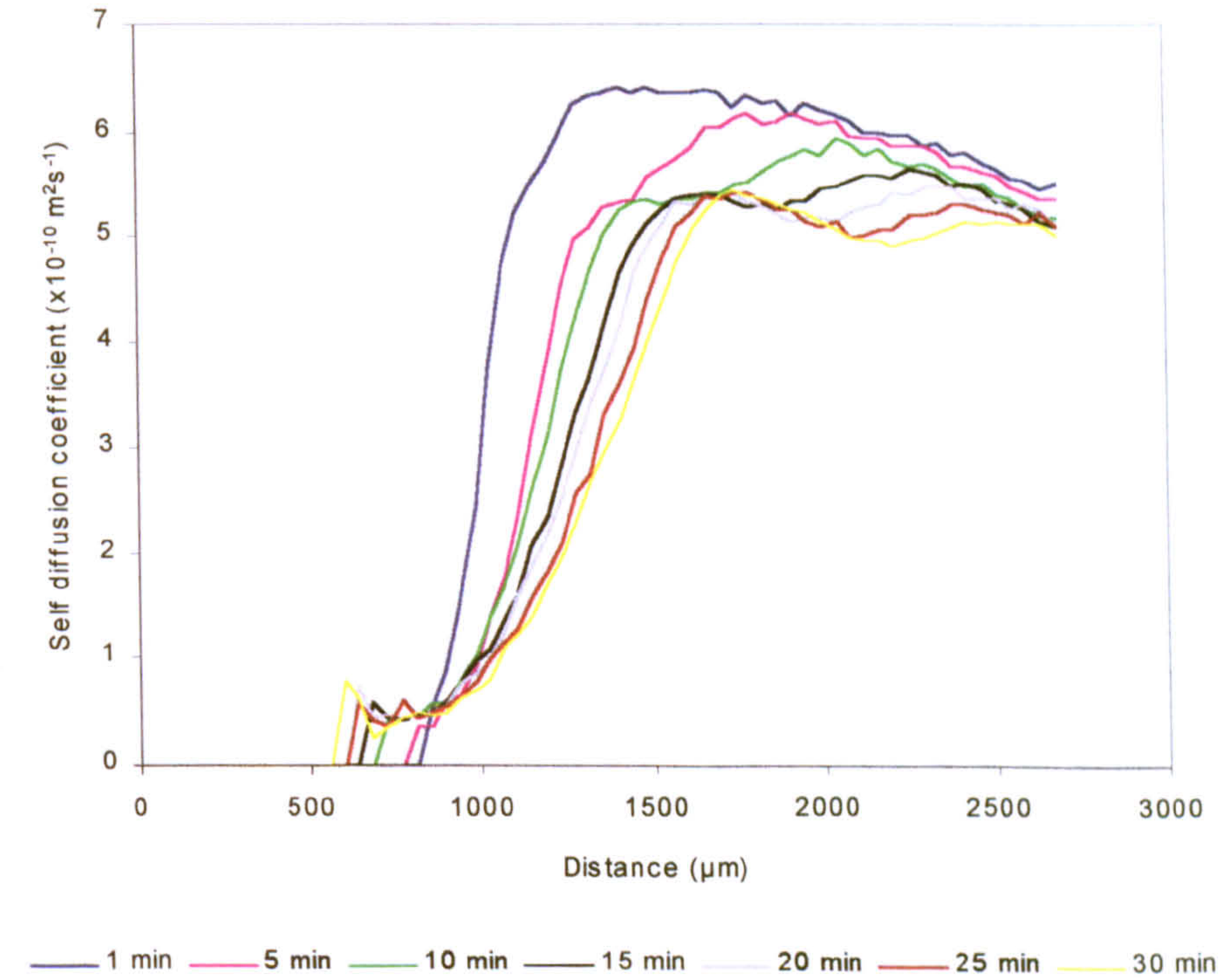

Figure 8.1 Influence of time on the SDC of water inside bioadhesive bonds formed by dry alginate matrices of different M:G ratio

Bioadhesive bonds were formed between dry (a) 69.4% G and (b) 44.4% G alginate matrices and purified pig gastric mucus at 20±1°C (mean, n=4). Standard deviation bars have been omitted for clarity.

The shape and development of the SDC profiles are similar to that of the SDC profiles shown in figures 7.1a-7.1c. The diffusion front of the low G alginate appeared to have a lower gradient than the diffusion front of the high G alginate over 30 mins. The characteristic dip in the low G alginate profile appear to be approximately symmetrical about the nadir point, compared with the characteristic dip in the high G alginate profile, which seemed to skewed to one side.

8.3.1.2. The influence of the M:G ratio on the SDC profiles of bioadhesive bonds formed by dry alginate matrices

Figures 8.2, 8.3 and 8.4 show how the M:G ratio influenced the diffusion front, zenith and nadir points, respectively. These points were measured from the SDC profiles of bioadhesive bonds formed by dry alginate matrices.

The P_{DF} values of both alginates decreased non-linearly at a similar rate over time, suggesting that the M:G ratio did not influence the ingress of water into the dry matrix core (figure 8.2a). The SDC_{DF} of the high G alginate gradually decreased with time whilst the SDC_{DF} of the low G alginate increased with time (figure 8.2b), although the SDC_{DF} values of both low and high G alginates were not statistically significantly different over 30 min ($p>0.05$).

The P_{zen} value of both alginates increased at the same rate, with the P_{zen} values of the low G alginate being higher than the P_{zen} values of the high G alginate (figure 8.3a). This suggests that the low G alginate matrices swelled more than the high G alginate matrices. The high G alginate SDC profile developed a zenith point after 5 mins compared with 10 mins in the low G alginate profile. The SDC_{zen} values of both low and high G alginates slightly increased with time (figure 8.3b), but were not statistically significantly different between 10-30 mins ($p>0.05$).

The P_{nad} value of the low G alginate increased at a faster rate than the P_{nad} of the high G alginate (figure 8.4a). The high G alginate profile developed a nadir point after 5 mins compared with 10 mins in the low G alginate profile. The SDC_{nad} of both low and high G alginates gradually increased over time (figure 8.4b), but were not statistically significantly different between 10-30 mins ($p>0.05$).

(a)

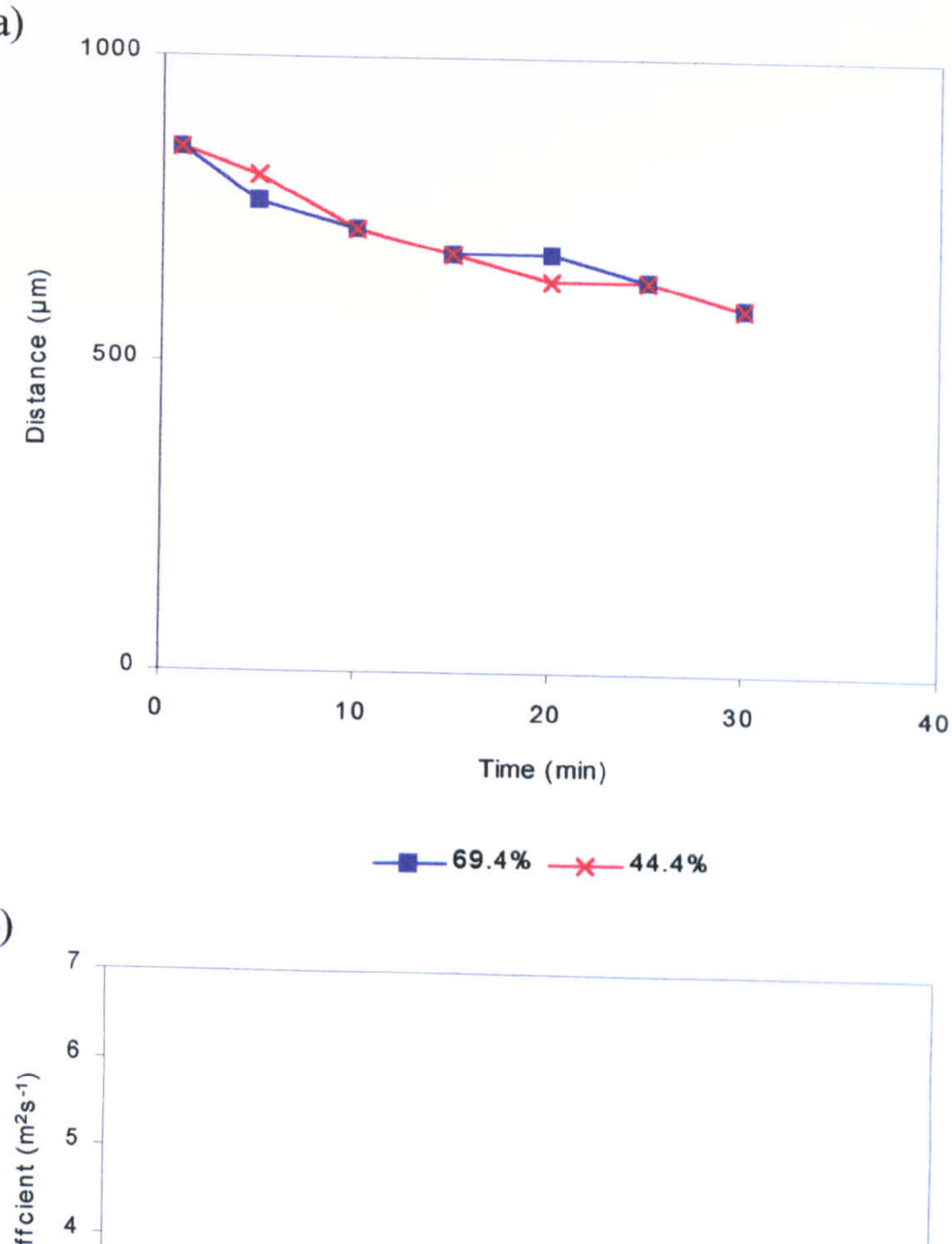

(b)

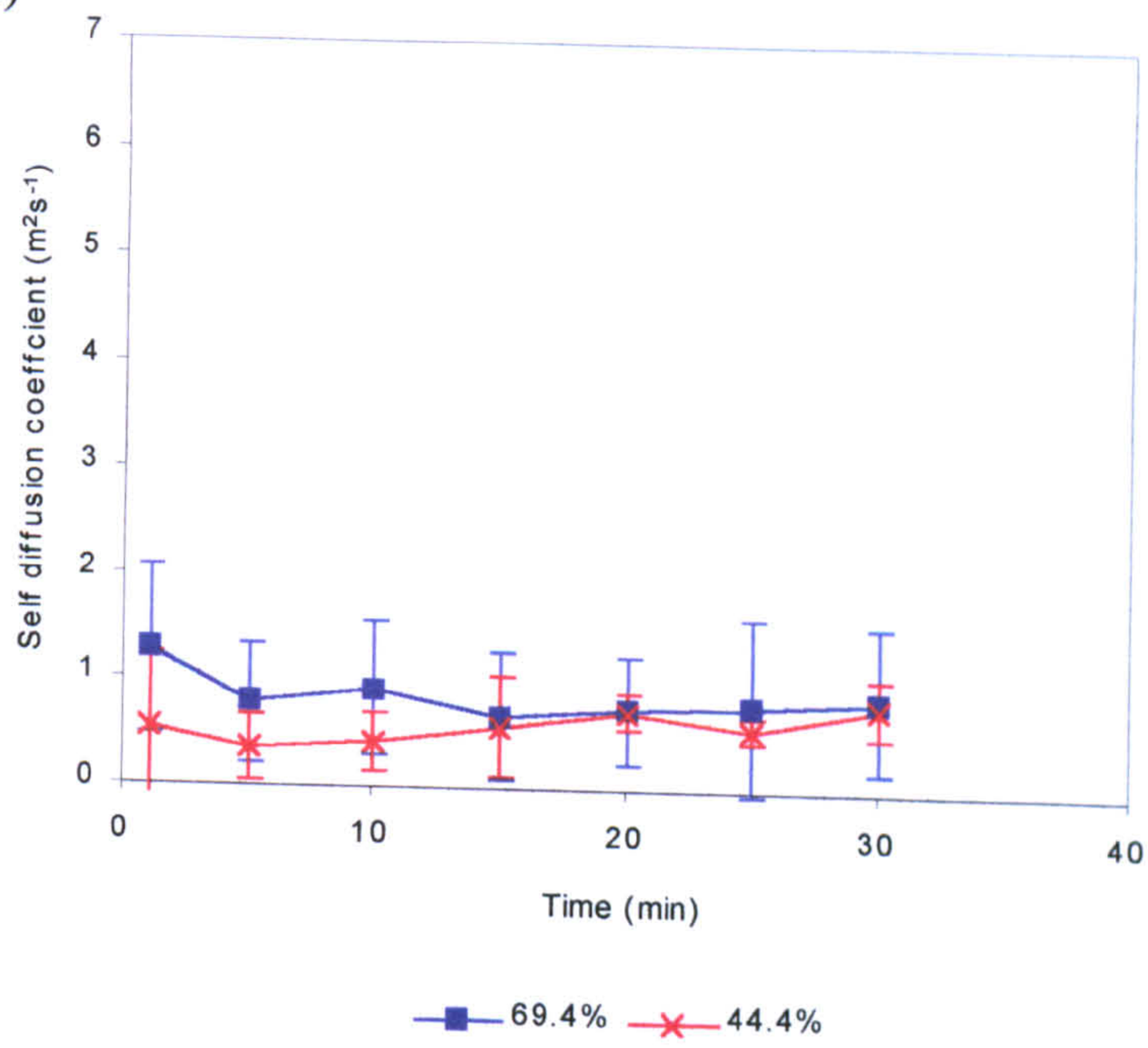

Figure 8.2 Influence of time on the diffusion front - dry alginate matrices of different M:G ratio

The effect of time on (a) P_{SD} and (b) SDC_{SD} taken from the SDC profiles of water inside bioadhesive bonds formed between dry 69.4% G and 44.4% G alginate matrices and purified pig gastric mucus at 20±1°C (mean, n=4, ±1 SD).

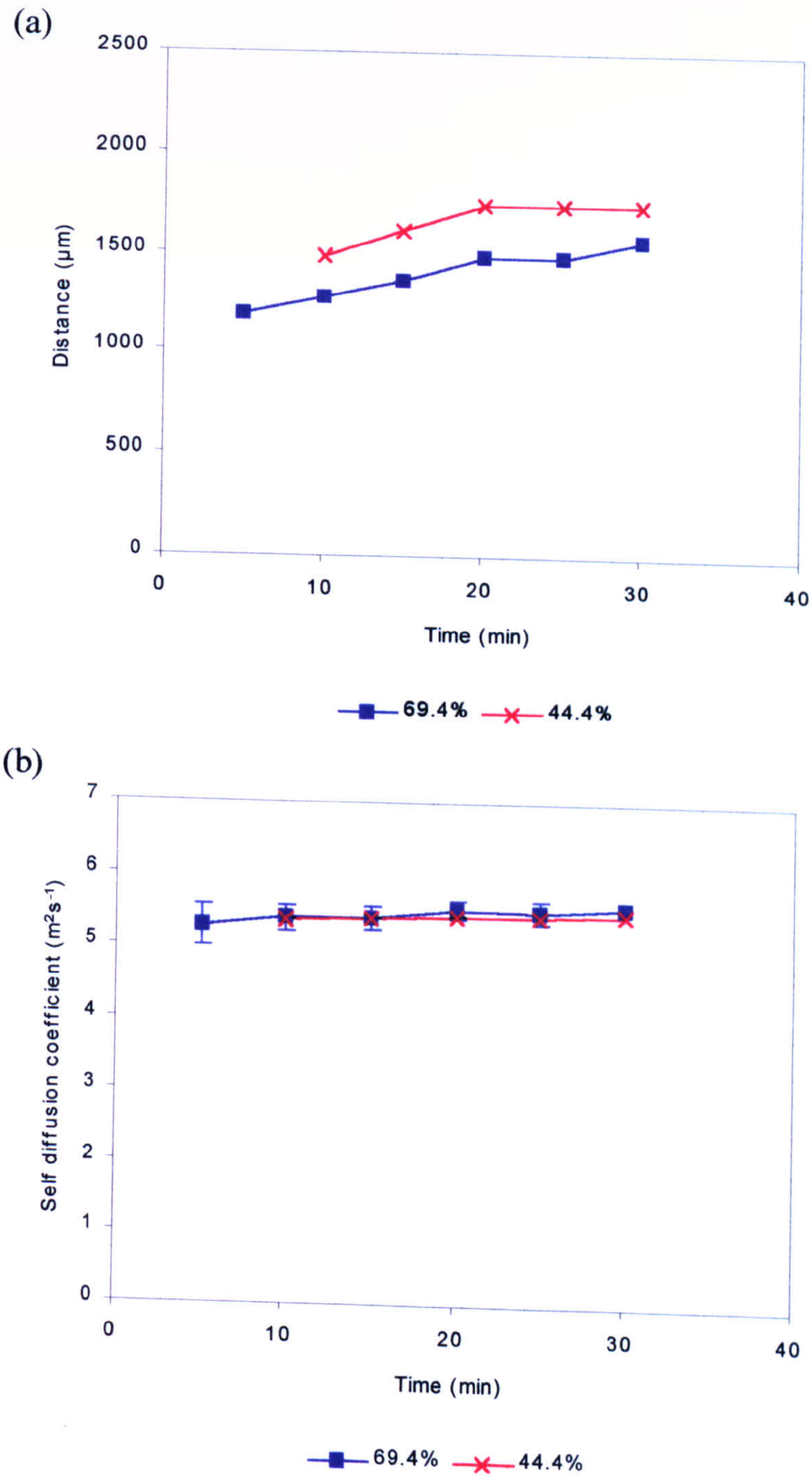

Figure 8.3 Influence of time on the zenith - dry alginate matrices of different M:G ratio

The effect of time on (a) P_{zen} and (b) SDC_{zen} taken from the SDC profiles of water inside bioadhesive bonds formed between dry 69.4% G and 44.4% G alginate matrices and purified pig gastric mucus at 20±1°C (mean, n=4, ±1 SD).

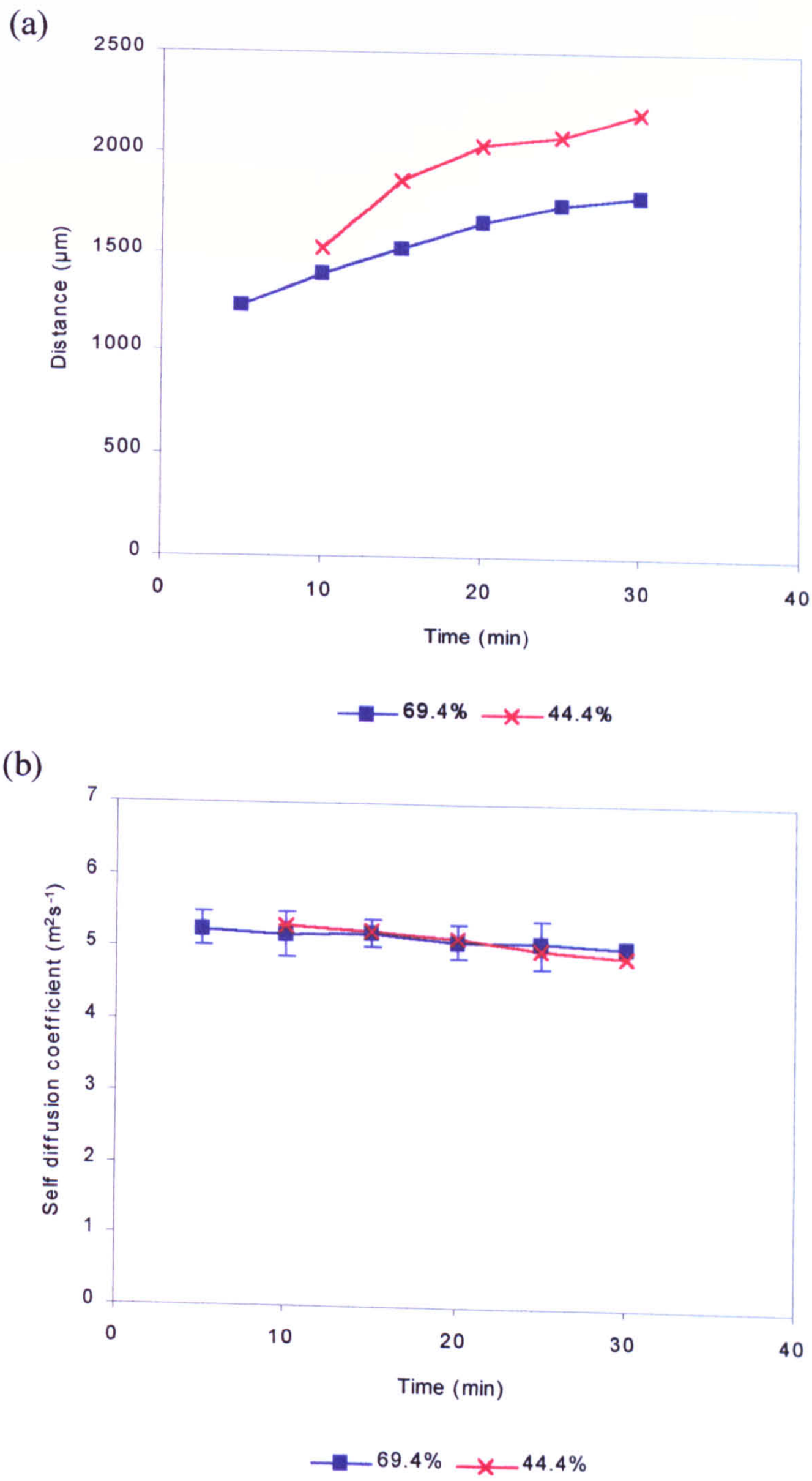

Figure 8.4 Influence of time on the nadir - dry alginate matrices of different M:G ratio

The effect of time on (a) P_{nad} and (b) SDC_{nad} taken from SDC profiles of water inside bioadhesive bonds formed between dry 69.4% G and 44.4% G alginate matrices and purified pig gastric mucus at 20±1°C (mean, n=4, ±1 SD).

8.3.1.3. Comparison of SDC and concentration profiles of water inside bioadhesive bonds formed by dry matrices

The concentration and SDC profiles of water inside bioadhesive joints formed by dry alginate matrices are shown in figure 8.5.

The water concentration profiles of bioadhesive bonds formed by dry alginate matrices were similar to those shown in figures 7.5a-7.5c. The penetrant fronts of both low and high G alginates sharply increased after 5 mins. The gradients of the penetrant fronts decreased after 20 mins, suggesting that water penetration into the matrix became more Fickian over time (Crank, 1975, and Valtier *et al*, 1995). The water concentration profiles did not develop characteristic dips similar to those seen in the SDC profiles.

Figure 8.5 also shows the approximate positions of the core-gel, mucus-gel and mucus-mucus interfaces in the concentration and SDC profiles. Mucus directly next to the alginate matrices again became more fluorescent over time. The mucus-mucus interface marks the limit of this region. The diffusion and penetrant fronts of both low and high G alginates seemed to approximately correspond with the viscous alginate gel layers. The characteristic dip in the SDC profiles corresponded to the region of increasingly fluorescent mucus. This is similar to the concentration and SDC profiles of figures 7.5a-7.5c.

(a)

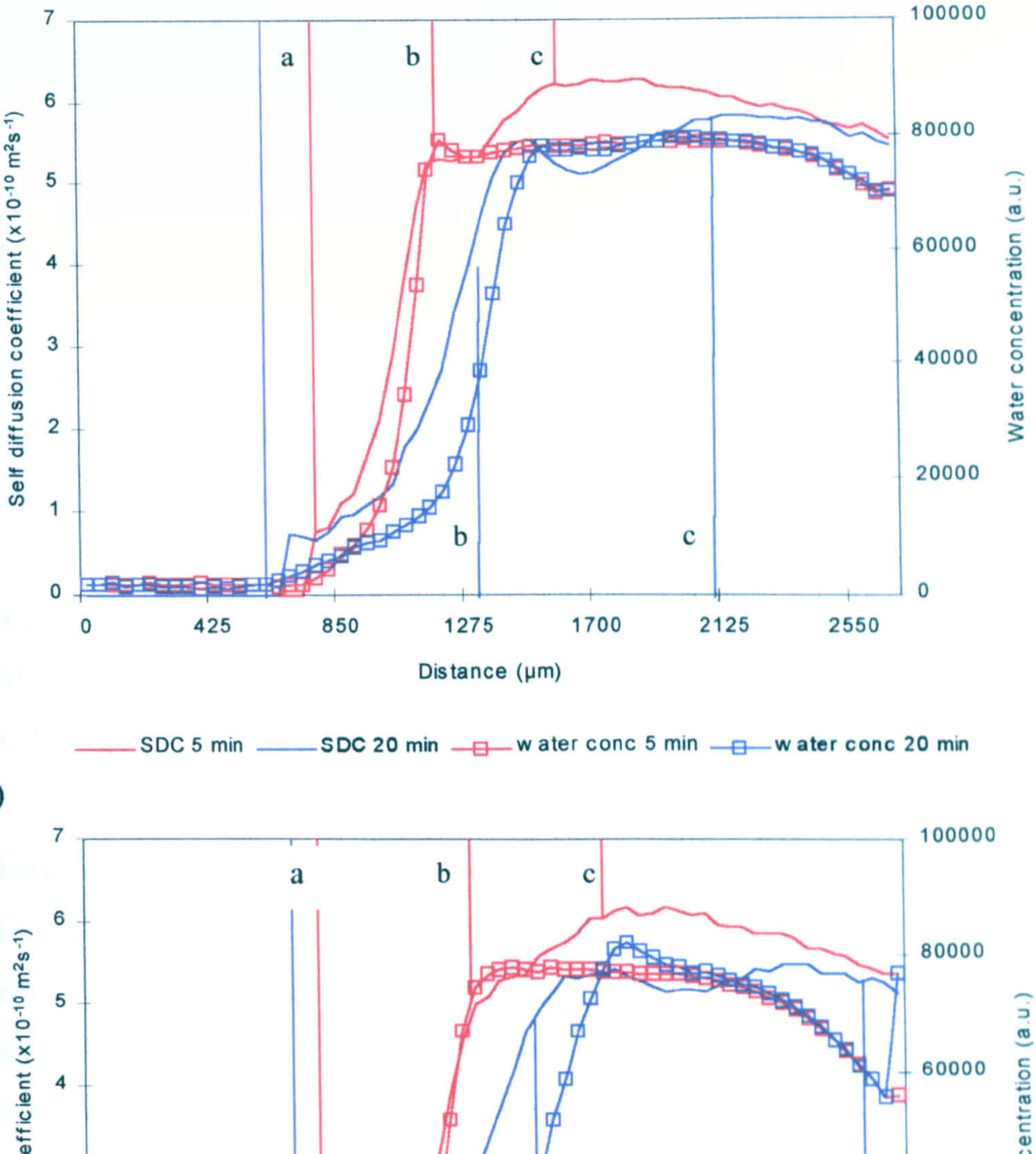

(b)

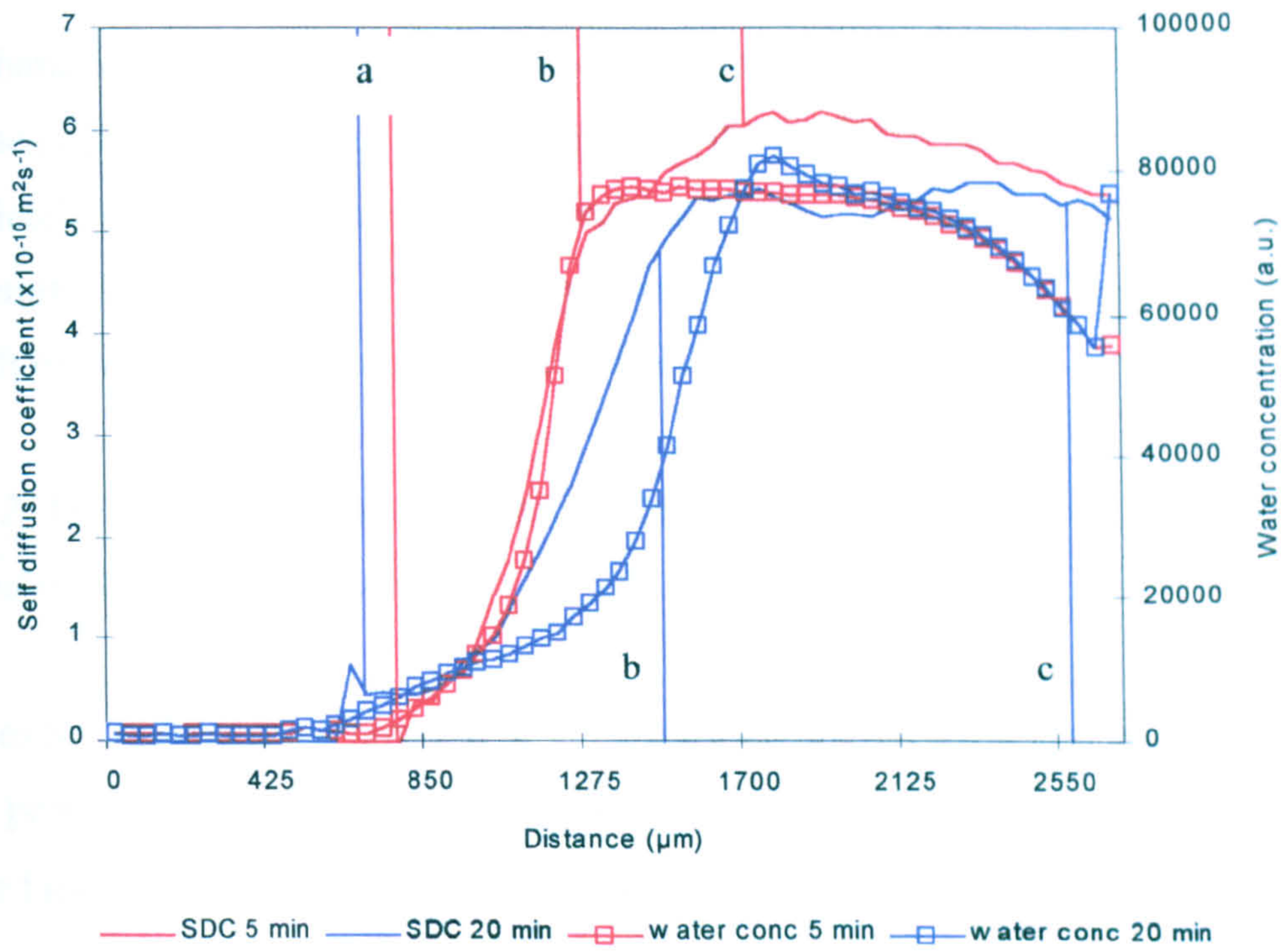

Figure 8.5 The concentration and SDC of water inside bioadhesive bonds of dry alginate matrices.

The SDC and concentration of water inside bioadhesive bonds formed between dry (a) 69.4% G and (b) 44.4% G alginate matrices and purified pig gastric mucus in physiological saline at 20±1°C (mean, n=4). The positions of (a) the dry core-viscous gel interface, (b) the viscous gel-mucus gel interface and (c) the mucus-mucus interface have been marked on the profiles. Standard deviation bars have been omitted for clarity

8.3.2. Influence of the M:G ratio on water inside bioadhesive bonds formed by prehydrated matrices

8.3.2.1. Water diffusion inside bioadhesive bonds formed by prehydrated matrices

The SDC profiles of water inside bioadhesive bonds formed by dry alginate matrices of differing M:G ratios are shown in figure 8.6 (figure 8.6a is a repeat of figure 7.6b and was included here for easy comparison).

After 1 min, the diffusion fronts of both low and high G alginates increased rapidly to $\approx 10 \times 10^{-9}$ m^2 sec^{-1}. The SDC profile of the high G alginate then decreased to a plateau of $\approx 8 \times 10^{-10}$ m^2 sec^{-1}, whereas the profile of the low G alginate just decreased.

The characteristic shape of the high G alginate profile did not change over time, except that the peak decreased over time. The peak in the profile of the low G alginate completely disappeared after 5 mins, resulting in the overall shape of the SDC profile becoming more 'rounded'. The SDC profiles of both low and high G alginates appeared to shift to the right, which may be due to continued matrix swelling.

8.3.2.2. The influence of the M:G ratio on the SDC profiles of bioadhesive bonds formed by dry alginate matrices

Figures 8.7 and 8.8 show how the M:G ratio influenced the diffusion front, zenith and nadir points, respectively. These points were measured from the SDC profiles of water inside bioadhesive bonds formed by prehydrated alginate matrices.

The P_{DF} value of both low and high G alginates decreased over 30 mins, with the P_{DF} value of the low G alginate decreasing at a faster rate than the P_{DF} value of the high G alginate (figure 8.7a). The SDC_{DF} value of the high G alginate did not change over time. In comparison, the SDC_{DF} value of the low G alginate seemed to increase over time (figure 8.7b). There was no evidence to suggest that the SDC_{DF} values of low and high G alginates were statistically significantly different over 30 mins ($p>0.05$).

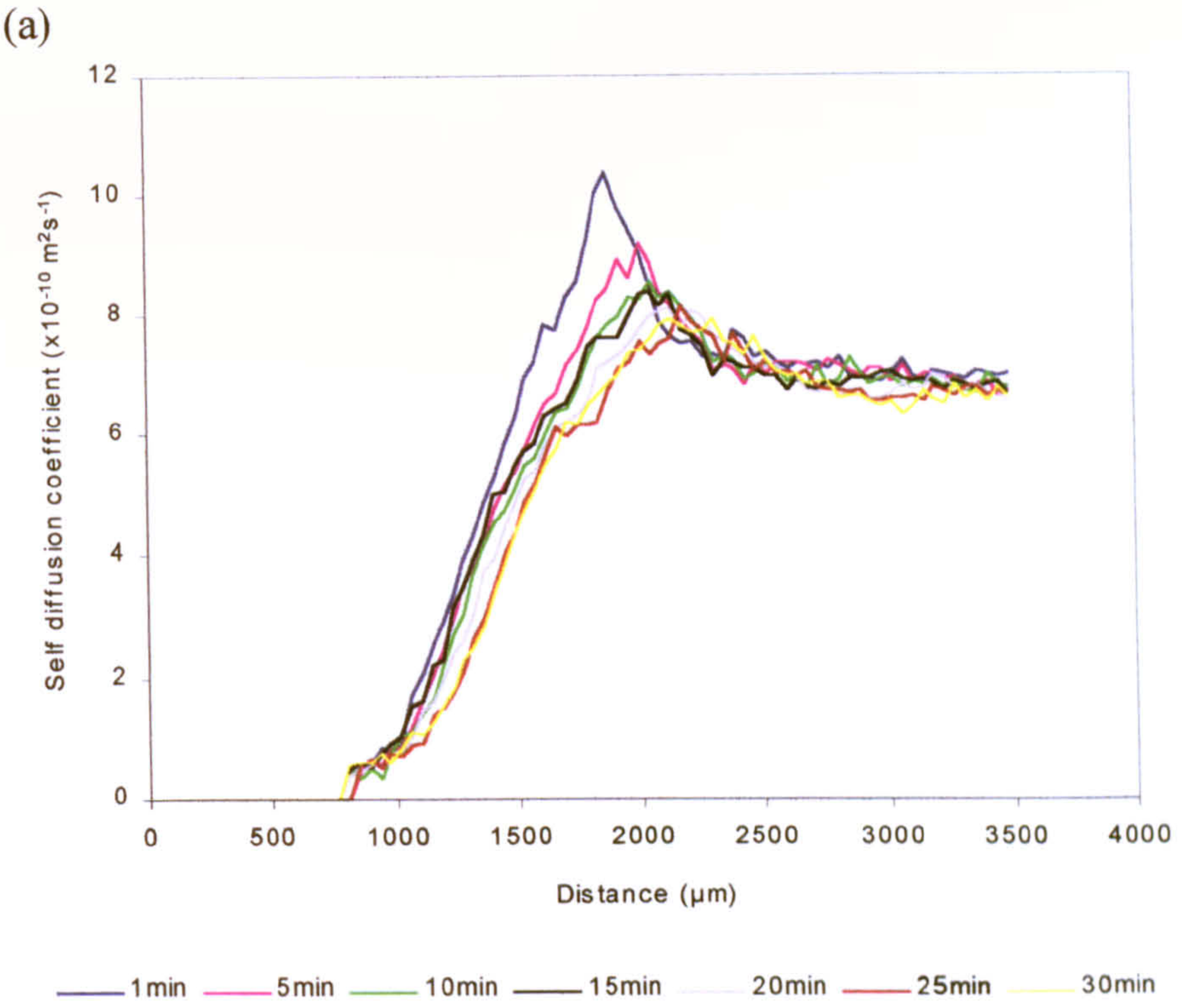

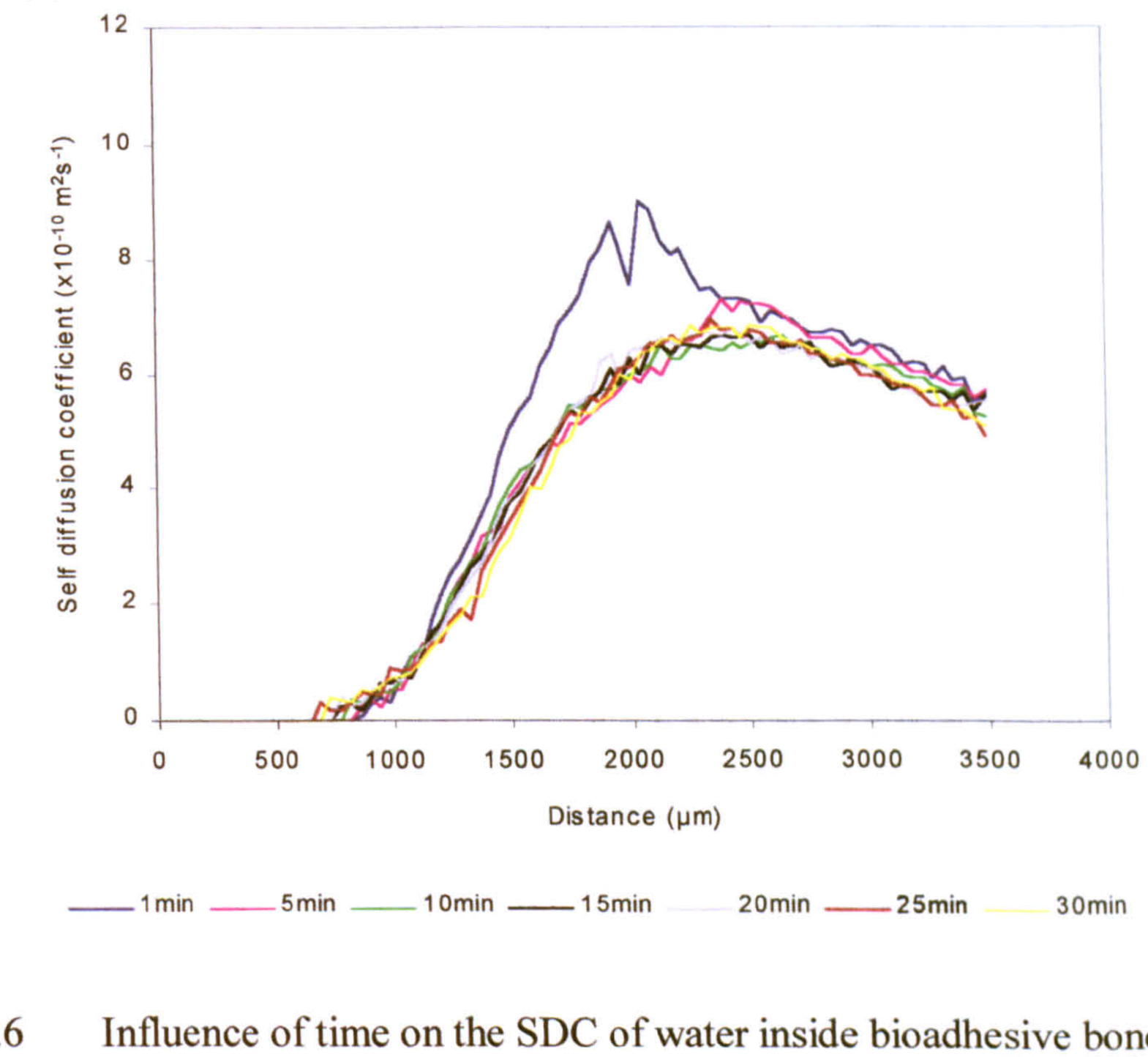

Figure 8.6 Influence of time on the SDC of water inside bioadhesive bonds formed by prehydrated alginate matrices of different M:G ratio

Bioadhesive bonds were formed between (a) 69.4% G and (b) 44.4% G alginate matrices, prehydrated in physiological saline for 10 mins, and purified pig gastric mucus at 20±1°C (mean, n=4). Standard deviation bars have been omitted for clarity.

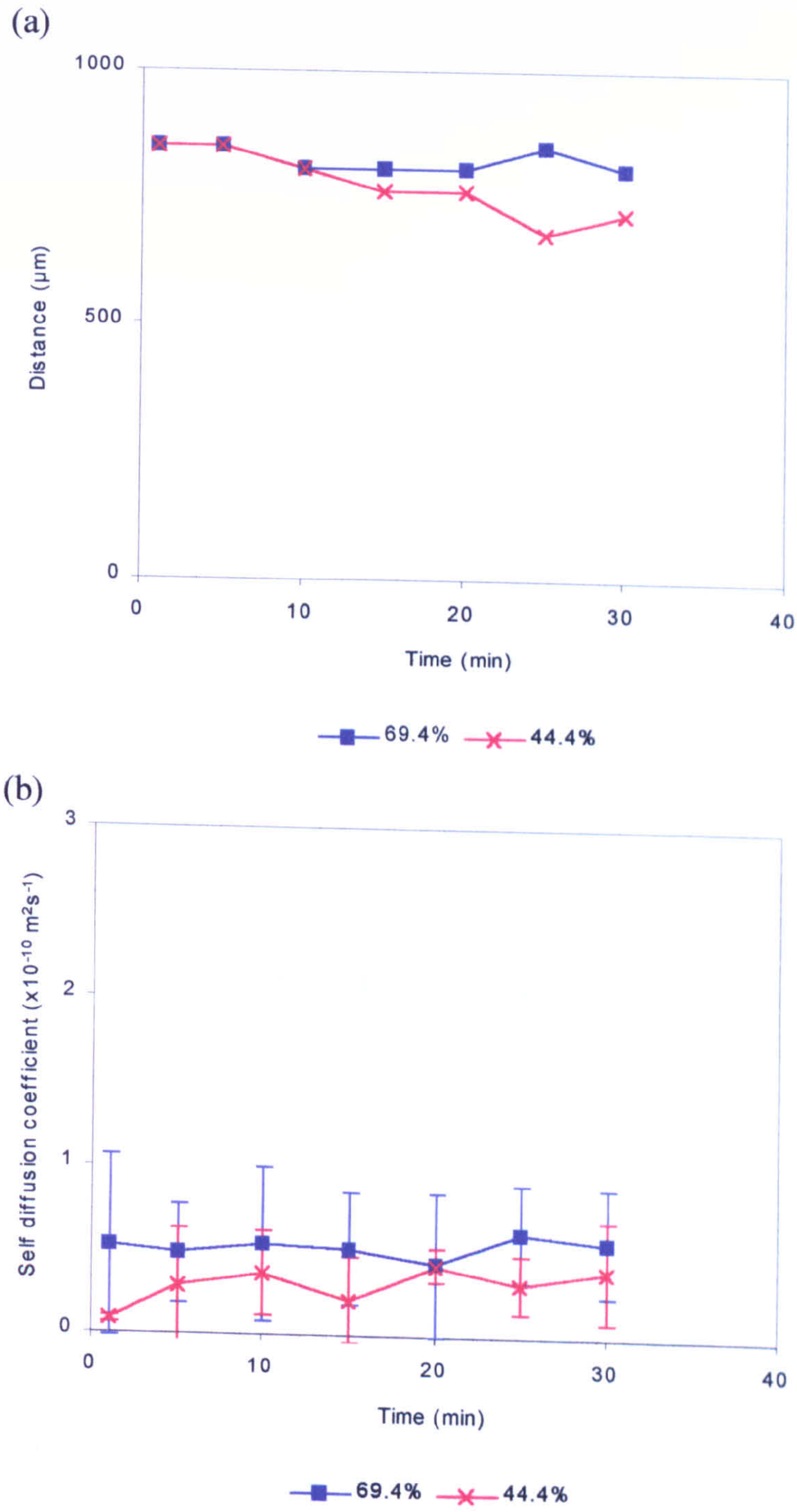

Figure 8.7 Influence of time on the diffusion front - prehydrated alginate matrices of different M:G ratio

The effect of time on (a) P_{SD} and (b) SDC_{SD} taken from SDC profiles of water inside bioadhesive bonds formed between 69.4% G and 44.4% G alginate matrices, prehydrated in physiological saline for 10 mins, and purified pig gastric mucus at 20±1°C (mean, n=4, ±1 SD).

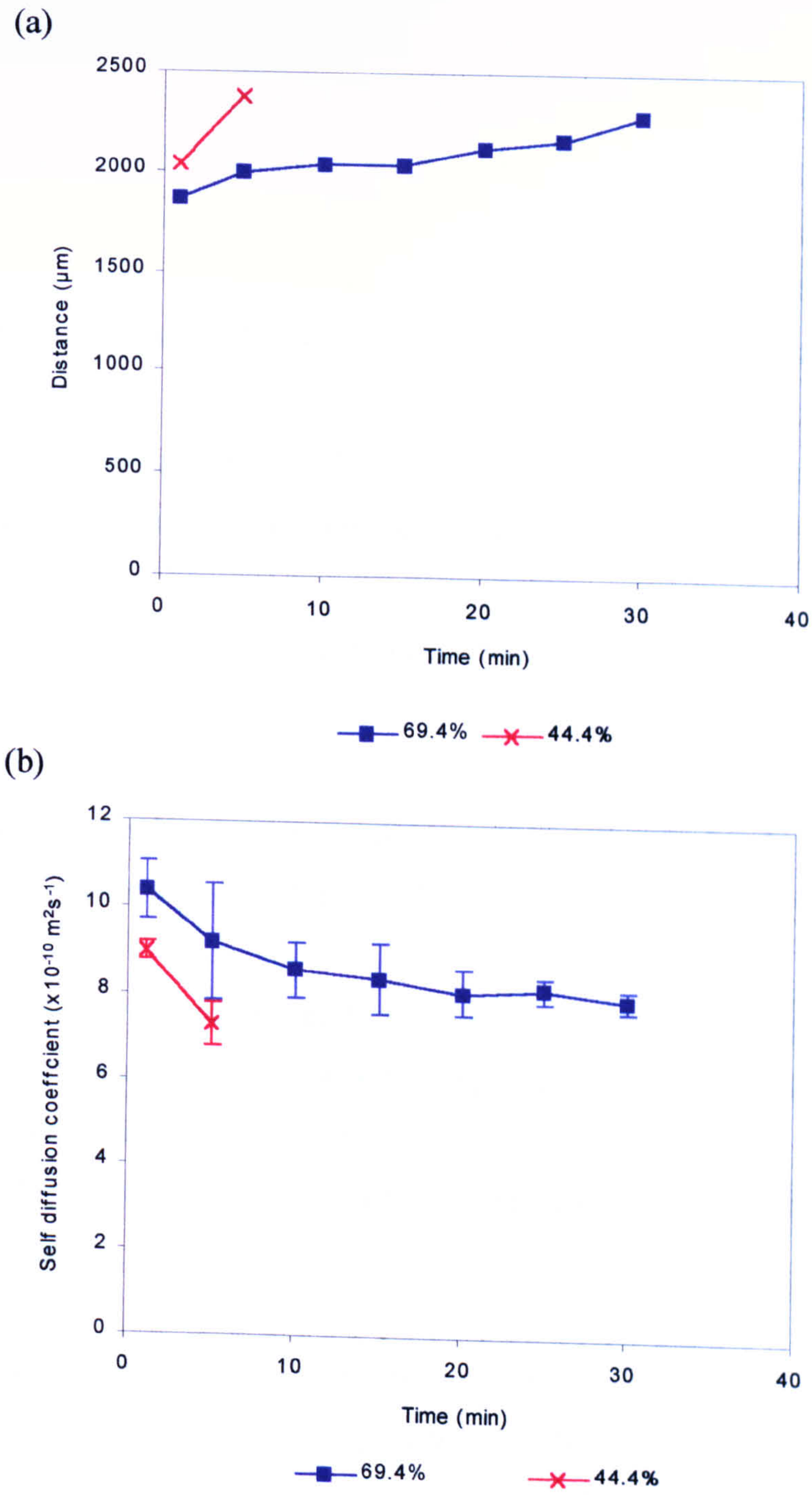

Figure 8.8 Influence of time on the zenith - prehydrated alginate matrices of different M:G ratio

The effect of time on (a) P_{zen} and (b) SDC_{zen} taken from e SDC profiles of water inside bioadhesive bonds formed between 69.4% G and 44.4% G alginate matrices, prehydrated in physiological saline for 10 mins, and purified pig gastric mucus at 20±1°C (mean, n=4, ±1 SD).

The P_{zen} value of both alginates increased with time, although the P_{zen} of the low G alginate disappeared after 5 mins (figure 8.8a). This suggests that the prehydrated matrices continue to swell. The SDC_{zen} values of both G alginates decreased over time, although the SDC_{zen} of the low G alginate was obviously unable to be measured after 5 mins (figure 8.8b). There was no evidence to suggest that the SDC_{zen} of both low and high G alginates were statistically significantly different in the first 5 mins ($p>0.05$).

The SDC profiles of low and high G alginates did not develop characteristic dips, like those observed in profiles of dry alginate matrices.

8.3.2.3. Comparison of SDC and concentration profiles of water inside bioadhesive bonds formed by prehydrated matrices

The concentration and SDC profiles of water inside bioadhesive bonds formed by prehydrated matrices are shown in figure 8.9.

The penetrant fronts in water concentration profiles of both low and high G alginates showed sharply increased after 5 mins, with the penetrant front gradient being higher in the high G alginate than in the low G alginate. The gradient of the high G alginate penetrant front decreased after 20 mins, whereas the penetrant front of the low G alginate did not change.

Figure 8.9 also shows the approximate positions of the core-gel and mucus-gel interfaces in the concentration and SDC profiles. The diffusion and penetrant fronts of both low and high G alginates seemed to correspond with the viscous alginate gel layer. The shape of diffusion fronts were similar to those inside the gel layers of hydrating HPMC and PVA matrices (Rajabi-Siahboomi *et al*, 1996 and Madhu *et al*, 1998).

8.3.3. Influence of the M:G ratio on uptake of physiological saline by alginate matrices

Figure 8.10 showed that the rate of saline uptake by the alginate matrices was rapid in the first 5 min, but decreased over 30 mins. The shape of the graphs suggests that the alginate matrices continue to take up saline after 30 mins. The low G alginate matrices

(a)

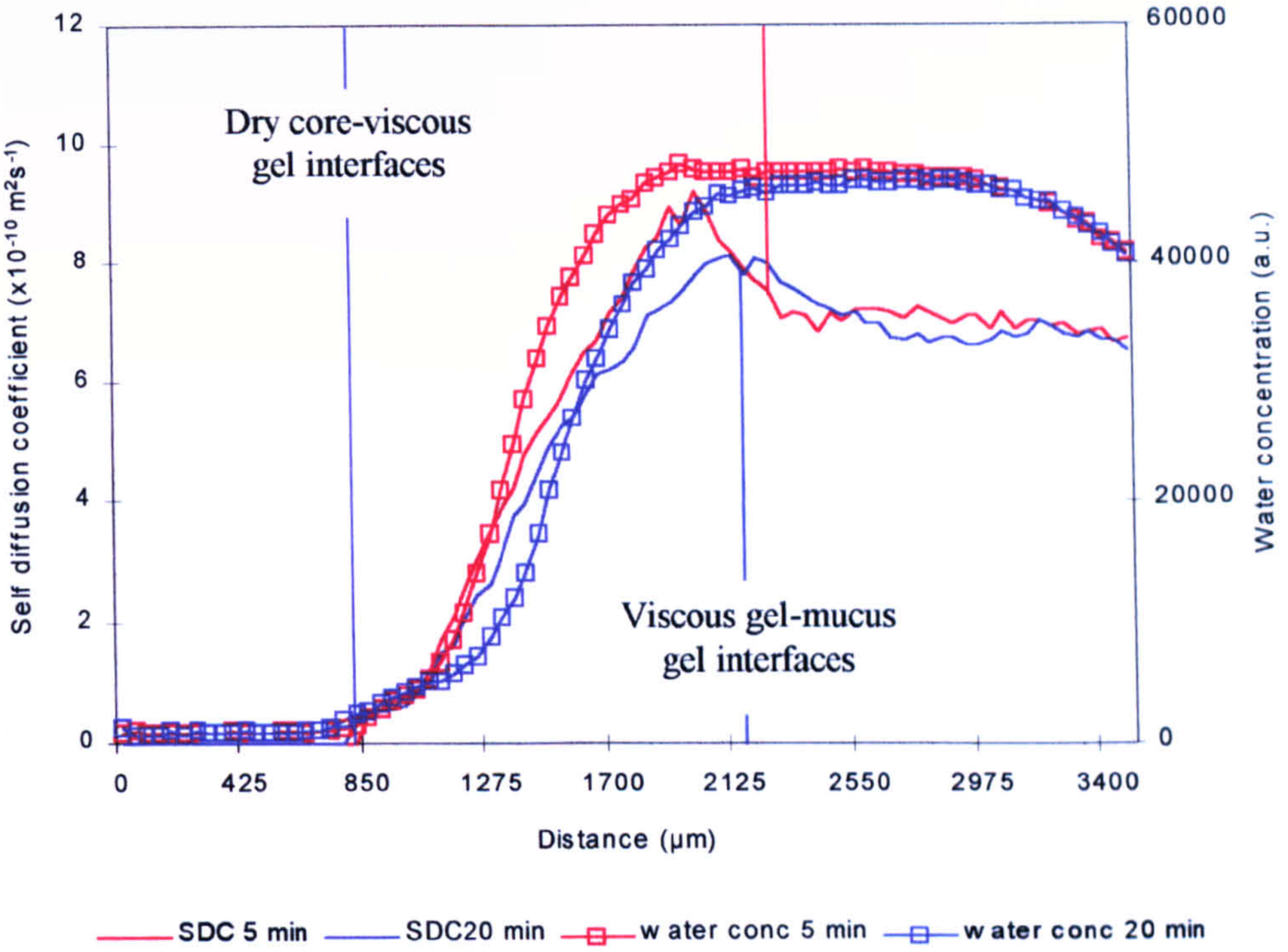

(b)

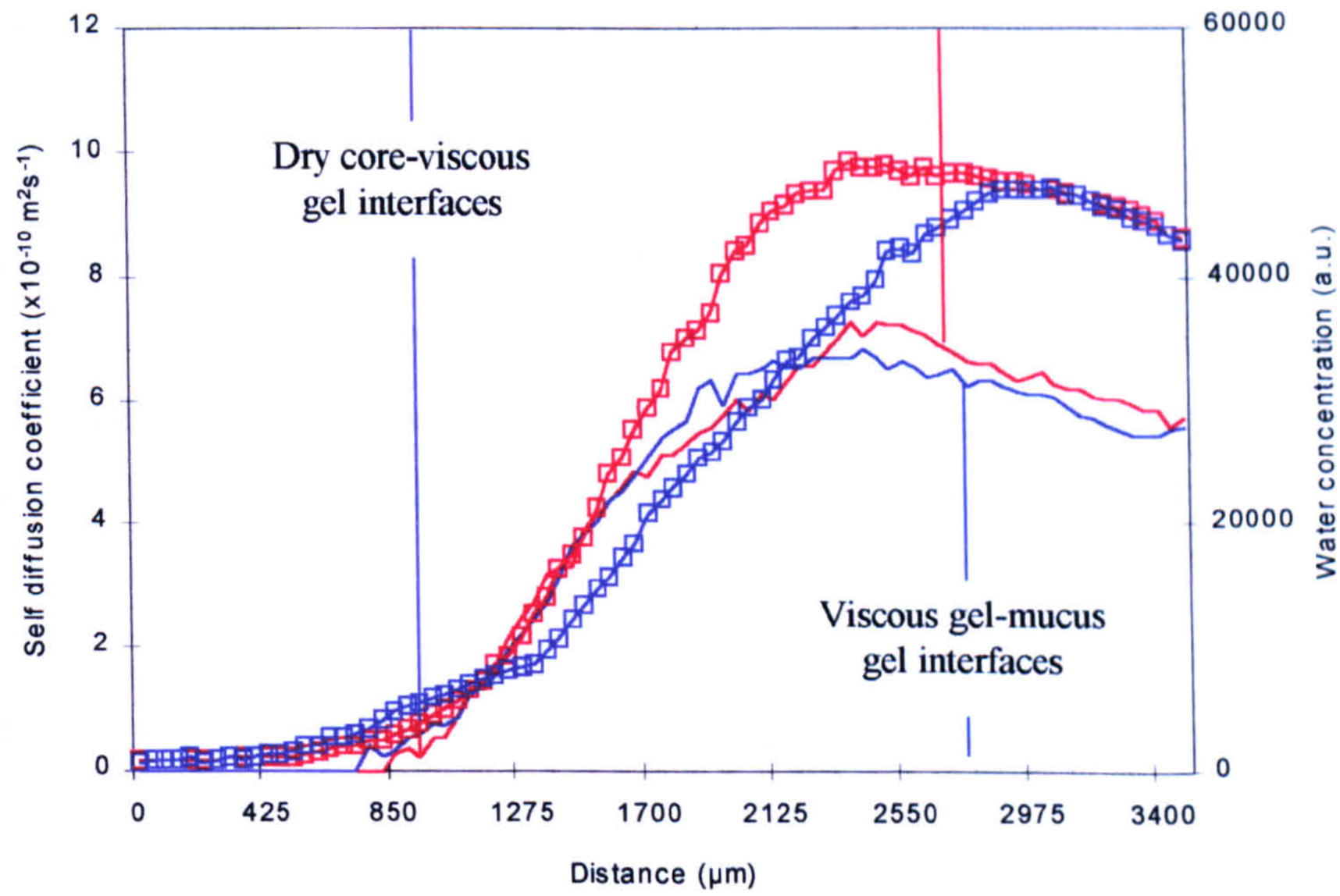

Figure 8.9 Relationship between concentration and SDC of water inside bioadhesive bonds of prehydrated alginate matrices.

Profiles of SDC and concentration of water inside bioadhesive bonds formed between (a) 69.4% G and (b) 44.4% G alginate matrices, prehydrated in physiological saline for 10 min, and purified pig gastric mucus in physiological saline at 20±1°C (mean, n=4). The positions of (a) the dry core-viscous gel interface and (b) the viscous gel-mucus gel interface have been marked on the profiles. Standard deviation bars have been omitted for clarity

took up a statistically significantly more saline than the high G alginate matrices over 30 min ($p<0.05$).

Table 8.1 Influence of the M:G ratio on the saline uptake kinetics of alginate matrices.

Transport parameter	**Percentage content of guluronate in alginate**	
	44.4%	**69.4%**
Case I (ml $min^{-0.5}$)	0.030	0.025
Case II (ml min^{-1})	0.001	0.000
Constant (ml)	-0.001	0.000
r^2	0.999	0.999
Diffusional exponent	0.591	0.507
Kinetic constant	0.025	0.024
r^2	0.997	0.997

Table 8.1 showed that uptake of saline in the low G alginate matrices had lower Fickian and Case II transport exponents than uptake in the high G alginates. The diffusional exponents indicate that matrices of both low and high G alginates take up saline by anomalous diffusion, with uptake being nearer to Case II transport in the low G alginate matrices.

8.3.4. Influence of the M:G ratio on the mobility of solutes inside bioadhesive bonds formed by alginate matrices

Table 8.2 The rate of transport (R_T) of FITC-dextran in the mucus adjacent to the alginate matrices

Guluronate (%)	**n**	**R_T (x10^{-6} cm^2s^{-1})**		**±SD (x10^{-6})**	
		Dry	**Prehydrated**	**Dry**	**Prehydrated**
69.4	7	3.39	7.99	3.5	5.1
44.4	8	1.49	13.30	1.7	8.3

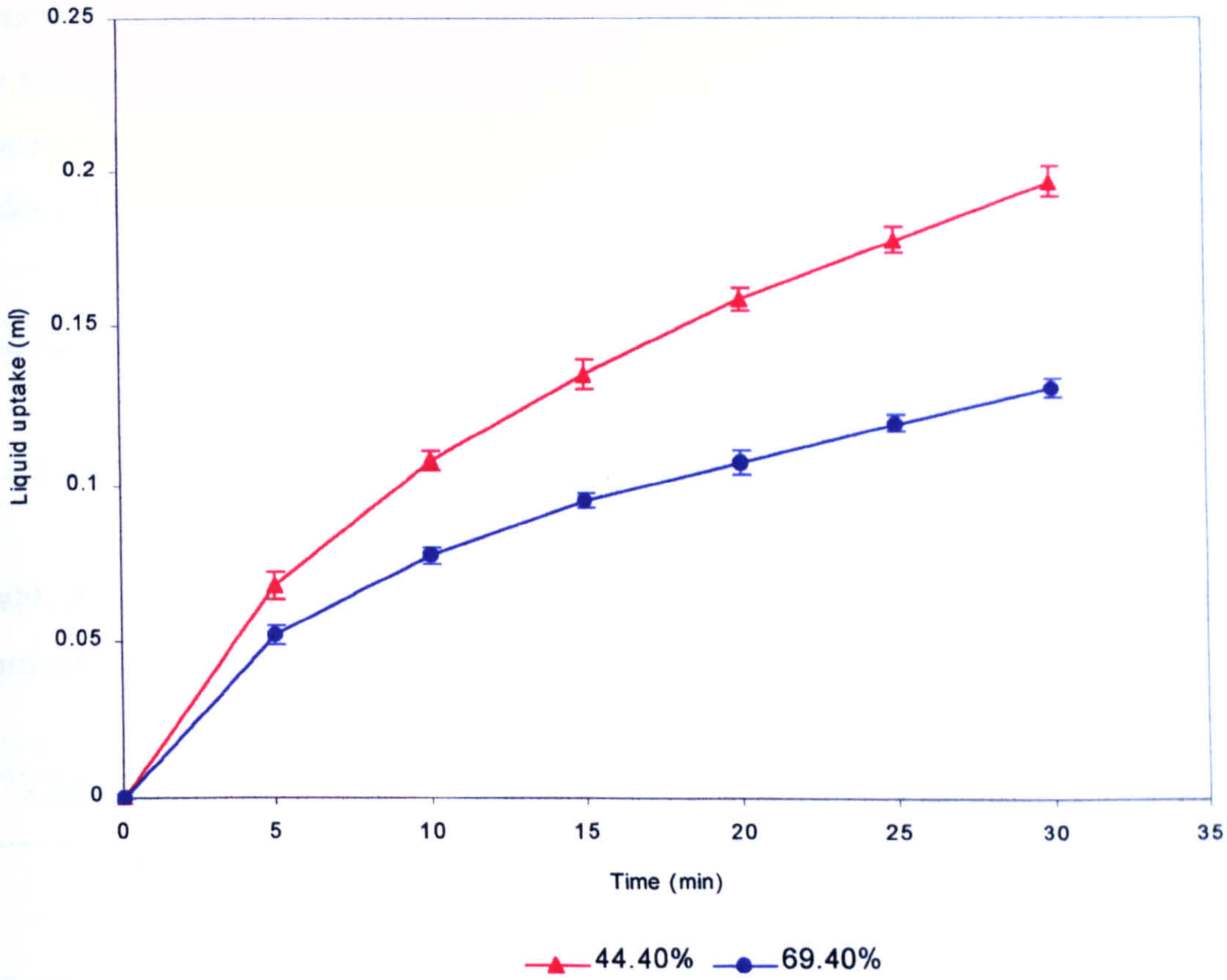

Figure 8.10 Influence of M:G ratio on the volume of liquid taken up by alginate matrices

Liquid uptake kinetics of 69.4% G and 44.4% G alginates were determined by measuring uptake of physiological saline by sodium alginate matrices at 37±1°C (mean, n=5, ±1 SD).

The R_T values in the mucus of bioadhesive bonds formed by dry alginate matrices appeared to increase as the guluronate content of alginate increased. In comparison, the R_T values in the mucus of bioadhesive bonds formed by prehydrated alginate matrices appeared to decrease as the guluronate content of alginate increased. However, the R_T values were not statistically significantly different in each case ($p>0.05$).

8.3.5. Influence of the M:G ratio on the bioadhesive bond strength

8.3.5.1. Bioadhesive bonds formed by dry sodium alginate matrices

Table 8.3 Influence of the M:G ratio on the W_a and F_{max} of bioadhesive bonds formed by dry alginate matrices.

Guluronate (%)	n	W_a (mJ)	±SD	F_{max} (N)	±SD
69.4	14	0.0071	0.004	0.694	0.47
44.4	14	0.0082	0.005	0.944	0.77

The W_a and F_{max} values of bioadhesive bonds formed by dry alginate matrices appeared to decrease as the guluronate content of alginate increased. However, the W_a or F_{max} values were not statistically significantly different ($p>0.05$).

8.3.5.2. Bioadhesive bonds formed by prehydrated sodium alginate matrices

Table 8.4 Influence of the M:G ratio on the W_a and F_{max} of bioadhesive bonds formed by prehydrated alginate matrices.

Guluronate (%)	n	W_a (mJ)	±SD	F_{max} (N)	±SD
69.4	16	0.0050	0.001	0.339	0.10
44.4	16	0.0040	0.002	0.323	0.16

The W_a and F_{max} values of bioadhesive bonds formed by prehydrated alginate matrices appeared to increase as the guluronate content of alginate increased. However, the W_a or F_{max} values were not statistically significantly different ($p>0.05$).

8.3.5.3. The cohesive strength of alginate viscous gel layers

Table 8.4 The cohesive strength of self-adhered alginate viscous gel layers

Guluronate (%)	n	W_a (mJ)	±SD	F_{max} (N)	SD
69.4	4	0.1802	0.060	4.28	0.10
44.4	4	0.0547	0.004	2.88	0.25

Table 8.5 shows that the W_a and F_{max} values of self-adhered alginate viscous gel layers were considerably stronger than the W_a and F_{max} values of bioadhesive bonds formed by either dry or prehydrated alginate matrices (section 8.3.5.1 and 8.3.5.2). This suggests that W_a and F_{max} of bioadhesive bonds are not indicative of fractures in the viscous alginate gel layer.

8.3.5.4. The cohesive strength of native pig gastric mucus

The W_a and F_{max} of self-adhered pig gastric mucus layers are reported in table 7.6 (section 7.3.5.4). The W_a and F_{max} of self-adhered pig gastric mucus layers were considerably weaker than W_a and F_{max} of bioadhesive bonds formed by either dry or prehydrated alginate matrices (section 8.3.5.1 and 8.3.5.2). This suggests that W_a and F_{max} of bioadhesive bonds are not indicative of fractures in the mucus gel layer.

8.4. Discussion

8.4.1. Influence of M:G ratio on bioadhesion of dry alginate matrices

The M:G ratio may influence some physicochemical properties of alginate, for example polymer flexibility, solubility and solution rheology, which may affect alginate bioadhesion. The relationships between these properties and M:G ratio have been discussed in the introductory chapter. This study found that the M:G ratios did not significantly influence the W_a and F_{max} values of bioadhesive bonds formed by dry alginate matrices ($p>0.05$) (table 8.3). However, this study only used 30:70 and 60:40 ratios of M:G, which may not differ greatly enough to produce a significant influence in

the bioadhesive bond strength. Future experiments studying a wider range of M:G alginates needs to be carried out.

At first sight, it seems that the M:G ratios used in this study seemed to influence the diffusion of water in the mucus gel directly adjacent to the alginate matrix (figure 8.1). The SDC profile of the high G alginate developed a characteristic dip in this region after 5 mins, whereas the SDC profile of the low G alginate developed a similar dip after 10 mins. This was also observed in the P_{nad} and SDC_{nad} values (figure 8.3). Close examination of both 5 mins SDC profiles showed that the difference in the SDC of water in this region was very small and may be within the noise of the experiment, thus suggesting no real difference in the profiles. This is supported by the SDC_{DF} (figure 8.2b), SDC_{zen} (figure 8.3b) and SDC_{nad} values (figure 8.4b), which were not significantly different at any one time over 30 mins ($p>0.05$). Therefore, this suggests that the low and high G alginate matrices did not influence the diffusion of water inside bioadhesive bonds formed between dry matrices and pig gastric mucus.

The characteristic dip in the SDC profiles of both low and high G alginates (figure 8.1) are similar in shape to each other and are also similar in shape to those in the SDC profiles shown in figures 7.1, 7.2 and 7.3. The mucus adjacent to the matrix became more fluorescent over time, providing evidence for an increase in the concentration of mucin. This region corresponded to the section of the SDC profiles containing the characteristic dips (figure 8.5). Together, this suggests that the low and high G alginate matrices dehydrated the mucus layer and that this was independent of M:G ratio. The SDC_{nad} values of low and high G alginates (figure 8.4b), which were not statistically significantly different over time ($p>0.05$), provide supporting evidence for this.

The R_T of FITC-dextrans in mucus near the alginate matrix were also not significantly influenced by M:G ratio, suggesting that there was no influence on the diffusion retarding properties in the mucus. However, the molecular sieve properties of mucus outlined in section 7.4.1 may interfere with and hamper this particular technique.

The M:G ratio seemed to influence the swelling of the alginate matrices. The P_{zen} values of the SDC profiles, which mark the approximate outer limit of the viscous gel layer, suggest that the low G alginate matrices swell more than the high G alginate matrices

(figure 8.3a). Electron micrographs of the dry alginate matrices show that the low G alginate have larger intergranular pores than the high G alginate, suggesting increased porosity. Since the molecular weight and particle size are similar, the larger pores of the low G alginate matrices may allow a deeper penetration of water into the dry core before the alginate hydrates and closes these intergranular pores. The swelling of hydrophilic matrices may be equally composed of hydration and swelling of the polymer as well as the expansion of the dry core as a result of release of tablet compression forces (Rajabi-Siahboomi *et al*, 1994). Therefore, the deeper penetration may result in a greater expansion of the dry core as well as the formation of a larger viscous alginate gel layer.

This is supported by the liquid uptake studies of the matrices, which show that the low G alginate matrices take up significantly more saline than the high G alginate matrices at any one time over 30 mins ($p<0.05$) (figure 8.10). Also, the transport exponents of liquid uptake (table 8.1) indicate that the saline uptake in the low G alginate matrices was closer to Case II transport than in the high G alginate matrices.

The low G alginate matrices contained a large number of fines (figures 2.4), which may influence the uptake of water. Wan and Choong, 1986, have shown that incorporating 50% w/w fines in rapidly disintegrating Phenacetin tablets decreased liquid uptake by decreasing the porosity of the tablets. However, the properties of rapidly disintegrating tablets and hydrophilic matrices are considerably different. Also, the chemical nature of these fines is unknown and consequently their influence, if any, on the uptake of saline cannot be reliably predicted.

Several bioadhesive studies have related the degree of polymer swelling to bioadhesion, arguing that a more swollen polymer will have larger interstitial pores, which may facilitate the interpenetration and entanglement of the mucin polymers and may increase the bioadhesive interaction (e.g. Park and Robinson, 1985, and 1987). Unfortunately, the P_{zen} measurement cannot differentiate between the swelling of the alginate viscous gel and the expansion of the dry matrix core. Therefore, the P_{zen} measurements cannot be related to the bioadhesion of the alginate matrix.

The influence of M:G ratio on the swelling and liquid uptake properties of alginate matrices was not reflected in the W_a and F_{max} values of the bioadhesive bonds (table 8.3). This implies that the capillary suction effect of the intergranular pores of the dry alginate matrices was not important in the bioadhesion of dry alginate matrices. The bioadhesion of polyacrylic acid tablets have showed that bioadhesive bond strength was independent of capillary suction (Lejoyeux *et al*, 1989a and 1989b). The influence of M:G ratio on the diffusion of water inside the bond and the liquid uptake properties of the alginate again shows that the uptake of saline does not correlate with the dehydration of the mucus by the dry alginate matrix.

8.4.2. Influence of M:G ratio on bioadhesion of prehydrated alginate matrices

The M:G ratios used in this study did not again significantly influence the W_a and F_{max} values of bioadhesive bonds formed by prehydrated alginate matrices ($p>0.05$) (table 8.4). Similarly, the R_T values of FITC-dextrans in the mucus adjacent to the viscous alginate gel layer were not affected by the low and high G alginates ($p>0.05$) (table 8.2).

The M:G ratios used in this study seemed to influence the diffusion of water inside bioadhesive bonds formed by prehydrated alginate matrices (figure 8.6). The diffusion front of the low G alginate decreased considerably after 5 min, resulting in the disappearance of the peak in the SDC profile. The diffusion front gradient of the high G alginate did not seem to change over time, although the SDC_{zen} value decreased over time.

This may be due to the continued hydration of the alginate matrices. The saline uptake studies show that the low G alginate matrices take up significantly more saline at any one time than the high G alginate matrices. The increased hydration drive of the low G alginate matrix causes the increased diffusion of water from the viscous alginate gel and reduces the SDC since there is an increasing higher concentration of alginate in the viscous gel. This supported by the water concentration profiles (figure 8.9), which showed a decrease in the concentration of water in this region for the low G alginate but not for the high G alginate.

Comparison of the SDC_{zen} values of low and high G alginates did not show any statistically significantly differences in the first 5 mins ($p>0.05$). Likewise, the SDC_{DI} values of both alginates were not statistically significantly different over 30 mins ($p>0.05$). This suggests that at the time when the W_a and F_{max} of the bioadhesive bonds were determined (after 5 mins), there was no influence of M:G ratio on diffusion inside the bond.

Therefore, the influence of diffusion on the bioadhesion of prehydrated alginate matrices cannot really be determined from the SDC profiles after 5 mins. The SDC profiles at later times suggest that the diffusion of water may not be important in the bioadhesion of prehydrated alginate since the influence of M:G ratio on the diffusion of water was not reflected in the W_a and F_{max} values of the bonds. However, the W_a and F_{max} values at later times need to be determined in order to fully substantiate this theory

The SDC profiles of both alginates did not develop a characteristic dip, similar to those observed in the SDC profiles of dry matrices. This suggests that mucus dehydration was not a major factor involved in the bioadhesion of prehydrated alginate matrices.

8.5 Conclusions

The M:G ratios used in this study did not influence the work of adhesion or the maximum detachment force of bioadhesive bonds formed by dry alginate matrices. The characteristic dips in the SDC profiles suggest that the dry alginate matrices dehydrated the adjacent mucus layer. The shape of the dips over time and the SDC_{mud} values suggest that this mechanism was independent of M:G ratio. The saline uptake of the low and high G matrices was different, although this was attributed in part to a possible difference in the porosity of the matrices. This suggested that mechanisms such as capillary suction may not be involved in the bioadhesion of dry alginate matrices and that liquid uptake studies cannot be used as a reliable measure of the dehydrative potential of alginate matrices.

Similarly, the M:G ratios used in this study did not influence the work of adhesion or the maximum detachment force of bioadhesive bonds formed by prehydrated alginate

matrices. The SDC profiles showed that bioadhesion of prehydrated alginate matrices did not involve mucus dehydration.

Chapter 9

Influence of particle size on bioadhesion of dry and hydrated sodium alginate matrices

9.1. Introduction

The rates of hydration and gel layer formation of hydrophilic matrices may be influenced by the size of the particles (Alderman, 1984, and Melia, 1991), subsequently affecting the movement of liquid into the matrices. The movement of water from mucus into the alginate matrices may be important in alginate bioadhesion (chapters 7 and 8). Therefore, the aim of this chapter was to study the influence of particle size on the uptake of saline by alginate matrices and the bioadhesive bond strength of dry and prehydrated alginate matrices.

9.2. Methods

The methods described in chapter 6 were used to test the alginate matrices. The physicochemical properties of the sodium alginates and pig gastric mucus used in this chapter are described in chapter 3. The statistical analysis of data was carried out according to the method described in section 6.7.

9.3. Results

This chapter will refer to matrices manufactured from 63-90 μm alginate particles as '63-90 μm matrices', those manufactured from 90-125 μm alginate particles as '90-125 μm matrices' and those manufactured from 125-180 μm alginate particles as '125-180 μm matrices'.

9.3.1. Influence of particle size on the uptake of physiological saline by alginate matrices

Figure 9.1 shows that the rate of saline uptake by the alginate matrices was rapid in the first 5 mins but decreased over 30 mins. The shape of the graphs suggests that the alginate matrices continue to take up saline after 30 mins. The 90-125 μm matrices took up significantly more saline over 30 mins than either the 63-90 μm or the 125-180 μm matrices ($p<0.02$). The uptake of saline by the 63-90 μm and 125-180 μm matrices was not statistically significantly different ($p>0.02$).

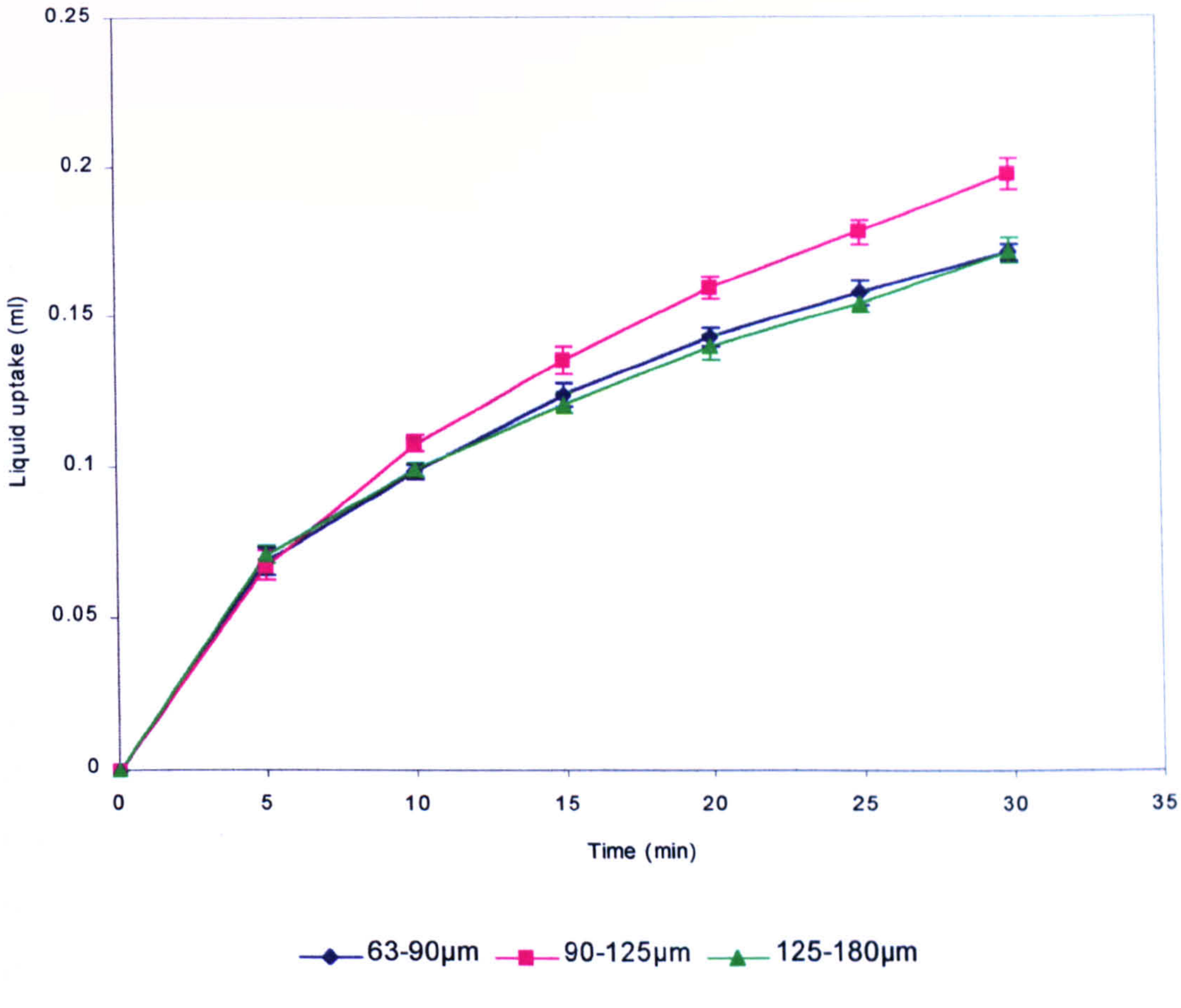

Figure 9.1 Influence of particle size on the volume of liquid taken up by alginate matrices

The liquid uptake profiles of 63-90 µm, 90-125 µm and 125-180 µm alginate matrices were determined by measuring the uptake of physiological saline by alginate matrices at 37±1°C (mean, n=5, ±1 SD).

Table 9.1 Influence of particle size on saline uptake kinetics of alginate matrices.

Transport parameter	Particle size of alginate		
	63-90 μm	90-125 μm	125-180 μm
Case I (ml $min^{-0.5}$)	0.032	0.030	0.032
Case II (ml min^{-1})	0.000	0.001	0.000
Constant (ml)	-0.001	-0.001	0.000
r^2	1.000	0.999	1.000
Diffusional exponent	0.513	0.591	0.486
Kinetic constant	0.0304	0.027	0.033
r^2	0.999	0.997	1.000

Table 9.1 shows that the 63-90 μm and 125-180 μm matrices had similar Fickian diffusion and Case II transport exponents. In comparison, the 90-125 μm matrices had lower Fickian and marginally higher Case II exponents than the other matrices. The diffusional exponents suggested that the alginate matrices take up saline by anomalous diffusion, with the 90-125 μm matrices being nearer to Case II transport and the 125-180 μm being nearer to Fickian diffusion.

9.3.2. Influence of particle size on bioadhesive bond strength

9.3.2.1. Bioadhesive bonds formed by dry alginate matrices

Table 9.2 Influence of particle size on the W_a and F_{max} of bioadhesive bonds formed by dry alginate matrices.

Particle size (μm)	n	W_a (mJ)	±SD	F_{max} (N)	±SD
63-90	14	0.0077	0.004	0.846	0.61
90-125	14	0.0082	0.005	0.944	0.77
125-180	14	0.0067	0.003	0.648	0.36

Table 9.2 shows that the W_a and F_{max} values appeared to increase as particle size increased from 63-90 μm to 90-125 μm, but decreased as particle size increased from

90-125 μm to 125-180 μm. However, there was no evidence to suggest that the W_a and F_{max} values were statistically significantly different ($p>0.05$).

9.3.2.2. Bioadhesive bonds formed by prehydrated alginate matrices

Table 9.3 Influence of particle size on W_a and F_{max} of bioadhesive bonds formed by prehydrated alginate matrices.

Particle size (μm)	n	W_a (mJ)	±SD	F_{max} (N)	±SD
63-90	13	0.0037	0.001	0.277	0.09
90-125	13	0.0038	0.001	0.317	0.15
125-180	13	0.0043	0.001	0.324	0.11

Table 9.3 shows that W_a and F_{max} appeared to increase as particle size increased, although there was no evidence to suggest that the W_a and F_{max} values were statistically significantly different ($p>0.05$).

9.3.2.3. The cohesive strength of alginate viscous gel layers

Table 9.4 The cohesive strength of self-adhered alginate viscous gel layers

Particle size (μm)	n	W_a (mJ)	±SD	F_{max} (N)	±SD
63-90	4	0.0402	0.003	2.49	0.11
90-125	4	0.0547	0.004	2.88	0.25
125-180	4	0.0462	0.004	2.64	0.21

Table 7.5 shows that W_a and F_{max} values of self-adhered alginate viscous gel layers were considerably stronger than the W_a and F_{max} values of bioadhesive bonds formed by either dry or prehydrated alginate matrices (section 9.3.2.1 and 9.3.2.2). This suggests that W_a and F_{max} of bioadhesive bonds were not indicative of fractures in the viscous alginate gel layer.

9.3.2.4. The cohesive strength of native pig gastric mucus

The W_a and F_{max} of self-adhered pig gastric mucus layers are reported in table 7.6 (section 7.3.5.4). The W_a and F_{max} values of self-adhered pig gastric mucus layers were considerably weaker than the W_a and F_{max} values of bioadhesive bonds formed by either dry or prehydrated alginate matrices (section 9.3.2.1 and 9.3.2.2). This suggests that W_a and F_{max} of bioadhesive bonds were not indicative of fractures in the mucus gel layer.

9.4. Discussion

9.4.1. Influence of particle size on bioadhesion of dry alginate matrices

The particle size range used in this study did not significantly influence the W_a or F_{max} values of bioadhesive bonds formed by dry alginate matrices ($p>0.05$) (table 9.2), but did significantly affect the uptake of saline by the matrices. The 90-125 μm matrices took up significantly more saline at any one time than the 63-90 μm or 125-180 μm matrices ($p<0.02$) (figure 9.1). The uptake of the 90-125 μm matrices was also nearer to Case II transport than the uptake of the other matrices.

This relationship between particle size and uptake was not expected since smaller particles of hydrophilic polymers tend to hydrate more quickly than larger particles (Alderman, 1984). This may result in a more rapid formation of a viscous alginate gel layer, which would decrease the ingress of saline and decrease saline uptake. Therefore, the uptake of saline was expected to increase as particle size increased.

The different sizes of the particles may also affect the packing density and thus porosity of the matrices. Electron micrographs (figures 2.3 and 2.4) show that the porosity of the 63-90 μm and 125-180 μm matrices appeared to be similar, reflecting the saline uptake profiles. However, micrographs of the 90-125 μm matrices show larger intergranular pores than the other matrices, suggesting an increased porosity. The larger pores may allow a deeper penetration of water into the dry core before the alginate hydrates and forms a viscous gel layer. This may result in an increased release of tablet compression forces in the dry core (Rajabi-Siahboomi *et al*, 1994), which may further increase the porosity of the tablet, thus driving the continued increase in saline uptake. This type of

phenomenon may have also been observed in the saline uptake of low and high G alginate matrices. However, further work investigating this relationship between porosity and uptake in alginate matrices needs to be carried out.

The micrographs also showed that all the matrices contained fines, the number of which seemed to increase as particle size increased (figure 2.4). Wan and Choong, 1986, have shown that incorporating 50% w/w fines in rapidly disintegrating Phenacetin tablets decreased liquid uptake by decreasing the porosity of the tablets. However, the properties of rapidly disintegrating tablets and hydrophilic matrices are considerably different. Also, the chemical nature of these fines is unknown and consequently their influence, if any, on the uptake of saline cannot be reliably predicted. Further work needs to be carried out on the effect of the fines on the properties of the alginate matrices.

This study suggests that the porosity of the matrices and the subsequent capillary suction effect were not major factors involved in the bioadhesion of dry alginate matrices. Lejoyeux *et al*, 1989a and 1989b, also found that the bioadhesive bond strength of polyacrylic acid tablets was independent of porosity and capillary suction effect. This study also found that the saline uptake kinetics were not reliable indicators of the bioadhesive potential of dry alginate matrices.

9.4.2. Influence of particle size on bioadhesion of prehydrated alginate matrices

The particle sizes used in this study also did not significantly influence either W_a and F_{max} of bioadhesive bonds formed by prehydrated alginate matrices ($p>0.05$) (table 9.2). Therefore, the implication of this to the liquid uptake studies and the bioadhesion of alginate matrices has been previously discussed in section 9.4.1. The influence of matrix porosity and capillary suction on the bioadhesion of prehydrated alginate matrices was not unsurprising since the mucus forms a bioadhesive bond with a viscous alginate gel.

9.4. Conclusion

The particle size range used in this study did not influence the work of adhesion or the maximum detachment force of bioadhesive bonds formed by dry or prehydrated alginate matrices. The 90-125 μm matrices seemed to be more porous than matrices of higher and lower particle sizes and this factor seemed to be responsible for the increased uptake of saline by the matrices. This suggests that factors influencing the uptake of saline by alginate matrices, such as porosity and capillary uptake, were not major factors involved in the bioadhesion of dry and prehydrated alginate. It also indicated that saline uptake may not be a reliable measure of the bioadhesive bond strength of alginate matrices.

Chapter 10

General discussion and future work

10.1. General discussion

Several mechanisms have been put forward to explain the phenomenon of bioadhesion, based on polymer interpenetration, entanglement, surface thermodynamics or secondary forces of attraction. The work in this thesis has focussed on developing techniques and conducting studies, which investigate the movement and concentration of water inside alginate matrices and the bioadhesive bonds formed by them. These have been proposed as important factors in the bioadhesion of hydrophilic matrices (Smart *et al*, 1991, and Mortazavi and Smart, 1993).

To date, the hydration and movement of water inside a bioadhesive bond have been investigated using relatively basic and rudimentary methods, which were unable to measure water diffusion and concentration. Thus, the initial aim of this project was to develop non-destructive techniques to measure the mobility and state of hydration inside matrices and bioadhesive bonds formed by alginate hydrophilic matrices.

Chapter 5 details the development of a method using magnetic resonance imaging (MRI) to successfully measure the SDC profiles of water inside the bioadhesive bond formed by dry and hydrated alginate matrices. The technique of MRI has been used to spatially resolve the SDC profile of water inside hydrating hydrophilic matrices (Rajabi-Siahboomi *et al*, 1996). Data from this method can be easily manipulated to obtain profiles of water concentration inside the bond. MRI could not resolve the interfacial positions of the mucus and matrix in the sample, but a suitable method based on measuring the relative autofluorescence of alginate and mucus by confocal microscopy was devised for this.

Fluorescence photobleaching techniques may be used to measure the mobility of fluorescent solutes in a polymer gel network but could not be applied to the bioadhesive bond as the majority of these techniques can only measure solute transport in homogeneous samples. Chapter 4 details the development of a fluorescence recovery after photobleaching (FRAP) technique to measure the rate of transport (R_f) of solutes in a bioadhesive bond. The interaction of mucin with a bioadhesive polymer may increase the diffusion retarding properties of either polymer networks (Degim and

Kellaway, 1998). Therefore, solute mobility may be used as a measure of this interaction.

These methods were combined with basic studies of liquid uptake kinetics and bond strength through detachment force testing to study the influence of some physicochemical factors on the properties of bioadhesive bonds formed between alginate matrices and pig gastric mucus. As the bioadhesion of dry and hydrated polymers may differ considerably (Lehr, 1994, and Smart, 1993), separate studies were undertaken using dry and prehydrated alginate matrices.

10.1.1. Bioadhesion of dry alginate matrices

The dehydration of the adjacent mucus gel layer has been put forward as an important mechanism involved in the bioadhesion of dry hydrophilic matrices (Smart *et al*, 1991, and Mortazavi and Smart, 1993). The SDC profile of water inside bioadhesive bonds formed between dry alginate matrices and pig gastric mucus provided evidence to suggest that these matrices dehydrate the directly adjacent mucus layer. The SDC profile developed a characteristic dip in that part of the profile corresponding to the mucus layer directly next to the alginate matrix, which increased in size over time irrespective of molecular weight or M:G ratio (figures 7.1a-7.c and 8.1a-8.1b). This relationship is reflected in the F_{max} values of bioadhesive bonds formed by dry alginate matrices (table 7.3 and 8.3).

Mucus is a viscoelastic gel composed of macromolecular cross-linked mucin molecules forming a mesh structure with water filled pores that functions as a barrier to diffusion (Bhat *et al*, 1995). Several mechanisms have been put forward to explain the diffusion retardation of water and small molecular weight solutes. The mucin network may immobilise water molecules to form the equivalent of an unstirred water layer (Smithson *et al*, 1981) or it may hold water molecules in a structured form, such as to make them unavailable for free diffusion (Williams and Turnburg, 1980). The mesh structure of the mucin network may also provide a diffusional barrier by increasing the tortuosity of the diffusion pathway and the negatively charged residues on the mucin molecule may confer some sort of electrical repulsion, especially to neutral or positively charged species (Lee and Nicholls, 1987).

The characteristic dip represents a region where the SDC of water has decreased. This increased restriction of water diffusion in this region may reflect a lowering of unbound water content caused by the dry alginate matrices dehydrating the mucus. Dehydration of mucus involves removing water from the mucus, more specifically, water that is freely available to diffuse from the mucus into the alginate matrix. This effectively increases the proportion of water bound by the mucin molecules, which will also increase the diffusion retarding ability of mucus. Mucus dehydration will effectively increase the concentration of mucin in the mucus gel, thus increasing its contribution to the retarding of diffusion (Smith *et al*, 1986). Also, Li *et al*, 1996, used Fourier transform pulsed field gradient spin echo ^{1}H-NMR to show that the fraction of bound water increases with increasing concentration of mucin. Further work studying the T_2 relaxation times of water bound to mucin during bioadhesion needs to be carried out.

The autofluorescence of mucus directly adjacent to the dry alginate matrices was observed to increase over time. The autofluorescence of mucus is proportional mucin concentration (figure 5.6), suggesting an increase in the concentration of mucin over time. This region of increasingly fluorescent mucus appeared to correspond with that part of the SDC profile containing the characteristic dip (figures 7.5a-7.5b and 8.5a-8.5b).

Visual evidence and the SDC profiles (figures 7.5a-7.5b and 8.5a-8.5b) show that the dry alginate matrices form hydrated viscous alginate gel layers and as mucus is the only source of water available in the sample geometry used, it is reasonable to deduce that hydration of dry alginate and the formation of the viscous layer may be the underlying mechanism causing mucus dehydration.

Electron micrographs showed that the dry alginate matrices were porous (figures 2.3 and 2.4), suggesting that capillary suction may be an underlying mechanism of mucus dehydration. Matrix porosity and capillary suction were thought to be important mechanisms controlling the uptake of saline by the dry alginate matrices. The influence of molecular weight, M:G ratio and particle size on the saline uptake of alginate matrices was not reflected in the W_a and F_{max} values (tables 7.3, 8.3 and 9.2) of the bioadhesive bonds or in the SDC profiles (figures 7.1a-7.1b and 8.1a-8.1b), suggesting

that capillary suction effect may not be an important factor in the bioadhesion of dry alginate matrices or in the dehydration of mucus.

The independence of mucus dehydration on molecular weight and M:G ratio is also reflected by the rate of transport (R_T) values of fluorescently tagged dextrans in the mucus region of the bioadhesive bond (tables 7.2 and 8.2). However, native mucus has been shown to retard diffusion of molecules greater than ≈14 kDa (Desai and Vadgama, 1991, and Williams and Turnberg, 1980), which may obviously affect the R_T values of the 580 kDa FITC-dextran used in this study. In contrast, Sigma mucin has a viscous liquid-like network structure, completely dissimilar to the elastic gel structure of native mucus, which may have a significantly influence on the diffusion of the dextran. In addition, large linear, flexible polymers may diffuse by the phenomenon of reptation. Further work needs to be carried out on this technique to see if mucus is exerting a molecular sieve effect on the diffusion of solutes.

The flexible, linear conformation of alginate may facilitate interdiffusion and entanglement of the alginate chains with the mucin gel network. Linear polyethylene glycol molecules (PEG) of up to 570,000 Da may interpenetrate a polymer gel network (Sahlin and Peppas, 1997). Detachment force testing showed that bioadhesive bonds formed by dry 220,000 Da or 315,000 Da alginate matrices had significantly stronger work of adhesion (W_a) values than bonds formed by dry matrices of 35,000 Da alginate ($p<0.02$) (table 7.3). The longer chains of the 220,000 Da and 315,000 Da alginates may form a more entangled interaction with the mucin network than the shorter chains of the 35,000 Da alginate. The more entangled polymer networks may take a longer time and more work to untangle and separate than less entangled networks. The relationship between molecular weight and alginate solution viscosity, which shows that viscosity is scaled to molecular weight, provides supporting evidence to suggest this mechanism (table 2.1).

The relative proportion of M and G blocks in alginate may influence the flexibility of the alginate chain, since polymannurate blocks are more flexible than polyguluronate blocks (Smidsrod and Draget, 1996), which may in turn affect the ability of the alginate chains to interpenetrate the mucin network. The W_a and F_{max} values of bioadhesive

bonds formed by low and high G alginate matrices were not significantly different ($p>0.05$), which suggests that polymer interpenetration is not a major factor in the bioadhesion of dry alginate matrices. However, the alginates used in this study were approximate 60:40 and 30:70 M:G ratios, which may not be significantly different in respect to alginate chain flexibility. Further work in this area is needed before attributing polymer interpenetration as a mechanism not involved in dry alginate bioadhesion.

The chemical structure of alginate (figure 1.2) showed that alginate molecules have a large number of –COOH groups, which may be able to H-bond to mucus glycoprotein (Tobyn *et al*, 1992). The number and density of these groups will increase with increasing molecular weight, but will not be affected by M:G ratio although their availability to bond with mucin may be. This suggests that secondary chemical bonding may be important in the bioadhesion of dry alginate matrices.

The evidence put forward by these studies suggests that the bioadhesion of dry alginate matrices may involve several different mechanisms, such as mucus dehydration, polymer interpenetration and secondary chemical bonding. These different mechanisms may occur simultaneously or may become predominant at different stages of bioadhesion.

10.1.2. Bioadhesion of prehydrated alginate matrices

In bioadhesive bonds formed by prehydrated alginate matrices, a surface viscous alginate gel layer will form the intimate contact with mucus and the bioadhesive bond. Cryogenic sections of alginate matrices after 10 mins of hydration (figure 2.5) showed two distinct regions within the viscous alginate gel layer. The outer region was extensively and evenly hydrated and the inner region was poorly and less evenly hydrated. The hydration of the inner gel layer became progressively uneven with increasing proximity to the dry alginate core. The structure of the viscous gel layers formed by the range of alginates matrices used in this project were similar to each other and were similar to SIF hydrated viscous alginate gel layers (Hodson *et al*, 1995). The

The diffusion retarding properties of this viscous alginate gel layer seemed to influence the dehydration of mucus by the prehydrated alginate matrices. The SDC profile of water inside the bioadhesive bonds formed by the 35,000 Da alginate matrix developed a characteristic dip, similar but smaller to those observed in the SDC profiles of bonds formed by dry alginate matrices (figure 7.6a). In contrast, the SDC profiles of the 220,000 Da and 315,000 Da alginates did not develop similar characteristic dips in their profiles (figures 7.6b and 7.6c). The SDC profiles of bonds formed by low G alginate matrices, which had molecular weights of ≈220,000 Da, also did not develop characteristic dips in their profile (figure 8.6b).

The hydrated alginate chains in the outer viscous gel region form a physically entangled mesh, which provides a diffusion retarding barrier to the ingress of water from the mucus into the dry matrix core. The extent to which the gel layer retards diffusion is dependent on the molecular weight and viscosity of the hydrophilic polymer (Alderman, 1984). The higher molecular weight alginate chains cause more entanglements per polymer chain than lower molecular weight alginate, resulting in more tortuous mesh network. It seems that this effect is independent of molecular weight, in respect to the bioadhesion of prehydrated alginate matrices.

However, the relationship between molecular weight of alginate and mucus dehydration was not reflected in the W_a and F_{max} values of bioadhesive bonds formed by the prehydrated alginate matrices (table 7.4), suggesting that the dehydration of mucus directly adjacent to the alginate matrix was not a major factor involved in the bioadhesion of prehydrated alginate matrices. The relationship between molecular weight and the W_a and F_{max} values was similar to that observed in the bioadhesive bonds formed by dry alginate matrices, but in that case only W_a was affected (table 7.3). This again suggests that mechanisms, such as polymer interpenetration and secondary chemical bonding, which are dependent on molecular weight, may be involved in the bioadhesion of prehydrated alginate matrices.

The mobility of fluorescent solutes (R_T) in the mucus region of the bioadhesive bond was not influenced by molecular weight or M:G ratio of the alginate (table 7.2 and 8.2). This was surprising given that the SDC of water in this region was influenced by

molecular weight (figures 7.6a-7.6c). This suggests that the diffusion of the 580 kDa fluorescently tagged dextran was affected by some sort of molecular sieve effect of the mucus, even though the rheology of Sigma mucin used in this study suggests a viscous liquid-like polymer structure and is dissimilar to native or purified mucus. Further work needs to be carried out on this technique to see whether this type of phenomena is occurring.

The evidence put forward by these studies suggest that the bioadhesion of prehydrated alginate matrices was similar to that of dry alginate matrices, except that the role of mucus dehydration in bioadhesion is dependent on the molecular weight and viscosity of the alginate.

10.1.3. The effect of mucus type on the bioadhesion of alginate matrices

The type of mucus used to form a bioadhesive bond may significantly influence the underlying mechanisms of bioadhesion. This project (table 2.7) and other studies (Kocervar-Nared *et al*, 1997, and Madsen *et al*, 1996) have shown that different types of gastric mucus had different rheological properties, in particular reconstituted freeze-dried gastric mucins were completely dissimilar to native or purified gastric mucus. These commercially and readily available freeze-dried mucins may contain salts, which can decrease the bioadhesive potential of some adhesive polymer, for example polyacrylic acids (Rossi *et al*, 1995).

In this study, the diffusion of water inside the bioadhesive bond formed by alginate matrices seemed to be influenced by the type of mucus. This effect is clearly observed in bioadhesive bonds formed by dry alginate matrices. In the bioadhesive bonds formed by purified pig gastric mucin (figure 7.1b), the diffusion fronts contained a sharp increase in SDC near the viscous gel-core interface, indicating a region of Case II transport (Valtier *et al*, 1995). The diffusion fronts correspond to the hydrating viscous alginate gel layers formed by the dry alginate matrices as a result of mucus dehydration. In comparison, a similar sharp increase in the SDC of water was not observed in the diffusion fronts of bioadhesive bonds formed by Sigma partially purified pig gastric mucin (figure 5.3).

As mentioned previously, Sigma mucin has a viscous liquid-like network structure (table 2.7), which is completely dissimilar to the elastic gel structure of native or purified mucus. The polymer structure of native mucin, in particular the glycosylated region of the mucin molecule (Turner *et al*, 1985), may immobilise water molecules in a structured form (Williams and Turnburg, 1980), making them unavailable for free diffusion and forming a type of unstirred water layer (Smithson *et al*, 1981). Case II transport occurs predominantly in glassy polymers (Crank, 1975), suggesting that the viscous gel layer in bonds formed by purified pig mucus are more glassy and thus less hydrated than viscous gel layers in bonds formed with Sigma mucin. Together, this suggests that purified and native mucus may have less water available for the hydration of polymers, such as alginate, than Sigma mucin.

The availability of water for hydration of the adhesive polymer may have considerable implications in bioadhesive bonds where the adhesive polymer has the potential to over hydrate and form a slippery mucilage with low cohesive and adhesive strength. In these polymers, the type of mucus may have a significant effect on the bioadhesive bond strength and properties.

10.2. Further work

Since this project developed several novel methods to study certain properties of bioadhesive bonds, time only allowed a small range of alginates and physicochemical factors to be investigated. It would be interesting to use these techniques to conduct a more in depth study investigating the influence of a wider range of physicochemical factors on the bioadhesion of alginate. It would also be interesting to use other bioadhesive test methods, particularly surface thermodynamic analysis, rheological testing and ATR-FTIR, to study the bioadhesive interaction between alginate and mucus.

The methods developed in this project may cope equally well with liquid formulations as well as solid formulations. Thus, it would be interesting to study how the bioadhesion of alginate solutions differs to that of solid alginate. It would also be interesting to use these techniques to study the formation of bioadhesive bonds by other adhesive polymers, in particular, well-known adhesives such as carbopol or sodium CMC.

The fluorescence photobleaching technique developed in this project to measure the mobility of fluorescent solutes inside bioadhesive bonds has a few limitations. Firstly, the method can only measure R_T in a single localised spot, thus providing limited information on solute mobility and polymer network tortuosity inside bioadhesive bonds. Secondly, the molecular size of the fluorescently tagged marker may be susceptible to a molecular sieve effect of mucus. Therefore, this technique needs to be further developed in order to determine simultaneous R_T at multiple locations throughout the bioadhesive bond and to counter-act the molecular sieve effect of mucus. The mathematical model used to analyse fluorescence recovery in this technique may be easily adapted to produce a Koppel-like multipoint analysis photobleaching technique.

It was also noticed that the mucus layer directly adjacent to the alginate matrices in bioadhesive bonds formed by dry alginate matrices became more fluorescent over time, which was attributed to an increase in mucin concentration and suggested the dehydration of mucus by the alginate matrix. Therefore, it may be possible to measure the dehydration of mucus by adhesive polymer by fluorescently imaging the bioadhesive bond. This would be a positive addition to the range of techniques used to study bioadhesion. This technique would be able to spatially resolve patterns of hydration inside a bioadhesive bond and fluorescence microscopes are considerably cheaper than NMR microscopes.

Finally, the detachment force test used in this project produced variable results, which were attributed to the flexibility of mucosal tissue, and may colour the observed bioadhesive bond strength of some polymer. Therefore, further work should concentrate on developing methods either to measure and account for flexibility in mucosal tissue or to standardise the flexibility of mucosal tissue.

Bibliography

Alderman, D.A. (1984) *A review of cellulose ethers in hydrophilic matrices for oral controlled-release dosage forms.* Int. J. Pharm. Tech. & Prod. Mfr., 5, (3), 1-9.

Ahuja, A., Khar, R.K. and Ali, J. (1997) *Mucoadhesive drug delivery systems.* Drug Dev. Ind. Pharm., 23, (5), 489-515.

Allen, A. (1981) *Structure and function of gastrointestinal mucus.* In: Physiology of the intestinal tract. Ed. Johnson, L.R., Raven Press, New York, 617-639.

Allen, A. (1983) *Mucus - a protective secretion of complexity.* Trends. Biochem. Sci., 8, 169-173.

Allen, A. (1998) *Personal communication.*

Allen, A. and Carroll, N.J.H. (1985) *Adherent and soluble mucus in the stomach and duodenum.* Digest. Diseases Sci., 30, (11), 55S-62S.

Allen, A. and Pearson, J.P. (1993) *Mucus glycoproteins of the normal gastrointestinal tract.* In: Mucus glycoproteins in the gastrointestinal tract. Ed. Corfield, T. 193-199.

Allen, A. (1989) *Gastrointestinal mucus.* In: Handbook of physiology - The gastrointestinal system III. Ed. Forte, J.G., Amer. Physiol. Soc., 359-382.

Allen, A., Cunliffe, W.J., Pearson, J.P., Sellars, L.A. and Ward, R. (1984) *Studies on gastrointestinal mucus.* Scan. J. Gastro., 19, 107-114.

Allen, A., Flemstrom, G., Garner, A. and Kivilaakso, E. (1993) *Gastroduodenal mucosal protection.* Physio. Rev., 73, (4), 823-857.

Andrade, J.D., King, R.N., Greggonis, D.E. and Coleman, D.L. (1979) *Surface characterisation of poly(hydroxyethyl methacrylate) and related polymers. I. Contact angle methods in water.* J. Polym. Sci. Polym. Symp., 66, 313-336.

Anlar, S., Capan, Y., Guvan, O., Gogus, A., Dalkara, T., and Hincal, A.A. (1994) *Formulation and in vitro-in vivo evaluation of buccoadhesive morphine sulfate tablets.* Pharm. Res., 11, (2), 231-236.

Ashraf, M., Iuorno, V.L., Coffin-Beach, D., Anderson Evans, C. and Augsberger, L.L. (1994) *A novel nuclear magnetic resonance (NMR) imaging method for measuring the water front peneration rate in hydrophilic polymer matrix capsule plugs and its role in drug release.* Pharm. Res., 11, (5), 733-737.

Axelrod, D., Koppel, D.E., Sclessinger, J., Elson, E., and Webb, W.W. (1976) *Mobility measurement by analysis of fluorescence photobleaching recovery kinetics.* Biophys. J., 16, 1055-1069.

Bansil, R., Stanley, E. and LaMont, J.T. (1995) *Mucin biophysics.* Annual Rev. Physiol., 57, 635-657.

Bell, A.E. (1983) *Physical studies on the structure of gastric mucus gel.* Ph.D. Thesis, University of Newcastle.

Bell, A.E., Allen, A., Morris, E.R. and Ross-Murphy, S.B. (1984) *Functional interactions of gastric mucus glycoprotein.* Int. J. Macromol., 6, 309-315.

Bell, A.E., Sellars, L.A., Allen, A., Cunliffe, W.J., Morris, E.R. and Ross-Murphy, S.B. (1985) *Properties of gastric and duodenal mucus: Effect of proteolysis, disulfide reduction, bile, acid, ethanol and hypertonicity on mucus gel structure.* Gastroenetrol., 88, 269-280.

Bhat, P.G., Flanagan, D.R. and Donovan, M.D. (1995) *The limiting role of mucus in drug absorption: Drug permeation through mucus solution.* Int. J. Pharm., 126, 179-187.

Blanco-Fuente, H., Vila-Dorrio, B., Anguiano-Igea, S., Otero-Espinar, F.J. and Blanco-Mendez, J. (1996) *Tanned leather: a good model for determining hydrogels bioadhesion.* Int. J. Pharm., 138, 103-112.

Blonk, J.C.G., Don, A., Van Aalst, H. and Birmingham, J.J. (1993) *Fluorescence photobleaching recovery in the confocal laser scanning microscope.* J. Micros., 169, (3), pp363-374.

Bodde, H.E., DeVries, M.E. and Junginger, H.E. (1990) *Mucoadhesive polymers for the buccal delivery of peptides, structure-adhesiveness relationships.* J. Contr. Rel., 13, 225-231.

Bouckaert, S., Lefebvre, R.A. and Remon, J.P. (1993) *In vitro/in vivo correlation of the bioadhesive properties of a buccal bioadhesive miconazole slow-release tablet.* Pharm. Res., 10, (6), 853-856.

Bowtell, R.W. (1998) *Personal communication.*

Bowtell, R.W., Brown, G.D., Glover, P.M. McJury, M. and Mansfield, P. (1990) *Resolution of cellular structures by NMR microscopy at 11.7T.* Proc. R. Soc. Lond. A 333, 457-467.

Bowtell, R.W., Sharp, J.C., Paters, A., Mansfield, P., Rajabi-Siahboomi, A.R. and Melia, C.D. (1994) *NMR microscopy of hydrating hydrophilic matrix pharmaceutical tablets.* Mag. Res. Imag., 12, (2), 361-364.

British Pharmacopoeia (1998) I & II, HMSO

Brunger, A. Peters, R. and Schulten, K. (1985) *Continuous fluorescence microphotolysis to observe lateral diffusion in membranes. Theoretical methods and applications.* J. Chem. Phys., 82, 2147-2160.

Buckton, G and Cappucinello, M.M. (1998) *Modelling mucoadhesion by use of surface energy terms obtained by the Lewis acid-Lewis base approach. III. An interaction between Teflon and Carbopol.* Pharm. Res., 15, (3), 502-503.

Carlstedt, I., Hermann, A., Hovenberg, H., Lindel, G., Nordman, H., Wickstrom, C. and Davies, J.R. (1995) *Soluble and insoluble mucins - Identification of distinct populations.* Biochem. Soc. Trans., 23, 845-851.

Carlstedt, I., Sheehan, J.K., Corfield, A.P. and Gallagher, J.T. (1985) *Mucous glycoproteins: A gel of a problem.* Essays Biochem., 20, 40-76.

Chickering III, D.E. and Mathiowitz, E. (1995a) *Bioadhesive microspheres. I. A novel electrobalance-based method to study adhesive interactions between individual microspheres and intestinal mucosa.* J. Contr. Rel., 34, (3), 251-261.

Chickering III, D.E., Jacob, J.S. and Mathiowitz, E. (1995b) *Bioadhesive microspheres. II. Characterisation and evaluation of bioadhesion involving hard, bioerodible polymers and soft tissue.* React. Poly., 25, 189-206.

Chickering III, D.E., Jacob, J.S., Desai, T.A., Harrison, M., Harris, W.P., Morrell, C.N., Chauturvedi, P. and Mathiowitz, E. (1997) *Bioadhesive microspheres. III. An in vivo transit and bioavailability study of drug-loaded alginate and poly(fumaric-co-sebacic anhydride) microspheres.* J. Contr. Rel., 48, 35-46.

Christmann, V., Rosenberg, J., Seega, J. and Lehr, C. M. (1997) *Simultaneous in vivo visualisation and localisation of solid oral dosage forms in the rat gastrointestinal tract by magnetic resonance imaging (MRI).* Pharm. Res., 14, 1066-1072.

Clamp, J.R. and Creeth, J.M. (1984) *Some non-mucin components of mucus and their possible biological roles.* In. Mucus and mucosa. Pitman, London (Ciba Foundation symposium 109). 121-163.

Clare, K. (1993) *Algin.* In. Industrial gums. Polysaccharides and their derivatives. Ed. Whistler, R.L. and BeMillar, J.N., 3rd Edn., Academic Press, Inc.

Cottrell, I.W. and Kovacs, P. (1980) *Alginates.* In. Handbook of water-soluble gums and resins. Ed. Davidson, R.L., McGraw-Hill, New York.

Crank, J. (1975) *The mathematics of diffusion.* 2nd Edition, Oxford University Press, Oxford.

Cutts, L.S. (1994) *Applications of the confocal laser scanning microscope in pharmaceutical research.* Ph.D. Thesis, Nottingham University.

Cutts, L.S., Roberts, P.A., Adler, J., Davies, M.C. and Melia, C.D. (1995) *Determination of localised diffusion coefficients in gels using confocal scanning microscopy.* J. Micros., 180, (2), 131-139.

Degim, Z. and Kellaway, I.W. (1998) *An investigation of the interfacial interaction between poly(acrylic acid) and glycoprotein.* Int. J. Pharm., 175, 9-16.

Desai, M.A. and Vadgama, N.P. (1991) *Estimation of effective diffusion coefficients of model solutes through gastric mucus: Assessment of a diffusion chamber technique based on spectrophotometric analysis.* Analyst, 116, 1113-1116.

Dinarvind, R., Wood, B. and D'Emanuele, A. (1995) *Measurement of the diffusion of 2,2,2-trifluoroacetamide within thermoresponsive hydrogels using NMR imaging.* Pharm. Res., 12, (9), 1376-1379.

Dixon, A. (1998) *Resolution, sensitivity, speed.* Appl. Note, 102, BioRad Microscience Division.

Draget, K.I. and Smidsrod, O. (1998a) *The effect of molecular weight on alginate gels.* 2nd Biopol. Res. Conf., University of Newcastle.

Draget, K.I., Simensen, M.K., Onsoyen, E. and Smidsrod, O. (1998b) *Use of G-block polysacharides.* Int. Pat. Appl. WO 98/02488.

Draget, K.I., Skjak-Braek, G. and Smidsrod, O. (1994) *Alginic acid gels: The effect of alginate chemical composition and molecular weight.* Carb. Polym., 25, 31-38.

Draget, K.I., Skjak-Braek, G., Christensen, B.E. and Gaserod, O. (1996) *Swelling and partial solubilisation of alginic acid gel beads in acidic buffer.* Carb. Polym., 29, (3), 209-215.

Duce, S.L. and Hall, L.D. (1995) *Visualisation of the hydration of food by nuclear magnetic resonance imaging.* J. Food Eng., 26, 251-257.

Duce, S.L., Amin, M.H.G., Horsfield, M.A., Tyszka, M and Hall, L.D. (1995) *Nuclear magnetic resonance imaging of dairy products in 2-dimensions and 3-dimensions.* Int. Dairy J., 5, (4), 311-319.

Duchene, D. and Ponchel, G. (1992) *Principle and investigation of the bioadhesion mechanism of the solid dosage form.* Biomaterials., 13, (10), 709-714.

Durrer, C., Irache, J.M., Puisieux, F., Duchene, D. and Ponchel, G. (1994a) *Mucoadhesion of latexes. I. Analytical methods and kinetic studies.* Pharm. Res., 11, (5), 674-679.

Durrer, C., Irache, J.M., Puisieux, F., Duchene, D. and Ponchel, G. (1994b) *Mucoadhesion of latexes. II. Adsorption isotherms and desorption studies.* Pharm. Res., 11, (5), 680-683.

Elson, E.L. and Magde, D. (1974) *Fluorescence correlation spectroscopy. I Conceptual basis and theory.* Biopolymers, 13, 1-27.

Esposito, P., Colombo, I. and Loverich, M. (1994) *Investigation of surface properties of some polymers by a thermodynamic and mechanical approach: possibility of predicting mucoadhesion and biocompatibility.* Biomaterials, 15, (3), 177-182.

Fahie, B.J. Nangia, A., Chopra, S.K. Fyfe, C.A., Grondey, H. and Blazek, A. (1997) *Use of NMR imaging in the optimisation of a compression-coated regulated release system.* J. Contr. Rel., 51, 179-184.

Feder, T.J., Brust-Mascher, I., Slattery, J.P., Baird, B. and Webb, W.W. (1996) *Constrained diffusion or immobile fraction on cell surfaces: A new interpretation.* Biophys. J., 70, 2767-2773.

Ferrari, F., Bertoni, M., Bonferoni, M. C., Rossi, S., Gazzaniga, A., Conte, U. and Caramella, C. (1995) *Influence of porosity and formula solubility on disintegrant efficiency in tablets.* STP Pharm. Sci., 5, (2), 16-121.

Ferrari, F., Bertoni, M., Caramella, C. and Waring, M. J. (1994) *Comparative-evaluation of hydrocolloid dressings by means of water- uptake and swelling force measurements.* Int. J. Pharm., 112, (1), 29-36.

Ferrari, F., Geddo, M., Gazziniga, A., Carmella, C. and Conte, U. (1988) *Water uptake to fast disintegrating tablets and Weibull function* S.T.P. Pharma., 4, 481-484.

Fiebrig, I., Varum, K.M., Harding, S.E., Davis, S.S. and Stokke, B. (1997) *Colloidal gold and colloidal gold labelled wheat germ agglutinin as molecular probes for identification in mucin/chitosan complexes.* Carb. Polym., 33, 91-99.

Fiebrig, I., Harding, S.E. and Davis, S.S. (1994) *Sedimentation analysis of potential interactions between mucins and a putative bioadhesive polymer.* Prog. Coll. Polym. Sci., 93, 66-73.

Fiebrig, I., Harding, S.E., Rowe, A.J., Hyman, S.C. and Davis, S.S. (1995) *Transmission electron microscopy studies on pig gastric mucin and its interaction with chitosan.* Carb. Polym., 28, 239-244.

Florence, A.T. and Attwood, D. (1988) *Physicochemical principles of pharmacy.* 2nd Ed., MacMillan Press Ltd, London.

Foster, S.N.E., Pearson, J.P., Hutton, D.A., Allen, A. and Dettmar, P.W. (1994) *Interactions of polyacrylates with porcine pepsin and the gastric mucus barrier-A mechanism for mucosal protection.* Clin. Sci., 87, (6), 719-726.

Forstner, J.F. and Forstner, G.G. (1994) *Gastrointestinal mucus.* In: Physiology of the intestinal tract. 3rd Edn., Ed. Johnson, L.R., Raven press, New York, 1255-1282.

Fyfe, C.A. and Blazek, A.I. (1997) *Investigation of hydrogel formation from hydroxypropylmethylcellulose (HPMC) by NMR spectroscopy and NMR imaging techniques.* Macromol., 30, (20), 6230-6237.

Fyfe, C.A. and Blazek, A.I. (1998) *Complications in investigation of the swelling of hydrogel matrices due to the presence of trapped gas.* J. Contr. Rel., 52, 221-225.

Gacesa, P. (1988) *Alginates.* Carb. Polym., 8, 161-182.

Gaserod, O., Joliffe, I.G., Hampson, F.C., Dettmar, P.W. and Skjak-Brack, G. (1998) *The enhancement of the bioadhesive properties of calcium alginate gel beads by coating with chitosan.* Int. J. Pharm., 175, 237-246.

Gissenger, D. and Stamm, A. (1980) *Comparative evaluation of the properties of some tablet disintegrants.* Drug Dev. Ind. Pharm., 6, 511-536.

Glicksman, M. (1987) *Utilisation of seaweed hydrocolloids in the food industry.* In. Hydrobiologia. Ed Ragan, M.A. and Bird, C.J., 12th Int. Seaweed Symp, 151-152, 31-47.

Gorden, N., Loy, S. and Wells, N. (1991) *Alginates, xanthan gum and gellan gum seminar.* Conf. Proc., University of Nottingham, Kelco Int.

Grant, G.T., Morris, E.R., Rees, D.A., Smith, P.J.C. and Thom, D. (1973) *Biological interactions between polysaccharides and divalent cations: The egg-box model.* Febs Lett., 32, (1), 195-198.

Grasdelen, H., Larsen, B. and Smidsrod, O. (1977) ^{13}C-N.M.R. studies of alginate. Carb. Res., 56, C11-C15.

Grebenkamper, K and Galla, H.J. (1994) *Translational diffusion measurements of a fluorescent phospholipid between MDCK-I cells support the lipid model of the tight junctions.* Chem. Phys. Lipids, 71, 133-143.

Green, H.C. (1936) *Process for making alginic acid and product.* U.S. Pat. No. 2,036,934.

Gribbon, P. and Hardingham, T. E. (1998) *Macromolecular diffusion of biological polymers measured by confocal fluorescence recovery after photobleaching.* Biophys. J., 75, 2, 1032-1039

Gum, J.R. (1995) *Mucins: Their structure and biology.* Biochem. Soc. Trans., 23, 795-799.

Gupta, P.K., Leung, S.H.S. and Robinson, J.R. (1990) *Bioadhesives/mucoadhesives in drug delivery to the gastrointestinal tract.* In: Bioadhesive dug delivery systems. Ed. Lenaerts, V. and Gurny, R. CRC Press, Boca raton, Florida.

Hall, A., Browne, M. & Howard, V. (1991) *Confocal microscopy-the basics explained.* Proceedings RMS, 26, (2), 63-68.

Harding, S.E. (1989) *The macro structure of mucus glycoproteins in solution.* Adv. Carb. Chem. Biochem., 47, 345-381.

Harding, S.E., Davis, S.S., Deacon, M.P. and Fiebig, I. (1999) *Biopolymer mucoadhesives.* Biotech. Genet. Eng. Rev., 16, 41-86.

Hassan, E.E. and Gallo, J.M. (1990) *A simple rheological method for the in vitro assessment of mucin-polymer bioadhesive bond strength.* Pharm. Res., 7, (5), 491-495.

Haug, A. and Smidsrod, O. (1965) *Fractionation of alginates by precipitation with calcium and magnesium ions.* Acta Chem. Scand., 19, 1221-1226.

Haug, A., Larson, B. and Smidsrod, O. (1966) *A study of the constitution of alginic acid by partial acid hydrolysis.* Acta Chem. Scand., 20, 183-190.

Haugland, R.P. (1992) *Handbook of fluorescent probes and research chemicals* 5th edition, Molecular Probes Inc, Eugene, U.S.A.

He, P., Davis, S.S., Illum, L. (1998) *In vitro evaluation of the mucoadhesive properties of chitosan microspheres.* Int. J. Pharm., 166, 75-68.

Helliwell, M. (1993) *The use of bioadhesives in targeted delivery within the gastrointetstinal tract.* Adv. Drug Del. Rev., 11, 221-251.

Hills, B. (1995) *Food processing: A MRI perspective.* Trends Food Sci. Tech., 6, pp111-117.

Hodsdon, A. C., Mitchell, J. R., Davies, M. C., Melia, C. D. (1995) *Structure and behavior in hydrophilic matrix sustained-release dosage forms. 3. The influence of pH on the sustained-release performance and internal gel structure of sodium alginate matrices.* J. Contr. Rel., 33, 1, 143-152.

Hodson, A.C. (1994) *Xanthan gum and sodium alginate as sustained-release carriers in hydrophilic matrix tablets.* Ph.D. Thesis, University of Nottingham.

Huang, Z.P. and Thompson, N.L. (1993) *Theory for two-photon excitation in pattern photobleaching with evanescent illumination.* Biophys. J., 47, (3), 241-249.

Hugo, W.B. and Russell, A.D. (1987) *Pharmaceutical Microbiology, 4th Ed.* Blackwell Scientific Publications, Oxford.

Hutton, D.A. (1991) *Studies on mucin isolation and proteolysis.* Ph.D. Thesis, University of Newcastle.

Hutton, D.A.. Pearson, J.P., Allen, A. and Foster, S.N.E. (1990) *Mucolysis of the colonic mucus barrier by faecal proteinases.* Clin. Sci., 78, 265-271.

Hyde, T.M., Gladden, L.F. and Payne, R. (1995) *A nuclear magnetic resonance imaging study of the effect of incorporating a macromolecular drug in poly(glycolic acid-co-DL-lactic acid).* J. Contr. Rel., 36, 261-275.

Illan, E., Amselem, S., Weisspapir, M., Schwarz, J., Yogev, A., Zawoznik, E. and Friedman, D. (1996) *Improved oral delivery of desmopressin via a novel vehicle mucoadhesive submicron emulsion.* Pharm. Res., 13, (7), 1083-1087.

Inoue, S. (1990) *Foundations of confocal scanned imaging in light microscopy.* In: Handbook of biological confocal microscopy. Ed. J.B. Pawley, Plenum Press, New York.

Irache, J.M., Durrer, C., Duchene, D. and Ponchel, G. (1994) *In vitro study of lectin-latex conjugates for specific bioadhesion.* J. Contr. Rel., 31, 181-188.

Jabbari, E. and Peppas, N.A. (1994) *Polymer-polymer interdiffusion and adhesion.* J.M.S.-Rev. Macromol. Chem. Phys., C34, (2), 205-241.

Jabbari, E., Wieniewski, N. and Peppas, N.A. (1993) *Evidence of mucoadhesion by chain interpenetration at a poly(acrylic acid)/mucin interface using ATR-FTIR spectroscopy.* J. Contr. Rel., 26, 99-108.

Jacques, Y. & Buri, P. (1992) *Optimisation of an ex vivo method for bioadhesion quantification.* Eur. J. of Pharm. Biopharm., 38, (6), 195-198.

Jeacoke, R. *Confocal microscopy in the food industry.* Appl. Note, BioRad Microscience Division, 1, 1-5

Jimenez-Castellanos, M.R., Zia, H. and Rhodes, C.T. (1993) *Assessment of an in vitro method for measuring the bioadhesiveness of tablets.* Int. J. Pharm., 89, 223-228.

Jones, D.S., Woolfson, A.D., Brown, A.F. (1997) *Textural, viscoelastic and mucoadhesive properties of pharmaceutical gels composed of cellulose polymers.* Int. J. Pharm., 151, (2), 223-233.

Kaeble, D.H. and Moacanin, J (1977) *A surface energy analysis of bioadhesion.* Polymer, 18, 475.

Kearney, P. and Marriott, C. (1987) *The effects of mucus glycoproteins on the bioavailability of tetracycline. III. Everted gut studies.* Int. J. Pharm., 38, 211-220.

Kelco. *Alginate products for scientific water control, 3rd Ed.* Kelco, Merck & Co. Inc.

Kerr, L.J., Kellaway, I.W., Rowlands, C. and Parr, G.D. (1990) *The influence of poly(acrylic) acids on the rheology of glycoprotein gels.* Proc. Int. Symp. Contr. Rel. Bioact. Mat., 17, 122-123.

Kerss, S., Allen, A. and Garner, A. (1982) *A simple method for measuring thickness of the mucus gel layer adherent to rat, frog and human gastric mucosa: Influence of feeding, prostaglandins, N-acetylcysteine and other agents.* Clin. Sci., 63, 187-195.

Knight, J. (1997) *Personal communication.*

Kocevar-Nared, J., Kristl, J., and Smid-Korbar, J. (1997) *Comparative rheological investigation of crude gastric mucin and natural gastric mucus.* Bioamaterials, 18, 677-681.

Koppel, D.E. (1979) *Fluorescence redistribution after photobleaching. A new multipoint analysis of membrane translational dynamics.* Biophys. J., 28, 281-291.

Kubitscheck, U., Tschodrichrotter, M., Wedekind, P. and Peters, R. (1996) *2-photon scanning microphotolysis for 3-dimensional data-storage and biological transport measurements.* J. Micros., 182, (3), 225-233.

Kubitscheck, U., Wedekind, P. and Peters, R. (1994a) *Scanning microphotolysis: A new photobleaching technique based on fast intensity modulation of a scanned laser beam and confocal imaging.* Confocal and Near-field microscopy, April 25-28, Munich, Germany. Abstract.

Kubitscheck, U., Wedekind, P. and Peters, R.(1994b) *Lateral diffusion measurement at high spatial resolution by scanning microphotolysis in a confocal microscope.* Biophys. J., 67, 948-956.

Lardner, T.J. (1977) *The measurement of cell membrane diffusion coefficients.* J. Biomech., 10, 167-170.

Larhed, A.W., Artursson, P., Grasjo, J. and Bjork, E. (1997) *Diffusion of drugs in native and purified gastrointestinal mucus.* J. Pharm. Sci., 86, (6), 660-665.

Larsson, K. (1980) *Interfacial phenomena - Bioadhesion and biocompatability.* Desalination, 35, 105-114.

Lauterbur, P.C. (1973) *Image formation by induced local interactions: Examples employing nuclear magnetic resonance.* Nature, 242, 190-191.

Le Gloahec, V.C.E. (1938) *Method for treating seaweed.* U.S. Pat. No. 2,128,551.

Lee, S.P. and Nicholls, J.F. (1987) *Diffusion of charged ions in mucus gel: Effect of net charge.* Biorheology, 24, 565-569.

Lehr, C.M. (1998) *The molecular basis of bioadhesion.* J. Pharm. Pharmcol., 50(Suppl), 11.

Lehr, C.M. (1994) *Bioadhesion technologies for the delivery of peptide and protein drugs to the gastrointestinal tract.* Crit. Rev. Ther. Drug Carrier Sys., 11, (2&3), 119-160.

Lehr, C.M. (1996) *From sticky stuff to sweet receptors - Achievements, limits and novel approaches to bioadhesion.* Eur. J. Drug Metab. and Pharm., 21, 2, 139-148.

Lehr, C.M., Bouwstra, J.A., Bodde, H.E. and Junginger, H.E. (1992a) *A surface energy analysis of mucoadhesion: Contact angle measurements on polycarbophil and pig intestinal mucosa in physiologically relevent fluids.* Pharm. Res., 9, (1), 70-75.

Lehr, C.M., Bouwstra, J.A., Bodde, H.E. and Junginger, H.E. (1993) *A surface energy analysis of mucoadhesion II. Prediction of mucoadhesive performance by spreading coefficients.* Eur. J. Pharm. Sci., 1, 19-30.

Lehr, C.M., Bouwstra, J.A., Bodde, H.E., Spies, F., van Munsteren, C., Vermeij-Keers, C. and Junginger, H.E. (1990) *Surface energy analysis and visualisation studies of mucoadhesion.* Proc. Int. Symp. Contr. Rel. Bioact. Mater., 17, 91-92.

Lehr, C.M., Bouwstra, J.A., Kok, W., Noach, A.B.J., de Boer, A.G. and Junginger, H.E. (1992b) *Bioadhesion by means of specific binding of tomato lectin.* Pharm. Res., 9, (4), 547-553.

Lehr, C.M., Poelma, F.G.J., Junginger, H.E. and Tukker, J.J. (1991) *An estimate of turnover time of intestinal mucus gel layer in the rat in situ loop.* Int. J. Pharm., 70, 235-240.

Lejoyeux, F., Ponchel, G. and Duchene, D. (1989a) *Influence of some technological parameters on the bioadhesive characteristics of polyacrylic acid matrices.* STP Pharma, 5, 893-898.

Lejoyeux, F., Ponchel, G., Wouessidjewe, D., Peppas, N.A. and Duchene, D. (1989b) *Bioadhesive tablets influence of the testing medium composition on bioadhesion.* Drug. Dev. Ind. Pharm., 15, (12), 2037-2048.

LeNeel, T., MorletRenaud, C., Lipart, C., Gouyette, A., Truchaud, A. and Merle, C. (1997) *Image analysis as a new technique for the study of water uptake in tablets.* STP Pharma Sci., 7, (2), 117-122.

Leung, S.H.S. and Robinson, J.R. (1990) *Polymer structure features contributing to mucoadhesion II.* J. Contr. Rel., 12, 187-194.

Leussen, H.L., de Leeuw, B.J., Langemeyer, W. E., de Boer, A.G., Verhoef, J.C. and Junginger, H.E. (1996) *Mucoadhesive polymers in peroral peptide drug delivery. VI. Carbomer and chitosan improve the intestinal absorption of the peptide drug buserelin in vivo.* Pharm. Res., 13, (11), 1668-1672.

Li, C., Bhatt, P.P. and Johnston, T.P. (1998) *Evaluation of a mucoadhesive buccal patch for delivery of peptides: In vitro screening of bioadhesion.* Drug Dev. Ind. Pharm., 24, 10, 919-926.

Li, C.Y., Zimmerman, C.L. and Wiedmann, T.S. (1996) *Diffusivity of bile salt/phospholipid aggregates in mucin.* Pharm. Res., 13, (4), 535-541.

Lin, S. Y. and Lin, K. H. (1996) *Water uptake and drug release behaviour of drug-loaded compacts prepared from different grades of ethylcellulose.* Eur. J. Pharm. Biopharm., 42, (3), 193-198.

Linker, A and Jones, R.S. (1964) *A polysaccharide resembling alginic acid from a Psuedomonas micro-organism.* Nature, 204, 187-188.

Linker, A and Jones, R.S. (1966) *A new polysaccharide resembling alginic acid isolated from Psuedomonads.* J. Biol. Chem., 241, (16), 3845-3851.

Livingston, E.H., Miller, J. and Engel, E. (1995) *Bicarbonate diffusion through mucus.* Amer. J. Physiol., 269, G453-457.

Longer, M.A. and Robinson, J.R. (1986) *Fundamental aspects of bioadhesion.* Pharm. Int., 7, (5), 114-117.

Lopez, A., Dupou, L., Altibelli, A., Trotard, J. and Tocanne, J.F. (1988) *Fluorescence recovery after photobleaching (FRAP) experiments under conditions of uniform disk illumination.* Biophys. J., 53, 963-970.

Mader, K., Crennilleux, Y., Domb, A.J., Dunn, J.F. and Swartz, H.M. (1997) *In vitro/in vivo comparison of drug release and polymer erosion from biodegradable P(FAD-SA) polyanhydrides – A non-invasive approach by the combined use of electron paramagnetic resonance spectroscopy and nuclear magnetic resonance.* Pharm. Res., 14, (6), 821-826.

Madhu, B. Hjartstam, J. and Soussi, B. (1998) *Studies of the internal flow process in polymers by ^{1}H NMR microscopy at 500MHz.* J. Contr. Rel., 56, 95-104.

Madsen, F., Eberth, K. and Smart, J.D. (1996) *A rheological evaluation of various mucus gels for use in in-vitro mucoadhesion testing.* Pharm. Sci., 2, 563-566.

Madsen, F., Eberth, K. and Smart, J.D. (1998a) *A rheological assessment of the nature of interactions between mucoadhesive polymers and a homogenised mucus gel.* Biomaterials, 19, 1083-1092.

Madsen, F., Eberth, K. and Smart, J.D. (1998b) *A rheological examination of the mucoadhesive/mucus interaction: the effect of the mucoadhesive type and concentration.* J. Contr. Rel., 50, 167-178.

Maggi, L., Carena, E., Torre, M.L., Giunchedi, P. & Conte, U. (1994) *In vitro/ex vivo methods for the evaluation of bioadhesive polymers.* A preliminary report. S.T.P. Pharm. Sci., 4, (5), 343-348.

Mansfield, P. and Grannell, P.K. (1973) *NMR diffraction in solids?* J. Phys., C6, L422-426.

Mansfield, P. and Grannell, P.K. (1975) *Diffraction and microscopy in solids and liquids by NMR.* Phys. Rev., B12, 3618-3634.

Mantle, M and Allen, A. (1978) *A colourimetric assay for glycoproteins based on the Periodic acid/Schiff stain.* Biochem. Soc. Trans., 6, 607-609.

Marriot, C. and Gregory, N.P. (1990) *Mucus physiology and pathology.* In: Bioadhesive dug delivery systems. Ed. Lenaerts, V. and Gurny, R. CRC Press, Boca raton, Florida.

Marshall, P., Snaar, J.E.M., Bowtell, R.W., Dettmar, P.W., Onsoyen, E., Hampson, F.C. and Melia, C.D. (1998) *A study of the bioadhesive bond using magnetic resonance imaging and detachment force analysis.* Proc. Int. Symp. Contrl. Rel. Bioact. Mater., 25, 34-35.

Melia, C.D. (1991) *Hydrophilic matrix sustained release systems based on polysaccharide carriers.* Crit. Rev. Therap. Drug Carrier Sys., 8, (4), 395-421.

Melia, C.D., Rajabi-Siahboomi, A.R. and Bowtell, R.W. (1998) *Magnetic resonance imaging of controlled release pharmaceutical dosage forms.* Pharm. Sci. Tech. Today, 1, (1), 32-39.

Melia, C.D., Wheatstone, J., Cutts, L.S. and Marshall, P. (1999) Eur. J. Pharm. Biopharm., unpublished.

Mikos, A.G. and Peppas, N.A. (1989) *Measurement of the surface tension of mucin solutions.* Int. J. Pharm., 53, 1-5.

Mikos, A.G. and Peppas, N.A. (1990a) *Bioadhesive analysis of controlled-release systems. IV. An experimental method for testing the adhesion of microparticles with mucus.* J. Contr. Rel., 12, 31-37.

Mikos, A.G. and Peppas, N.S. (1990b) *Scaling concepts and molecular theories of adhesion of synthetic polymers to glycoproteinic networks.* In: Bioadhesive drug delivery systems. Ed. Lenaerts, V. and Gurny, R. CRC Press, Boca raton, Florida.

Mikos, A.G., Mathiowitz, E., Langer, R. and Peppas, N.A. (1991) *Interaction of polymer microspheres with mucin gels as a means of characterising polymer retention on mucus.* J. Coll. Interface Sci., 143, (2), 366-373.

Mitchell, J.R. and Blanshard, J.M.V. (1976) *Rheological properties of alginate gels.* J. Text. Stud., 7, 219-234.

Mitchell, K., Ford, J. L., Armstrong, D. J., Elliott, P. N. C., Hogan, J. E. and Rostron, C. (1993) *The influence of the particle-size of hydroxypropylmethylcellulose K15M on its hydration and performance in matrix tablets.* Int. J. Pharm., 100, (1-3), 175-179.

Morra, M. and Cassinelli, C. (1997) *Bacterial adhesion to polymer surfaces: A critical review of surface thermodynamic approaches.* J. Biomater. Sci. Polym. Edn., 9, (1), 55-74.

Mortazavi, S.A. and Smart, J.D. (1993) *An investigation into the role of water movement and mucus gel dehydration in mucoadhesion.* J. Contr. Rel., 25, 197-203.

Mortazavi, S.A. and Smart, J.D. (1994a) *An in-vitro method for assessing the duration of mucoadhesion.* J. Contr. Rel., 31, (2), 207-212.

Mortazavi, S.A. and Smart, J.D. (1994b) *Factors influencing gel-strengthening at the mucoadhesive mucus interface.* J. Pharm. Pharmcol., 46, 86-90.

Mortazavi, S.A. and Smart, J.D. (1995) *An investigation of some factors influencing the in vitro assessment of mucoadhesion.* Int. J. Pharm., 116, 223-230.

Mortazavi, S.A., Carpenter, B.G. and Smart, J.D. (1992) *An investigation of the rheological behaviour of the mucoadhesive/mucosal interface.* Int. J. Pharm., 83, 221-225.

Moussa, I. S., Lenaerts, V. and Cartilier, L. H. (1998) *Image analysis studies of water transport and dimensional changes occurring in the early stages of hydration in cross-linked amylose matrices.* J. Contr. Rel., 52, (1-2), 63-70.

Mumtaz, A. M. and Ch'ng, H.S. (1995) *Evaluation of bioadhesive buccal tablets containing triamcinolone acetonide in healthy volunteers.* Int. J. Pharm., 121, 249-254.

Munnelly, H.M., Roess, D.A., Wade, W.F. and Barisas, B.G. (1998) *Interferometric fringe fluorescence photobleaching recovery interrogates entire cell surfaces.* Biophys. J., 75, 1131-1138.

Naisebett, B. and Woodley, J. (1994) *The potential use of tomato lectin for oral drug delivery: 1. Lectin binding to rat small intestine in vitro.* Int. J. Pharm., 107, 223-230.

Naisebett, B. and Woodley, J. (1995) *The potential use of tomato lectin for oral drug delivery: 3. Bioadhesion in vivo.* Int. J. Pharm., 114, 227-236.

Nakumura, F., Ohta, R., Machida, Y. and Nagai, T. (1996) *In vitro and in vivo nasel mucoadhesion of some water-soluble polymers.* Int. J. Pharm., 134, 173-181.

Nebgen, G., Gross, D., Lehmann, V. and Muller, F. (1995) *^1H NMR microscopy of tablets.* J. Pharm Sci, 84, (3), pp283-291.

Needleman, I.G. and Smales, F.C. (1995) *In vitro assessment of bioadhesion for periodontal and buccal delivery.* Biomaterials, 16, 617-624.

Park, H. and Robinson, J.R. (1984) *Bioadhesive polymers as platforms for oral-controlled drug delivery: method to study bioadhesion.* Int. J. Pharm., 19, 107-127.

Park, H. and Robinson, J.R. (1985) *Physico-chemical properties of water insoluble polymers important to mucin/epithelial adhesion.* J. Contr. Rel., 2, 47-57.

Park, H. and Robinson, J.R. (1987) *Mechanisms of mucoadhesion of poly(acylic acid) hydrogels.* Pharm. Res., 4, (6), 457-464.

Park, K. (1989) *A new approach to study mucoadhesion: Colloidal gold staining.* Int. J. Pharm., 53, 209-217.

Park, K. and Park, H. (1990) *Test methods of bioadhesion.* In: Bioadhesive dug delivery systems. Ed. Lenaerts, V. and Gurny, R. CRC Press, Boca raton, Florida.

Paudler, W.W. (1987) *Nuclear magnetic resonance-general concepts and applications.* John Wiley & Sons, New York.

Pawley, J.B. (1990) *Handbook of biological confocal microscopy.* Ed. J.B. Pawley, Plenum Press, New York.

Peppas, N.A. (1998) *Molecular calculations of poly(ethylene glycol) transport across a swollen poly(acrylic acid)/mucin interface.* J. Biomater. Sci. Polymer Edn., 9, (6), 535-542.

Peppas, N.A. and Lustig, S.R. (1985) *The role of cross-links, entanglements, and relaxations of the macromolecular carrier in the diffusional release of biologically active materials. conceptual and scaling relationships.* Annals. N.Y. Acad. Sci., 446, 26-41 .

Peppas, N.A. and Sahlin, J.J. (1989) *A simple equation for the description of solute release III. Coupling of diffusion and relaxation.* Int. J. Pharm., 57, 169-172.

Peppas, N.A. and Buri, P.A. (1985) *Surface, interfacial and molecular aspects of polymer bioadhesion on soft tissues.* J.Contr. Rel., 2, 257-275.

Peppas, N.A., Narasimhan, B., Snaar, J.E.M., Bowtell, R.W. and Melia, C.D. (1997) *Magnetic resonance imaging analysis of soluble drug delivery carriers.* Proc. Int. Symp. Contrl. Rel. Bioact. Mater., 24, 171-172.

Perisamy, N. and Verkman, A.S. (1998) *Analysis of fluorophore diffusion by continuous distributions of diffusion coefficients: Application to photobleaching measurements of multicomponent and anomalous diffusion.* Biophys. J., 75, 557-567.

Perisamy, N., Bickenese, S. and Verkman, A.S. (1996) *Reversible photobleaching of fluorescein conjugates in air-saturated viscous solutions: Singlet and triplet state quenching by tryptophan.* Photochem. Photobiol., 63, (3), 265-271.

Peters, R. (1986) *Fluorescence microphotolysis to measure nucleocytoplasmic transport and intracellular mobility.* Biochem. Biophys. Acta, 864, 305-359.

Peters, R., Brunger, A. and Schulten, K. (1981) *Continuous fluorescence microphotolysis: A sensitive method for study of diffusion processes in single cells.* Biophys., 78, (2), 962-966.

Peters, R., Peters, J., Tews, K.H., Bahr, W. (1974) *A microfluorimetric study of translational diffusion in erythrocyte membranes.* Biochem. Biophy. Acta, 367, 282-294.

Ponchel, G., Touchard, F., Duchene, D. and Peppas, N.A. (1987) *Bioadhesive analysis of controlled-release systems. I. Fracture and interpenetration analysis in poly(acrylic acid)-containing systems.* J. Contr. Rel., 5, 129-141.

Potter, K., Balcom, B., Carpenter, T.A. and Hall, L.D (1994a) *The gelation of sodium alginate with calcium ions studied by magnetic resonance imaging (MRI).* Carb. Res., 257, 117-126.

Potter, K., Carpenter, T.A. and Hall, L.D (1994b) *Magnetic resonance imaging (MRI) of calcium alginate gels.* Mag. Res. Imaging, 12, (2), 309-311.

Potter, K., Carpenter, T.A. and Hall, L.D. (1993a) *Mapping the spatial variation in alginate concentration in calcium alginate gels by magnetic resonance imaging (MRI).* Carb. Res., 246, 43-49.

Potter, K., Herrod, N.J., Carpenter, T.A. and Hall, L.D (1993b) *Visualisation of the geometries of objects fabricated from calcium alginates, using magnetic resonance imaging.* Carb. Res., 239, 249-256.

Pronova. *General information.* Alginates. Pronova Biopolymers.

Rajabi-Siahboomi, A.R., Bowtell, R.W., Mansfield, P., Davies, M.C. and Melia, C.D. (1996) *Structure and behavior in hydrophilic matrix sustained release dosage forms. 4. Studies of water mobility and diffusion coefficients in the gel layer of HPMC tablets using NMR imaging.* Pharm. Res., 13, (3), 376-380.

Rajabi-Siahboomi, A.R., Bowtell, R.W., Mansfield, P., Henderson, A., Davies, M.C. and Melia, C.D. (1994) *Structure and behavior in hydrophilic matrix sustained release dosage forms. 2. NMR-imaging studies of dimensional changes in the gel layer and core of HPMC tablets undergoing hydration.* J. Contr. Rel., 31, 121-128.

Ranga Rao, K.V. and Buri, P. (1989) *A novel in situ methods to test polymers and coated microparticles for bioadhesion.* Int. J. Pharm., 52, 265-270.

Rillosi, M. and Buckton, G. (1995a) *Modelling mucoadhesion by use of surface energy terms obtained by the Lewis acid-Lewis base approach.* Int. J. Pharm., 117, 75-84.

Rillosi, M. and Buckton, G. (1995b) *Modelling mucoadhesion by use of surface energy terms obtained by the Lewis acid-Lewis base approach. II. Studies on anionic, cationic and unionisable polymers.* Pharm. Res. 12, 669-675.

Ritger, P.L. and Peppas, N.A. (1987a) *A simple equation for description of solute release. I. Fickian and non-Fickian release from non-swellable devices in the form of slabs, spheres, cylinders or discs.* J. Contr. Rel., 5, 23-36.

Ritger, P.L. and Peppas, N.A. (1987b) *A simple equation for description of solute release. II. Fickian and anomalous release from swellable devices.* J. Contr. Rel., 5, 37-42

Robert, C., Buri, P. and Peppas, N.A. (1988) *Experimental method for bioadhesive testing of various polymers.* Acta Pharm. Tech., 34, (2), 95-98.

Romero, A.P., Caramella, C., Ronchi, M., Ferrari, F. and Chulia, D. (1991) *Water uptake and force development in an optimised prolonged release formulation.* Int. J. Pham., 73, pp239-248.

Rossi, S., Bonferoni, M.C., Lippoli, G., Bertoni, M., Ferrari, F., Caramella, C. and Conte, U. (1995) *Influence of mucin type on polymer-mucin rheological interactions.* Biomaterials, 16, 1073-1079.

Rudnic, E.M. and Rhodes, C.T., (1982) *Evaluations of the mechanism of disintegrant action.* Drug Dev. Ind. Pharm., 8, 87-109.

Sahlin, J.J. and Peppas, N.A. (1996) *Hydrogels as mucoadhesive and bioadhesive materials: A review.* Biomaterials, 17, 1553-1561.

Sahlin, J.J. and Peppas, N.A. (1997) *Enhanced hydrogel adhesion by polymer interdiffusion: Use of linear poly(ethylene glycol) as an adhesion promoter.* J. Biomater. Sci. Polym. Edn., 8, (6), 421-436.

Sam, A. P., Vandenheuij, J. T. M. and Tukker, J. J. (1992) *Mucoadhesion of both film-forming and non-film-forming polymeric materials as evaluated with the Wilhelmy plate method.* Int. J. Pharm., 79, (2-3), 97-105.

Sandzen, B., Blom, H. and Dahlgren, S. (1988) *Gastric mucus gel layer thickness measured by direct light microscopy. An experimental study in the rat.* Scand. J. Gastroenterol., 23, 1160-1164.

Sanzgiri, Y.D., Topp, E.M., Bernedetti, L. and Stella, V.J. (1994) *Evaluation of mucoadhesive properties of hyaluronic acid benzyl esters.* Int. J. Pharm., 107, 91-97.

Sargent, J.A. (1988) *Low temperature scanning electron microscopy.* Micros.Analysis, 1, 7-9.

Schnurrer, J. and Lehr, C.M. (1996) *Mucoadhesive properties of the mussel adhesive protein.* Int. J. Pharm., 141, 251-256.

Sellars, L.A., Allen, A., Morris, E.R. and Ross-Murphy, S. (1991) *The rheology of pig small intestinal and colonic mucus: Weakening of gel structure by non-mucin components.* Biochem. Biophys. Acta, 1115, 174-179.

Sellars, L.A., Allen, A., Morris, E.R., Ross-Murphy, S.B. (1988) *Mucus glycoprotein gels. Role of glycoprotein polymeric structure and carbohydrate side-chains in gel formation.* Carb. Res., 178, 93-110.

Shapiro, M., Jarema, M.A. and Gravina, S. (1996) *Magnetic resonance imaging of an oral gastrointestinal-therapeutic-system (GITS) tablet.* J. Contr. Rel., 38, 123-127.

Shojaei, A.H. and Li, X. (1997) *Mechanisms of buccal mucoadhesion of novel coploymers of acrylic acid and polyethylene glycol monomethlether monomethacrylate.* J. Contr. Rel., 47, 151-161.

Shumen, H., Murray, J.M. and Dilullo, C. (1989) *Confocal microscopy: An overview.* Biotech., 7, 154-163.

Smart, J.D. (1991) *An in vitro assessment of some mucosa-adhesive forms.* Int. J. Pharm., 73, 69-74.

Smart, J.D. (1993) *Drug delivery using buccal-adhesive systems.* Adv. Drug. Del. Rev., 11, 253-270.

Smart, J.D. and Kellaway, I.W. (1989) *Pharmaceutical factors influencing the rate of gastrointestinal transit in an animal model.* Int. J. Pharm., 53, 79-83.

Smart, J.D., Carpenter, B. and Mortazavi, S.A. (1991) *Is mucus dehydration an important factor in mucoadhesion?* Proc. Int. Symp. Contr. Rel. Bioact. Mater., 18, 629-670.

Smart, J.D., Kellaway, I.W. and Worthington, H.E.C. (1984) *An in-vitro investigation of mucosa-adhesive materials for use in controlled drug delivery.* J. Pharm. Pharmcol., 36, 295-299.

Smidsrod, O. (1974) *Molecular basis for some physical properties of alginates in the gel state.* Faraday Disc. Chem. Soc., 57, 263-275.

Smidsrod, O. and Draget, K.I. (1996) *Chemistry and physical properties of alginates.* Carb. Eur., 14, 6-13.

Smidsrod, O. and Grasdalen, H. (1984) *Polyelectrolytes from seaweeds.* Hydrobiologia, 116/117, 19-28.

Smith, B.A. and McConnell, H.M. (1978) *Determination of molecular motion in membranes using periodic pattern photobleaching.* Proc. Natl. Acad. Sci. U.S.A., 75, 2759-2763.

Smith, G.W., Wiggins, P.M., Lee, S.P. and Tasman-Jones, C. (1986) *Diffusion of butyrate through pig coloninc mucus in vitro.* Clin. Sci., 70, 271-276.

Smithson, K.W., Millar, D.B., Jacobs, L.R. and Gray, G.M. (1981) *Intestinal diffusion barrier: Unstirred water layer or membrane surface mucous coat.* Science, 214, 1241-1244.

Snaar, J.E.M., Bowtell, R. Melia, C.D. Morgan, S. Narasimhan, B. and Peppas, N.A. (1998) *Self-diffusion and molecular mobility in PVA-based dissolution-controlled systems for drug delivery.* Mag. Res. Imaging, 16, (5-6), 691-694.

Song, L., Hennik, E.J., Young, T., and Tanke, H.J. (1995) *Photobleaching kinetics of fluorescein in quantitative fluorescence microscopy.* Biophys. J., 68, 2588-2600.

Song, L., Varma, C.A.G.O., Verhoeven, J.W. and Tanke, H.J. (1996) *Influence of the triplet excited state on the photobleaching kinetics of fluorescein in microscopy.* Biophys. J., 70, 2959-2968.

Soumpasis, D.M. (1983) *Theoretical approach of fluorescence recovery experiments.* Biophys. J., 41, 95-97.

Stanford, E.C.C. (1881) *Manufacture of useful products from seaweeds.* Brit. Pat. No. 142.

Swaminathan, R., Bickinese, S., Perisamy, N. and Verkman, A.S. (1996) *Cytoplasmic viscosity near the cell plasma membrane: Translational diffusion of a small fluorescent solute measured by total internal reflection-fluorescence photobleaching recovery.* Biophy. J., 71, 1140-1151.

Tanner, J.E. and Stejskal, E.O. (1968) *Restricted self-diffusion of protons in colloidal systems by the pulsed-gradient, spin-echo method.* J. Chem. Phys., 49, (4), 1768-1777.

Teng, C.L.C. and Ho, N.F.H. (1987) *Mechanistic studies in the simultaneous flow and adsorption of polymer-coated latex particles on intestinal mucus. I. Methods and physical model development.* J. Contr. Rel., 6, 133-149.

Thompson, N.L., Burghardt, T.P. and Axelrod. D. (1981) *Measuring surface dynamics of biomolecules by total internal reflection fluorescence with photobleaching recovery or correlation spectroscopy.* Biophy. J., 33, 435-454.

Tobyn, M.J. (1994) *Factors affecting in vitro gastric mucoadhesion.* Ph.D. Thesis, University of Strathclyde.

Tobyn, M.J., Johnson, J.R. and Gibson, S.A.W. (1992) *Investigations into the role of hydrogen bonding in the interaction between mucoadhesives and mucin at gastric pH.* J.Pharm. Pharmcol., 44(Suppl), 11P.

Tobyn, M.J., Johnson, J.R. and Dettmar, P.W. (1995) *Factors affecting in vitro gastric mucoadhesion. I. Test conditions and instrumental parameters.* Eur. J. Pharm. Biopharm., 41, (4), 235-241.

Tobyn, M.J., Johnson, J.R., Dettmar, P.W. (1996a) *Factors affecting in vitro gastric mucoadhesion. III. Influence of polymer addition on the observed mucoadhesion of some polymers.* Eur. J. Pharm. Biopharm., 42, (5), 331-335.

Tobyn, M.J., Johnson, J.R., Dettmar, P.W. (1996b) *Factors affecting in vitro gastric mucoadhesion. II. Physical properties of polymers.* Eur. J. Pharm. Biopharm., 42, (1), 56-61.

Tur, K.M. and Ch'ng, H.S. (1998) *Evaluation of possible mechanism(s) of bioadhesion.* Int. J. Pharm., 160, 61-74.

Turner, N.C., Martin, G.P. and Marriott, C. (1985) *The influence of native porcine gastric mucus gel on hydrogen ion diffusion: the effect of potentially ulcerogenic agents.* J. Pharm. Pharmacol., 37, 776-780.

Valtier, M., Tekely, P. Kiene, L. and Canet, D. (1995) *Visualisation of solvent polymers by NMR microscopy with radio-frequency flied gradients.* Macromol., 28, 4075-4079.

Van Kamp, H.V., Bolhuis, G.K., de Boer, A.H., Lerk, C.F. and Lie-A-Huen, L. (1986) *The role of water uptake on tablet disintegration.* Pharm. Acta. Helv., 61, (1), 22-29.

Veiga, F., Salsa, T. and Pina, M.E. (1998) *Oral controlled release dosage forms. II. Glassy polymers in hydrophilic matrices.* Drug Dev. Ind. Pharm., 24, (1), 1-9.

Veillard, M. (1990) *Buccal and gastrointestinal drug delivery systems.* In: Bioadhesion-Possibilities and future trends. Ed. Gurny, R. and Junginger, H.E., Wissenschaftliche Velagegesellschaft, Stuttgart.

Wan, L.S.C., Heng, P.W.S. and Wong, L.F. (1991) *The effect of hydroxypropylmethylcellulose on water penetration into a matrix system.* Int. J. Pharm., 73, 111-116.

Wan, L.S.C. and Choong, Y.L. (1986) *The effect of excipients on the penetration of liquid into tablets.* Pharm. Acta. Helv., 61, 150-155.

Wan, L.S.C. and Heng, P.W.S. (1987) *Technique of measuring rapid water penetration rate into tablets.* Chem. Pharm. Bull., 35, 1615-1618.

Wan, L.S.C., Heng, P.W.S. and Wong, L.F. (1994) *Effect of additives on liquid uptake into hydroxypropylmethylcellulose matrices.* S.T.P. Pharma Sci., 4, (3), 213-219.

Wan, L.S.C. and Prasad, K.P.P. (1989) *Influence of quantity of granulating liquid on water uptake and disintegration of tablets with methylcellulose.* Pharm. Ind., 51, (1), 105-109.

Warburg, M and Christian, G. (1942) *Isolierung und kristallisation des garungsferments enolase* Biochem Z., 310, 384-421.

Wedekind, P., Kubitscheck, U. and Peters, R. (1994) *Scanning microphotolysis: A new photobleaching technique based on fast intensity modulation of a scanned laser beam and confocal imaging.* J. Micros., 176, (1), 23-33.

Wedekind, P., Kubitscheck, U., Heinrich, O. and Peters, R. (1996) *Line-scanning microphotolysis for diffraction-limited measurements of lateral diffusion.* Biophys. J., 71, 1621-1632.

Wells, K.S., Sandison, D.R. Strickler, J. and Webb, W.W. (1990) *Quantitative fluorescence imaging with laser scanning confocal microscopy.* In: Handbook of biological confocal microscopy. Ed. J.B. Pawley, Plenum Press, New York.

White, J.G., Amos, W.B. and Fordham, M. (1987) *An evaluation of confocal versus conventional imaging of biological structures by fluorescence light microscopy.* J. Cell Biol., 105, 41-48.

Williams, S.E. and Turnberg, L.A. (1980) *Retardation of acid diffusion by pig gastric mucus: A potential role in mucosal protection.* Gastroent., 79, (2), 299-304.

Wilson, T. (1989) *Trends in confocal microscopy.* Trends Neurosci., 12, (12), 486-493.

Winne, D. and Verheyen, W. (1990) *Diffusion coefficients in native mucus gel of a rat small intestine.* J. Pharm. Pharmcol., 42, 517-519.

Woolfson, A.D., McCafferty, D.F., Gorman, S.P., McCarron, P.A. and Price, J.H. (1992) *Design of an apparatus incorporating a linear variable differential transformer for the measurement of type III bioadhesion to cervical tissue.* Int. J. Pharm., 84, 69-76.

Woolfson, A.D., McCafferty, D.F., McCallion, C.R., McAdams, E.T. and Anderson, J.M.C.C. (1995a) *Moisture-activated, electrically conducting bioadhesive hydrogels as interfaces for bioelectrodes: Effect of formulation factors on cutaneous adherence in wet environments.* J. Appl. Poly. Sci., 56, 1151-1159.

Woolfson, A.D., McCafferty, D.F., McCarron, P.A. and Price, J.H. (1995b) *A bioadhesive patch cervical drug delivery system for the administration of 5-fluorouracil to cervical tissue.* J. Contr. Rel., 35, 49-58.